The University of Nottingham
UNITED KINGDOM · CHINA · MALAYSIA

Erten, Tayyibe (2016) A Hydrodynamic Study of Microbial Polysaccharides Considered For Use in Food and Health Products. PhD thesis, University of Nottingham.

Access from the University of Nottingham repository:
http://eprints.nottingham.ac.uk/33794/1/final%20draft%20of%20%20PhD%20thesis-T.Erten.pdf

Copyright and reuse:

The Nottingham ePrints service makes this work by researchers of the University of Nottingham available open access under the following conditions.

This article is made available under the University of Nottingham End User licence and may be reused according to the conditions of the licence. For more details see: http://eprints.nottingham.ac.uk/end_user_agreement.pdf

A note on versions:

The version presented here may differ from the published version or from the version of record. If you wish to cite this item you are advised to consult the publisher's version. Please see the repository url above for details on accessing the published version and note that access may require a subscription.

For more information, please contact eprints@nottingham.ac.uk

A Hydrodynamic Study of Microbial Polysaccharides Considered For Use in Food and Health Products

Tayyibe Erten

BSc., MSc.

Thesis submitted to the University of Nottingham for the degree of Doctor of Philosophy

February, 2016

National Centre for Macromolecular Hydrodynamics

School of Biosciences, University of Nottingham,

Sutton Bonington, Loughborough, Leicestershire, UK

This thesis is dedicated to my parents

ABSTRACT

Microbial polysaccharides are widely used in many industrial and therapeutic applications as bioactive compounds, drug release and encapsulation materials for pharmaceuticals, and as natural ingredients or additives in food applications. To increase the utilisation or to improve for the food and healthcare applications of these polysaccharides, it is critical to have the detailed knowledge of macromolecular properties and interactions with other polymers. In this study, to properly understand the relationship between physical properties and functionality, the microbial polysaccharides-namely xanthan, gellan, microbial hyaluronic acid (HA) and schizophyllan, which have widely been used for many food and medical applications, were investigated. Taking advantage of recent advances in hydrodynamic techniques, including analytical ultracentrifugation (AUC) based on sedimentation velocity and equilibrium, size exclusion chromatography coupled to multi angle light scattering (SEC-MALS) and viscometry, the solution properties of these polysaccharides were studied. Since conformation analyses are important for macromolecular structure-function relationships, the conformation of these microbial polysaccharides were examined using the accomplished method-Multi-HYDFIT. For schizophyllan and gellan, the samples were depolymerised using heat treatment to estimate the conformation. The results indicated that, the three microbial polysaccharides (xanthan, gellan, schizophyllan) adapted the rigid rod conformation whereas another polysaccharide-microbial HA adapted semi-flexible coil structure.

Then, the possible interactions of these polysaccharides were investigated with chitosan of different degrees of acetylation using the principle of co-sedimentation in AUC. Xanthan-chitosan mixture presented strong evidence by proving a clear

interaction on the basis of changes in the distribution of sedimentation coefficients in the solution form of mixture whereas the mixture of chitosan-schizophyllan and chitosan-HA did not show or prove any clear interactions at studied concentrations and solution conditions.

ACKNOWLEDGEMENT

I would like to express my deepest gratitude and sincere appreciation to my supervisors Professor Dr. Steve Harding and Dr. Gary Adams for their patience, encouragement, support, and guidance over the last four years. Without their assistance and help, this thesis would not be accomplished.

My special thanks go to Professor Dr. Arthur Rowe and Professor Dr. Tim Foster for their advice and support for this project. Deep gratitude goes to Dr. M. Samil Kok for his assistance and support.

I am also grateful to the whole NCMH team; Dr. Guy Channell, Dr. David Besong, Dr. Richard Gillis, Dr. Fahad Almutairi, Dr. Shahwar Imran Jiwani and Qushmua Alzahrani for their collaboration, advice and support.

I also would like to express my gratitude and deepest appreciation to my family back home. Without their invaluable prayers, support and encouragement, I could not complete this thesis.

I am indebted to all my friends who have supported me during these four years; Aytul Gokce, Seda Ozdemir, Ayse Sarihan, Rukiye Karadeniz, Zehra C. Araci, Bahar Kayali, F. Fusun Kucukapan, Kubra Aktas, Agne Tilunaite, Esra Kaya and Mehtap Aygun for their friendship and help.

Last but not least, I would like to thank Turkish Ministry of National Education who funded my postgraduate education.

LIST OF ABBREVIATIONS

a	Mark-Houwink exponent of viscosity
A_2 —*or B*	Second virial coefficient
A_3 —*or C*	Third virial coefficient
AFM	Atomic Force Microscopy
AUC	Analytical Ultracentrifugation
b	Mark-Houwink-Sakurada power law exponent of sedimentation
c	Concentration
DLS	Dynamic Light Scattering
DSC	Differential Scanning Calorimetry
d	Diameter
dn/dc	refractive index increment
D_t	Diffusion coefficient (extrapolated to infinite dilution)
F_c	Centrifugal force
F_b	Buoyant force
F_d	Frictional‖ force
f/f_0	Frictional ratio
FDA	Food and Drug Administration
HA	Hyaluronic Acid
I	Ionic strength
kDa	kilo Daltons
k_D	Concentration dependence coefficient
K_H	Huggins coefficient
K_K	Kraemer coefficient
k_s	Gralén concentration dependence parameter
k_s/η —*or R*	Wales-van Holde ratio
LAG	Low acyl gellan
LS	Light Scattering
L_p	Persistence length
ls-g*(s)	Least-square g*(s)
MALS	Multi-angle light scattering detector
MHKS	Mark-Houwink-Kuhn-Sakurada

M_L	Mass per unit length
m	Mass of particle
M_w	Weight average molecular weight
M_n	Number average molecular weight
M_z	z-average molecular weight
$M_{w,app}$	Apparent molecular weight
M*	M-star function of molecular weight
M*(r)	M-star function of molecular weight at a certain radius
N_A	Avogadro‘s constant
PBS	Phosphate buffer saline
R_θ	Rayleigh factor
r	Radial displacement
R_g	Radius of gyration
rpm	Revolution per minute
SEM	Scanning electron microscopy
s	Sedimentation coefficient
S	Svedberg units
$s_{T,b}$	Sedimentation coefficient achieved during experimental conditions
$s_{20,w}$	Sedimentation coefficient corrected from $s_{T,b}$ in the form of standard solvent of water at 20 °C
$s^0_{20,w}$	$s_{20,w}$extrapolated to zero concentration and elimination of non-ideality
SE	Sedimentation equilibrium
SEC	Size exclusion chromatography
SEC-MALS	Size exclusion chromatography coupled with multi angle light scattering
SV	Sedimentation velocity
T	Absolute temperature
V	Scattering volume
v	Velocity
κ_η	Mark-Houwink constant of viscosity
κ_s	Mark-Houwink constant of sedimentation
η	Viscosity of the solution

η_0	Viscosity of the solvent
η_{inh}	Inherent viscosity
η_{red}	Reduced viscosity
η_{rel}	Relative viscosity
η_{sp}	Specific viscosity
$[\eta]$	Intrinsic viscosity
ρ	Density of solution
ρ_o	Density of solvent
$\bar{\upsilon}$	Partial specific volume
$\omega^2 r$	Centrifugal field
θ	Angle of scattering light
ϕ	Flory-Fox constant
Δ	Target (error) function
ΔP	Differential pressure

TABLE OF CONTENTS

ABSTRACT ii
ACKNOWLEDGEMENT iv
LIST OF ABBREVIATIONS v
TABLE OF CONTENTS viii
LIST OF FIGURES xiii
LIST OF TABLES xxi
CHAPTER 1 1
INTRODUCTION 1
1.1. INTRODUCTION 1
1.2. MICROBIAL POLYSACCHARIDES 3
1.2.1. Xanthan 4
1.2.2. Gellan 7
1.2.3. Hyaluronic Acid 10
1.2.4. Schizophyllan 13
1.3. INTERACTION WITH CHITOSAN 15
1.4. THE AIM OF THIS STUDY 16
CHAPTER 2 17
HYDRODYNAMIC METHODS 17
2.1. ANALYTICAL ULTRACENTRIFUGATION 17
2.1.1. Sedimentation Velocity 18
2.1.2. Sedimentation Equilibrium 24
2.2. SIZE EXCLUSION CHROMATOGRAPHY COUPLED TO MULTI ANGLE LIGHT SCATTERING (SEC-MALS) 28
2.3. VISCOMETRY 34
2.3.1. Capillary Viscometry 36
2.3.2 Pressure Imbalance Differential Viscometry 38
2.4. DYNAMIC LIGHT SCATTERING 40
2.5. COMBINED HYDRODYNAMIC APPROACHES AND THE CONFORMATION OF MACROMOLECULES 42
2.5.1. Wales-van Holde Ratio 42
2.5.2. Mark-Houwink-Kuhn-Sakurada (MHKS) or Power Law Relations 43

2.5.3 Estimation of the Persistence Length (Lp) and Mass Per Unit Length (M_L) 45
2.5.4. Conformation Zoning 50
CHAPTER 3 52
HYDRODYNAMIC CHARACTERISATION OF XANTHANS OF DIFFERENT PYRUVATE AND ACETATE CONTENT 52
3.1. INTRODUCTION 52
3.2. MATERIALS 55
3.3. METHODS 56
3.3.1. Sedimentation Velocity (SV) 56
3.3.2. Sedimentation Equilibrium (SE) 57
3.3.3. Dynamic Light Scattering (DLS) 58
3.3.4. Capillary Viscometry 59
3.4. RESULTS 60
3.4.1. Sedimentation Velocity (SV) 60
3.4.2. Estimation of Molecular Weight 63
3.4.3. Dynamic Light Scattering 69
3.4.4 Intrinsic Viscosity 71
3.4.5. Conformational Analysis 74
3.5. DISCUSSION 77
3.6. CONCLUSION 80
CHAPTER 4 82
A STUDY ON SOLUTION PROPERTIES AND MOLECULAR CONFORMATION OF LOW ACYL GELLAN GUM 82
4.1. INTRODUCTION 82
4.2. MATERIALS 85
4.3. METHODS 86
4.3.1. Partial Specific Volume 86
4.3.2. Sedimentation Velocity (SV) 86
4.3.3. Sedimentation Equilibrium (SE) 87
4.3.4. Capillary and Differential Pressure Viscometry 88
4.4. RESULTS 89
4.4.1. Partial Specific Volume 89
4.4.2. Sedimentation Velocity (SV) 90

4.4.3. Estimation of Molecular Weight 92
4.4.4. Intrinsic Viscosity 95
4.4.5. Conformation Analysis 98
4.5. DISCUSSION 105
4.6. CONCLUSION 107
CHAPTER 5 109
MOLECULAR WEIGHT AND CONFORMATION STUDY OF SODIUM HYALURONATE IN AQUEOUS SOLUTION 109
5.1. INTRODUCTION 109
5.2. MATERIALS 112
5.3. METHODS 112
5.3.1. Sedimentation Velocity (SV) 112
5.3.2. Sedimentation Equilibrium (SE) 114
5.3.3. Size Exclusion Chromatography Coupled to Multi Angle Light Scattering (SEC-MALS) 115
5.3.4. Capillary and Differential Pressure Viscometry 116
5.4. RESULTS 117
5.4.1. Sedimentation Velocity (SV) 117
5.4.2. Estimation of Molecular Weight 120
5.4.3. Intrinsic viscosity 125
5.4.4. Conformation Analysis 128
5.5. DISCUSSION 139
5.6. CONCLUSION 141
CHAPTER 6 143
A STUDY ON SOLUTION PROPERTIES AND MOLECULAR CONFORMATION OF SCHIZOPHYLLAN 143
6.1. INTRODUCTION 143
6.2. MATERIALS 146
6.3. METHODS 147
6.3.1. Partial Specific Volume 147
6.3.2. Sedimentation Velocity (SV) 148
6.3.3. Sedimentation Equilibrium (SE) 149
6.3.4. Size Exclusion Chromatography Coupled to Multi Angle Light Scattering (SEC-MALS) 150

6.3.5. Capillary and Differential Pressure Viscometry 150
6.4. RESULTS 152
6.4.1. Partial Specific Volume 152
6.4.2. Sedimentation Velocity (SV) 153
6.4.3 Estimation of Molecular Weight 155
6.4.4. Intrinsic Viscosity 159
6.4.5. Conformation Analysis 160
6.5. DISCUSSION 169
6.6. CONCLUSION 171
CHAPTER 7 172
HYDRODYNAMIC CHARACTERISATION OF CHITOSAN AND ITS INTERACTION WITH TWO POLYANIONS: DNA AND XANTHAN 172
7.1 INTRODUCTION 173
7.2. MATERIALS 176
7.3. METHODS 177
7.3.1. Sedimentation Velocity (SV) 177
7.3.2. Sedimentation Equilibrium (SE) 178
7.3.3. Size Exclusion Chromatography Coupled to Multi Angle Light Scattering (SEC-MALS) 178
7.3.4. Intrinsic viscosity 179
7.4. RESULTS 181
7.4.1. Sedimentation Velocity (SV) 181
7.4.2. Estimation of Molecular Weight 184
7.4.3. Intrinsic Viscosity 190
7.4.4. Conformational Analysis 192
7.4.5. Interaction with Two Polyanions: DNA and Xanthan 201
7.5. DISCUSSION 204
7.7. CONCLUSION 207
CHAPTER 8 209
CONCLUDING REMARKS AND SUGGESTIONS FOR FUTURE WORK 209
8.1. Characterisation of Xanthans 209
8.2. Characterisation of Gellan 210
8.3. Characterisation of Microbial Hyaluronic Acid 211
8.4. Characterisation of Schizophyllan 212

8.5. Characterisation of chitosan – used as an interactant with xanthan and DNA 213
8.6. Suggestion for Future Work.....215
REFERENCES.....216
APPENDIX.....240

LIST OF FIGURES

Figure 1.1	Chemical structure of xanthan	5
Figure 1.2	Chemical structure of (a) native and (b) deacetylated gellan gum	8
Figure 1.3	Chemical structure of repeating disaccharide unit of hyaluronic acid.	11
Figure 1.4	Chemical structure of repeating unit of schizophyllan	13
Figure 2.1	Diagram of a macromolecule in the sedimentation process	19
Figure 2.2	Boundary movement of sodium hyaluronate (HAV1) in sedimentation velocity experiment at 0.1 mg/ml. Scans recorded every 2 min. Rotor speed = 40000rpm	21
Figure 2.3	Profile of sedimentation equilibrium process for sodium hyaluronate (HAV4) at 0.1M PBS and (loading) concentration 1.0 mg/ml. Rotor speed = 13000rpm	25
Figure 2.4	Schematic presentation of SEC-MALS components	29
Figure 2.5	Separation of two fractions (Sample1 and 2) through the SEC column. Sample 2 eluted out first being the highest molecular weight fraction followed by Sample 1	30
Figure 2.6	Events in the process of light scattering	32
Figure 2.7	A schematic representation of the shearing of a liquid between 2 parallel plates. The parallel arrows represent fluid velocities at different values of y	35
Figure 2.8	The Huggins (black squares), Kraemer (red circles) and Solomon- Ciuta (green triangles) plots for depolymerised gellan (45sec microwaved) (see Chapter 4)	38
Figure 2.9	Schematic diagram of four capillary bridge design of a classical pressure imbalance viscometer	39
Figure 2.10	Example of a Mark–Houwink–Kuhn–Sakurada (MHKS) power law double logarithmic plot for chitosan HAV1 (see Chapter 5) from an on-line differential pressure viscometer ViscoStar coupled to SEC-MALS. The a value from the slope (0.20 ± 0.01)	43
Figure 2.11	Example of Mark–Houwink–Kuhn–Sakurada (MHKS) power law double logarithmic plot of $s^0_{20,w}$vs Mw for gellan samples (see Chapter 4). The b value from the slope (0.22 ± 0.04)	44
Figure 2.12	HAUG Triangle	45
Figure 2.13	Contour plots of the CHIT1. The target function, Δ calculated based on variables values of L_p and M_L, and are represented on the full colour spectrum from blue (Δ = 0.005) to red (Δ≥0.65) L_p = (16 ± 0.2), M_L = (500 ± 30)	49

(see Chapter 7)

Figure 2.14 The sedimentation conformation zoning plot; A: extra rigid rod, B: rigid rod, C: semi-flexible coil, D: random coil, E: globular/heavily branched structure 51

Figure 3.1 Chemical structure of xanthan 53

Figure 3.2a Sedimentation coefficient distribution profiles (least squares g(s) vs. s plots) of xanthan samples at different concentrations in pH= 7.0, I = 0.1 M buffer. (A) Standard LMW (B) Standard HMW, (C) High pyruvate, (D) Low pyruvate 61

Figure 3.2b Sedimentation coefficient distribution profiles (least squares g(s) vs. s plots) of xanthan samples at different concentrations in pH= 7.0, I = 0.3 M buffer. (A) Standard LMW (B) Standard HMW, (C) High pyruvate, (D) Low pyruvate 62

Figure 3.3a Concentration dependence (reciprocal) of the sedimentation coefficient plot (after correction to standard solvent conditions) for xanthan samples pH= 7.0, I = 0.1 M buffer. (A) Standard LMW (B) Standard HMW, (C) High pyruvate, (D) Low pyruvate 63

Figure 3.3b Concentration dependence (reciprocal) of the sedimentation coefficient plot (after correction to standard solvent conditions) for xanthan samples pH= 7.0, I = 0.3 M buffer. (A) Standard LMW (B) Standard HMW, (C) High pyruvate, (D) Low pyruvate 64

Figure 3.4 SEDFIT-MSTAR analysis of Low Pyruvate in 0.3 M PBS at a loading concentration of 0.35 mg/ml (A) molecular weight distribution, c(M) vs. M plot; (B) log concentration ln c(r) vs. r^2 plot, where r is the radial distance from the centre of rotation; (C) M* vs. r plot: the value of M* extrapolated to the cell base = $M_{w,app}$ the apparent weight average molecular weight for the whole distribution. (D) Point or local apparent weight average molecular weight at radial position r (open circle) plotted against the local concentration c(r). 66

Figure 3.5a Concentration dependence of apparent diffusion coefficient ($D_{20,w}$) vs concentration plot of xanthan samples; pH= 7.0, I = 0.1 M buffer. (A) Standard LMW (B) Standard HMW, (C) High pyruvate, (D) Low pyruvate 69

Figure 3.5b Concentration dependence of apparent diffusion coefficient ($D_{20,w}$) vs concentration plot of xanthan samples; pH= 7.0, I = 0.3 M buffer. (A) Standard LMW 70

(B) Standard HMW, (C) High pyruvate, (D) Low pyruvate

Figure 3.6a The intrinsic viscosity plots from capillary viscometry: Huggins, Kraemer and Solomon-Ciuta extrapolations for xanthan samples; pH= 7.0, I = 0.1 M buffer. (A) Standard LMW (B) Standard HMW, (C) High pyruvate, (D) Low pyruvate 72

Figure 3.6b The intrinsic viscosity plots from capillary viscometry: Huggins, Kraemer and Solomon-Ciuta extrapolations for xanthan samples; pH= 7.0, I = 0.1 M buffer. (A) Standard LMW (B) Standard HMW, (C) High pyruvate, (D) Low pyruvate 73

Figure 3.7 The conformation zoning plot for xanthan samples in both ionic strengths (I=0.1M and I=0.3M) which are adopted extra rigid rod structures (Zone A) 77

Figure 4.1 Chemical structure of (a) native and (b) deacetylated gellan gum adapted from 83

Figure 4.2 Determination of partial specific volume of LAG using density measurement in NaI at 20^{o}C. 89

Figure 4.3 Sedimentation coefficient distribution profiles using least squares g*(s) method of SEDFIT obtained from sedimentation velocity experiment for gellan samples in 0.25mM NaI; (A) LAG, (B) LAG1, (C) LAG2, (D) LAG3, (E) LAG4, (F) LAG5 91

Figure 4.4 Concentration dependence (reciprocal) of the sedimentation coefficient plot (after correction to standard solvent conditions) for gellan samples in 0.25mM NaI (A) LAG, (B) LAG1, (C) LAG2, (D) LAG3, (E) LAG4, (F) LAG5 92

Figure 4.5 SEDFIT-MSTAR analysis of LAG in 25mM NaI at a loading concentration of 0.3 mg/ml (A) molecular weight distribution, c(M) vs. M plot; (B) log concentration ln c(r) vs. r^2 plot, where r is the radial distance from the centre of rotation; (C) M* vs. r plot: the value of M* extrapolated to the cell base = $M_{w,app}$ the apparent weight average molecular weight for the whole distribution. (D) Point or local apparent weight average molecular weight at radial position r (open circle) plotted against the local concentration c(r). 93

Figure 4.6 The reciprocal plots of the apparent weight average molecular weight ($M_{w,app}$) against concentration c (g/ml) for gellan samples in 0.25mM NaI (A) LAG, (B) LAG1, (C) LAG2, (D) LAG3, (E) LAG4, (F) LAG5 94

Figure 4.7	The intrinsic viscosity plots from capillary viscometry: Huggins, Kraemer and Solomon-Ciuta extrapolations for gellan samples in 25mM NaI; (A) LAG, (B) LAG1, (C) LAG2, (D) LAG3, (E) LAG4, (F) LAG5	97
Figure 4.8	Mark–Houwink–Kuhn–Sakurada (MHKS) power law double logarithmic plot of $s^0_{20,w}$ vs M_w for gellan samples	99
Figure 4.9	Mark–Houwink–Kuhn–Sakurada (MHKS) power law double logarithmic plot for gellan samples	100
Figure 4.10	Contour plots for gellan samples. The target function, Δ calculated based on variables values of L_p and M_L, and are represented on the full colour spectrum from blue (Δ = 0.17) to red ($\Delta \geq 0.95$)	103
Figure 4.11	The conformation zoning plot for gellan samples which are adapted rigid rod structures (Zone B)	105
Figure 5.1	Chemical structure of repeating disaccharide unit of hyaluronic acid	109
Figure 5.2	Sedimentation coefficient distribution profiles using the least squares g*(s) method of SEDFIT obtained from sedimentation velocity experiment for sodium hyaluronate samples (A) HAV1, (B) HAV2, (C) MHAV1, (D) MHAV2, (E) HAV3, (F) HAV4, (G) HAV5, (H) HAV6	118
Figure 5.3	Concentration dependence (reciprocal) of the sedimentation coefficient plot (after correction to standard solvent conditions) for sodium hyaluronate samples in 0.1M PBS (A) HAV1, (B) HAV2, (C) MHAV1, (D) MHAV2, (E) HAV3, (F) HAV4, (G) HAV5, (H) HAV6	119
Figure 5.4	SEDFIT-MSTAR analysis of HAV4 in 0.1 M PBS at a loading concentration of 1.0 mg/ml (A) molecular weight distribution, c(M) vs. M plot; (B) log concentration ln c(r) vs. r^2 plot, where r is the radial distance from the centre of rotation; (C) M* vs. r plot: the value of M* extrapolated to the cell base = $M_{w,app}$ the apparent weight average molecular weight for the whole distribution. (D) Point or local apparent weight average molecular weight at radial position r (open circle) plotted against the local concentration c(r)	121
Figure 5.5	Plots of $M_{w,app}$ against concentration for (A) conventional plot of HAV3 (B) reciprocal plot of MHAV1 and MHAV2 (C) reciprocal plot of HAV4, HAV5 and HAV6	123
Figure 5.6a	Elution profiles of the sodium hyaluronate samples: HAV1 (black line), HAV2 (red line), HAV3 (green line)	124

	at concentration 0.5 mg/ml, MHAV1 (blue line) and MHAV2 (purple line) at concentration 1.0mg/ml examined by SEC-MALS.	
Figure 5.6b	Elution profiles of the sodium hyaluronate samples: HAV4 (black line), HAV5 (red line), HAV6 (green line) at concentration 5.0 mg/ml examined by SEC-MALS	125
Figure 5.7	The intrinsic viscosity plots from capillary viscometry: Huggins, Kraemer and Solomon-Ciuta extrapolations for sodium hyaluronate samples; (A) HAV1, (B) HAV2, (C) MHAV1, (D) MHAV2, (E) HAV3, (F) HAV4, (G) HAV5, (H) HAV6	126
Figure 5.8	Mark–Houwink–Kuhn–Sakurada (MHKS) power law double logarithmic plot of $s^0_{20,w}$ vs M_w for all sodium hyaluronate samples	129
Figure 5.9	Mark–Houwink–Kuhn–Sakurada (MHKS) power law double logarithmic plot from on-line differential pressure viscometry coupled to SEC-MALS for sodium hyaluronate samples; (A) HAV1, (B) HAV2, (C) MHAV1, (D) MHAV2, (E) HAV3, (F) HAV4, (G) HAV5, (H) HAV6	130
Figure 5.10	Bushin-Bohdanecky plot for sodium hyaluronate samples, where L_p = (9.4 ± 0.03) nm from the slope	133
Figure 5.11	Contour plots for sodium hyaluronate samples (A) HAV1, (B) HAV2, (C) MHAV1, (D) MHAV2, (E) HAV3, (F) HAV4, (G) HAV5, (H) HAV6. The target function, Δ calculated based on variables values of L_p and M_L, and are represented on the full colour spectrum from blue (Δ = 0) to red ($\Delta \geq 0.95$)	137
Figure 5.12	The conformation zoning plot for sodium hyaluronate samples. All samples fall in the zone for which are adapted semi-flexible coil structures (Zone C)	139
Figure 6.1	Chemical structure of repeating unit of schizophyllan	144
Figure 6.2	Determination of partial specific volume of schizophyllan using density measurement in 0.1M PBS at 20^{o}C.	152
Figure 6.3	Sedimentation coefficient distribution profiles using least squares g*(s) method of SEDFIT obtained from sedimentation velocity experiment for schizophyllan samples (A) GM1, (B) INV1, (C) GM2, (D) INV2	154
Figure 6.4	Concentration dependence (reciprocal) of the sedimentation coefficient plot (after correction to standard solvent conditions) for schizophyllan samples (main component) in 0.1M PBS at pH 7.0 (A) GM1, (B) INV1, (C) GM2, (D) INV2	155

Figure 6.5	As (Figure 5.4) but the analysis of GM1 at a loading concentration of (0.6 mg/ml). $M_{w,app}$ from extrapolation of M* to cell base = 2043 kDa, and the meaning of the fitted lines in "c" and "d" are explained in the legend Figure 6.4	156
Figure 6.6	The reciprocal plots of the apparent weight average molecular weight ($M_{w,app}$) against concentration c (g/ml) for schizophyllan samples (A) GM1, (B) INV1, (C) GM2, (D) INV2	157
Figure 6.7	Molecular weight distribution for all schizophyllan samples in 0.1 M PBS buffer obtained from transformation of the g(s) versus s distribution using the Extended Fujita method of Harding et al., (2011) (A) GM1 at c=0.2mg/ml, (B) INV1, (C) GM2, (D) INV2 at c=0.4mg/ml	158
Figure 6.8	Intrinsic viscosity plots from capillary viscometry: Huggins, Kraemer and Solomon-Ciuta extrapolations for schizophyllan samples (A) GM1, (B) INV1, (C) GM2, (D) INV2	160
Figure 6.9	Mark–Houwink–Kuhn–Sakurada (MHKS) power law double logarithmic plot of $s^0_{20,w}$ vs M_w for all schizophyllan samples	161
Figure 6.10	Mark–Houwink–Kuhn–Sakurada (MHKS) power law double logarithmic plot from on-line differential pressure viscometry coupled to SEC-MALS for schizophyllan samples (A) GM1, (B) INV1, (C) GM2, (D)INV2	162
Figure 6.11	Yamakawa-Fujii plot for schizophyllan samples, where L_p = (134 ± 4) nm from the slope and the an assumed value for M_L= 2150 $g.mol^{-1}.nm^{-1}$	165
Figure 6.12	Contour plots of schizophyllan samples; (A) GM1, (B) INV1, (C) GM2, (D) INV2. The target function, Δ is calculated based on the variables values of L_p and M_L, and is represented on the full colour spectrum from blue (Δ = 0) to red ($\Delta \geq 0.95$)	167
Figure 6.13	The conformation zoning plot for schizophyllan samples which are adapted rigid rod structures (Zone B)	169
Figure 7.1	Chemical structure of chitosan	173
Figure 7.2	Sedimentation coefficient distribution profiles using least squares g*(s) method of SEDFIT obtained from sedimentation velocity experiment for chitosan samples (A) CHIT1, (B) CHIT2, (C) CHIT3, (D) CHIT4, (E) CHIT5, (F) CHIT6	182
Figure 7.3	Concentration dependence (reciprocal) of the sedimentation coefficient plot for chitosan samples (A)	183

CHIT1 (B) CHIT2 (C) CHIT3 (D) CHIT4 (E) CHIT5 (F) CHIT6

Figure 7.4 As (Figure 5.4) but the analysis of CHIT4 at a loading concentration of (0.5 mg mL-1). $M_{w,app}$ from extrapolation of M* to cell base = 80 kDa, and the meaning of the fitted lines in "c" and "d" are explained in the legend Figure 4.9 185

Figure 7.5a The conventional plot of the apparent weight average molecular weight ($M_{w,app}$) against concentration c (g/ml) ($M_{w,\,app}$ vs c) 186

Figure 7.5b The reciprocal plot of the apparent weight average molecular weight ($M_{w,app}$) against concentration c (g/ml) ($M_{w,\,app}$ vs c) 186

Figure 7.6 Elution profile of commercial and laboratory-prepared chitosan samples in 0.2 M, pH 4.3, acetate buffer, (A) CHIT1 (B) CHIT2 (C) CHIT3 (D) CHIT4 (E) CHIT5 (F) CHIT6 (black line) examined by SEC-MALS at concentration 0.5 mg/ml. The open squares correspond to molecular weights calculated from SEC-MALS 187

Figure 7.7 Molecular weight distribution for all chitosan samples in 0.2 M, pH 4.3, acetate buffer obtained from transformation of the g(s) versus s distribution at concentration (0.2 mg/ml), using the Extended Fujita method of Harding et al., (2011) (A) CHIT1 (B) CHIT2 (C) CHIT3 (D) CHIT4 (E) CHIT5 (F) CHIT6 189

Figure 7.8 The intrinsic viscosity plots from capillary viscometry: Huggins, Kraemer and Solomon-Ciuta extrapolations for chitosan samples (a) CHIT1 (b) CHIT2 (c) CHIT3 (d) CHIT4 (e) CHIT5 (f) CHIT6 191

Figure 7.9 Mark–Houwink–Kuhn–Sakurada (MHKS) power law double logarithmic plot of $s^0_{20,w}$ vs M_w for all chitosan samples 192

Figure 7.10 Mark–Houwink–Kuhn–Sakurada (MHKS) power law double logarithmic plot for chitosan samples (A) CHIT1 (B) CHIT2 (C) CHIT3 (D) CHIT4 (E) CHIT5 (F) CHIT6 194

Figure 7.11 Bushin-Bohdanecky plot for commercial (CHIT1 to CHIT4) and laboratory-prepared (CHIT5 and CHIT6) chitosan samples, where L_p = (10 ± 1) nm from the slope 196

Figure 7.12 Yamakawa-Fujii plot for commercial and laboratory-prepared chitosan samples, where L_p = (18 ± 1) nm from the slope 197

Figure 7.13 Contour plots of chitosan samples (A) CHIT1, (B) CHIT2, (C) CHIT3, (D) CHIT4, (E) CHIT5 and (F) CHIT6. The target function, Δ calculated based on 199

variables values of L_p and M_L, and are represented on the full colour spectrum from blue ($\Delta = 0$) to red ($\Delta \geq 0.95$)

Figure 7.14 The conformation zoning plot for chitosan samples, commercial (CHIT1 to CHIT4) which have rigid rod structures, and laboratory-prepared (CHIT5 and CHIT6) which have semi-flexible coil structures 200

Figure 7.15 Normalized sedimentation coefficient distribution profiles obtained from sedimentation velocity experiment for unmixed controls and mixture for chitosan samples (CHIT5 and CHIT6) with DNA 202

Figure 7.16 Normalized sedimentation coefficient distribution profiles obtained from sedimentation velocity experiment for unmixed controls and mixture for chitosan samples (CHIT5 and CHIT6) with xanthan-STD 204

Figure 7.17 Multi-Gaussian fit using MULTIG (locally written software, run under pro Fit™, interactive Preview Window, floating the position (s value), area and standard deviation of each peak Quansoft, Zurich) (A) Multi-Gaussian fit to the CHIT5-DNA mixture and (B) Multi-Gaussian fit to the CHIT6-DNA mixture. With the routine MULTIG fitting was initially performed manually via the interactive Preview Window, floating the position (s value), area and standard deviation of each peak 206

LIST OF TABLES

Table 1.1	Classification of polysaccharides considering the source	2
Table 3.1	Pyruvate and acetate content of the xanthans	56
Table 3.2	Summary of sedimentation coefficient ($s^0_{20,w}$) and concentration dependence of sedimentation (k_s) for all xanthan samples	62
Table 3.3	Estimated molecular weight of xanthan from the Mark-Houwink-Kuhn-Sakurada equation ($s = \kappa_s . M^b$)	68
Table 3.4	Summary of diffusion coefficient ($D^0_{20,w}$) for all xanthan samples	70
Table 3.5	Summary of Intrinsic viscosity values of xanthan samples obtained from capillary viscometry	74
Table 3.6	Wales-van Holde ratio (R) determined from intrinsic viscosity and concentration dependence coefficient results for xanthan samples	75
Table 4.1	Summary of $s^0_{20,w}$and k_s for original low acyl gellan and depolymerised gellan samples	90
Table 4.2	Summary of weight average molecular weights (M_w) results for original low acyl and depolymerised gellan samples	95
Table 4.3	Summary of intrinsic viscosity values of gellan samples obtained from capillary viscometry	96
Table 4.4	Mark-Houwink-Kuhn-Sakurada (MHKS) Power Law exponents	98
Table 4.5	Wales-van Holde ration, R, for original low acyl and depolymerised gellan samples	101
Table 5.1	Summary of $s^0_{20,w}$and k_s for sodium hyaluronate samples	120
Table 5.2	Summary of weight average molecular weights (M_w) results for sodium hyaluronate samples from sedimentation equilibrium and SEC-MALS	122
Table 5.3	Summary of Intrinsic viscosity values of sodium hyaluronate samples obtained from capillary viscometry and differential pressure viscometry	127
Table 5.4	Mark-Houwink-Kuhn-Sakurada (MHKS) power law exponent a, from SEC-MALS and Wales-van Holde ratio R, for sodium hyaluronate samples	131
Table 5.5	Summary of the persistence length, L_p and the mass per unit length, M_L values for sodium hyaluronate samples	136

Table 6.1	Persistence length L_P and mass per unit length M_L of schizopyhyllan	145
Table 6.2	Summary of $s^0_{20,w}$and k_s for schizophyllan samples	153
Table 6.3	Summary of weight average molecular weights (M_w) results for schizophyllan samples from sedimentation velocity, equilibrium and SEC-MALS	156
Table 6.4	Summary of intrinsic viscosity values of schizophyllan samples obtained from capillary viscometry and differential pressure viscometry	159
Table 6.5	Mark-Houwink-Kuhn-Sakurada (MHKS) power law exponent a, from SEC-MALS and Wales-van Holde ration, R, for schizophyllan samples	163
Table 6.6	Summary of the persistence length L_p and the mass per unit length M_L values for schizophyllan samples	167
Table 7.1	Summary of $s^0_{20,w}$and k_s for chitosan samples	182
Table 7.2	Summary of weight average molecular weights (M_w) results for chitosan samples from sedimentation velocity, equilibrium and SEC-MALS	187
Table 7.3	Intrinsic viscosity values of (Commercial) and (Laboratory-prepared) chitosan samples obtained from capillary viscometry and differential pressure viscometry	189
Table 7.4	Mark-Houwink-Kuhn-Sakurada (MHKS) power law exponent a, from SEC-MALS and Wales-van Holde ration, R for chitosan samples	192
Table 7.5	Summary of the persistence length L_p and the mass per unit length M_L values for chitosan samples obtained from global HYDFIT analyses	197
Table 7.6	Sedimentation coefficients at $s_{20,w}$ at a total concentration of 1.0 mg/ml, for chitosan, DNA, xanthan and chitosan-DNA and chitosan-xanthan complexes	201

CHAPTER 1

INTRODUCTION

1.1. INTRODUCTION

Carbohydrates are the most abundant class of natural organic compound, which have different functions in both plant and animal tissues. The carbohydrates are classified into three groups according to their chemical structure: monosaccharides, disaccharides and polysaccharides (Patel, 2007). Polysaccharides consist of monosaccharide units linked with glycosidic bonds. The variety and complexity in polysaccharides originate from different types of monosaccharides in the backbone and the variety of glycosidic linkage between them. This diversity leads to many potential industrial applications, particularly, cosmetics, pharmaceuticals and food applications. Ubiquitously availability and renewable properties of polysaccharides make them useful in almost all sectors of human activities (e.g. materials science, nutrition, health care and energy) (Persin et al., 2011).

Polysaccharides, in many forms, play an important role as an energy provider or storage, a structural unit and as a protector for cells in all living organisms. They can be classified according to their molecular structure (homopolysaccharide or heteropolysaccharide), their molecular shape (e.g. linear, branched, alternating repeat), their properties (e.g. gelling, non-gelling) and their electrostatic charge (e.g. anionic, cationic or neutral). However, categorisation by their origin (e.g. higher

plants, microorganisms, marine plants) is the most commonly used (Table 1.1) (Huber et al., 2005).

Among all types of polysaccharides (e.g. animal, marine), microbial polysaccharides promise more benefits as compared to other polysaccharides that have the same functions in terms of availability, well-manageable process conditions and stable chemical characteristics (Giavasis and Biliaderis, 2007a). Since microorganisms are

Table1.1: Classification of polysaccharides considering the source[1]

Source/Origin	**Polysaccharide Examples**
Higher Plants	
Cell wall associated	cellulose, hemicellulose, pectin
Energy stores (seeds, roots, tubers)	starch, guar gum, locust bean gum
Exudates	gum arabic, gum karaya
Marine plants (seaweed extracts)	carrageenan, alginate, agar
Microorganisms	xanthan, gellan
Animal	glycogen, glycosaminoglycans, chitin, chitosan
Chemical derivatives (of varied native origin)	hydroxyproply starch, starch acetate, starch phosphate, carboxymethylcellulose, hydroxyproply methylcellulose, methylcellulose
Synthetic	polydextrose

[1]adapted from (Huber et al., 2005) and (Izydorczyk, 2005).

also more susceptible for genetic manipulation than higher organisms, the biosynthetic or degradation pathways by manipulation of enzymes can be improved. Thus, the production of polysaccharides can be improved indirectly (Tombs and Harding, 1997).

1.2. MICROBIAL POLYSACCHARIDES

Microbial polysaccharides produced by microorganisms show particular diversity in structural and functional properties. These polysaccharides may be produced for different purposes such as (i) cell defence, (ii) prevention phagocytosis, (iii) protection from dehydration, (iv) adhesion to the surfaces or the other cells, (v) energy reserve and part of the cell wall (Giavasis, 2013). According to their functions, there are three types of polysaccharides: intracellular polysaccharides (carbon or energy supplier for organism), structural polysaccharides (constituent for cell wall and structure) and extracellular polysaccharides that are also called "exopolysaccharides" (EPS). Since isolation and purification of cell wall polysaccharides are difficult, exopolysaccharides are widely used in many industrial applications as bioactive compounds, drug release and encapsulation materials for pharmaceuticals, as natural ingredients or additives in food applications. For industry, they have been used for oil drilling and recovery and biodegradable plastics (Kumar and Mody, 2009). The Gram negative bacteria (Xanthomonas, Sphingomonas, Streptococcus etc.) and the fungi from the Basidiomycetes (Schizophyllum, Sclerotium etc.) family are popularly used to obtain microbial polysaccharides for many biotechnological applications. For example, xanthan produced from Xanthanonas campestris has been used as a thickener, viscosifier, emulsifier and stabiliser for food industry and an encapsulation agent with chitosan

for pharmaceutical applications whereas schizophyllan from Schizophyllum commune is used for medical applications due to its antitumor, antinflammatory and immunostimulating properties (Zhang et al., 2013).

Although several microbial polysaccharides have already been discovered, this study will only focus on just xanthan, gellan, bacterial hyaluronic acid and schizophyllan in terms of their properties and applications.

1.2.1. Xanthan

Xanthan gum is a natural polysaccharide discovered in 1950s by American scientists at the Northern Regional Research Laboratories (NRRL). After safety and toxological research studies, xanthan was approved by United States Food and Drug Administration (FDA) and European Economic Community respectively. It is widely used as a thickening agent, dispersant agent and stabiliser in food, pharmaceutical, cosmetic and agricultural applications (Rosalam and England, 2006, García-Ochoa et al., 2000) since its transformation from substrate to macromolecule is comparatively higher (~70%) and less expensive than any other microbial polysaccharide (Sutherland, 1998).

Xanthan is an anionic, extracellular microbial polysaccharide produced by Xanthomanas campestris (Rodd et al., 2000, Berth et al., 1996, Khouryieh et al., 2007). The primary structure of xanthan consists of a linear β-(1→4) D-glucan backbone with trisaccharide chains containing D-glucoronic acid unit between two D-mannoses. These trisaccharide chains are linked to a backbone at C-3 on every second unit (Figure 1.1). Approximately half of the terminal D-mannose units contain

a pyruvic acid residue linked via a keto group to the 4 and 6 positions, whose distribution patterns are described (Kool et al., 2014).

The annual worldwide production of xanthan is 30000 tons and its market is approximately US$270 million (Kalogiannis et al., 2003, Phillips and Williams, 2009).

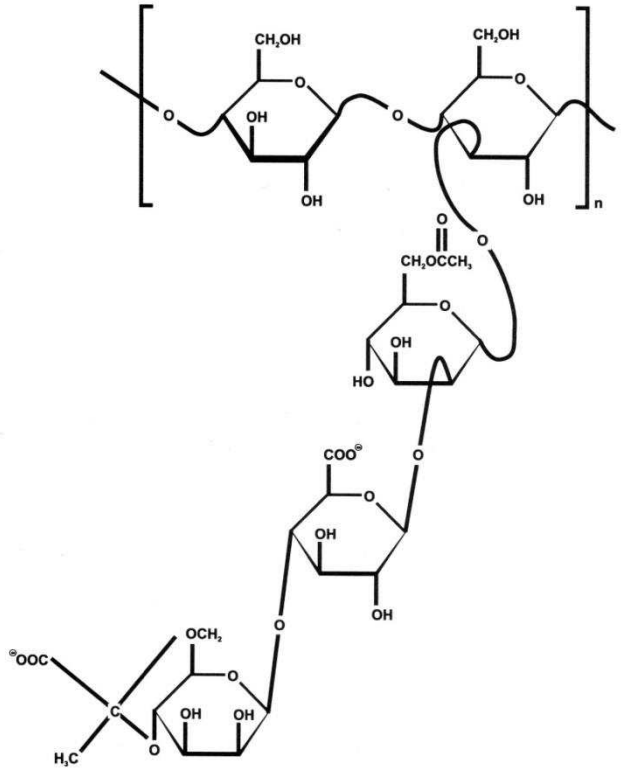


Figure 1.1: Chemical structure of xanthan adapted from (Tombs and Harding, 1997)

Xanthan molecules are very large, anionic heteropolysaccharides with high molecular weights (M_w) (~ 2.80-7.40 x 10^6 Da) (Sato et al., 1984, Berth et al., 1996) and high viscosity at low concentrations (Dhami, 1996).

The approval of xanthan from US Food and Drug Administration and European Economic Community makes it not only attractive as a food additive, but also for

use in biomedical and pharmaceutical application. Due to the ability of dissolution in both cold and hot water, stability over a wide range of pH values and temperatures, it is favourable for many applications (Sutherland, 2006). For instance, in the food industry, it has been used as a stabiliser in syrups, sauces and dressings, which enables the emulsion stability in salt and acid, which contributes the texture and pourability and increases the flavour release while stabilising the viscosity at wide range of temperatures and pH ranges (Giavasis, 2013). Xanthan has also been used for bakery products to bind water and enhance the texture, for beverages to improve mouthfeel and solubility at even low pH and, for dairy products to reduce syneresis, stabilize the emulsions and control ice crystals formation, and for meat products to bind water and inhibit syneresis (Palaniraj and Jayaraman, 2011).

Xanthan generates synergistic gels with gluco and galactomannans by heating above its conformation transition temperature then cooling so that the total required amount of polysaccharide is reduced. Besides that, this synergistic gel is also used to enhance the functionality of foods related to health concern such as prevention of obesity. The study on mixtures of konjac glucomannan-alginate-xanthan as an additive tablets (PGX) for control satiety has demonstrated that addition of 5g PGX tablet to meal decreased the anticipatory consumption and increased the satiety feeling along with a low calorie diet (Kacinik et al., 2011).

Xanthan has gained interest from other industries. In the oil industry, it is used for oil recovery as an additive, for oil drilling, pipeline cleaning and fracturing since it has good stability against salt and temperature. In paper, paints and wallpaper-adhesive industry, it controls rheological behaviour and aids the suspension. In textile and carpet printing, it enhances processing and regulates the colour migration. Xanthan is also used for personal care products such as shampoos, creams, toothpastes, where it

improves the pumpability and stabilises the emulsions (Palaniraj and Jayaraman, 2011).

For medical and pharmaceutical applications, xanthan has also been used as an encapsulation agent along with modified starches, polyvinyl alcohol, cellulose esters, kappa-carrageenan, guar gum and mostly chitosan in nanoparticle, microsphere, hydrogel and matrix systems (Benny et al., 2014). Since xanthan-chitosan can form a gel under lower pH, the complex has been considered as a continuous release matrix for drugs. For example, Popa et al. worked on chitosan-xanthan hydrogel to encapsulate theophylline (THP) and concluded that THP inclusion into drug has confirmed higher bioavailability than raw complex. Therefore, this chitosan–xanthan complex was recommended for the application of oral drug delivery systems such as chronic pulmonary obstructive disease (Popa et al., 2010). This xanthan-chitosan hydrogel system is also used to encapsulate vitamins, polyphenols, enzymes and probiotic bacteria see e.g. (Liu et al., 2011a, Argin-Soysal et al., 2009, Draganescu et al., 2013).

1.2.2. Gellan

Gellan gum, an extracellular polysaccharide, was first discovered and produced in 1978 by Kelco (San Diego, USA). It was approved as a food additive firstly in Japan (1988) then in USA and EU (1992), respectively. Now, it is added as a commercial gelling agent for food usage in many countries e.g. Canada, Australia and Southeast Asia (Morris et al., 2012). It is an anionic heteropolysaccharide produced by Sphingomanas elodea (Kumar and Mody, 2009). The linear molecular structure consists of a repeating tetrasaccharide of two substituents of β- D-glucose, one of β-D glucoronate and one of α-L-rhamnose. The native form of gellan has two types of

acyl residues: an L-glyceryl residue on O(2) of the 3-linked glucose substituent of the tetrasaccharide chain and an acetyl group at O(6) of the same residue (Figure 1.2). Both these residues are removed by an alkaline process and this deacetylated gellan is called ‘low acyl gellan’ and ‘high acyl gellan’ according to mildness of the process (Morris et al., 2012, Prajapati et al., 2013).

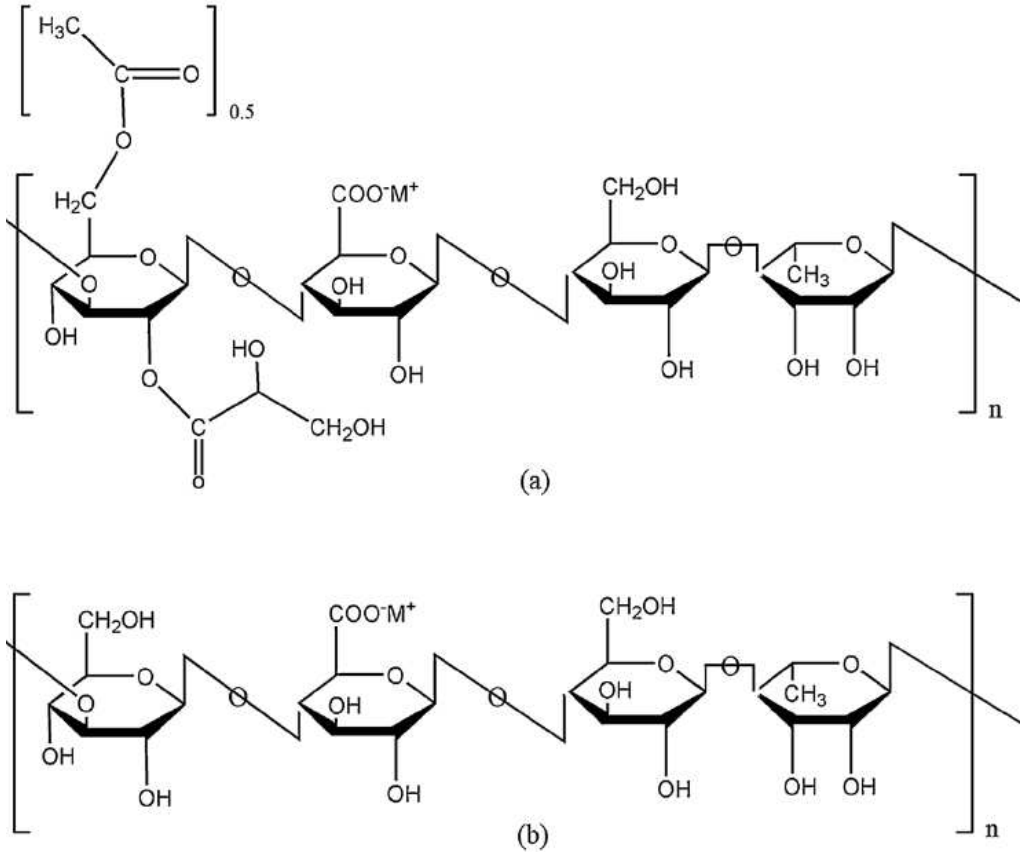


Figure 1.2. Chemical structure of (a) native and (b) deacetylated gellan gum adapted from (Prajapati et al., 2013)

Gellan gum is in the GRAS (Generally Recognised as Safe) list for food applications. Gellan gum forms thermoreversible, brittle and rigid gels in the presence of mono and divalent cations, which enables its use in many applications (Morris et al., 2012). Due to its ability to form clear gels, it can be used in many food applications as a viscosifier, gelling agent and texture modifier for the products such

as dessert gels, confectionery products, pie fillings, processed meats and milkshakes. Gellan gum can be also used as an agar substitution for Japanese food applications such as hard bean jelly, mitsumame, tokoroten noodles (Morris, 2006). It was proposed as a gelatine alternative due to its textural and rheological properties (Morrison et al., 1999). Like xanthan, gellan showed synergistic interactions when blended with other polysaccharides such as carrageenan, xanthan, konjac glucomannan, xyloglucan (Rodríguez-Hernández and Tecante, 1999, Miyoshi et al., 1996, Nitta et al., 2003). Valli and Miskiel suggested that using gellan gum with agar, gelatin and carrageenan increased the acid and thermal stability and enhanced the texture and releasing flavour of the food products such as desserts. Because of the functionality at wide range of pH, low acyl gellan gum can be used in fruit fillings for pastry products and pies (Valli and Miskiel, 2001). Xu et al. examined the interaction of gellan-glucomannan blend and its usage as a film for food packaging where the nisin (natural antimicrobial agent) was added into film to assess the antimicrobial activity. Results indicated that increasing the amount of gellan in the blend improved the antimicrobial activity for releasing the nisin (Xu et al., 2007).

The nontoxic, biocompatible and biodegradable properties make gellan an attractive substance for medicinal and pharmaceutical applications (Picone and Cunha, 2013). The gellan based materials for these areas were investigated over the last twenty years for different applications such as tissue engineering, dental care, bone repair, gene delivery and drug delivery by many researchers (Osmałek et al., 2014). For drug delivery, it has considered for different delivery methods such as for oral and nasal deliveries, solid dosage forms, beads and microcapsule forms while it was investigated for tissue engineering, wound healing, artificial vein design and gene

delivery purposes for medicinal application (Osmałek et al., 2014). Moreover, Li et al. studied the Ca-activated three dimensional gellan films for insulin delivery by in vivo and in vitro studies post characterisation of optimum film conditions. The in-vivo studies proved that the bioviability of insulin was maintained in gellan film, which indicated an evidence of possible application of gellan in protein delivery (Li et al., 2001).

Since gellan is considered to be a 'soluble dietary fibre', it can be considered for human healthcare applications and nutritional perspectives (Valli and Miskiel, 2001). While acid gelation of low acyl gellan can be used for controlling satiety (Norton et al., 2011), it also demonstrated serum cholesterol levels lowering effect (Kogan et al., 2007).

1.2.3. Hyaluronic Acid

Hyaluronic acid or hyaluronan (HA) is a linear, negatively charged and unbranched polysaccharide, which was first discovered in 1934 in the vitreous humor of cattle eyes (Lapčík et al., 1998). It is chemically classified as a glycosaminoglycan and consists of repeating disaccharide unit of β-(1→4) N-acetyl-D-glucosamine and β-(1→3) linked D-glucuronic acid (Figure1.3) (Hokputsa, 2003).

HA is found in the skin (dermis, epidermis), umbilical cord and vitreous body of the eye as sodium hyaluronate in the human body (Kogan et al., 2007). It is also present in other mammalian synovial fluids and connective tissues such as rooster comb, where commercial HA is obtained by extraction using protease digestion, HA ion-pair precipitation (with e.g., cetylpyridinium chloride), and membrane ultrafiltration. (Kogan et al., 2007, Hokputsa et al., 2003a).

HA is produced by Streptoccocus species e.g. Streptococcus zooepidemicus. (Haxaire et al., 2000).

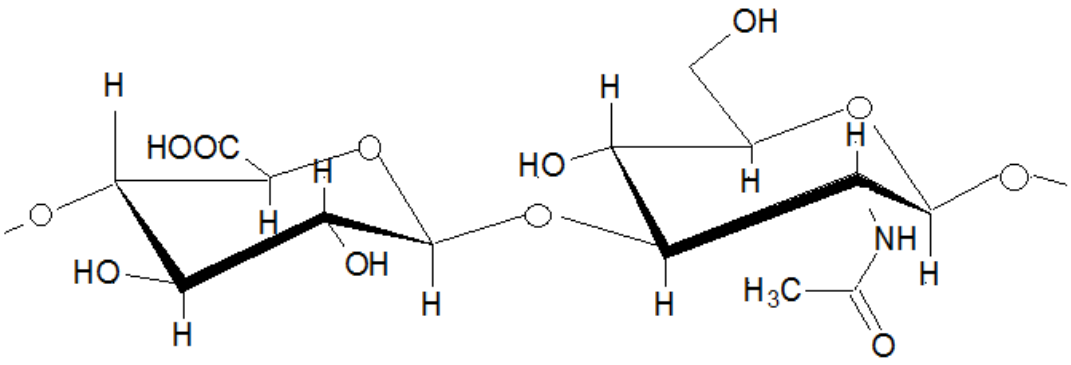


Figure 1.3: Chemical structure of repeating disaccharide unit of hyaluronic acid. Figure reproduced from (Hokputsa, 2003).

The unique physicochemical and rheological characteristics have been extensively investigated and attracted for possible medical and pharmaceutical applications. The molecular weights of HA preparations have been previously determined to be between 7.3 x 10^4 – 3.3 x 10^6 Da (Hokputsa et al., 2003a, Rinaudo, 2008, Preston and Wik, 1992) and it is an important property, which governs the characteristics and applications of HA. For example, HA with high molecular weight can be used for ophthalmology, orthopaedics, wound healing and cosmetics, whereas HA with low molecular weight can be used for the inhibition of tumour growth, initiating the expression of inflammatory moderators and promotion of angiogenesis (Liu et al., 2011b).

The current worldwide HA market is anticipated to be worth over $1 billion with more than a ton being produced in the medical market (Chong et al., 2005). Reflecting the extensive applications in medical and cosmetic applications, microbial fermentation has appeared as an alternative for bulk production of HA to provide the

adequate production. Furthermore, the price is also decreased and the degree of purity is enhanced by microbial production of the polysaccharide (Milas and Rinaudo, 2004). HA has been used widely in the medical industry since the 1970s due to the distinctive properties including biodegradable, biocompatible, non-immunogenic and non-inflammatory (Jin et al., 2010, Chong et al., 2005). It is used as a visco-supplement for osteoarthritis to replace synovial fluids in arthritis and relieve the pain in the knee (Hochberg, 2000, Tascıoglu and Öner, 2003, Altman, 2000). In ophthalmology, it is used in eye surgery to aid the implantation of artificial lens and improve the corneal wound healing (Miyazaki et al., 1996). It has also been used for aqueous eye drops to improve their viscosity and stability (Gurny et al., 1987, Lapčík et al., 1998). To prevent post-surgical adhesion, HA is an attractive material since it is naturally found in the human body. HA is used as a mucoadhesive to modulate the wound healing process by mending the sliding function of the tendons by injection of auto-crosslink HA (Renier et al., 2005, Rinaudo, 2008). Stabilised or cross-linked forms of HA are considered to moisturise the skin and repair the elasticity for skin products in cosmetics, and as dermal filling compounds to achieve reduction of facial lines and wrinkles (Brown and Jones, 2005, Narins et al., 2003, Bergeret-Galley et al., 2001). The therapeutic effects of HA have been studied in cancer. In cancer tissues, HA supports tumour cell migration by dehydration, which opens a space and interaction with surface cell receptor (Lokeshwar et al., 2000). HA has extensively been used in tissue engineering with other polymers such as chitosan. Tan et al. concluded that the chitosan-HA hydrogel enhanced cell adhesion and encapsulation, and supported the survival of the cells and maintained cell morphology, thereby the possible use of this hydrogel in tissue engineered cartilage (Tan et al., 2009). HA has already been added in the list of drug

delivery systems to be considered for dermal, nasal, pulmonary, parental, liposomal, implantable drug delivery and gene delivery. For drug delivery, chitosan is the main polysaccharide that is mostly chosen for polyelectrolyte complex with HA (Liao et al., 2005).

1.2.4. Schizophyllan

Schizophyllan is a non-ionic, water-soluble homopolysaccharide that is produced by fermentation from filamentous fungi Schizophyllum commune. It consists of a linear chain of β-D-(1-3)-glucopyranosyl groups, to which β-D-(1-6)-glucopyranosyl groups are attached (Figure 1.4) (Kumari et al., 2008, Bot et al., 2001). Due to these glucosyl side-chains being on the outside of a triple helical structure, it is readily dissolved in water (Bot et al., 2001).

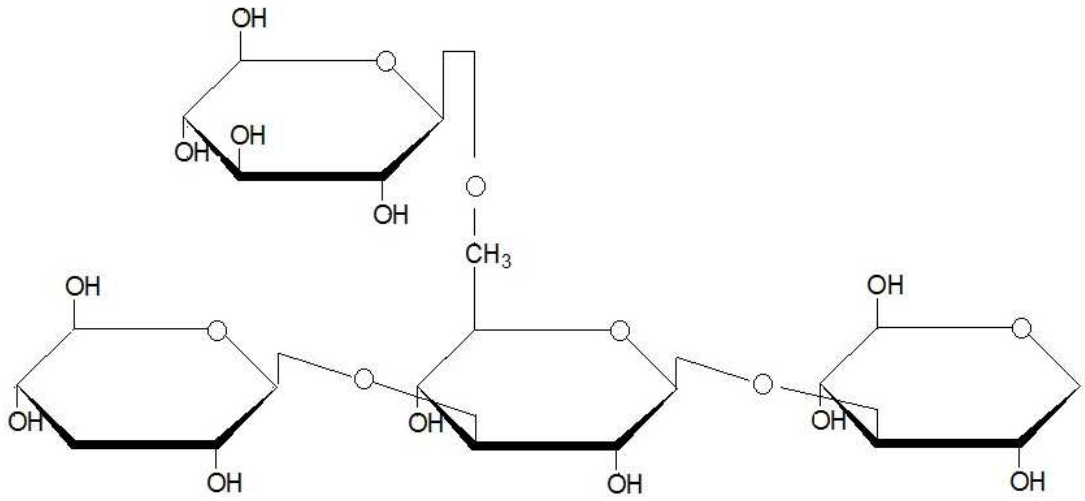


Figure 1.4: Chemical structure of repeating unit of schizophyllan (reproduced from (Takedatsu et al., 2012)

Owing to its high capacity for binding water (in cosmetics-skin and hair products), high heat stability (petroleum recovery) and bioactivity characteristics (antitumor, anti-inflammatory, antibacterial activities), it has been considered for many potential application in industrial and pharmaceutical applications (Leathers et al., 2006, Tombs and Harding, 1997).

Schizophyllan was firstly discovered by Japanese researchers (Zhang et al., 2013) and approved for use in Japan in 1986 for drug administration. Schizophyllans are also referred to as 'Biological Response Modifiers' (BRMs) with other bioactive fungal polysaccharides such as lentinan, scleroglucan through the capability of inducing an immune response against viral and bacterial infections, inflammation and tumour cells (Giavasis, 2014). Schizophyllan has been investigated as an immune enhancer against the Sendai virus, which is lethal for mice and results indicated schizophyllan has an effect on antiviral activity and increased immune response (Hotta et al., 1993). Kakumu et al. also observed that sizofiran, which is a commercial form of pharmacological schizophyllan, regulated the cellular immune responses of patients with hepatitis B virus (Kakumu et al., 1991). Schizophyllan has been found to have a therapeutic effect on gastric, breast, lung, cervical, head and neck cancers with anticancer drugs. It has also helped in the inhibition of metastasis (Bohn and BeMiller, 1995, Giavasis and Biliaderis, 2007b, Giavasis, 2014). Kimura et al. showed schizophyllan acted as an assistant immunotherapeutic agent and supported recovery of damaged cellular immunity after chemotherapy, radiation and surgery on patients with head and neck cancers (Kimura et al., 1994). The use of schizophyllan in cancer treatment was found efficient together with chemotherapy and radiation (Giavasis and Biliaderis, 2007b). Kojima et al. indicated the relationship between molecular weight and antitumor activity of schizophyllan

and observed that the antitumor activity has reduced when the molecular weight decreased and the conformation was of the random coil type (Kojima et al., 1986).

1.3. INTERACTION WITH CHITOSAN

It has been proven that microbial polysaccharides can interact with other polysaccharides such as gluco-and-galactomannans, guar gum, carrageenan and most commonly chitosan which is a nontoxic, bioadhesive and biocompatible with anionic polysaccharides (Rinaudo et al., 1999, Casas and García-Ochoa, 1999, Rodríguez-Hernández and Tecante, 1999). Since chitosan is a cationic polysaccharide, it has been considered for interaction studies with anionic polysaccharides such as xanthan, gellan and hyaluronic acid (Argin-Soysal et al., 2009, Luppi et al., 2009, Picone and Cunha, 2013). For example, since xanthan-chitosan and gellan-chitosan can form gels at lower pH values, the complex has been considered as a potential for controlled drug release from drug delivery systems (Phaechamud and Ritthidej, 2008, Vilela et al., 2015), whereas chitosan-hyaluronic has been considered for gene delivery and tissue engineering (Tan et al., 2009). However, knowledge and understanding the behaviour of these interactions is needed for developing new applications in the food, cosmetics, medical and pharmaceutical industries. To achieve this, the hydrodynamic techniques such as sedimentation velocity can be useful to investigate these interactions, which previously provided information about the synergistic interaction between xanthan-konjac glucomannan-alginate (Abdelhameed et al., 2010) and mucin-chitosan mixtures (Fiebrig et al., 1995).

1.4. THE AIM OF THIS STUDY

To properly understand the relationship between physical properties and functionality of microbial polysaccharides, the physical characteristics such as homogeneity, molecular weight, conformation and interaction conditions are required for the targeted applications of these polysaccharides. Therefore, the aim of this study is firstly to examine the solution properties of microbial polysaccharides- namely xanthan, gellan, hyaluronic acid and schizophyllan- in terms of sedimentation coefficient, molecular weight, distribution of molecular weight, intrinsic viscosity and the conformation. To investigate these biophysical properties and to take advantage of development in instrumentation and data analysis methods, analytical ultracentrifugation (AUC), Size Exclusion Chromatography Coupled to Multi Angle Light Scattering (SEC-MALS), Dynamic Light Scattering (DLS) and viscometry techniques were used. Hydrodynamic parameters derived from these techniques were then used to assess the gross conformation of polysaccharides by power law, conformation zoning, Wales-van Holde methods and Multi-HYDFIT program. After the determination of hydrodynamic properties of microbial polysaccharides in solution, the possible interactions of xanthan with chitosan as a mixture were then investigated. Thus, this knowledge can hopefully help to improve food and healthcare applications of these polysaccharides by increasing the understanding of these types of systems.

CHAPTER 2

HYDRODYNAMIC METHODS

2.1. ANALYTICAL ULTRACENTRIFUGATION

Analytical ultracentrifugation (AUC) is a powerful separation technique for characterising the hydrodynamic properties of macromolecular solutions and has a wide applicability to assess the solution behaviour in a broad range of solvents. (Cole et al., 2008). This method was firstly developed by Svedberg and co-workers in the 1920s and it was very popular until the 1970s. With the introduction of new methods such as light scattering, electron microscopes (EM), polyacrylamide gel electrophoresis (PAGE) and size exclusion chromatography (SEC), which provide rapid determination of molecular weight for macromolecules, this technique lost its popularity – see for example (Mächtle and Börger, 2006). However, many of these other techniques require calibration using standards and rely on a series of assumptions that are frequently invalid (Ralston, 1993) and also have limitations for determination of the molecular weight especially polydisperse and interacting macromolecules. Regarding new instrumentation (Beckman XL-I and XL-A) and numerical data analysis methods in the 1980s, the AUC became popular once again for protein and protein interactions in solutions and polysaccharide solutions (Harding, 1992). The analytical ultracentrifuge technique has considerable advantages over other methods such as gel permeation chromatography and light scattering, since there is no need to use membranes, columns other separation media

or immobilisation materials (unlike electrophoresis, chromatography and Surface Plasmon Resonance) – which can cause problems due to anomalous interactions.

Basically, an analytical ultracentrifuge is a centrifuge with a detection system, which observes the distribution of sedimenting macromolecules in a centrifugal field by centrifugal force (Harding et al., 1992, Scott et al., 2005). It consists of centrifuge housing (motor, safety chamber, temperature control), rotor, measuring cells and optical detectors (absorbance, interference, fluorescence) -see for example (Mächtle and Börger, 2006).

With AUC, two main experiments can be performed, namely; sedimentation velocity where the velocity and shape of a sedimenting boundary are examined, and sedimentation equilibrium where slower speeds are applied to produce equilibrium between diffusional and centrifugal potentials -see for example (Abdelhameed, 2010).

2.1.1. Sedimentation Velocity

Sedimentation velocity in the analytical ultracentrifuge provides information about purity, state of association, conformation and conformational changes, shape, molecular weight and interaction with other molecules (Dam and Schuck, 2004). This experiment is performed in high centrifugal fields, where the rotor is accelerated to ~30000-50000 rpm depending on the macromolecule. In this field, the solution of interest is subjected to a centrifugal field; the solute is subjected to three forces - sedimenting (centrifugal) force, F_c, the buoyant force, F_b, and the frictional force, F_d. Under the effect of these forces, the macromolecule in solution starts to accelerate and reach terminal velocity (Figure 2.1).

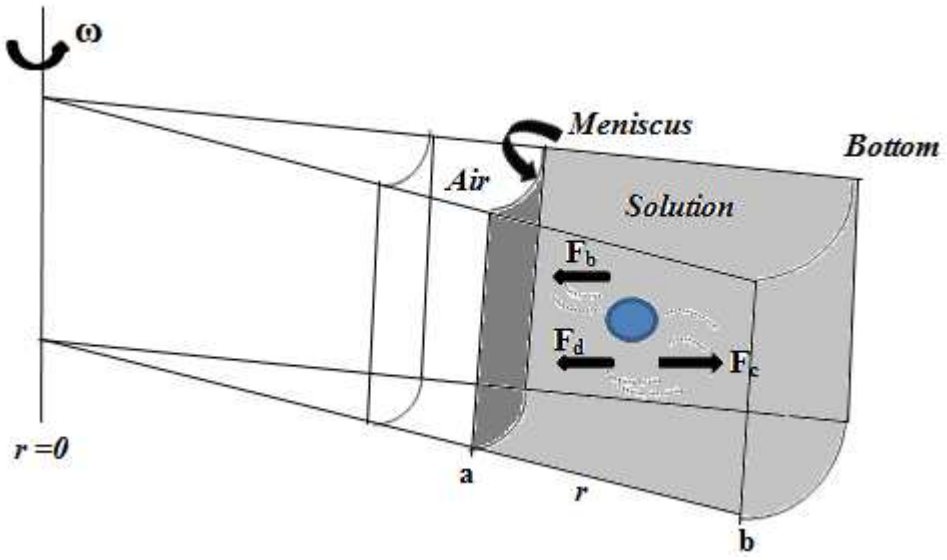


Figure 2.1: Diagram of a macromolecule in the sedimentation process. Figure reproduced from (Van Holde, 1985).

The centrifugal force, F_c which is related to the mass of molecule (m) and the distance from the centre of rotation (r) and the angular velocity (ω) is firstly experienced by the molecule.

$$F_c = \omega^2 rm \tag{2.1}$$

At the same time, the buoyant force, F_b which is equal to the weight of the fluid displaced:

$$F_b = -\omega^2 r m_0 \tag{2.2}$$

where m_0 is the mass of fluid displaced and:

$$m_0 = m\bar{\upsilon}\rho \tag{2.3}$$

Where $\bar{\upsilon}$ is the partial specific volume and ρ is the density of the solvent (g/ml).

When the density of the particle is greater than that of the solvent, the particle will begin to sediment. As the particle begins to move along a radial path towards the bottom of the cell, the velocity of the molecule will increase because of the

increasing radial distance. Thus, frictional force, F_d will also be exerted on the macromolecule as result of the movement of the molecule through a viscous solution with the velocity (v):

$$F_d = - fv \tag{2.4}$$

where f is the frictional coefficient and depends on the shape and size of the particle. As a result, at terminal velocity the three forces come into balance (Ralston, 1993):

$$F_c+F_b+F_d = 0 \tag{2.5}$$

By replacing the molecular mass, m (g) by M/N, (M is the molar mass or molecular weight ($g.mol^{-1}$ or Da) and N is Avogadro's number 6.02×10^{23} mol^{-1}), the equation can be written as:

$$\omega^2 r \frac{M}{N} - (1-\bar{\upsilon}\rho) - fv = 0 \tag{2.6}$$

Therefore, the sedimentation coefficient, s, is obtained from the equation below:

$$s = \frac{M(1-\bar{\upsilon}\rho)}{Nf} = \frac{v}{\omega^2 r} \tag{2.7}$$

The sedimentation coefficient, s, is defined as the velocity of the particle per unit gravitational acceleration and it depends on the properties of the particle. The unit for the s is the Svedberg unit (abbreviation S), in honour of The Svedberg which is 10^{-13} seconds (Ralston, 1993).

In the centrifugal field, application of high angular velocity causes rapid sedimentation of the molecule towards the cell bottom and a moving boundary is formed between the solute and solvent. From the rate of motion of this boundary (see, Figure 2.2), the sedimentation coefficient and distribution of sedimentation

coefficient can be calculated (Van Holde, 1985). Since the sedimentation velocity is expressed as $v = dr_b/dt$, the equation can be:

$$s = \frac{v}{\omega^2 r} = \frac{dr_b/dt}{\omega^2 r} \quad (2.8)$$

Integrating from this equation:

$$\ln \frac{r_b(t)}{r_{b\ (t_0)}} = \omega^2 s\ (t-t_o) \quad (2.9)$$

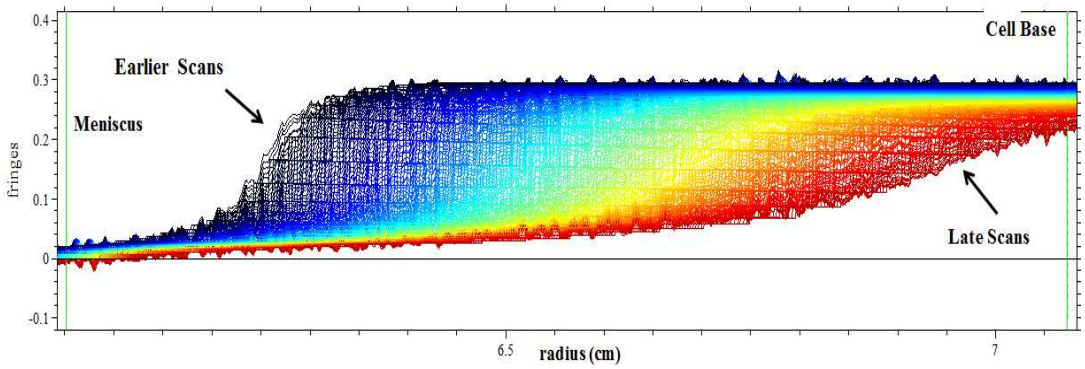


Figure 2.2: Boundary movement of sodium hyaluronate (HAV1) in sedimentation velocity experiment at 0.1 mg/ml. Scans recorded every 2 min. Rotor speed = 40000rpm

Plotting $\ln(r_b/r_m)$ versus time t, yielded a slope of straight line $\omega^2 s$, which leads to determine the sedimentation coefficient (s).

The sedimentation coefficient, s, is affected from temperature as well as the solvent viscosity and density. Therefore, it is expressed as $s_{T,b}$ where, T, is the temperature at which the experiment was carried out and, b, indicates the buffer used to dissolve sample. To normalise these contributions to standard conditions (density and viscosity in water at 20.0 °C), the equation below is used (Ralston, 1993):

$$s_{20,w} = \{(1-\bar{\upsilon}\rho_{20,w}) / (1-\bar{\upsilon}\rho_0)\} \cdot \{\eta_0 / \eta_{20,w}\} s_{T,b} \quad (2.10)$$

where ρ_o and η_o are respectively the density and viscosity of the solvent or buffer, b, at temperature T and $\rho_{20,w}$ and $\eta_{20,w}$ the corresponding values of water at 20.0^o C. Sedimentation coefficients are concentration dependent and they exhibit a decrease in the measured sedimentation coefficient with increasing concentration if the solute is pure and non-associating (Ralston, 1993). Therefore, the measured s value at a given concentration will be an apparent one because of non-ideality effects arising from co-exclusion and charge effects. These effects are more severe for polysaccharides and can be eliminated by measuring the $s_{20,w}$ for a range of different cell loading concentration and then extrapolation to zero concentration (Harding, 2005a). Plotting $1/s_{20,w}$ versus c is applied using the following equation:

$$1/s_{20,w} = (1/s^0_{20,w}).(1+k_s c) \qquad (2.11)$$

Where k_s is the Gralen parameter and shows the concentration dependency. It is also used to estimate the conformation with intrinsic viscosity (Harding, 2005b). In sedimentation velocity experiments, any changes in boundary positions and in the whole radial concentration profile can be observed by the optical system- either UV/visible absorption (especially proteins and other macromolecules with an absorbing chromophore) or Raleigh Interference optics (for any macromolecule – including polysaccharide). The distribution of sedimentation coefficient is measured by the ability of capturing multiple data on-line with AUC model XL-I and XL-A with the help of these optical systems.

Sedimentation coefficient distributions are popularly calculated using the ls-g*(s) model incorporated into the SEDFIT program (Schuck et al., 2002) based on Lamm equation (Equation 2.12). The sedimentation coefficient distribution is affected by diffusion and this diffusion correction is usually small for polysaccharides since

absence of diffusion during the time of the experiment can be assumed for molecules with very large frictional coefficients (Ralston, 1993).

$$\frac{dc}{dt} = D.\left[\frac{d^2c}{dr^2} + \frac{1}{r}\frac{dc}{dr}\right] - s\omega^2\left[r\frac{dc}{dr} + 2c\right] \qquad (2.12)$$

This SEDFIT program (Schuck, 1998, Schuck et al., 2002) enables the plot of g*(s) vs. s and the distribution and integration of a peak or resolved peaks can be defined. These plots can then be used to calculate the weight average s of the sedimenting species. Normally, due to the nature of interference optical system, a time invariant noise is present during the calculation of g*(s) from the radial derivative dc/dr. Using least squares boundary modelling – ls-g*(s) –which was introduced by Schuck (1998) and Dam & Schuck (2004), this noise can be eliminated.

However, the SEDFIT program provides the correction of density and viscosity of the solvent at the experimental conditions to standard conditions as noted above.

A sedimentation coefficient distribution, c(s) vs s. or g*(s) vs s. can be transformed into apparent molecular weight distribution if the conformation is known (Harding, 2005b). Fujita (Fujita, 1962) and earlier Cantow (Cantow, 1959) had investigated the possibility of transforming a distribution of sedimentation coefficient s into a distribution of molecular weight for linear polymers. They concluded that the sedimentation velocity determination of g*(s) enables the estimation of molecular weight distribution of a given macromolecule if the information about the relation between s and M is obtained. The conversion is as follows:

$$(M) = (ds/dM) \cdot g(s) \qquad (2.13)$$

The linking of g*(s) to f(M) is achieved by manipulation of the "power law" relation (MHKS) (Tombs and Harding, 1997):

$$s = \kappa_s M^b \qquad (2.14)$$

Recently, Harding, Schuck and co-workers has extended the application for carbohydrate polymers, mucin and glycoconjugates and named as "Extended Fujita *Method"*(Harding et al., 2011). Manipulation of these equations above, Harding et al. yields the following relation:

$$f(M) = b.(\kappa_s^{1/b}).(s^{b-1/b}).g(s) \qquad (2.15)$$

where b is the conformation parameter with the limits of 0.4-0.5 for a flexible coil, 0.67 for a compact sphere and 0.15 for a rigid rod (Tombs and Harding, 1997). κ_s can be calculated from equation (2.14) with at least one value of M and corresponding value of s (from sedimentation velocity experiment).

2.1.2. Sedimentation Equilibrium

Sedimentation equilibrium is another main experiment that can be run in the AUC. This experiment provides thermodynamic information about the solution molar mass and non-ideality, and enables the molecular weight to be estimated (Cole et al., 2008, Harding, 2005a). Unlike sedimentation velocity, the experiment is performed under moderate centrifugal fields, where the sedimentation and diffusion forces on the solution are balanced. Thus, a steady state equilibrium distribution of molecules occurs instead of a sedimenting boundary (Figure 2.3) (Mächtle and Börger, 2006, Harding, 2005b). This steady state is a function of molecular weight (Harding, 2005b).

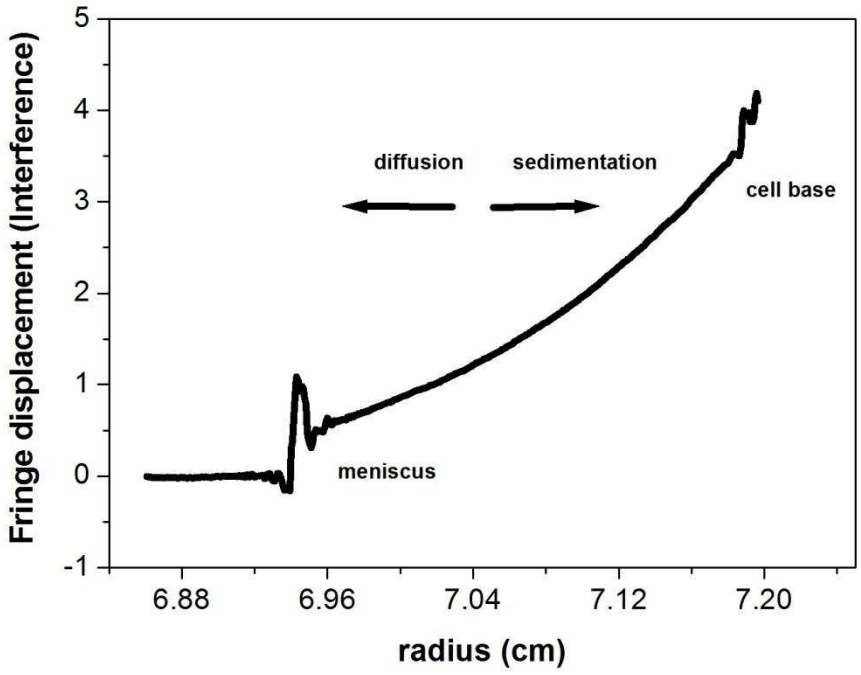


Figure 2.3: Profile of sedimentation equilibrium process for sodium hyaluronate (HAV4) at 0.1M PBS and (loading) concentration 1.0 mg/ml. Rotor speed = 13000rpm

For equilibrium experiments, the rotor speed is an important parameter, where it should be high enough to sediment the molecule from meniscus, but not too high to sediment the molecule in the cell base. The length of the solution column in the radial direction also affects the experiment duration time since the equilibrium time is proportional to the square of solution column length. Using a shorter column provides a rapid equilibrium time (Ralston, 1993).

When the sedimentation equilibrium method is applied to polysaccharides, there will be a redistribution of total polysaccharide and the different molecular weight species along the cell, and the high molecular weight species are observed near the cell base

(Harding, 2005a). Therefore, the complete concentration distribution profile through the cell needs to be considered to obtain the true (average) molecular weight.

To calculate the molecular weight M, the concentration distribution c(r) is measured by the following equation, which is used for monodisperse, non-associating macromolecular solutions (Van Holde, 1985):

$$\frac{d\ ln\ c}{d\ (r^2)} = \frac{\omega^2 M(1-\bar{\upsilon}\rho_0)}{2RT} \qquad (2.16)$$

Where M is the solute molar weight (as g/mol), ω the angular velocity of the rotor, and c the concentration of the solute (in g/L) at a radial distance, r from the axis of rotation, whereas R is the gas constant and the T is temperature. From the equation 2.16, a data fitting plot of log (c) versus $(r)^2$ for a single, ideal solute at sedimentation equilibrium yields a slope proportional to the molar mass (Ralston, 1993). Ideally, the plot should be obtained as a straight line for monodisperse molecules. However, for polydisperse solution, this straight line tends to be curvilinear either upward-bending (polydispersity/association) or downward-bending (non-ideality) (Mächtle and Börger, 2006).

The MSTAR algorithm was developed by Creeth and Harding (1982) as a method, which allows more accurate assessment of the apparent weight average molecular weight $M_{w,app}$ throughout the cell (Creeth and Harding, 1982). The "app" indicates that the obtained values are affected by thermodynamic non-idealiy and the "ideal" values can be yielded by extrapolation of $M_{w,app}$ to zero concentration. Recently, the MSTAR algorithm has been built into the SEDFIT platform as SEDFIT-MSTAR which employs a more rigorous method for yielding the baseline and meniscus concentration for the Rayleigh interference optical systems (Schuck et al., 2014). M*

function (Creeth and Harding, 1982) is an operational point average molecular weight and is defined as follows:

$$M^*(r) = \frac{c(r) - c_m}{k c_m \left(r^2 - r_m^2\right) + 2k \int_{r_m}^{r} (c(r) - c_m) r dr} \quad (2.17)$$

where r = radial position, M*(r) = molecular weight at the specific radial position, c(r) = concentration of solute at radial position r, c_m = concentration of the solute at meniscus and k is obtained from equation 2.18:

$$k = \frac{(1 - \bar{\upsilon}\rho)\omega^2}{2RT} \quad (2.18)$$

Extrapolation of M*(r) to the cell base yields the apparent weight average molecular weight $M_{w,app}$, for the whole distribution (Creeth and Harding, 1982):

$$M^*(r = r_b) = M_{w,app} \quad (2.19)$$

Non-ideality arising from co-exclusion and polyelectrolyte effects is a problem particularly for measuring the molecular weight of polysaccharides. Although using long path length cells (20mm) allows working with low concentrations (~0.2mg/ml), it is still insufficient to eliminate the non-ideality effect for some macromolecules. To correct this effect, the measurement of $M_{w,app}$ over a range of concentration and extrapolation to zero concentration allows the molecular weight to be estimated (Harding, 2005a) :

$$M_{w,app} = M_w \cdot \frac{1}{1 + 2BM_w c} \quad (2.20)$$

where B is the second thermodynamic virial coefficient (ml.mol/g^2).

2.2. SIZE EXCLUSION CHROMATOGRAPHY COUPLED TO MULTI ANGLE LIGHT SCATTERING (SEC-MALS)

The SEC-MALS instrument combines three analytical methods together. These are light scattering, viscometry and differential refractive index (Figure 2.4). This technique allows separation of components of a heterogeneous solution based on their volume using size exclusion chromatography columns. This technique determines absolute molecular weight and molecular weight distribution for these separated fractions using the laser light scattering method and then further viscometric analysis on the separated materials (Morris et al., 2002). Exclusion from the columns takes place according to macromolecule size (larger particles elute first). For a homologous solution, this results in separation according to decreasing molecular mass –see for example (Hokputsa et al., 2002, Jumel et al., 2002). Additional hydrodynamic parameters (intrinsic viscosity and radius of gyration) can be obtained at the same time of the experiment: the addition of an on-line viscometer allows determination of the intrinsic viscosity [η] as a function of elution volume, V_e. Data obtained through SEC-MALS complements the results obtained through other methods.

Columns are packed with gel beads from where the solvent moves as mobile phase. When sample solution containing a mixture of diverse sized macromolecules is passed through the column, larger molecules pass through the column along with the mobile phase and do not enter all of the pores of the beads. Since small molecules enter a greater proportion of the pores of the gel beads, they elute after larger molecules (Figure 2.5).

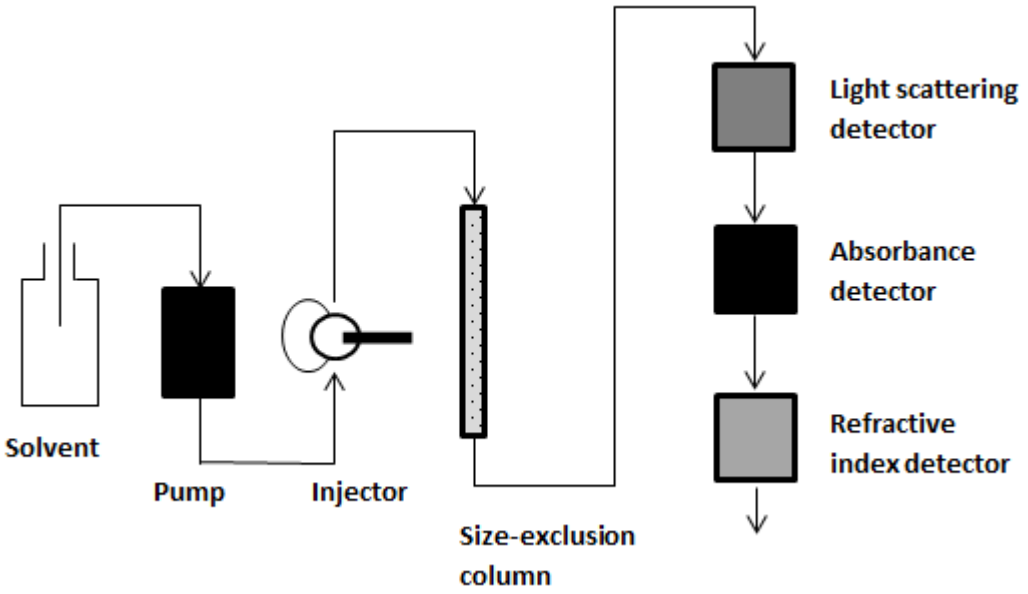


Figure 2.4: Schematic presentation of SEC-MALS components (Philo and Arakawa, 2000)

Molecular weight determination in SEC is based on the principle that the molecular weight is linked to the size of the particle. Thus, the first eluting molecule is assumed to have higher molecular weight. This method is rapid and simple but molecular weight evaluation can be more complicated if the subjected samples have self-association or some interaction(s) with the column material. This, in turn, can change the elution time and can lead to the misleading evaluation of molecular weight. Particle shape and hydrodynamic radius will also affect the elution volume and if SEC is used alone, it requires the calibration of the column with standard materials of the same conformation type – almost impossible for polysaccharides without the addition of an on-line molecular weight detector. Therefore, coupling of light scattering with SEC can provide a better and reliable evaluation of molecular weight.

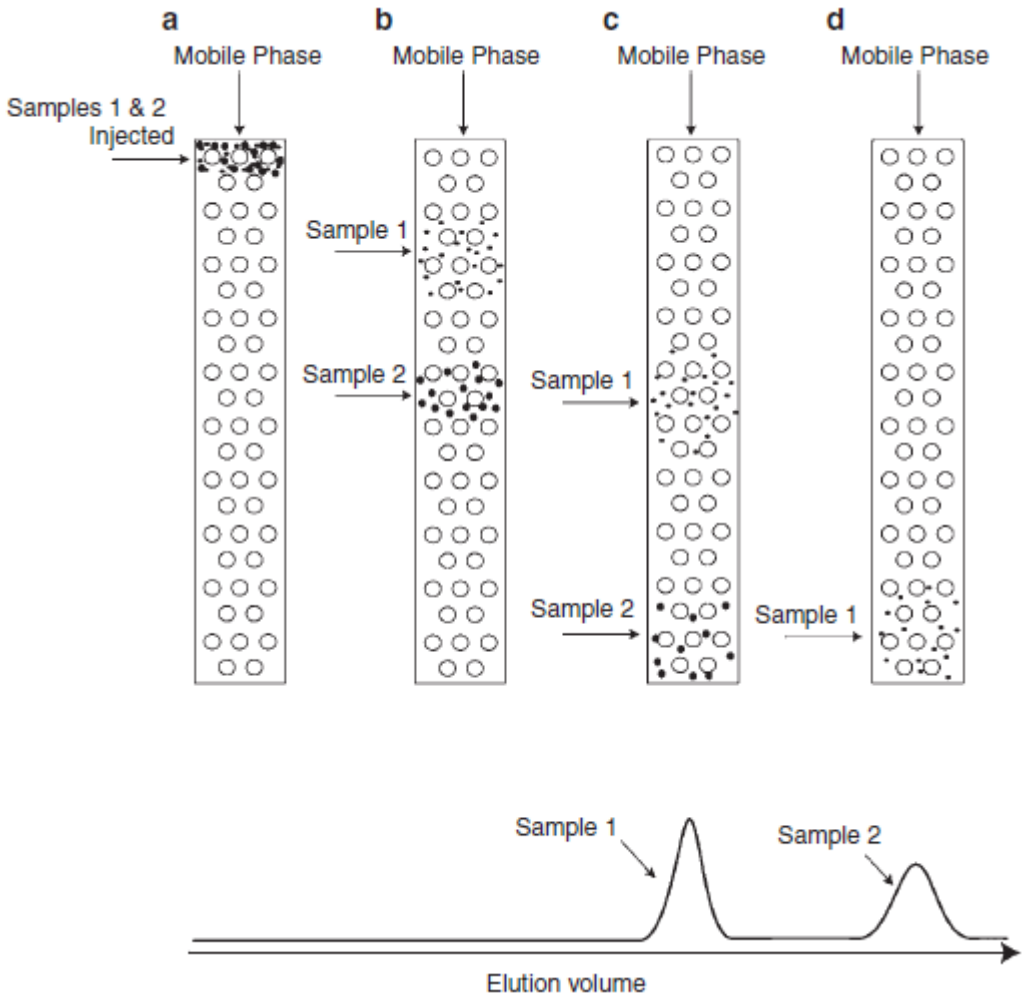


Figure 2.5: Separation of two fractions (Sample1 and 2) through the SEC column. Sample 2 eluted out first being the highest molecular weight fraction followed by Sample 1. Adapted from (Wyatt, 2013a)

From the SEC columns, the separated molecules enter into the light scattering (LS) device. In LS, the separated molecules are stricken by laser light and reflect light (details are mentioned later) in multiple directions by the LS photometer, which is equipped with multiple detectors at various fixed angle(s). This allows measurement of scattered light intensity at a number of angles and thus can be extrapolated to

infinitely low angle (0°) intensities to compute absolute molecular weight. For a well separated sample, the M_w (weight average molecular weight) – the primary parameter obtained - M_z (z-average molecular weight) and M_n (number average molecular weight) along with the molecular weight distribution can be determined. For large sized particles, the radius of gyration can also be obtained as an additional parameter (Wyatt, 2013a).

In the light scattering device, the amount of light scattered is directly proportional to the polymer molar mass and concentration. According to the classical theory of light scattering (Static light scattering theory), light scattering means the partial scattering of electromagnetic radiation hitting the particles. The interaction of electrons of the molecules with the oscillating electrical field of light induces charge separation. This leads to the formation of an oscillating dipole and the molecules emit light (Wyatt, 1993). The wavelength of the scattered light is almost the same as the incident light. (Figure 2.6) This theory is based on the measurement of scattering angle unlike the quasi-electrical theory of photons (DLS), which is based on measurement of change in the light intensity.

For larger molecules like polysaccharides, there is a decrease in the scattering light due to intramolecular interference. In multi angle light scattering (MALS) the scattered light intensity is measured at several angles to calculate molecular weight (molar mass) by extrapolation to zero angle.

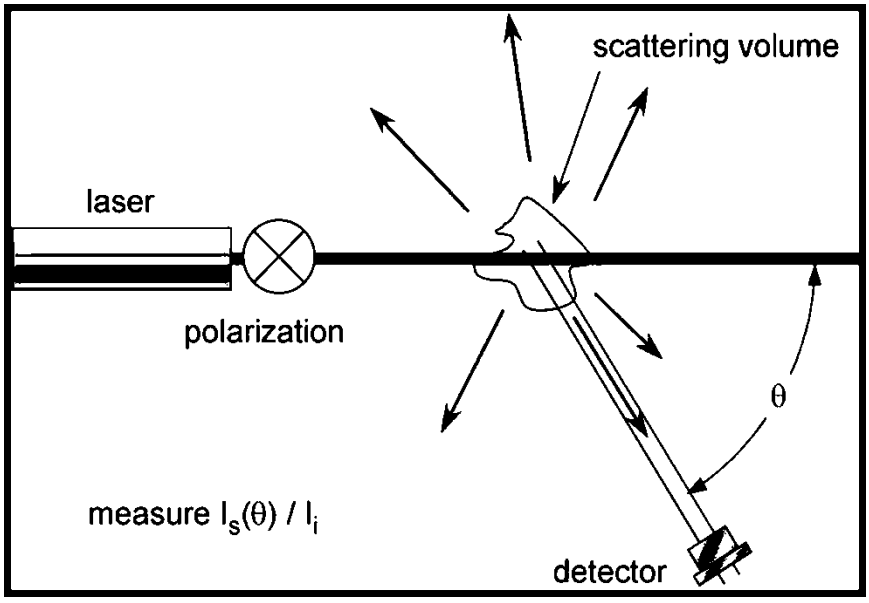


Figure 2.6: Events in the process of light scattering (reproduced-courtesy of Wyatt Technology Corporation).

The relationship between the Rayleigh excess factor and the physical characteristics of the scattering molecule can be given as (Berth et al., 1998):

$$\frac{Kc}{R_\theta} = \frac{1}{M_W P(\theta)} + 2A_2c + 3A_3c^2 \ldots\ldots \quad (2.21)$$

where c is the concentration of solution, P (θ) is particle scattering factor and defines the angular dependence of scattered light, which depends on shape and size of macromolecules, the A thermodynamic virial coefficient called 2nd, 3rd etc., which is are also known as B, C etc. and are equal to zero for an ideal solution, and K is an optical parameter related to the polymer in its solvent defined as:

$$K = 4\pi^2 (dn/dc)^2 n_0 N^{-1} \lambda_0^{-4} \quad (2.22)$$

where dn/dc is the refractive index increment (ml/g), η_0 is the refractive index of the solvent, N_A is Avogadro's number (6.02 x 10^{23} mol^{-1}), λ is the vacuum wavelength of the incident light (cm).

At low angles, when θ approaches zero and (θ) = 1, the third and higher virial coefficients can be eliminated and the equation (2.21) rearranges as (e.g. Wyatt, 2003)

$$\frac{Kc}{R_\theta} = \frac{1}{M_w} + 2A_2c \qquad (2.23)$$

If the macromolecule is at low concentration with low angle, the equation is becomes:

$$\frac{Kc}{R_\theta} = \frac{1}{M_w} \qquad (2.24)$$

Using the above mentioned relationship (equation 2.23), a plot of R_θ/Kc versus $sin^2\theta/2$ can give us the apparent molecular weight ($M_{w,app}$) and second virial coefficient A_2 from the intercept and slope respectively (Fee et al., 2003a). When samples are attached to the SEC in a chromatography mode, the Debye plot of Kc/R_θ vs $\sin^2$ *(θ/2)* is used for molecular weight determination. This plot is based on Zimm formalism. This method allows M_w calculation of medium sized molecules (in a size range of 10-100 nm root mean square radius, R_g). For molecules with any above this value Berry formalism can be applied. Debye formalisms is applicable over a wider range of molecular weights (Wyatt, 1993).

To measure molar mass (molecular weight) averages, there is a need for the calculation of concentration of each slice (fraction) of the chromatogram. The system

considers each slice as a mono disperse sample. A differential refractive index detector attached to the instrument allows measurement of concentration for each slice of fraction. However, this calculation requires the dn/dc value of the macromolecule to calculate concentration (Wyatt, 1993) according to the following relation (equation 2.25).

$$c = \frac{V\,\alpha}{dn/dc} \tag{2.25}$$

where, c is the polymer concentration in solution, V is output voltage and α is the calibration constant of the DRI detector, i.e. a proportionality constant between the difference in refractive index between the pure solvent and the polymer solution (Δn), and the change in the output voltage (ΔV), with:

$$\alpha = \frac{d(\Delta n)}{d(\Delta V)} \tag{2.26}$$

The value for change in the refractive index that is dn/dc can be calculated experimentally for an unknown sample or otherwise predetermined values for known sample can be obtained from theory (Thiesen et al., 2000).

2.3. VISCOMETRY

Viscometry is a simple and inexpensive hydrodynamic technique to obtain information about conformation, conformational change, flexibility of the molecule, molecular weight and the state of aggregation or degradation (Harding, 2012). Viscosity is a measurement of the resistance of fluid to flow, which is affected by shape and size of the molecule. Figure 2.7 is considered where the liquid is held between two parallel plates. One of these plates is stationary, whereas other is

moving in the x direction with a constant velocity v. The resistance of this movement is measured by viscosity and the liquid in these plates is exposed to (shear strain) and can be referred to as d/dt (dx/dy). Thus, when the liquid is subjected to a constant shear strain, it will shear at a constant rate (Van Holde, 1985).

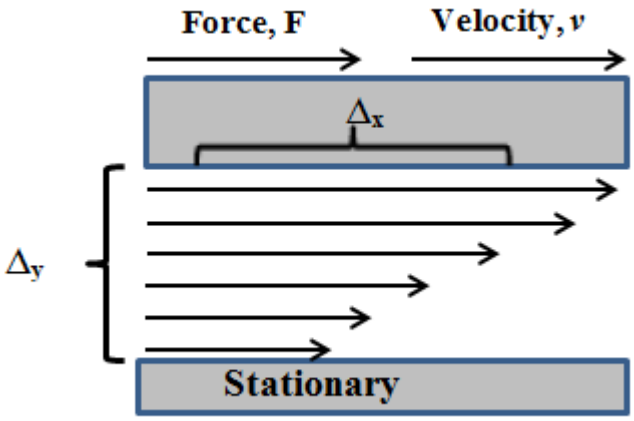


Figure 2.7: A schematic representation of the shearing of a liquid between 2 parallel plates. The parallel arrows represent fluid velocities at different values of y. Figure is reproduced from (Van Holde, 1985)

For the Newtonian fluids which obey the equation below:

$$\sigma = \eta \frac{d}{dt}\left(\frac{dx}{dy}\right) \tag{2.27}$$

where σ = shear stress, η is the viscosity of the liquid in $g.cm^{-1}.s^{-1}$ (commonly abbreviated to Poise). Einstein also defined the viscosity as a measure of the rate of energy dissipation of flow and shear rate which was given below:

$$\frac{F}{A\Delta y} \cdot \frac{dx}{dt} = \eta \cdot \left(\frac{v}{\Delta y}\right)^2 \tag{2.28}$$

In this equation, F.dx is the energy expended in the time dt and A. Δy is the volume of the fluid (Morris, 2001).

To determine of the viscosity of macromolecules in solution, the two types of viscometry -capillary viscometry and pressure imbalance differential viscometry- can be used for measurement.

2.3.1. Capillary Viscometry

Capillary or "Ostwald" viscometer is the most commonly used instrument for measuring the viscosity of dilute solutions. It is a glass capillary viscometer and suspended in a constant temperature with water bath ((Wang and Cui, 2005, Harding, 1997). The principle of this measurement is the determination of time needed for a volume of liquid to flow through the capillary. For the macromolecule solution, the flow time of solution is measured as a concentration series particularly for polysaccharides. The relative viscosity is calculated from the ratio of flow time of the solution (t) to solvent (t_s):

$$\eta_{rel} = (t/t_s).(\rho/\rho_o) \quad (2.29)$$

(ρ/ρ_0) is the ratio of the density of the solution to that of solvent; at low concentrations this ratio is ~1.00. If the concentrations studied are low enough, the density of the solution can be assumed approximately identical to that of solvent. The following viscosity parameters that show the effect of a dispersed solute on a solution proved useful (see Harding 1997 and references therein):

The specific and relative viscosities (η_{sp} *and* η_{rel}):

$$\eta_{sp} = \eta_{rel} - 1 \quad (2.30)$$

The reduced specific viscosity (η_{red}), in ml/g:

$$\eta_{red} = \eta_{sp}/c = (\eta_{rel}-1)/c \quad (2.31)$$

and the inherent viscosity (η_{inh}), also in ml/g:

$$\eta_{inh} = ln\eta_{rel}/c \quad (2.32)$$

where c represents the solute concentration (g/ml)

The reduced viscosity and the inherent viscosity are concentration dependent. (Harding, 1998). Therefore, the reduced viscosity or the inherent viscosity has to be extrapolated to zero concentration to eliminate non-ideality effects due to exclusion volume and polyelectrolyte (Harding, 1997). A plot η_{red} vs. concentration yields the intrinsic viscosity, $[\eta]$ at the intercept and the slope is related to the concentration dependence, K_H.

$$\eta_{red} = [\eta] (1 + K_H.[\eta].c) \quad (2.33)$$

where K_H is the Huggins constant (Huggins, 1942). Alternatively, the Kraemer method of plotting $ln(\eta_{rel})$ vs. concentration can also be used to calculate the intrinsic viscosity and the corresponding Kraemer constant, K_K (Kraemer, 1938).

$$(ln\eta_{rel})/c = [\eta] (1 - K_K.[\eta].c) \quad (2.34)$$

Another important relation is the Solomon-Ciuta relation that is a combination of the Huggins and Kraemer lines (Solomon and Ciută, 1962) (see also Harding, 1997).

$$[\eta] \sim (1/c). [2 (\eta_{sp} - ln (\eta_{rel}))]^{1/2} \quad (2.35)$$

The Solomon-Ciuta equation gives the approximate evaluation of $[\eta]$ without the requirement of a concentration extrapolation, although this is still useful to check for

consistency of the data. So, it is often applied at a given concentration; but in this study, this equation is used at the same concentration series as Huggins and Kraemer in order to confirm the results determined from both equations.

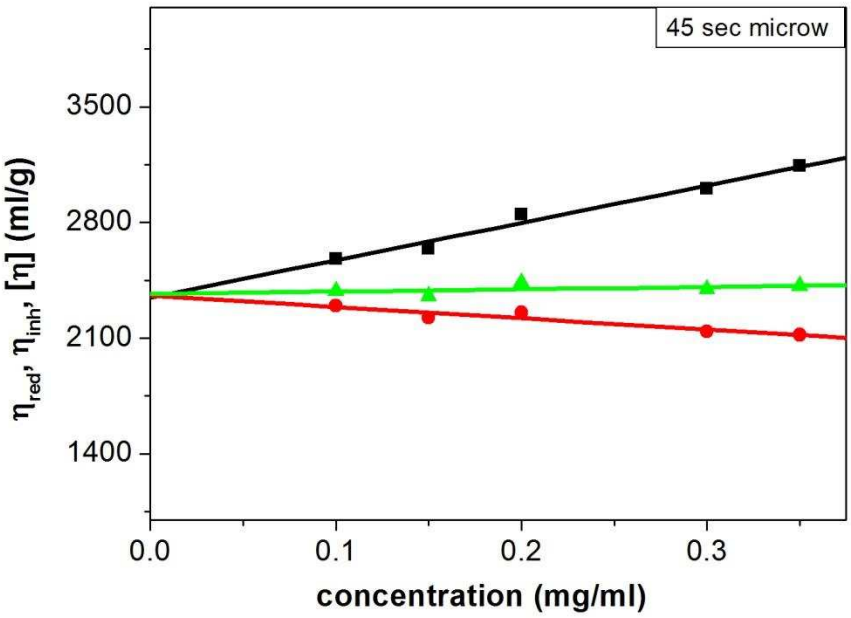


Figure 2.8: The Huggins (black squares), Kraemer (red circles) and Solomon-Ciuta (green triangles) plots for depolymerised gellan (45sec microwaved) (see Chapter 4).

2.3.2 Pressure Imbalance Differential Viscometry

This technique measures the relative viscosity by using a sensitive pressure transducer which measures the difference in pressure between solution and solvent through metal capillaries (Harding, 2012). It enables us to measure low relative viscosities and at low concentrations by taking advantage of the four-arm capillary bridge design as shown in Figures 2.9.

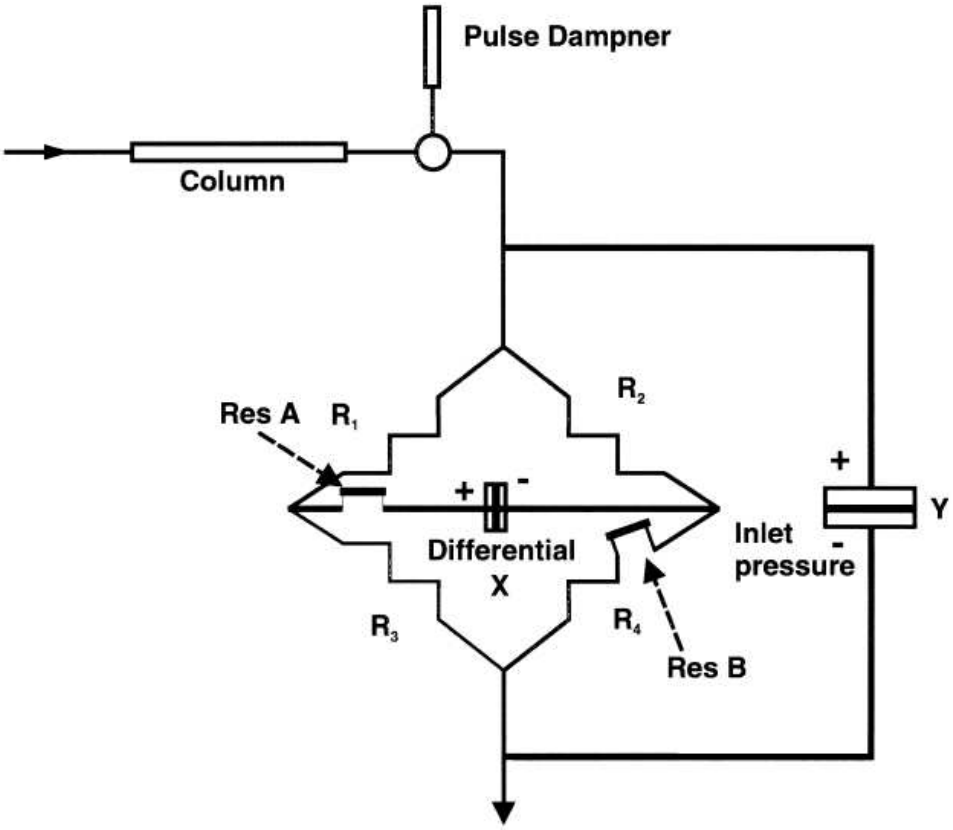


Figure 2.9: Schematic diagram of four capillary bridge design of a classical pressure imbalance viscometer adapted from (Harding, 1997)

The principle of the differential pressure measurement is explained as follows: solvent flows in all four capillaries (R1, R2, R3 and R4) at baseline conditions and the pressure across the bridge is zero. As the polymer solution is injected, it fills the capillaries R1, R2 and R3 while solvent from a reservoir is still flowing through R4 (Wang and Cui, 2005). This causes a pressure imbalance within the bridge that is detected by ΔP, where the specific viscosity η_{sp} of sample can be determined as (Waters and Leiske, 2005):

$$\eta_{sp} = \eta\,(\eta_0 - 1\,) = 4\Delta P(IP - 2\Delta P) \qquad (2.36)$$

where η and η_0 are the solution and the solvent viscosities, respectively. This method provides great sensitivity at high dilution and fast measurements. By continuous injection by a flow cell, it can be combined with on-line concentration detector (refractometer- coupled on-line to the SEC-MALS-) thus η_{rel} can be converted into η_{red}.

2.4. DYNAMIC LIGHT SCATTERING

Dynamic Light Scattering -also termed as Quasi-Elastic Light Scattering (QELS)- is the method which is used to measure hydrodynamic radii and translational diffusion coefficient (D_t) –see for example (Harding, 2012). A dynamic light scattering or ―DLS instrument can be used for estimating the z-average molecular "size" in terms of the hydrodynamic radius r_H in solution, a parameter inversely related to the translational diffusion coefficient (D_t) by using the Stoke-Einstein equation:

$$D_t = \frac{k_B T}{6\pi\eta r_H} \qquad (2.37)$$

Where, r_H is hydrodynamic radius (nm); k_B is the Boltzmann constant (1.38×10^{-16} erg/K); T is temperature (K); η_0 is solvent viscosity (Poise); D_t is translational diffusion coefficient (cm^2/s).

With this technique, the fluctuations in scattered light intensity which caused by Brownian movements of the particles in solution can be measured and the translational diffusion coefficient is estimated from the time scale of these fluctuations which rely on the speed the movement of molecule. Small molecules moves faster, which causes rapid intensity fluctuations and they scatter the very little light whereas larger particles diffuse slower (Claes et al., 1992).

The data from DLS is analysed by autocorrelation analysis that is defined as:

$$g^{(2)}(\tau) = \frac{<i\,(t).\ i(t+\tau)>}{<i>^2} \qquad (2.38)$$

where $g^{(2)}(\tau)$ is auto correlation function, i(t) intensity of the scattered light at time t and with that sometime later *i(t + τ)* (Van Holde et al., 2006a). The diffusion coefficient can be calculated from the slope of a plot of between correlation function and delay time using the following relation (Van Holde et al., 2006b, Tuinier, 1998, Harding et al., 1990).

$$\ln[g^2(\tau) - 1] = \ln c - 2h^2 D_\tau \qquad (2.39)$$

where, $h = 4\pi n\lambda^{-1}\sin(\theta/2)$, θ = scattering angle, n = refractive index, c= concentration (g/ml).

Since the translational diffusion coefficient (D_t) depends on the viscosity and temperature of solvent, it is usually normalised to standard conditions to the viscosity of water at a temperature of 20.0°C (293.14K) (Van Holde et al., 2006b)

$$D_{20,w} = [293.1/T].\ [\eta_{T,b}/\ \eta_{20,w}].\ D_{T,b} \qquad (2.40)$$

where $\eta_{T,b}$ is viscosity of buffer at T temperature (K); $\eta_{20,w}$ is viscosity of water at 20°C (Harding, 1999).

Since diffusion coefficients are concentration dependent (due to non-ideal effects, similar to those effecting viscosity) the "apparent" translational diffusion coefficients ($D_{20,w}$) are needed to be extrapolated to zero concentration, where these effects tend to zero.

$$D_{20,w} = D^0_{20,w}\ (1+ k_D c) \qquad (2.41)$$

$D^0_{20,w}$ is standardised translational diffusional coefficient at zero concentration, $D_{20,w}$ is translational diffusion coefficient at standard condition, k_D is the concentration dependence coefficient (Morris, 2001). In practise, the non-ideality effects on the diffusion coefficient are much smaller compared to other hydrodynamic coefficients, so it is often possible to approximate k_D ~0.

Low concentrations can also cause the problems because of the effect of dust and large particle contamination and these effects can be reduced by filtering solutions through appropriate filters.

Although high angles are permitted for nearly spherical scatters such as proteins, this is not the case for the macromolecular components, particularly the polysaccharides where rotational diffusion can contribute to the DLS autocorrelation calculations – at low angles these effects are small (Harding, 2012).

2.5. COMBINED HYDRODYNAMIC APPROACHES AND THE CONFORMATION OF MACROMOLECULES

2.5.1. Wales-van Holde Ratio

Wales-van Holde ratio (Wales and Van Holde, 1954) is the simplest guidance/indicator of a molecule conformational flexibility. This method utilizes the concentration-dependence or the Gralén parameter, k_s from the sedimentation velocity experiment and intrinsic viscosity $[\eta]$. Thus, Wales-van Holde ratio R is;

$$R = k_s / [\eta] \qquad (2.42)$$

The limits are ~ 1.6 for a compact sphere or a non-draining random coil (Creeth and Knight, 1965) and <1 for rods (Tombs and Harding, 1997).

2.5.2. Mark-Houwink-Kuhn-Sakurada (MHKS) or Power Law Relations

The conformation of polysaccharides can be estimated through the molecular weight dependency of the hydrodynamic parameters such as intrinsic viscosity $[\eta]$, sedimentation coefficient ($s^0_{20,w}$), radius of gyration (R_g) or the diffusion coefficient ($D^0_{20,w}$) molar mass dependency of a number of hydrodynamic parameters. In this study, the relations linking $[\eta]$ and $s^0_{20,w}$, with the molecular weight are studied and the equations were given as (see (Harding et al., 1991b):

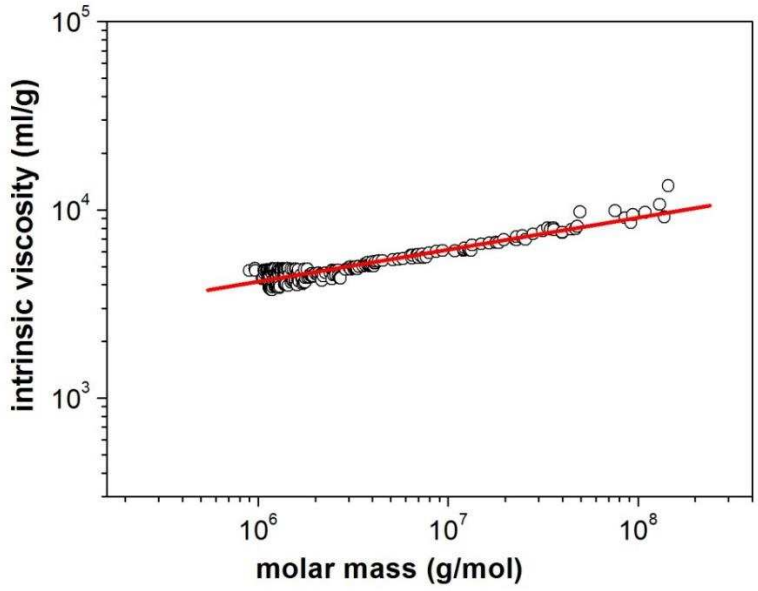


Figure 2.10: Example of a Mark–Houwink–Kuhn–Sakurada (MHKS) power law double logarithmic plot for chitosan HAV1 (see Chapter 5) from an on-line differential pressure viscometer ViscoStar coupled to SEC-MALS. The a value from the slope is (0.20 ± 0.01).

$$[\eta] = \kappa_{\eta}.M^{a} \quad (2.43)$$

The a parameter is obtained from the double logarithmic plot of $[\eta]$ versus $M_{w.}$. The value of a can be used as an estimation of gross macromolecular conformation and an a value of ~0 correspond to spheres, ~0.5-0.8 to random coils, and up to 1.8 for rigid rods.

$$s^{0}_{20,w} = \kappa_{s}.M^{b} \quad (2.44)$$

The conformation parameter, b is yielded from the double logarithmic plot of $s^{0}_{20,w}$ versus M_w. This is analogous to the relation of intrinsic viscosity with molecular weight, but the b values of ~ 0.67 has been established for compact sphere or highly branched macromolecules, 0.4-0.5 for random coils, and ~ 0.15 for rigid rods.

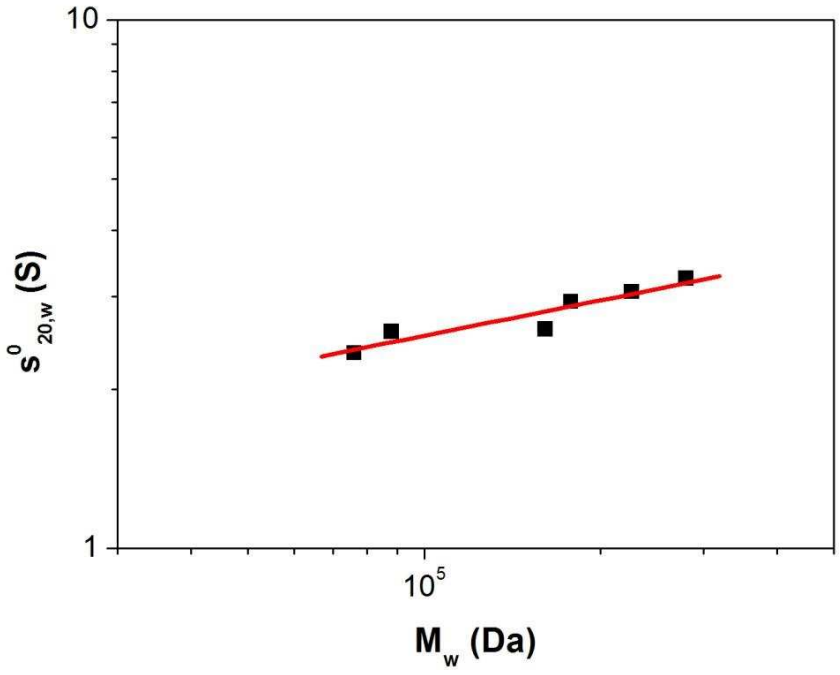


Figure 2.11: Example of Mark–Houwink–Kuhn–Sakurada (MHKS) power law double logarithmic plot of $s^{0}_{20,w}$ vs M_w for gellan samples (see Chapter 4). The b value from the slope is (0.22 ± 0.04).

The values of a and b are then used to determine conformation using the 'Haug Triangle' which is a representation of the gross conformation of macromolecules. The three extremes of conformation, compact sphere, random coil and rigid rod, are placed at the corners of triangle (Tombs and Harding, 1997).

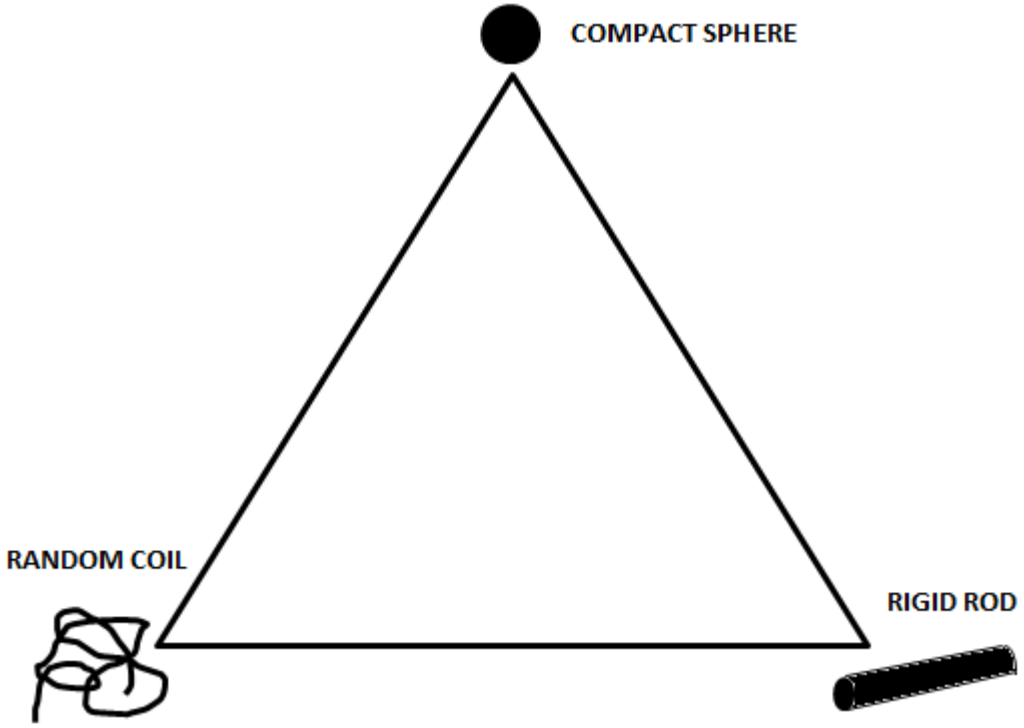


Figure 2.12: HAUG Triangle. Figure reproduced from (Tombs and Harding 1997)

2.5.3 Estimation of the Persistence Length (L_p) and Mass Per Unit Length (M_L)

The linear flexibility of polymer chain can be described with persistence length (L_p) and mass per unit length (M_L). L_p is defined as the average projection length along the initial direction of the polymer chain and M_L is the mass of the molecule(s) within the polymer divided by its length. Theoretically, L_p is $L_p = 0$ for a random

coil whereas $L_p = \infty$ for the rigid rod (e.g. see (Harding, 1997). However in practice limits, for random coil ~1nm (e.g pullulan) and for rigid rod ~200nm (e.g. xanthan) are more suitable (Tombs and Harding, 1997). Persistence length can be estimated using different approaches either sedimentation coefficient (Yamakawa and Fujii, 1973, Hearst and Stockmayer, 1962) or intrinsic viscosity (Bohdanecky, 1983, Stockmayer and Fixman, 1963), equations. The choice of appropriate methods enable to estimate an optimum measurement for the polymer flexibility (Kök et al., 2009).

2.5.3.1. Bushin-Bohdanecky Method

This method is a commonly used to estimate chain persistence lengths (L_p) especially for semi-flexible polymers, and has been applied to range of polysaccharides such as xyloglucan (Patel et al., 2008b), methylcellulose (Morris et al., 2009b) and konjac glucomannan (Kök et al., 2009). Persistence length is estimated using viscosity and molecular weight data with the equation below (Bushin et al., 1981a, Bohdanecky, 1983):

$$\left(\frac{M_w^2}{[\eta]}\right)^{1/3} = A_0 M_L \Phi^{-1/3} + B_0 \Phi^{-1/3} \left(\frac{2L_P}{M_L}\right)^{-1/2} M_w^{1/2} \qquad (2.45)$$

where Φ is the Flory-Fox constant (2.86 x 10^{23} mol^{-1}), A_0 and B_0 are constants and are taken as ~1.32 and ~1.10, respectively (Bushin et al., 1981b). However, the value of mass per unit length (M_L) is needed for the calculation.

2.5.3.2 Yamakawa–Fujii Method

This method provides another way for estimating chain persistence length, L_p using sedimentation coefficient and molecular weight information. The slope of $s^0_{20,w}$ vs

$(M_w)^{1/2}$ gives the value of L_p and M_L but it also requires knowledge about one of these parameters (L_p or M_L) (Yamakawa and Fujii, 1973). However, the original equation given by Yamakawa and Fujii (1973) was misprinted. Freire and Garcia de la Torre (Freire and Garcia De La Torre, 1992) provided the corrected relation as follows:

$$s^0 = \frac{M_L(1-\bar{\upsilon}\rho_0)}{3\pi\eta_0 N_A}\, x \left[1.843\left(\frac{M_w}{2M_L L_P}\right)^{1/2} + A_2 + A_3\left(\frac{M_w}{2M_L L_P}\right)^{-1/2} + \ldots.\right] \qquad (2.46)$$

If the persistence length L_p is much larger than the mean chain diameter, d, Yamakawa and Fujii (Yamakawa and Fujii, 1973) have shown that $A_2 = -\ln(d/2L_p)$ and $A_3 = 0.1382$.

2.5.3.3 Global analysis method (HYDFIT)

The different methods can bring about bias and discrepancies on results. To prevent this variability, Multi-HYFIT program was developed by Ortega and Garcia de la Torre (2007) to enable estimates for consensus values of L_p and M_L and chain diameter d, by considering two or more data sets of intrinsic viscosity *([η]),* sedimentation coefficient (s), radius of gyration (R_g) and translational diffusion coefficient (D_t) for varying molecular weights of the same molecule. This program carries out minimisation of the target function Δ using Bushin-Bohdanecky (Bohdanecky, 1983, Bushin et al., 1981a) and Yamakawa-Fujii (Yamakawa and Fujii, 1973) equations within the several variables. The optimization process can be implemented giving different weightings to each property (Ortega and García de la Torre, 2007). To simplify and accelerate the minimization of the process, the least effective parameter or well defined parameter from known molecular structure (eg.

M_L) can be fixed. The results of simulation analysis showed that L_p is comparatively insensitive to the value chosen d.

The Multi-HYDFIT program runs the parameters *([η], Rg, s*) in order to find a minimum of the target (error) function, Δ (Ortega and García de la Torre, 2007, Morris et al., 2008).

Target function, Δ is calculated using an equivalent radius which is defined by Ortega and Garcia de la Torre as 'the radius of the equivalent sphere having same value of the particular properties'. The translational friction coefficient, f (can be obtained from sedimentation coefficient s or diffusion coefficient D_t), the radius of gyration R_g, intrinsic viscosity *[η]* and relaxation time τ are comprised from these particular property (Ortega and García de la Torre, 2007). The method equivalent radii that is interested in this study are obtained from sedimentation coefficient i.e. translational frictional coefficient (a_T), intrinsic viscosity (a_I) and radius of gyration (a_G).

$$a_T = \frac{f}{6\pi\eta_0} \tag{2.47}$$

where $\eta_0$is the viscosity of water at 20°C,

$$a_I = \left(\frac{3[\eta]M_w}{10\pi N_A}\right)^{1/3} \tag{2.48}$$

where N_A is Avogadro's number and

$$a_G = \sqrt{5/3}R_G \tag{2.49}$$

where R_G is radius of gyration.

The target function, Δ can be obtained from these equations below:

$$\Delta^2 = \frac{1}{N_s}\sum_{i=1}^{N_s}\left[(\sum_T W_T)^{-1}\sum_T W_T\left(\frac{a_{T_{(cal)}}-a_{T_{(exp)}}}{a_{T_{(\exp)}}}\right)^2\right] \quad (2.50)$$

$$\Delta^2 = \frac{1}{N_s}\sum_{i=1}^{N_s}\left[(\sum_I W_I)^{-1}\sum_I W_I\left(\frac{a_{I_{(cal)}}-a_{I_{(exp)}}}{a_{I_{(\exp)}}}\right)^2\right] \quad (2.51)$$

where N_s is the number of samples, W_T and W_I are the statistical weights for equivalent radii a_T and a_I and the subscripts cal and exp indicates values from calculated and experimental values, respectively. Therefore, Δ is a dimensionless estimate of the consensus between calculated values for the frictional coefficient, intrinsic viscosity and radius of gyration for a certain persistence length, L_p and the experimentally measured parameters (Ortega et al., 2011, Patel et al., 2008b).

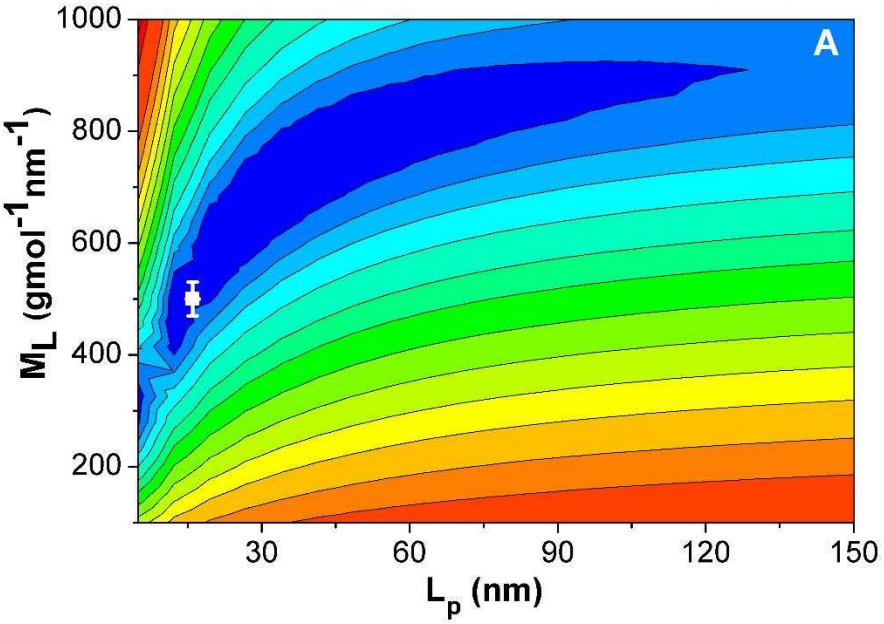


Figure 2.13: Contour plots of the CHIT1. The target function, *Δ* calculated based on variables values of L_p and M_L, and are represented on the full colour spectrum from blue (*Δ* = 0.005) to red (*Δ*≥0.65) L_p = (16 ± 0.2), M_L = (500 ± 30) (see Chapter 7).

2.5.4. Conformation Zoning

The sedimentation conformation zoning plot provides the estimation of 'overall' solution conformation of a macromolecule using M_L. Pavlov and co-workers suggested the use of five conformation types which ranges from Zone A (extra-rigid rod) to Zone E (globular or branched) by plotting of $k_s M_L$ versus [s]/M_L. (Pavlov et al., 1997, Pavlov, 2013). This plot is obtained from the knowledge of the intrinsic sedimentation coefficient, [s] along with the concentration dependence of the sedimentation coefficient, k_s and mass per unit length, M_L which is the mass of the molecule(s) within the polymer divided by its length.

[s] is evaluated from this equation:

$$[s] = \frac{s^0_{20,w}\eta_0}{(1-\bar{\upsilon}\rho_0)} \tag{2.52}$$

Where $s^0_{20,w}$ sedimentation coefficient, η_0 and ρ_0 are the viscosity and the density of the solvent, respectively. $\bar{\upsilon}$ is the partial specific volume of the macromolecule.

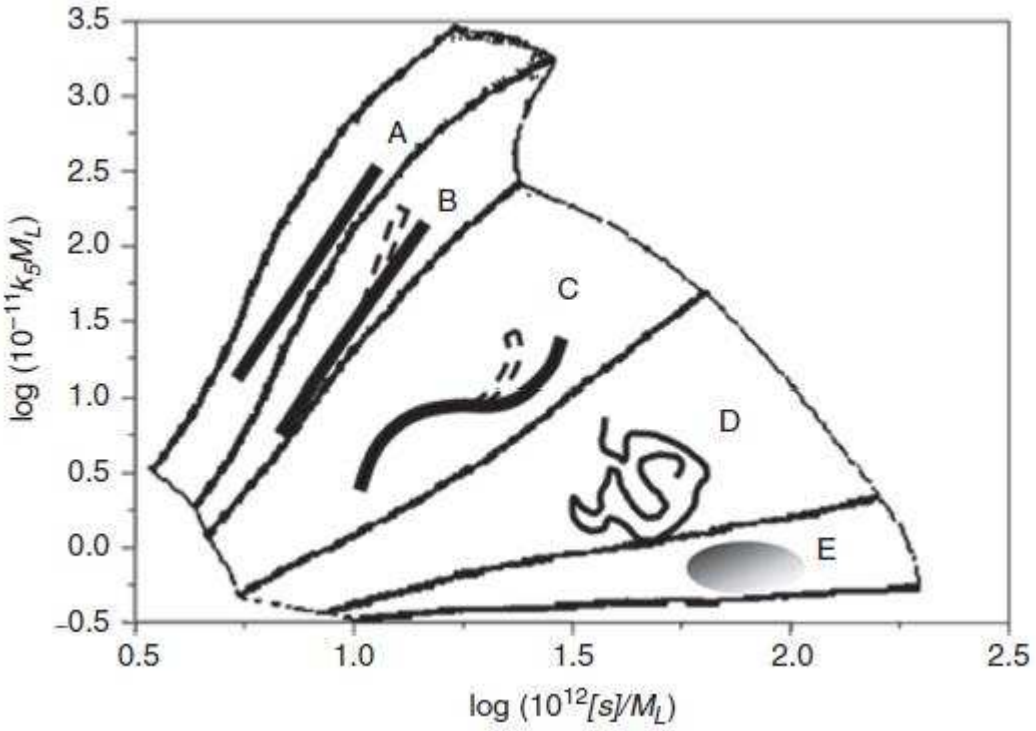


Figure 2.14: The sedimentation conformation zoning plot; A: extra rigid rod, B: rigid rod, C: semi-flexible coil, D: random coil, E: globular/heavily branched structure. Adapted from (Morris and Harding, 2013).

CHAPTER 3

HYDRODYNAMIC CHARACTERISATION OF XANTHANS OF DIFFERENT PYRUVATE AND ACETATE CONTENT

3.1. INTRODUCTION

Xanthan is an anionic, extracellular microbial polysaccharide produced by Xanthomanas campestris (Rodd et al., 2000, Berth et al., 1996, Khouryieh et al., 2007). The primary structure of xanthan consists of a linear β-(1→4) D-glucan backbone with branched trisaccharide chains containing D-glucoronic acid unit between two D-mannoses. These trisaccharide chains are linked to a backbone at C-3 on every second unit. Approximately half of the terminal D-mannose units contain a pyruvic acid residue linked via a keto group to the 4 and 6 positions, whose distribution patterns are beginning to be described (Kool et al., 2014). The D-mannose linked to the main chain contains an acetyl group at position C-6 as shown in Figure 3.1 (Tombs and Harding, 1997).

In aqueous solutions, xanthan undergoes a conformational transition depending on temperature, ionic strength, pH and acetyl and pyruvyl substituent content (Chazeau et al., 1995). At high temperature and low ionic strength, the xanthan backbone exists in an disordered form in solution whereas it exists in ordered form at low

temperature and high ionic strength due to electrostatic repulsion between side chains (Khouryieh et al., 2007).

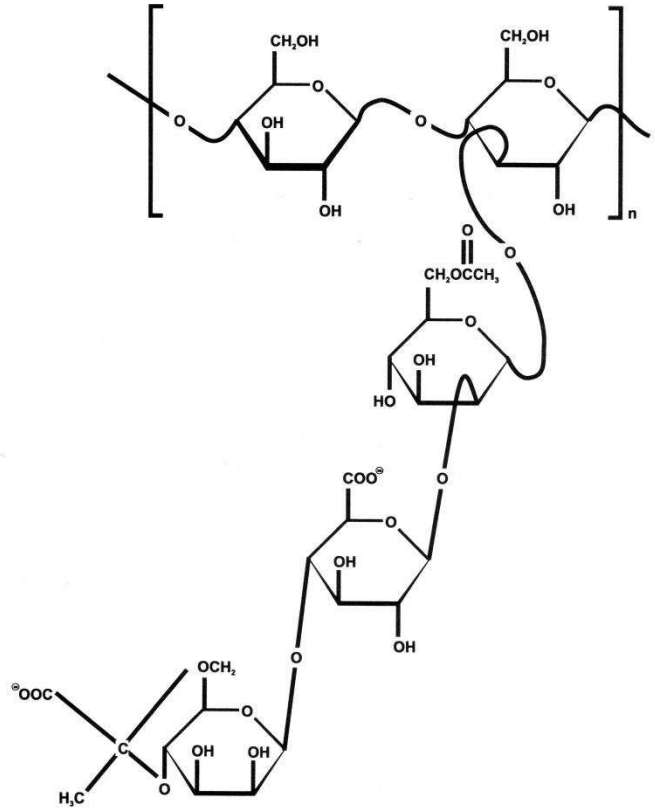


Figure 3.1: Chemical structure of xanthan. Adapted from (Tombs and Harding, 1997)

Xanthan gum is also very soluble in both cold and hot water due to its polyelectrolyte characteristics. Xanthan solutions are highly viscous at very low concentrations (García-Ochoa et al., 2000) so the critical overlap concentration c* (the concentration at which the individual polymer molecule chains begin to overlap) is relatively lower than other gums such as guar which is 0.08 %w/w and carob which is 0.11 % w/w (Secouard et al., 2007). It has been reported as lower than 0.03% w/w (Cuvelier and Launay, 1986) and 0.025 % w/w which is equivalent to

0.25mg/ml (Pelletier et al., 2001). This low value of c* has subsequently caused some problems in terms of solution characterisation. The viscosity of xanthan also depends on temperature, salt concentration and pH (Sworn, 2009, García-Ochoa et al., 2000).

The acetyl and pyruvate substituents depend on the xanthan strain and fermentation process which may have an effect on viscosity and conformation of xanthan solutions. Researchers have claimed that the acetyl and pyruvate groups may have a significant effect on viscosity (Sandford et al., 1977, Smith et al., 1981, Cheetham and Nik Norma, 1989, Tako and Nakamura, 1984) , whereas other groups have disputed this (Callet et al., 1987, Shatwell et al., 1990, Bradshaw et al., 1983). Khouryieh concluded that acetate and pyruvate substituents can affect viscosity depending on temperature, salt type and concentration and sample concentration. However, due to the intermolecular and intramolecular association of these groups with the carbohydrate -backbone, these two groups play an important role on the conformation of xanthan (Khouryieh, 2006).

In the current investigation, four commercial xanthan samples have been studied: two with identical degrees of pyruvation ("Standard pyruvate" 3.9%) but different molecular weights, and two further ones of different degrees of pyruvation, namely "High" (6.5%) and "Low" (2%). These were characterized in dilute aqueous buffered solutions (pH 7.0, ionic strength 0.1M and 0.3 M) using high-precision viscometry, sedimentation velocity, sedimentation equilibrium and dynamic light scattering (DLS), facilitating a rigorous comparison with regards heterogeneity (sedimentation coefficient distribution), molecular weight and conformation (translational frictional ratio). Resolution of the controversy is deemed important because of the huge commercial significance of xanthan in the food and

biopharmaceutical industries. A major problem however in the characterization of xanthans is their very large size compromising the use of size exclusion chromatography based procedures, the low value of the "critical overlap concentration", c*, and large thermodynamic non-ideality of these substances. However, advantage can now be taken of some recent and relevant advances in the analysis of polymeric materials by analytical ultracentrifugation (Abdelhameed et al., 2010, Dam and Schuck, 2004, Schuck et al., 2014).

3.2. MATERIALS

Xanthan samples with "Standard pyruvate" (low and high molecular weight- "Standard LMW", and "Standard HMW" respectively), and low and high pyruvate contents "Low" and "High" respectively were supplied by Dupont (Paris). The two standard samples had been shown to have the same pyruvate content (3.9%), as determined by chemical analysis, with the high and low pyruvate samples having 6.5% and 2.0% respectively. The proportions of acetate in each sample had also been evaluated and are given in Table 3.1. Stock solutions of xanthan were prepared by dissolving a known amount in distilled deionised water, at room temperature with gentle stirring at 3 h followed by overnight dialysis against phosphate-chloride buffer supplemented with NaCl according to Green (Green, 1933) at pH 7.0 and an ionic strength, I, of 0.1 M and 0.3M. The concentrations, c (g/ml) of the stock xanthan solutions were measured after dialysis using an Atago (Japan) DD-7 refractometer calibrated with glucose standards, and a refractive increment dn/dc of 0.15 ml/g (Berth et al., 1996).

Table 3.1: Pyruvate and acetate content of the xanthans.

Xanthan	Pyruvate (%)	Acetate (%)
Standard LMW (STD)	3.9	6.2
Standard HMW (Supra)	3.9	6.2
High Pyruvate (TSF)	6.5	5.1
Low Pyruvate (TSC)	2.2	6.0

3.3. METHODS

3.3.1. Sedimentation Velocity (SV)

An Optima XL-I (Beckman Instruments, Palo Alto, USA) equipped with Rayleigh interference optics was used to determine the sedimentation behaviour and molecular homogeneity of xanthan samples. Solution concentrations ranging between 0.05 – 0.225 mg/ml for each xanthan were studied at a temperature of (20.0 ± 0.1) °C. 400µl of solution and an equal volume of the pH 7.0, I=0.1M and I=0.3M reference buffer (400µl) were injected into the solution and solvent channels of 12 mm optical path length double sector cells. The Rayleigh interference optical system was used to record changes in the concentration versus radial displacement profiles with time. Scans were taken at 2 min intervals for a run time of approximately 18 hours at 30000rpm. A partial specific volume, $\bar{\upsilon}$ of (0.602 ± 0.010) was used for the xanthans (Anderson, 1991, Dhami, 1996). For comparison purposes, sedimentation coefficients were normalised to standard solvent conditions, namely the density and viscosity of water at 20.0°C (Abdelhameed et al., 2010, Laue and Stafford III, 1999):

$$s_{20,w} = \{(1-\bar{\upsilon}\rho_{20,w}) / (1-\bar{\upsilon}\rho_0)\} \,.\, \{\eta_0 / \eta_{20,w}\} s_{T,b} \qquad (3.1)$$

where ρ_o and η_o are respectively the density and viscosity of the solvent or buffer, b, at temperature T and $\rho_{20,w}$ and $\eta_{20,w}$ the corresponding values of water at 20.0^{o}C. The data was analysed using the "least squares ls-g(s) model" SEDFIT program of Schuck and colleagues (Dam and Schuck, 2004) in terms of distributions of sedimentation coefficient distribution (see also (Harding, 2005c)). The g(s) vs. s profiles were used to provide an assessment of sample polydispersity. The s and $s_{20,w}$values are 'apparent' values because of non-ideality. To remove this effect, $s_{20,w}$ is extrapolated to zero concentration and $s^0_{20,w}$is obtained from reciprocal plot of $s_{20,w}(1/s_{20,w})$ vs. concentration (see for example, (Laue and Stafford III, 1999, Harding, 2005c, Tanford, 1961) :

$$1/s_{20,w} = (1/s_{20,w}).\,(1+k_s c) \qquad (3.2)$$

where $s^0_{20,w}$is the sedimentation coefficient at zero concentration and standard condition, k_s is the Gralen parameter (Gralen, 1944); see also (Harding, 2005b, Harding, 2005c).

3.3.2. Sedimentation Equilibrium (SE)

Sedimentation equilibrium experiments were also performed using the Beckman (Palo Alto, California, U.S.A.) Optima XL-I analytical ultracentrifuge and employing Rayleigh interference optics and an automatic on-line data capture system. The modified long (20.0 mm) optical path length double-sector titanium cells with sapphire windows were loaded with (~120 ml) of dialysed sample and a matching amount of reference buffer dialysate in appropriate channels. The balanced cells were then loaded into an analytical 8-hole titanium rotor An50-Ti and placed in

the AUC. After time was allowed for vacuum formation and for temperature equilibration (20.0 °C), the rotor was then accelerated to 2000 rpm; rotor speeds were selected to be sufficiently apart to give good molecular weight distributions (Scott and Schuck, 2005). Using the Rayleigh interference optical system, scans were taken every 1 h and equilibrium was reached after approximately

168 h. Record of the relative concentration distribution of the solute at equilibrium was analysed to give the weight average apparent molecular weight $M_{w,app}$ using SEDFIT-MSTAR program implemented by Schuck et al. (Schuck et al., 2014) . The use of the long path length cells (20.0 mm) meant that a low loading concentration (0.3 mg/ml) could be used to give a sufficient signal. At such low concentrations, non-ideality effects will be minimized (Harding, 2005c).

3.3.3. Dynamic Light Scattering (DLS)

Xanthan solutions ranging in concentration from 0.2 to 1.0mg/ml were filtered by using 0.45 mm pore size filter (Whatman, UK) to reduce supramolecular aggregates and injected into scrupulously clean cuvettes. These were placed into a dual angle Zetasizer Nano-S dynamic light scattering photometer (Malvern Instruments, Worcester, UK), controlled to a temperature of (20.0 ± 0.1)°C. A low scattering angle (12.8°) was chosen to minimize the complicating effects of rotational diffusion and other anisotropic effects. Data was automatically collected and analysed using Malvern's DTS (Version 4.2) software. Sample times and delay times were chosen automatically by the software. Consistent values for the apparent translational diffusion coefficient, D_t were found from multiple (>10) repeats. As with the sedimentation coefficient, the measured translational coefficient was normalised to

standard solvent conditions namely the viscosity of water at a temperature of 20.0 °C (293.14 K), see (Van Holde et al., 2006a).

$$D_{20,w} = [293.1/T] \, . \, [\eta_0/\eta_{20,w}] . \, D_{T,b} \quad (3.3)$$

where η_0 is the solvent viscosity of buffer at temperature T(K) - which in this case is 20.0 °C; $\eta_{20,w}$ is the viscosity of water at 20 °C (Harding, 1999).

Unlike other hydrodynamic parameters such as reduced viscosity and the sedimentation coefficient, translational diffusion coefficients show only either a small or negligible dependence on concentration to a cancellation of effects (Harding and Johnson, 1985a, Harding and Johnson, 1985b) but nonetheless measurement at different concentrations provides a useful check for any discontinuities due to possible coil overlap.

3.3.4. Capillary Viscometry

Xanthan solutions ranging from 0.06 mg/ml to 0.22 mg/ml were analysed using a Schott-Geräte U-tube viscometer system at a temperature of (20.0 ± 0.01) °C. The relative viscosity,η_{rel}, was obtained from the ratio of the flow time of the solution t (sec) to the flow time of solvent t_0:

$$\eta_{rel} = (t / t_0) \quad (3.4)$$

recorded accurately using photosensors. Because of the low concentrations used a density correction was deemed unnecessary (Yang, 1962, Harding, 1997). The reduced (specific) viscosity (ml/g) was evaluated from

$$\eta_{red} = (\eta_{rel} - 1) / c \quad (3.5)$$

and the inherent viscosity (ml/g) from

$$\eta_{inh} = (\ln \eta_{rel}) / c \quad (3.6)$$

where c represents the solute concentration (g/ml).

To eliminate non-ideality effects η_{red} and η_{inh} were extrapolated to zero concentration with the common intercept at c = 0 yielding the intrinsic viscosity $[\eta]$:

$$\eta_{red} = [\eta]\ (1 + K_H.[\eta].c) \quad (3.7)$$

and

$$(ln\eta_{rel})/c = [\eta]\ (1 - K_K.[\eta].c) \quad (3.8)$$

where K_H and K_K are respectively the Huggins (1942) and Kraemer (1938) constants. As an additional check, a combined relation due to Solomon & Ciuta (1962) was also used:

$$[\eta] \sim (1/c).\ [2\ (\eta_{sp} - ln\ (\eta_{rel}))]^{1/2} \quad (3.9)$$

The assumption has been made that there was no shear dependence of $[\eta]$ under creeping flow conditions in the capillary viscometer.

3.4. RESULTS

3.4.1. Sedimentation Velocity (SV)

The sedimentation coefficient, s, values for xanthan samples were determined by sedimentation velocity in the analytical ultracentrifuge as outlined above. These s values of xanthan samples were obtained at different series of concentrations (0.05 to 0.25 mg/ml) and two ionic strengths (0.1M and 0.3M) for each of xanthan sample. The g*(s) vs. s profiles (or sedimentation coefficient distribution) and are given in Figure 3.2a and Figure 3.2b. To reduce the non-ideality effect of xanthan, $s_{20,w}$ was extrapolated to zero concentration and $s^0_{20,w}$was obtained from reciprocal plot of

$s_{20,w}$ ($1/s_{20,w}$) vs. concentration (c) as indicated in Figure 3.3a and Figure 3.3b. The summary of sedimentation coefficient and concentration dependence of k_s of all xanthan samples at two ionic strengths (0.1M and 0.3M) is given in Table 3.2.

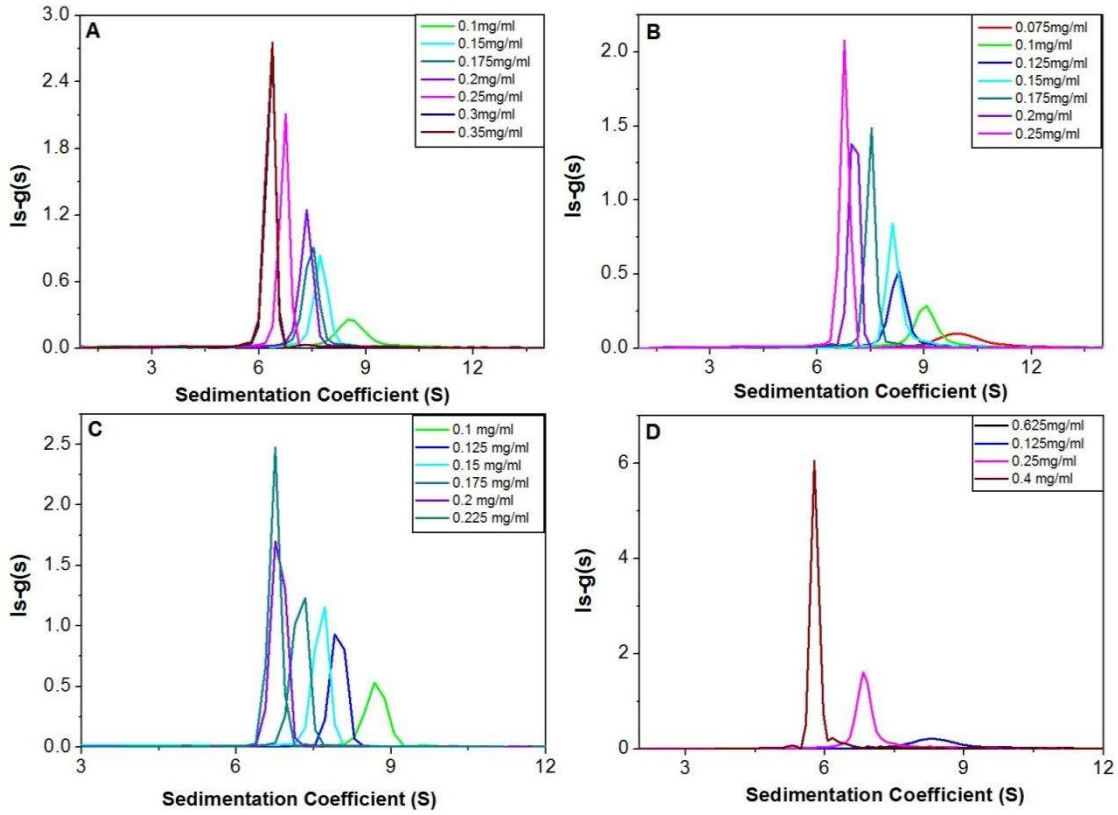


Figure 3.2a: Sedimentation coefficient distribution profiles (least squares g(s) vs. s plots) of xanthan samples at different concentrations in pH= 7.0, I = 0.1 M buffer. (A) Standard LMW (B) Standard HMW, (C) High pyruvate, (D) Low pyruvate.

The g*(s) vs. s plot shows the homogeneity of xanthan samples since there is only one peak in the distribution. The s values moved and decreased with increasing concentration (see for example (Cole et al., 2008)). This clear reduction of sedimentation coefficient is consistent with xanthan being highly non-ideal (Dhami et al., 1995).

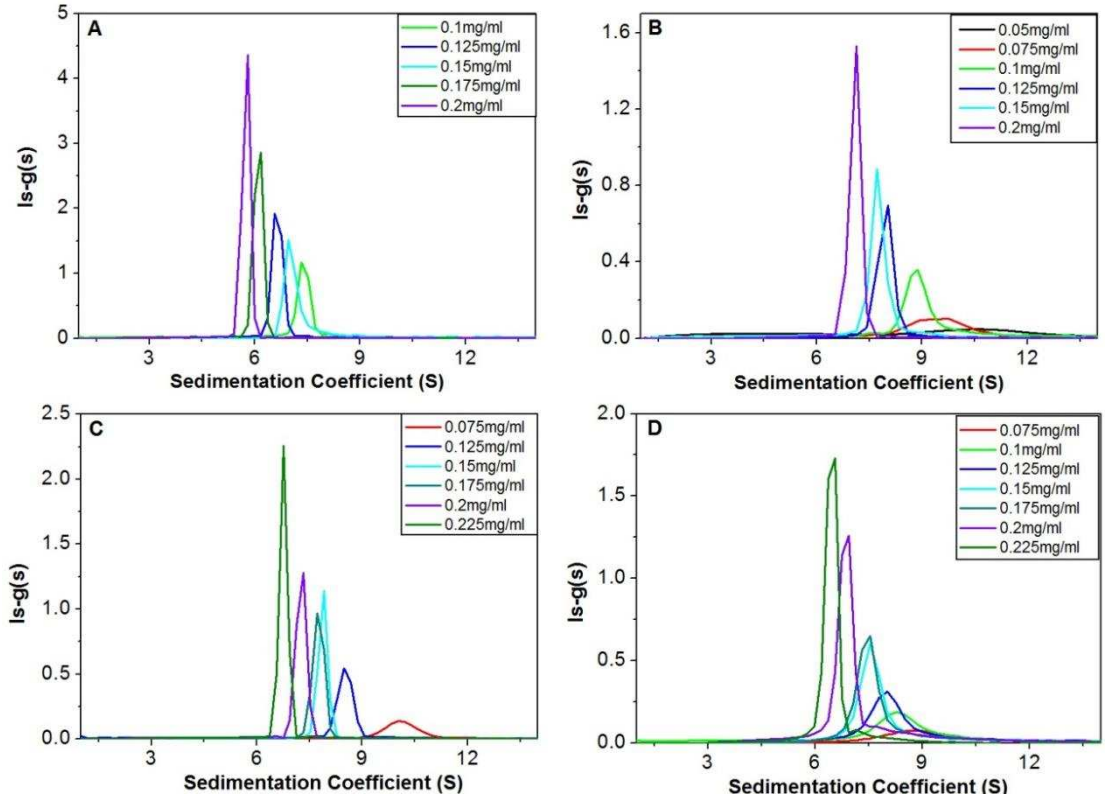


Figure 3.2b: Sedimentation coefficient distribution profiles (least squares g(s) vs. s plots) of xanthan samples at different concentrations in pH= 7.0, I = 0.3 M buffer. (A) Standard LMW (B) Standard HMW, (C) High pyruvate, (D) Low pyruvate.

Table 3.2: Summary of sedimentation coefficient ($s^0_{20,w}$) and concentration dependence of sedimentation (k_s) for all xanthan samples.

Sample	$s^0_{20,w}$ (S)	k_s (ml/g)	$s^0_{20,w}$ (S)	k_s (ml/g)
	0.1M	**0.1M**	**0.3M**	**0.3M**
Standard LMW	9.80 ± 0.34	1700 ± 160	10.10 ± 1.75	3600 ± 1290
Standard HMW	13.08 ± 0.52	4200 ± 310	13.54 ± 0.99	4800 ± 680
High pyruvate	11.07 ± 0.44	3000 ± 260	12.90 ± 0.60	4000 ± 340
Low pyruvate	10.95 ± 0.24	2300 ± 100	11.47 ± 0.50	3200 ± 310

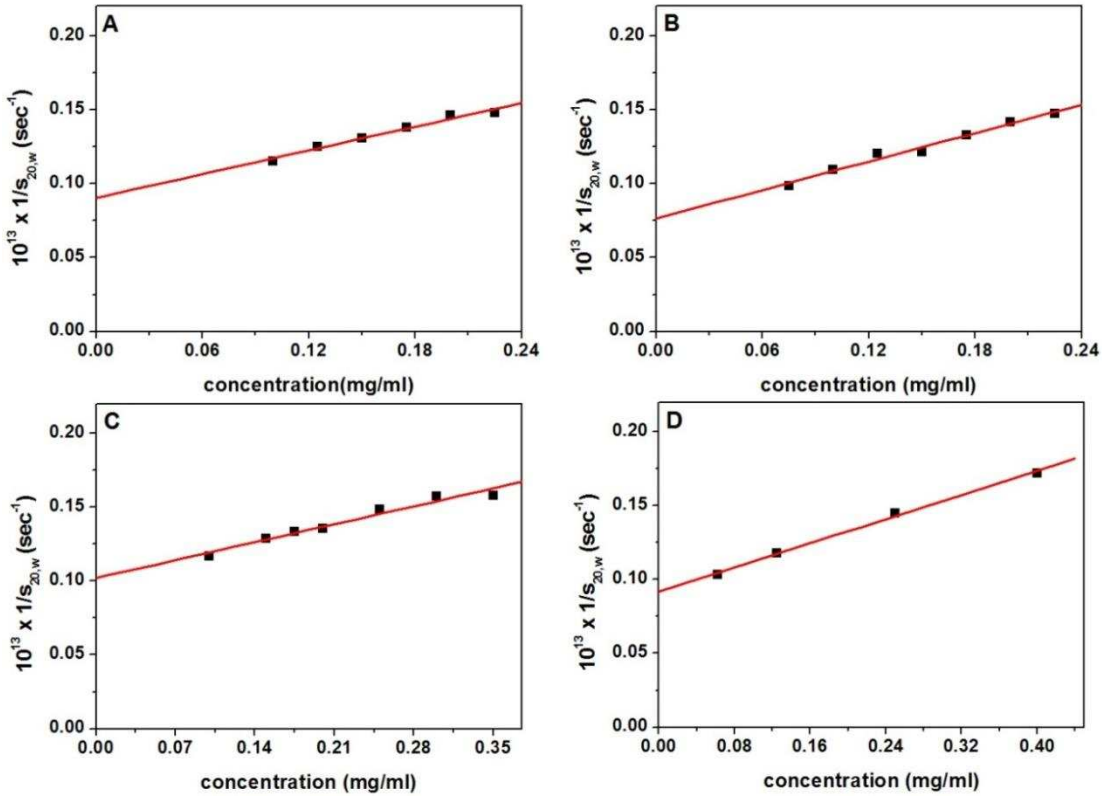


Figure 3.3a: Concentration dependence (reciprocal) of the sedimentation coefficient plot (after correction to standard solvent conditions) for xanthan samples pH= 7.0, I = 0.1 M buffer. (A) Standard LMW (B) Standard HMW, (C) High pyruvate, (D) Low pyruvate.

This study is thus in complete agreement with previous studies that were performed by Dhami and co-workers (Dhami et al., 1995) and Harding and co-workers (Harding et al., 2012).

3.4.2. Estimation of Molecular Weight

The molecular weight estimation of xanthan was attempted using size exclusion chromatography coupled to multi angle light scattering (SEC-MALS) and also sedimentation equilibrium (SE) in the analytical ultracentrifuge, both classical methods for measuring molecular weights of polymer. However, both presented

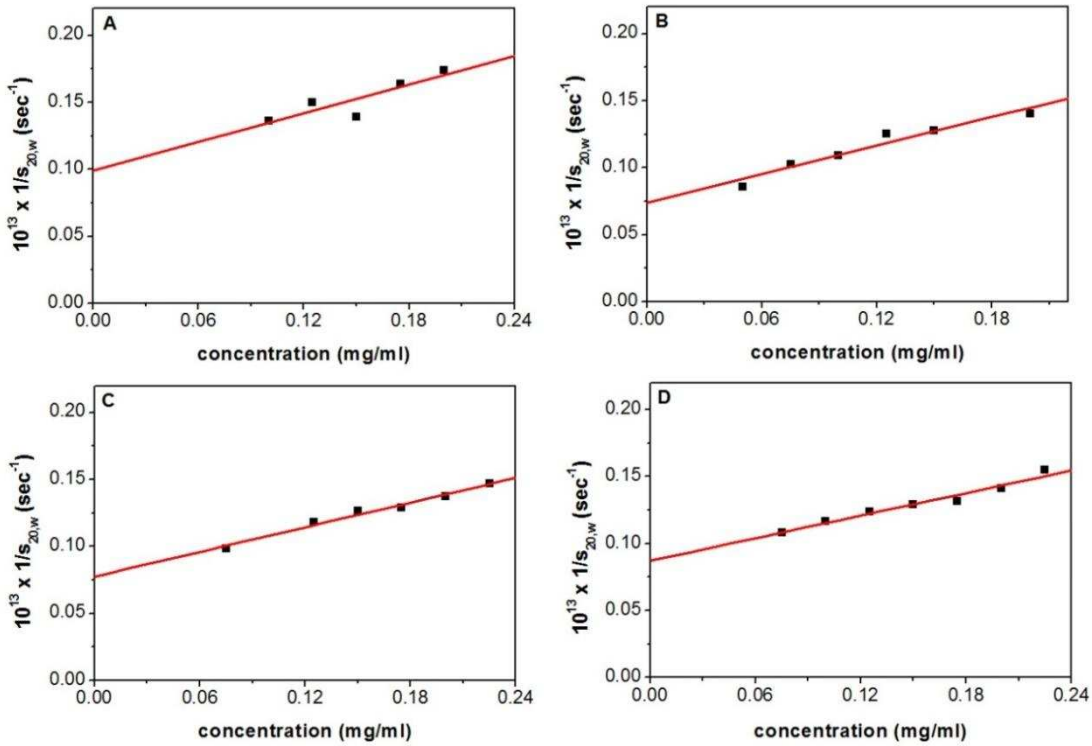


Figure 3.3b: Concentration dependence (reciprocal) of the sedimentation coefficient plot (after correction to standard solvent conditions) for xanthan samples pH= 7.0, I = 0.3 M buffer. (A) Standard LMW (B) Standard HMW, (C) High pyruvate, (D) Low pyruvate.

problems for xanthan. Although SEC-MALS in principle provides such information, it was not successful on these samples which were beyond the exclusion range of the columns (namely TSK G6000PW and TSK G4000PW). When the experiment was performed with SEC-MALS, the xanthan molecules appeared to interact with column matrix causing anomalous behaviour, while yielding the molecular weight data. Furthermore, the data was not consistent with previous xanthan studies (Dhami et al., 1995, Harding et al., 2012) for the same sedimentation coefficient values. Sedimentation equilibrium is itself not without difficulties for these macromolecules because of the almost unique challenge they pose. Even with long path length cells

(20 mm) the lowest concentration that can be used for sedimentation equilibrium based methods in the analytical ultracentrifuge is not as low with current instrumentation (the XL-I ultracentrifuge) than was previously attainable with the old generation Model E ultracentrifuge, as for example employed by Dhami et al. for estimation of $M_{w,app}$ in their study on Keltrol xanthan (Dhami et al., 1995). This is a particular problem for xanthan because of the strong thermodynamically non-ideality even at 0.3 mg/ml (Dhami, 1996). Normally, there is a straight forward solution to this problem -to measure the apparent weight average molecular weight and at a series of concentrations and extrapolate back to c = 0, where $M_{w,app} = M_w$, the ideal weight average molecular weight. In this case, this extrapolation has been impossible to do: the inability to perform a concentration series extrapolation to c = 0 is because of the c* limitation restricting the use of concentrations much greater than ~0.6 mg/ml (Dhami et al., 1995). Nonetheless we can take advantage of the earlier study by Dhami et al. (1995) and use the value obtained for the 2nd thermodynamic virial coefficient B to correct apparent weight average molecular weights, to true or thermodynamically ideal weight average molecular weights, M_w according to the equation;

$$1/M_{w,app} = \{1/M_w\}\{1+ 2BM_wc\} \qquad (3.10)$$

using a value for $BM_w = 2.01 \times 10^3$ ml/g (Dhami et al., 1995).

As a supplementary technique, another approach is to estimate the molecular weight from the (weight average) sedimentation coefficient using the power law relation. According to Harding (Harding, 2005c), a sedimentation coefficient distribution can be transformed into apparent molecular weight if the conformation of the sample is

known or estimated with respect to the 'Mark –Houwink-Kuhn-Sakurada' (MHKS) approach (Tombs and Harding, 1997) :

$$s^0_{20,w} = \kappa_s . M^b \quad (3.10)$$

where the b coefficient is obtained from double log plots of sedimentation coefficient $s^0_{20,w}$ vs. apparent molecular weight ($M_{w,app}$) (Harding, 1992). Eqn. (3.10) is generally much less sensitive to conformation differences but more reliable at giving

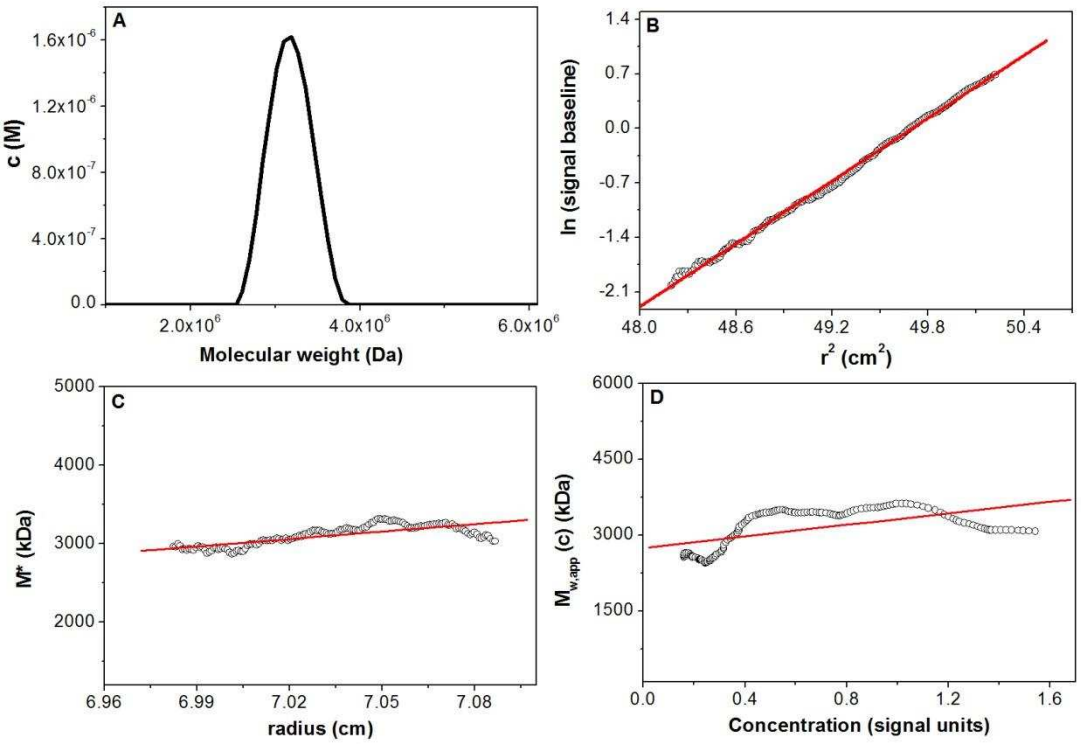


Figure 3.4: SEDFIT-MSTAR analysis of Low Pyruvate in 0.3 M PBS at a loading concentration of 0.35 mg/ml (A) molecular weight distribution, c(M) vs. M plot; (B) log concentration ln c(r) vs. r^2 plot, where r is the radial distance from the centre of rotation; (C) M* vs. r plot: the value of M* extrapolated to the cell base = $M_{w,app}$ the apparent weight average molecular weight for the whole distribution. (D) Point or local apparent weight average molecular weight at radial position r (open circle) plotted against the local concentration c(r).

molecular weight estimates. In this case, b and κ_s were obtained from the study by Dhami et al. (1995). To calculate this equation, another exponent from MHSK (Mark – Houwink – Sakurada – Kuhn) equation was used;

$$[\eta] = \kappa_\eta M^{a} \quad (3.11)$$

The relation between a and b exponents is presented by the Tsvetkov equation (Tsvetkov et al., 1971) :

$$a = 2\text{-}3b \quad (3.12)$$

a values that have been previously published in general range from 0.9 to 1.2 (see, for example, (Bindal et al., 2007, Morris and Harding, 2013)) correspond to b values ranging from 0.26 to 0.36. To get the κ_s value using Eqn. (3.10), this value of b together with the weight average sedimentation coefficient $s_{20,w}$ = 13.0S and the corresponding weight average molecular weight value M_w = 5.9 x 10^6 Da were used (yielding κ_s = 0.225 for b = 0.26 and κ_s = 0.047 for b = 0.36). In this way, it was possible to convert sedimentation coefficient values to equivalent molecular weights for all our xanthan samples, and these are presented in Table 3.3, allowing for uncertainty in the b and k_s coefficients.

It is seen that the (weight average) molecular weights M_w from sedimentation equilibrium are all within the range 3-8 million Da, values reinforced by the sedimentation velocity/power law method, with one possible exception - the predicted M_w for the Low Pyruvate xanthan from sedimentation velocity was half that from sedimentation equilibrium suggesting that this may have a stiffer conformation (lower b value) than the others - and the Keltrol xanthan studied by Dhami et al. (1995). Also, the two xanthans with the same pyruvate and acetate

contents appear also to have different molecular weights (M_w Standard LMW ~ 3 x 10^6 Da, M_w Standard HMW~ 6 x 10^6 Da), the Standard HMW being similar to the result for Keltrol xanthan (Dhami et al., 1995), and this difference is commensurate with the differences in the sedimentation coefficients.

Table 3.3: Estimated molecular weight of xanthan from the Mark-Houwink-Kuhn-Sakurada equation *($s = \kappa_s . M^b$)*.

Sample	10^6 x M_w (Da)[a]	10^6 x M_w (Da)[a]	10^6 x M_w (Da)[b]	Frictional ratio f/f_o
	0.1M PBS	**0.3M PBS**		
Standard LMW	1. 9 ± 1.2	2.6 ± 0.5	3.2 ± 0.1	12.2
Standard HMW	6.1 ± 0.04	6.9 ± 0.1	6.1 ± 0.2	14.0
High pyruvate	3.6 ± 0.5	5.9 ± 0.1	5.9 ± 0.2	14.4
Low pyruvate	3.4 ± 0.5	4.0 ±0.4	8.0 ± 0.1	19.7

a: Estimated from the sedimentation power law equation $s^0_{20,w} = \kappa_s . M^b$

b: From sedimentation equilibrium (corrected for non-ideality using the BM value of Dhami et al. (1995)).

The fifth column in Table 3.3 compares the translational frictional ratios f/f_o, calculated from the weight average molecular weights and the sedimentation coefficients (Tanford, 1961). The f/f_o is defined as the ratio of the frictional coefficient of the macromolecule divided by the corresponding parameter for a spherical particle of the same molecular weight and anhydrous volume. The Standard and high pyruvate xanthans - Standard LMW, Standard HMW and High, all have frictional ratios all within close range of each other (12.2 - 14.4) and all are very

large implying a highly asymmetric and highly expanded, swollen molecular structure in solution. The Low pyruvate xanthan is the exception with an even higher f/f_o of 19.7, commensurate of an even stiffer or more swollen structure: intriguingly a similar value was obtained for a xanthan in 1M guanidine hydrochloride (Morris et al., 2001).

3.4.3. Dynamic Light Scattering

The translational diffusion coefficients ($D^0_{20,w}$) of xanthan samples were found by using dynamic light scattering (DLS)**.** Translational diffusion coefficients

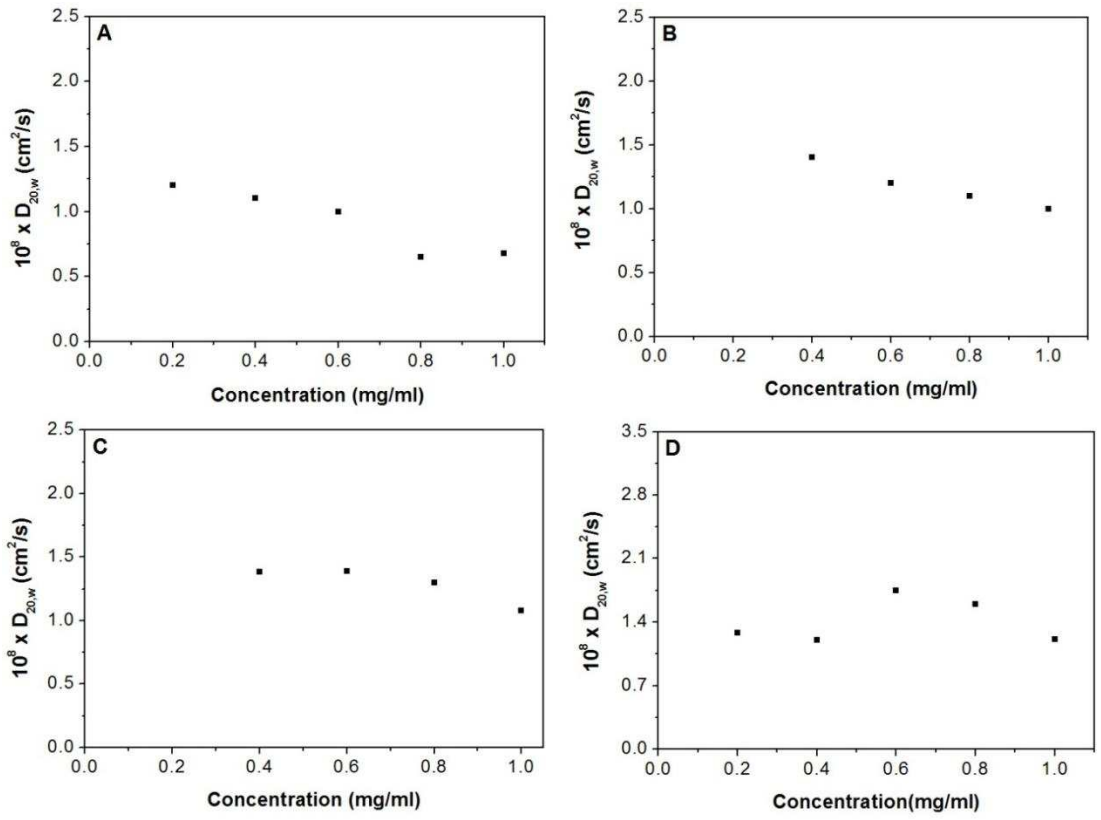


Figure 3.5a: Concentration dependence of apparent diffusion coefficient ($D_{20,w}$) vs concentration plot of xanthan samples; pH= 7.0, I = 0.1 M buffer. (A) Standard LMW (B) Standard HMW, (C) High pyruvate, (D) Low pyruvate.

Table 3.4: Summary of diffusion coefficient ($D^0_{20,w}$) for all xanthan samples.

Sample	10^{-8} x $D^0_{20,w}$ (cm^2/s)	10^{-8} x $D^0_{20,w}$ (cm^2/s)
	0.1M	**0.3M**
Standard LMW	1.37 ± 0.01	1.81 ± 0.2
Standard HMW	1.63 ± 0.13	2.27 ± 0.08
High pyruvate	1.63 ± 0.13	1.50 ± 0.21
Low pyruvate	1.47 ± 0.12	2.51 ± 0.16

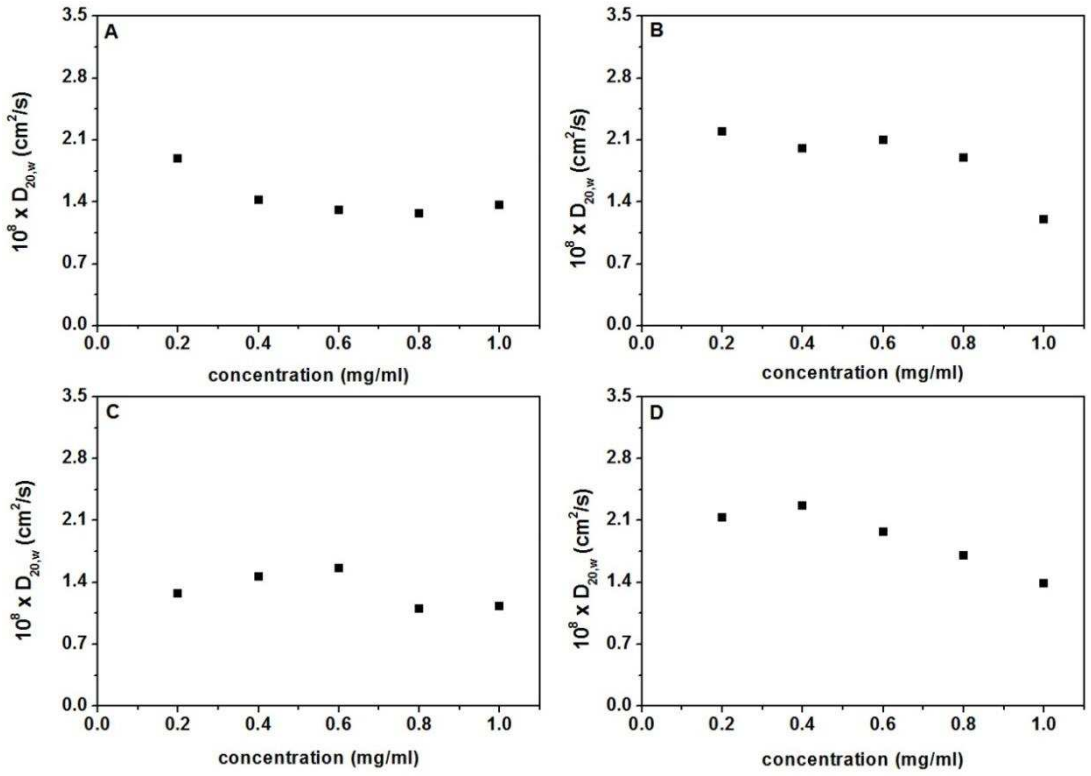


Figure 3.5b: Concentration dependence of apparent diffusion coefficient ($D_{20,w}$) vs concentration plot of xanthan samples; pH= 7.0, I = 0.3 M buffer. (A) Standard LMW (B) Standard HMW, (C) High pyruvate, (D) Low pyruvate.

were determined at the same concentration series (0.2mg/ml- 1.0 mg/ml) of each sample and two ionic conditions (I=0.1M and I=0.3M). Because of non-ideality and

the charge effect of xanthan, the translational diffusion coefficients at standard conditions were extrapolated to zero concentration and $D^0_{20,w}$ was obtained from the plot of $D_{20,w}$ vs. concentration as shown in Figure 3.5a and 3.5b.

A summary of $D^0_{20,w}$ results is presented in Table 3.4 and according to this table, the diffusion coefficients of xanthan samples were found between 1.37 x 10^{-8} to 2.51 x 10^{-8} cm^2/s. Since xanthan is a large macromolecule these values were expected at these ranges and reassuringly these values are in the same range as for previous studies on xanthan published by Southwick and co-workers (Southwick et al., 1979, Southwick et al., 1980).

3.4.4 Intrinsic Viscosity

The values of intrinsic viscosity obtained from the Huggins, Kraemer and Solomon-Ciuta extrapolation methods (using capillary viscometry) for all xanthan samples are indicated in Table 3.5. Figures 3.6a and 3.6b show the corresponding plots of viscosity (η_{red}, η_{inh} *and* $[\eta]$) versus concentration (g/ml) for xanthan samples. Intrinsic viscosities $[\eta]$ from 3 different extrapolation methods (Table 3.5) were all consistent with previously published values (2700-7000 ml/g) (see, e.g. (Tombs and Harding, 1998)), and generally to a higher precision than we obtained previously (Dhami et al., 1995). The values in Table 3.5 may be lower than the true values as they have been assumed there are no shear-dependence effects due to non-Newtonian behaviour.

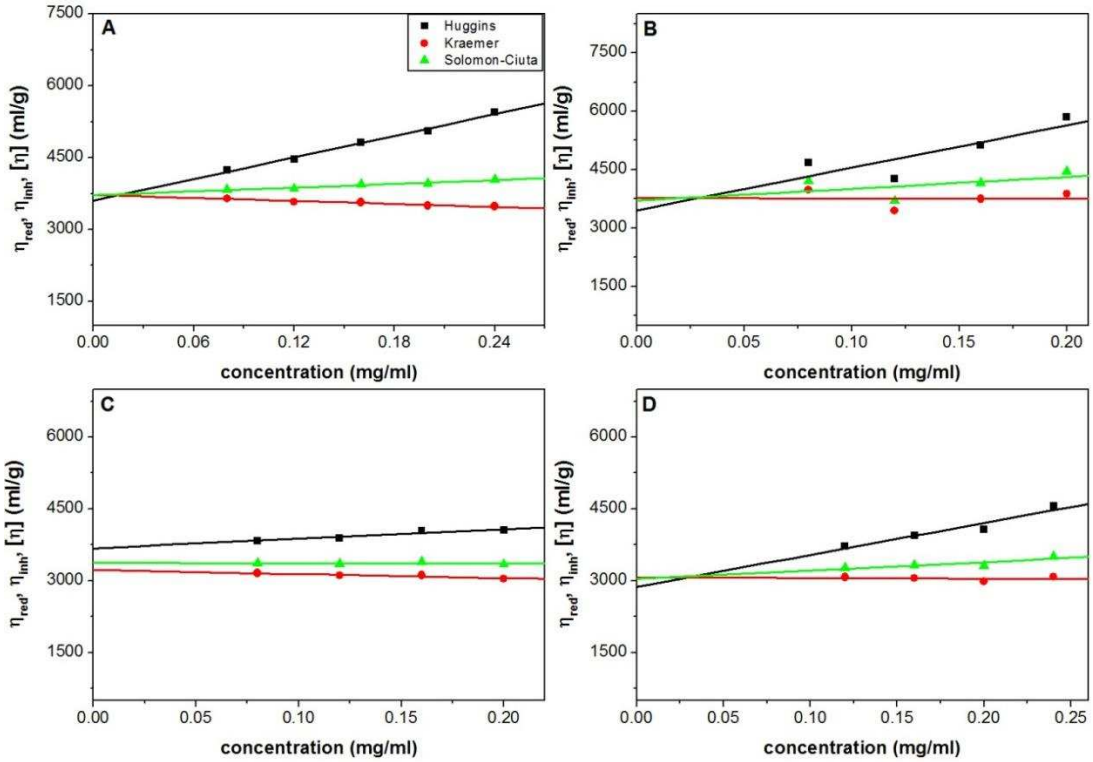


Figure 3.6a: The intrinsic viscosity plots from capillary viscometry: Huggins, Kraemer and Solomon-Ciuta extrapolations for xanthan samples; pH= 7.0, I = 0.1 M buffer. (A) Standard LMW (B) Standard HMW, (C) High pyruvate, (D) Low pyruvate.

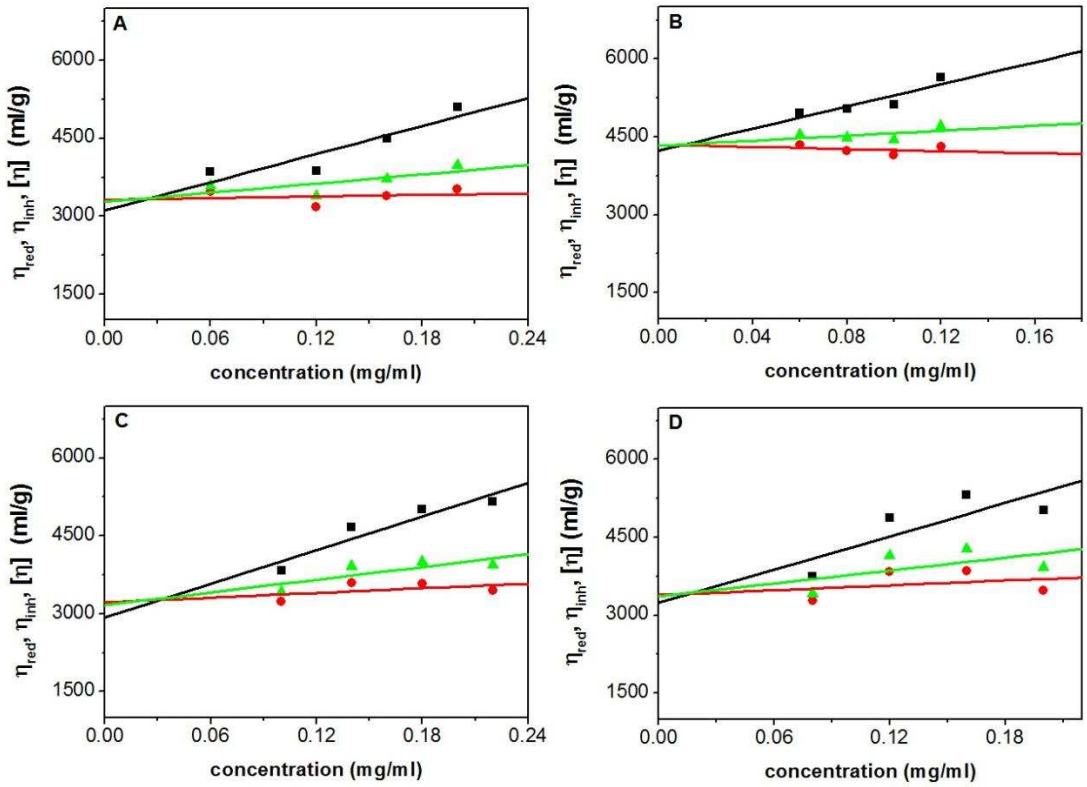


Figure 3.6b: The intrinsic viscosity plots from capillary viscometry: Huggins, Kraemer and Solomon-Ciuta extrapolations for xanthan samples; pH= 7.0, I = 0.3 M buffer. (A) Standard LMW (B) Standard HMW, (C) High pyruvate, (D) Low pyruvate

Table 3.5: Summary of Intrinsic viscosity values of xanthan samples obtained from capillary viscometry.

Sample	Solvent	Intrinsic viscosity *[η]* (mL/g)		
		Capillary viscometry		
		Huggins	Kraemer	Solomon-Ciuta
Standard LMW	**0.1M PBS**	3500 ± 760	3800 ± 460	3700 ± 540
Standard LMW	**0.3M PBS**	3100 ± 420	3300 ± 250	3300 ± 300
Standard HMW	**0.1M PBS**	3600 ± 60	3700 ± 25	3700 ± 30
Standard HMW	**0.3M PBS**	4200 ± 350	4300 ± 220	4300 ± 250
High pyruvate	**0.1M PBS**	3400 ± 130	3400 ± 80	3400 ± 100
High pyruvate	**0.3M PBS**	3000 ± 460	3200 ± 320	3200 ± 370
Low pyruvate	**0.1M PBS**	3400 ± 180	3400 ± 160	3400 ± 180
Low pyruvate	**0.3M PBS**	3200 ± 830	3400 ± 540	3400 ± 630

3.4.5. Conformational Analysis

3.4.5.1. Wales-van Holde Ratio (R)

Wales-van Holde ratio is (Wales and Van Holde, 1954) the simplest guidance/indicator of a molecule conformational flexibility. The limits are ~ 1.6 for a compact sphere or a non-draining random coil (Creeth and Knight, 1965), and <1 for rods (Tombs and Harding, 1997). Wales-van Holde ratio, R, is;

$$R = k_s / [\eta] \qquad (3.13)$$

The k_s is concentration dependence coefficient or the Gralen parameter and $[\eta]$ is intrinsic viscosity. The R results of xanthan samples are given in Table 3.6.

Table 3.6: Wales-van Holde ratio (R) determined from intrinsic viscosity and concentration dependence coefficient results for xanthan samples.

Sample	$k_s/[\eta]$	$k_s/[\eta]$
	0.1M	**0.3M**
Standard LMW	0.55	1.1
Standard HMW	1.13	1.1
High pyruvate	0.88	1.25
Low pyruvate	0.67	0.95

According to Table 3.6, it can be seen that xanthan samples have rigid rod conformation. When the ionic strength increased from 0.1M to 0.3M, the rigidity of xanthan Standard LMW, High pyruvate and Low pyruvate reduced. Xanthan Standard HMW was not affected from alteration of ionic strength. As it has been said earlier, xanthan Low pyruvate has the lowest pyruvate substituent and due to this, Wales-van Holde ratio (R) of xanthan Low pyruvate is the lowest since the pyruvate group on the side of xanthan induce disordered structure (Viebke, 2005).

3.4.5.2. Molecular Conformation Zoning

The sedimentation conformation zoning plot provide the estimation of 'overall' solution conformation of a macromolecule ranging from Zone A (extra-rigid rod) to Zone E (globular or branched) by plotting of $k_s M_L$ versus $[s]/M_L$. (Pavlov et al., 1997, Pavlov, 2013) Thus, it represents the conformation of polymer in solution

based on mass per unit length, M_L and persistent length, L_p parameters. Also, the important parameter is sedimentation coefficient, which can be estimated from the sedimentation coefficient and [s] is evaluated from this equation:

$$[s] = \frac{s^0_{20,w}\eta_{20,w}}{(1-\bar{\upsilon}\rho_{20,w})} \tag{3.14}$$

And M_L is the mass of the molecule(s) within the polymer divided by its length. In this study, M_L was taken as 2040 ($g.mol^{-1}.nm^{-1}$) from Kawakami and Norisuye (Kawakami and Norisuye, 1991) and [s] was calculated from sedimentation coefficient data.

Figure 3.7 demonstrates that the xanthan samples in both ionic strength (I=0.1M, I=0.3M) have adopted extra rigid rod conformation in Zone A. This method also shows an excellent agreement with results from Wales van Holde Ratio.

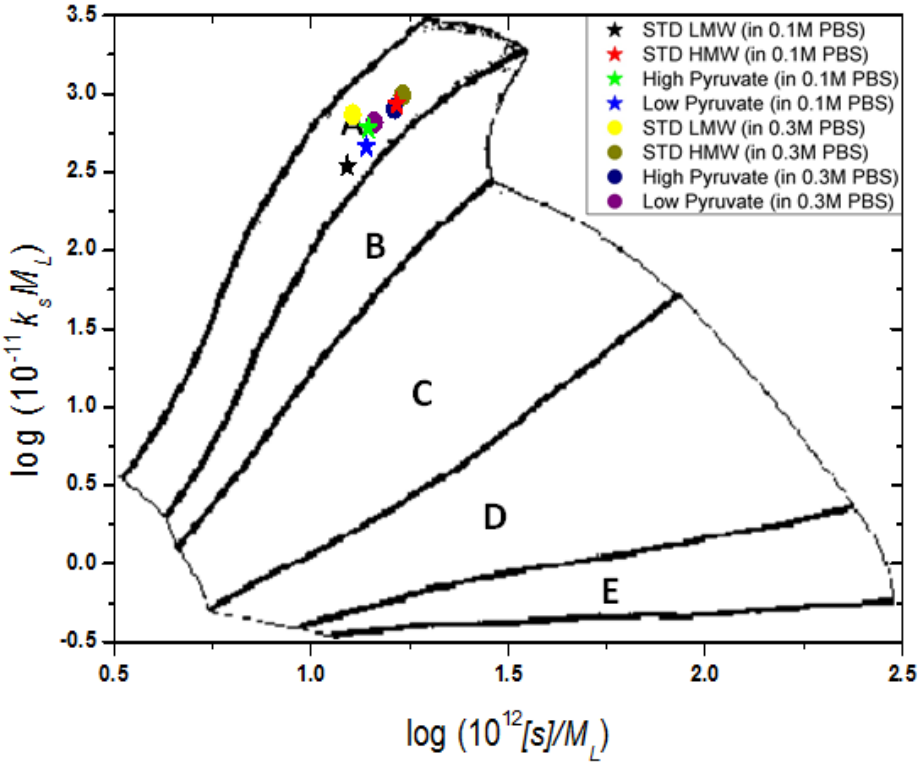


Figure 3.7: The conformation zoning plot for xanthan samples in both ionic strengths (I=0.1M and I=0.3M) which are adopted extra rigid rod structures (Zone A).

3.5. DISCUSSION

Despite the difficulties and challenges that xanthans present with regards molecular characterization, it was possible to make a measurable comparison of material with different pyruvate contents. All four xanthans appear unimodal in sedimentation velocity and reliable estimates for the sedimentation coefficients (corrected for non-ideality by extrapolation to c = 0) were made. The values obtained in this study are in complete agreement with previous studies performed by Dhami et al. (1995) and Harding et al. (2012) with values in the range 9-13.5S. (Dhami et al., 1995, Harding et al., 2012).

Sedimentation equilibrium experiments are less sensitive than sedimentation velocity and, although absolute (yield the weight average molecular weight M_w, directly) require higher concentrations (>0.3 mg/ml) to get a sufficient signal for reliable analysis. Xanthans are hugely non-ideal because of their high exclusion volumes, even under conditions of high ionic strength (I = 0.3 M), used to suppress the polyelectrolyte contribution. Because of the constraint of a low critical overlap concentration (~0.6 mg/ml) as it was found previously (Dhami et al., 1995) this removed the possibility of a standard concentration extrapolation of the apparent weight average molecular weight $M_{w,app}$ to c = 0 to yield M_w. Despite this, possible strategy for yielding estimates for M_w, based on the earlier measurements of the non-ideality contribution, and these estimates were, with one exception (the low pyruvate Low xanthan) supported by the sedimentation coefficient data and application of the power law relation (Eqn. (3.9)) linking s with molecular weight.

Intrinsic viscosities [η] from 3 different extrapolation methods agreed with previously published values (2700-7000 ml/g) (see, e.g., (Tombs and Harding, 1997)). Results showed the influence of ionic strength on xanthan Standard LMW, High pyruvate and Low pyruvate that when it decreased the intrinsic viscosity is increased. Since increasing ionic strength resulted in suppression of side chains, it helped the compaction of the macromolecule so the viscosity decreased with increasing ionic strength of solution. The viscosity values of xanthan Standard HMW did not decrease in contrast to Standard LMW, High pyruvate and Low pyruvate and it increased with ionic strength increment. According to Rinaudo however, the local stiffness of different polysaccharides can permit different viscosities at the same molecular weight (Rinaudo, 2006).

With reference to this, it can be said that increasing ionic strength probably increased the local stiffness of xanthan Standard HMW. Therefore, the viscosity of Standard HMW has higher when the ionic strength was 0.3M. Furthermore, the viscosity results are consistent with the sedimentation coefficients. It is also possible to comment on conflicting claims with regards the effect of pyruvate content on viscosity. Although Sanford et al. (1977) deduced that high pyruvate xanthan is more viscous than low pyruvate xanthan in solution with supporting electrolyte, Smith et al. (Smith et al., 1981), Bradshaw et al. (Bradshaw et al., 1983), Callet et al. (Callet et al., 1987), Khouryieh et al. (Khouryieh et al., 2007) and Pinto et al. (Pinto et al., 2011) have concluded that an increased pyruvate level does not lead to an increase in viscosity. At the ionic strength used in this study, it appears that intrinsic viscosities are independent of pyruvate content. In other research by Janin (Janin, 2015), it was showed that at lower ionic strengths the intrinsic viscosity increases with increasing pyruvate content, consistent with a lowering of classical charge shielding phenomena. At I = 0.3 M the influence of molecular weight on [η] may be being offset by the influence of differing levels of pyruvate, leading to a set of xanthans with apparently different molecular weights but all with apparently similar intrinsic viscosities.

Dynamic light scattering also proved highly useful. Estimated values for the translational diffusion coefficient ($D_{20,w}$) for these four xanthan samples in the concentration range from 0.2 mg/ml - 1.0 mg/ml are shown in Fig. 3.5. Encouragingly, only the Standard HMW and Low Pyruvate xanthans showed evidence of possible discontinuity >0.8 mg/ml and below this, values were generally ~2.0 x 10^8 cm^2/s. Although these values are in general agreement with a study by Southwick and co-workers (1979), they should be taken as only apparent values as

rotational diffusive effects may still be significant even at a scattering angle of 12.8° because of their very large, elongated structures (Burchard, 1992).

In terms of conformation, Wales-van Holde ratio and conformation zoning approaches indicated that the all samples adopted a rigid rod type conformation and showed an excellent agreement with Takada et al. (Takada et al., 1991), Berth at al. (Berth et al., 1996), Sattler et al. (Sattler et al., 2007) and Choi et al. (Choi and Yoo, 2009).

3.6. CONCLUSION

In this study, four different xanthan samples that have different acetate and pyruvate ratios has been characterised using the techniques; viscometry, analytical ultracentrifugation (AUC) and dynamic light scattering (DLS). The hydrodynamic properties were studied with two different ionic conditions; 0.1M and 0.3M. For the molecular weight determination, analytical ultracentrifuge (XL-I) and size exclusion chromatography coupled with multi angle light scattering (SEC-MALL) methods have been applied. Due to the electrostatic charge and extended structure of xanthan polymer, sedimentation equilibrium and SEC-MALL methods could not be carried successfully out. However, the sedimentation velocity in the analytical ultracentrifuge, viscometry and dynamic light scattering with low angle methods has been successfully applied to samples. Sedimentation velocity method also gave estimations about conformation and molecular weight of xanthan samples. For three xanthan samples- xanthan Standard LMW, High pyruvate and Low pyruvate - showed more rigidity with increasing ionic strength and the influence of ionic strength on xanthan is consistent with sedimentation coefficient, diffusion coefficient and the viscometry results. Increasing ionic strength has showed an adverse effect on

xanthan Standard LMW. Meanwhile, the conformation results showed a perfect agreement with the previous results, and the rigid rod conformation was proved by Wales van Holde Ratio and molecular conformation zoning.

CHAPTER 4

A STUDY ON SOLUTION PROPERTIES AND MOLECULAR CONFORMATION OF LOW ACYL GELLAN GUM

4.1. INTRODUCTION

Gellan gum is an extracellular anionic heteropolysaccharide produced by Sphingomanas elodea (Morris et al., 2012). The linear molecular structure consists of a repeating tetrasaccharide unit of two substituents β-D-glucose, one of β-D glucoronate and one of α-L-rhamnose. There are two types of acyl residues in native form: an L-glyceryl residue on O(2) of the 3-linked glucose substituent of the tetrasaccharide chain and an acetyl group at O(6) of the same residue (Figure 4.1). These residues are removed by an alkaline process and according to mildness of this process, the gellan is called 'low acyl gellan' and 'high acyl gellan'. (Prajapati et al., 2013).

Gellan gum forms thermoreversible, brittle and rigid gels in the presence of mono and divalent cations. These cations have an effect on the conformation of gellan gel, which undergoes a change from a single (disordered state) to double helix (ordered state) through decreasing temperature (Takahashi et al., 2004, Ogawa, 1999). The

effect and selectivity of mono and divalent cations on the conformation of gellan gel studies indicated that the divalent cations are more effective than monovalent

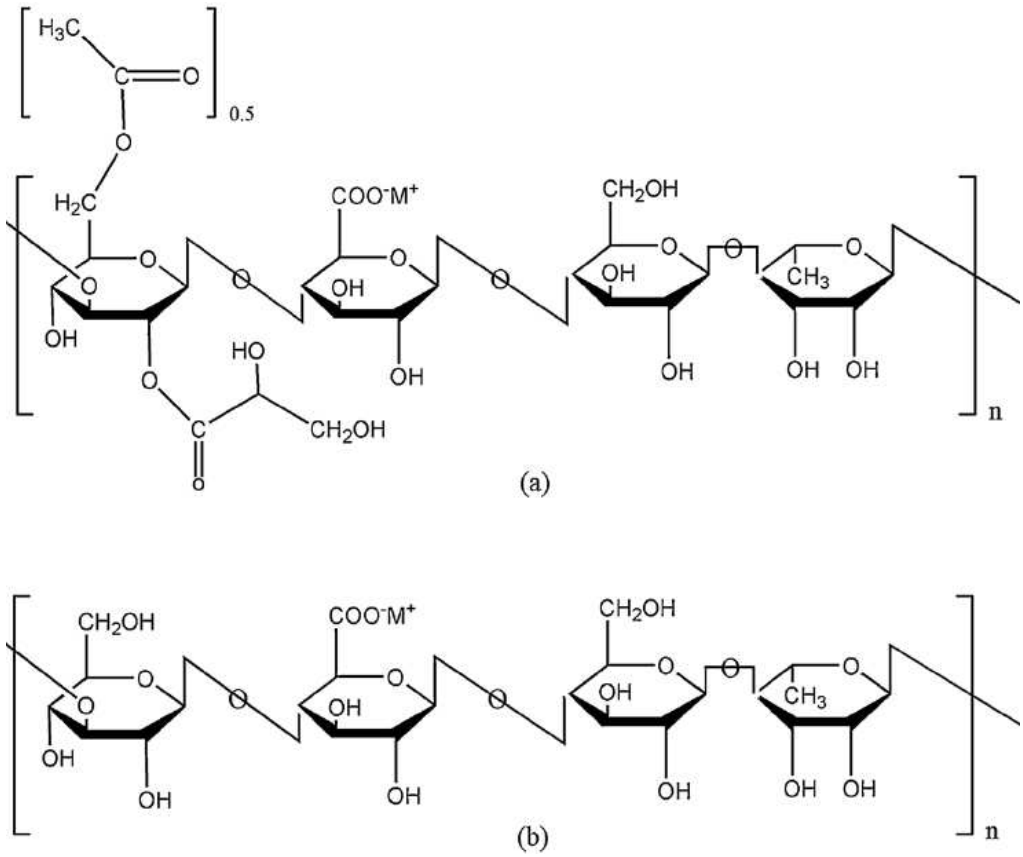


Figure 4.1. Chemical structure of (a) native and (b) deacetylated gellan gum adapted from (Prajapati et al., 2013)

cations in terms of double helix stability by shielding effectively the electrostatic repulsion on charge groups. Additionally, it was observed that there is not any difference between Ca^{++} and Mg^{++} for divalent cations and Cl, Br, I for monovalent cations whereas the order of monovalent cations is $K^{+} > Na^{+} > Li^{+}$ with regards to selectivity in gel state (Milas and Rinaudo, 1996, Kani et al., 2005, Ogawa et al., 2002).

The rheological and physicochemical properties of low and high acyl gellan have been extensively studied before (Miyoshi et al., 1994, Gunning et al., 1996, Caggioni et al., 2007) but attempts at determining solution properties of gellan gum have been hampered because of the aggregation caused by existing cations in the sample. Milas and co-workers (Milas et al., 1990) estimated the average molecular weight 4.9×10^5 Da for gellan in the presence of tetramethylammonium (TMA) salt, whereas Takahashi et al. (Takahashi et al., 2004) estimated 2.3×10^5 Da for gellan in 25mM NaCl salt using static light scattering. Since the conformation of polysaccharide in solution was considered to play an important role in the structure-function relationship and in interaction with other biopolymers, transition of the ordered double helix conformation to disordered coil conformation was also observed by these researchers by temperature changes. The persistence lengths of gellan were estimated to be ~9.4nm for disordered, ~98nm for the ordered conformation state by Takahashi et al. from six depolymerised Na-gellan samples which were obtained by ultrasonication (Takahashi et al., 2004).

In this current study, the "pressure cell" solubilisation method, which was applied for galactomannans by Picout and co-worker (Picout et al., 2002) to break the main chain of polysaccharide and induce the solubility, was used to obtain knowledge about solution properties of gellan gum in 25mM NaI solution by depolymerising the sample. This method was successfully employed previously by (Kök et al., 2009, Almutairi, 2015). The hydrodynamic properties of untreated low acyl gellan and depolymerised gellan samples were studied in solution to assess the structural unity in terms of sedimentation coefficient, molecular weight, intrinsic viscosity, conformation and overall conformational flexibility by taking advantage of using the sedimentation velocity and equilibrium in analytical ultracentrifugation (AUC). The

flexibility of samples in terms of persistence length (L_p) and mass per unit length (M_L) values were also estimated using a more recent approach, the global conformational analysis method an algorithm known as Multi-HYDFIT.

4.2. MATERIALS

The low acyl gellan gum (LAG) was provided by CP Kelco (Denmark) and samples were used as supplied without any further purification. A stock solution of gellan samples were dissolved in 25mM NaI solution by heating at 60°C for 20 min. The concentrations, c (g/ml) of the stock gellan solutions were measured after using an Atago (Japan) DD-7 refractometer calibrated with glucose standards, and a refractive increment dn/dc of 0.154 ml/g (Takashi et al, 2004). The solutions of gellan gum (LAG) were firstly ultrasonicated with a VWR Ultrasonicater Bath-USC 1700 THD series (VWR International, UK) at 480W and 45 kHz for 15hours to produce different molar mass of sample LAG1. Since the ultrasonication method was not effective as expected, then the gellan solutions were exposed to microwave (see, e.g. Wood et al, 2002) heating in an 800 W microwave oven (Panasonic UK Ltd. Bracknell, UK) using a high pressure vessel for different time periods (45sec-60sec) to produce different molar masses (LAG2-45 sec microwaved, LAG3-50sec microwaved, LAG4-55sec microwaved, LAG5-60sec microwaved). The temperature and pressure within the "bomb" were not measured.

4.3. METHODS

4.3.1. Partial Specific Volume

A DMA 5000M density meter (Anton Paar, UK) was used to measure the density of gellan solution (concentration ranging 0.5-2.5mg/ml) so as to determine the partial specific volume using the mechanical oscillator technique according to the procedure of Kratky et al. (Kratky et al., 1973). The partial specific volume was calculated using the equation below;

$$\bar{\upsilon} = \frac{1 - d\rho/dc}{\rho_0} \tag{4.1}$$

where $\bar{\upsilon}$ is the partial specific volume (ml/g), ρ_0 is the density of the solvent (g/ml), $d\rho/dc$ is the density increment which can be obtained from the limiting slope of the plot of solution density versus concentration.

4.3.2. Sedimentation Velocity (SV)

Sedimentation velocity experiments were performed using an Optima XL-I (Beckman Instruments, Palo Alto, USA) equipped with Rayleigh interference optics. Solution concentrations ranging between 0.1 – 1.4 mg/ml for each gellan were studied at a temperature of (20.0 ± 0.1) °C. 400µl of solution and an equal volume of the 0.25mM NaI reference buffer/solvent (400µl) were injected into the solution and solvent channels respectively of 12 mm optical path length double sector cells. Scans were taken at 2 min intervals for a run time of approximately 16 hours at 40000 rpm. A partial specific volume, $\bar{\upsilon}$ of -0.602 ml/g- was used for the gellan according to the density meter measurements. For comparison purposes, sedimentation coefficients

were normalised to standard solvent conditions, namely the density and viscosity of water at 20.0°C (Abdelhameed, 2010, Laue and Stafford III, 1999):

$$s_{20,w} = \{(1-\bar{\upsilon}\rho_{20,w}) / (1-\bar{\upsilon}\rho_0)\} \cdot \{\eta_0 / \eta_{20,w}\} s_{T,b} \qquad (4.2)$$

where ρ_0 and η_0 are respectively the density and viscosity of the solvent or buffer, b, at temperature T, and ρ_0 and $\eta_{20,w}$ the corresponding values of water at 20.0 °C. The data was analysed using the "least squares ls-g(s) model" SEDFIT program of Schuck and colleagues (Dam and Schuck, 2004) in terms of distributions of sedimentation coefficient distribution. The s and $s_{20,w}$ values are 'apparent' values because of non-ideality. To remove this effect, $s_{20,w}$ is extrapolated to zero concentration and $s^0_{20,w}$ is obtained from the reciprocal plot of $s_{20,w}$ ($1/s_{20,w}$) vs. concentration (see (Harding, 2005c)):

$$1/s_{20,w} = (1/ s°_{20,w}).(1+k_s c) \qquad (4.3)$$

where $s^0_{20,w}$ is sedimentation coefficient at zero concentration and standard condition, k_s is the Gralen parameter (Gralen, 1944); see also (Harding, 2005a).

4.3.3. Sedimentation Equilibrium (SE)

The weight average molecular weight, $M_{w,app}$ of gellan samples were determined using the Beckman (Palo Alto, California, U.S.A.) Optima XL-I analytical ultracentrifuge and employing Rayleigh interference optics and an automatic on-line data capture system. 20 mm optical path length double-sector cells with sapphire windows were loaded with (~130µl) of sample ranging 0.2-1.6mg/ml and a matching amount of reference buffer (0.25mM NaI) in appropriate channels. The balanced cells were then loaded into an analytical 8-hole titanium rotor An50-Ti and placed in

the AUC. After time was allowed for vacuum formation and for temperature equilibration (20.0 °C), the rotor was then accelerated to 4500 rpm for LAG, LAG1 and LAG2, 6000 rpm for LAG3 AND LAG4, and 9000 rpm for LAG5. Using the Rayleigh interference optical system, scans were taken every one hour and equilibrium was reached after approximately 72 hours for LAG3, LAG4 and LAG5, and 96 hours for LAG, LAG1 and LAG2. Record of the relative concentration distribution of the solute at equilibrium was analysed to give the weight average apparent molecular weight, $M_{w,app}$, using the SEDFIT-MSTAR program implemented by Schuck et al. (Schuck et al., 2014) based on the algorithm of Cölfen and Harding (Cölfen and Harding, 1997) and the M* function of Creeth and Harding (Creeth and Harding, 1982).

4.3.4. Capillary and Differential Pressure Viscometry

Untreated and treated gellan solutions ranging from 0.1 mg/ml to 1.25 mg/ml were analysed using a Schott-Geräte Ostwald viscometer system at a temperature of (20.0 ± 0.01) °C. The relative viscosity, η_{rel}, was obtained from the ratio of the flow time of the solution t (sec) to the flow time of solvent ($\eta_{rel} = (t/t_o)$), where the flow time was recorded accurately using photosensors. Because of the low concentrations, a density correction was deemed unnecessary (Harding, 1997). The reduced viscosity ($\eta_{red} = (\eta_{rel}-1)/c$) and the inherent viscosity ($\eta_{inh} = (ln\eta_{rel})/c$) were extrapolated to zero concentration to eliminate non-ideality effects with the common intercept at c=0 yielding the intrinsic viscosity $[\eta]$ from Huggins and Kraemer equations:

$$\eta_{red} = [\eta] (1 + K_H.[\eta].c) \quad (4.4)$$

and

$$(ln\eta_{rel})/c = [\eta]\ (1 - K_K.[\eta].c) \quad (4.5)$$

where K_H and K_K are the Huggins (1942) and Kraemer (1938) constants, respectively. As an additional check, a combined Solomon & Ciuta (1962) relation was also used:

$$[\eta] \sim (1/c).\ [2\ (\eta_{sp} - ln\ (\eta_{rel}\ ))]^{1/2} \quad (4.6)$$

The assumption has been made that there was no shear dependence of $[\eta]$ under creeping flow conditions in the capillary viscometer.

4.4. RESULTS

4.4.1. Partial Specific Volume

Partial specific volume is an important parameter to calculate of sedimentation coefficient and weight average molecular weight from sedimentation equilibrium

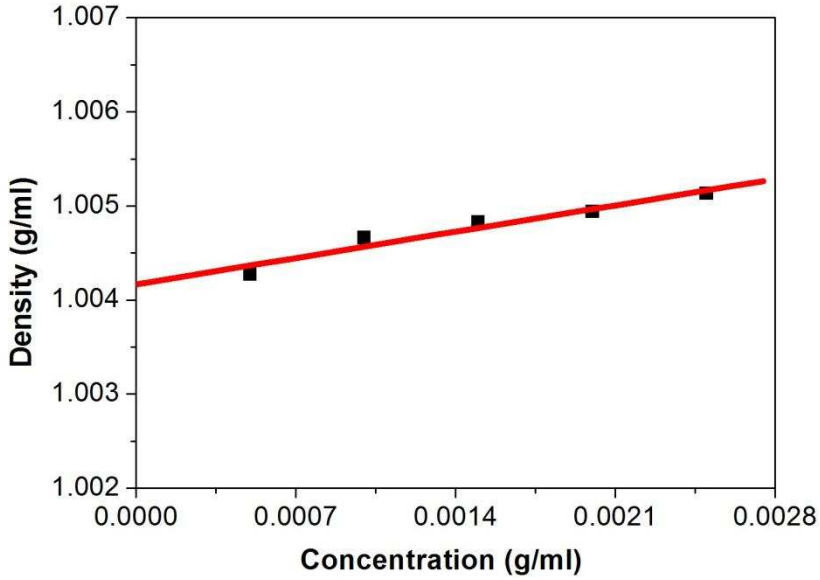


Figure 4.2. Determination of partial specific volume of LAG using density measurement in NaI at 20°C.

experiment. The partial specific volume, $\bar{\upsilon}$ of gellan was measured as (0.602 ± 0.05) ml/g and it was calculated from the slope of the solution density versus concentration (Figure 4.2). This value is comparable to the values for xanthan (Dhami, 1996) and similar with pullulan (Kawahara et al., 1984).

4.4.2. Sedimentation Velocity (SV)

Sedimentation velocity method was used to determine the heterogeneity of solutions and measure their sedimentation coefficients as well. The sedimentation coefficient (s), of untreated gellan and depolymerized gellan samples were measured at various concentrations by the least square ls-g*(s) method. Figure 4.3 shows the bimodal sedimentation coefficient distribution for all samples and the concentrations. In Figure 4.2, two peaks were identified for each concentration studied and for all samples. Peak 1 (the minor peak) is around ~1S which shows the small molecular weight component and peak 2 (the main component) is around ~2S - 3S, which indicated higher molecular weight component in the sample. The hyper sharp peaks can be observed at higher concentration for all samples, which is an indication of high concentration dependency and it was proved by k_s values in Table 4.1.

Table 4.1: Summary of $s^{0}_{20,w}$ and k_s for untreated and microwaved gellan samples.

Sample	$s^{\circ}_{20,w}$ (S)	k_s (ml/g)
LAG	3.24 ± 0.08	1510 ± 190
LAG1	3.06 ± 0.08	1040 ± 100
LAG2	2.93 ± 0.10	1090 ± 135
LAG3	2.60 ± 0.08	620 ± 70
LAG4	2.57 ± 0.02	590 ± 20
LAG5	2.34 ± 0.04	330± 20

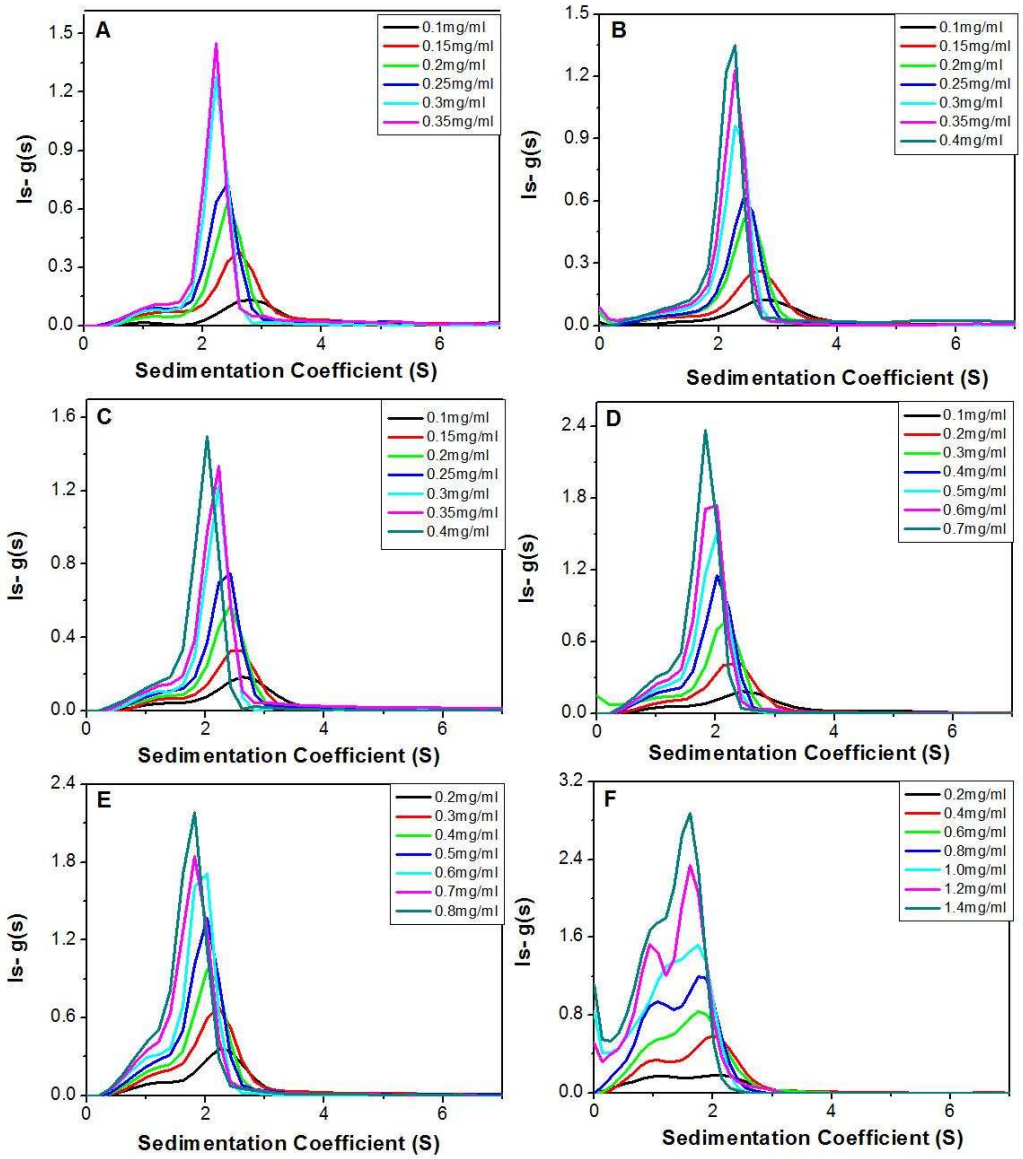


Figure 4.3: Sedimentation coefficient distribution profiles using least squares g*(s) method of SEDFIT obtained from sedimentation velocity experiment for gellan samples in 0.25mM NaI; (A) LAG, (B) LAG1, (C) LAG2, (D) LAG3, (E) LAG4, (F) LAG5.

The Figure 4.4 shows the reciprocal plots of apparent sedimentation coefficient versus concentration (for the main component) to eliminate the non-ideality effect. The slope of these plots gives the concentration dependence parameter k_s (Gralén coefficient) for each sample and presented on Table 4.1.

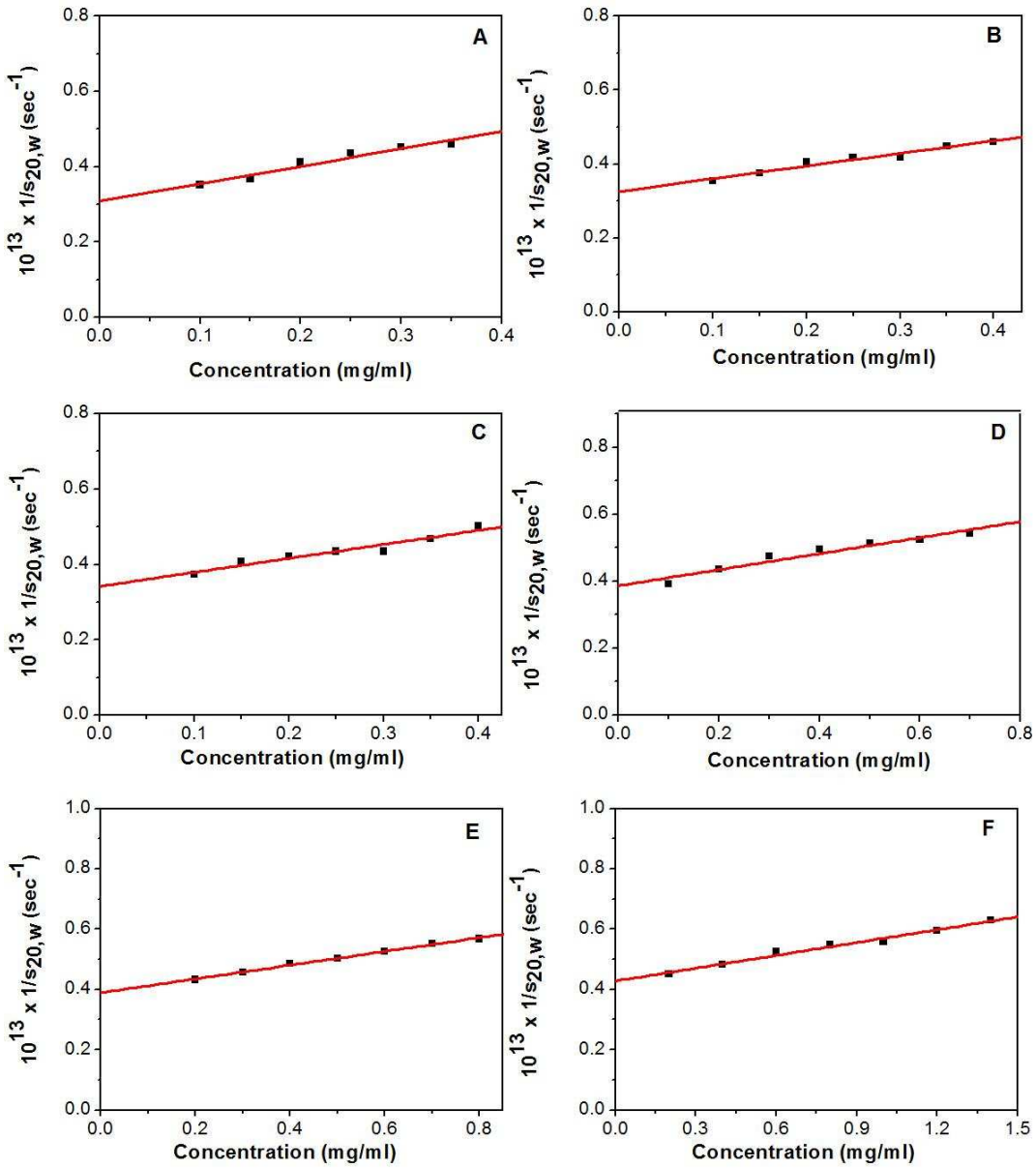


Figure 4.4: Concentration dependence (reciprocal) of the sedimentation coefficient plot (after correction to standard solvent conditions) for gellan samples in 0.25mM NaI (A) LAG, (B) LAG1, (C) LAG2, (D) LAG3, (E) LAG4, (F) LAG5.

4.4.3. Estimation of Molecular Weight

The weight average molecular weight of untreated and microwaved gellan samples were estimated by the sedimentation equilibrium method in the analytical

ultracentrifuge. The use of long optical path length cells (20.0 mm) enabled the investigation the gellan samples at relatively low concentration (0.2 mg/ml) for this experiment. Thus, the non-ideality effect in solution from excluded volume and charge effects can be minimized. To achieve this, the samples were run at different loading concentration ranges 0.2-1.6mg/ml. The data then was analysed using SEDFIT-MSTAR program to obtain weight average molecular weight (for example Figure 4.5).

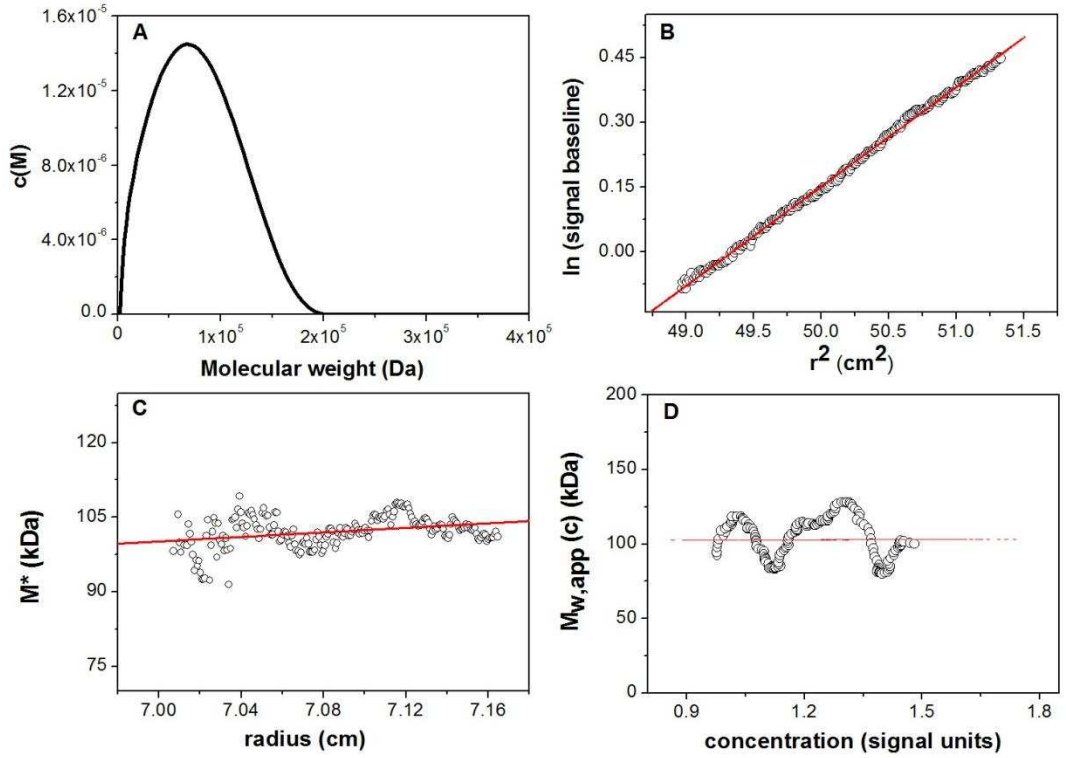


Figure 4.5: SEDFIT-MSTAR analysis of LAG in 25mM NaI at a loading concentration of 0.3 mg/ml (A) molecular weight distribution, c(M) vs. M plot; (B) log concentration ln c(r) vs. r^2 plot, where r is the radial distance from the centre of rotation; (C) M* vs. r plot: the value of M* extrapolated to the cell base = $M_{w,app}$ the apparent weight average molecular weight for the whole distribution. (D) Point or local apparent weight average molecular weight at radial position r (open circle) plotted against the local concentration c(r).

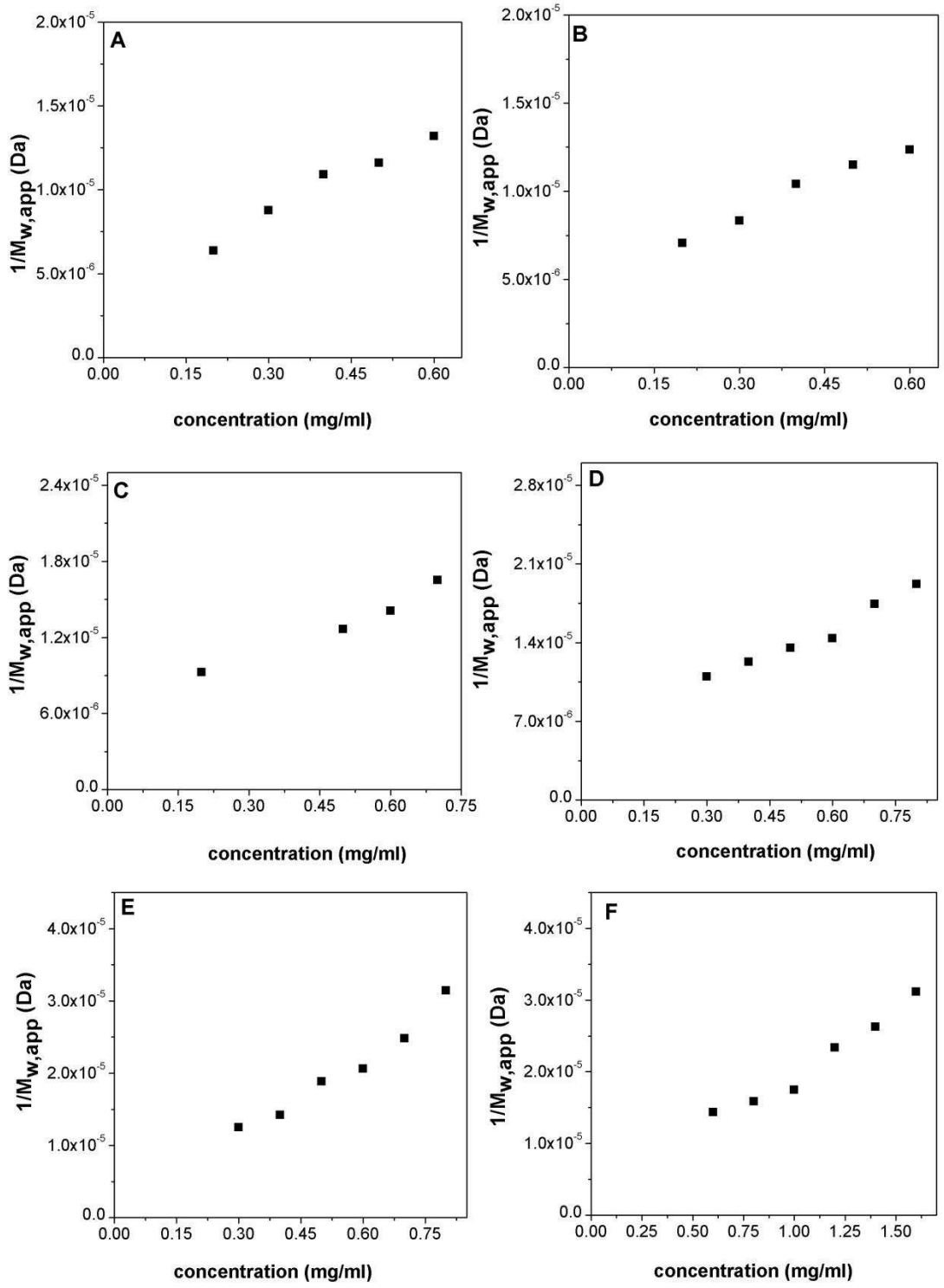


Figure 4.6: The reciprocal plots of the apparent weight average molecular weight ($M_{w,app}$) against concentration c (g/ml) for gellan samples in 0.25mM NaI (A) LAG, (B) LAG1, (C) LAG2, (D) LAG3, (E) LAG4, (F) LAG5.

The reciprocal plots of $M_{w,app}$ versus concentration were shown in Figure 4.6. The weight average molecular weight values were then yielded from the slope of these extrapolations and presented in Table 4.2. The results indicates that depolymerisation by microwave heating induced the reduction in molar mass with increasing heating time for gellan samples.

Table 4.2: Summary of weight average molecular weights (M_w) results for original low acyl and depolymerised gellan samples.

Sample	10^3 x M_w (Da)[a]
LAG	280 ± 13
LAG1	226 ± 26
LAG2	178 ± 29
LAG3	161 ± 24
LAG4	88 ± 30
LAG5	76 ± 20

4.4.4. Intrinsic Viscosity

The intrinsic viscosity values for gellan samples were measured by capillary viscometry and are presented in Table 4.3. Figure 4.7 demonstrated linear extrapolations in all samples for Huggins, Kraemer and Solomon-Ciuta plots. Heating the original gellan sample led to the degradation of the polymer chain, and resulted in a decrease in intrinsic viscosity. These results are also consistent with

those of sedimentation coefficient and molecular weight measurements, supporting the depolymerisation of gellan samples.

Table 4.3: Summary of intrinsic viscosity values of gellan samples obtained from capillary viscometry.

Sample	Intrinsic viscosity *[η]* (mL/g)		
	Huggins	**Kraemer**	**Solomon-Ciuta**
LAG	2820 ± 360	2800 ± 190	2830 ± 240
LAG1	2280 ± 340	2390 ± 230	2380 ± 360
LAG2	1860 ± 270	2050 ± 140	2010 ± 180
LAG3	1360 ± 30	1350 ± 25	1350 ± 40
LAG4	1100 ± 30	1090 ± 20	1100 ± 30
LAG5	490 ± 10	500 ± 7	500 ± 7

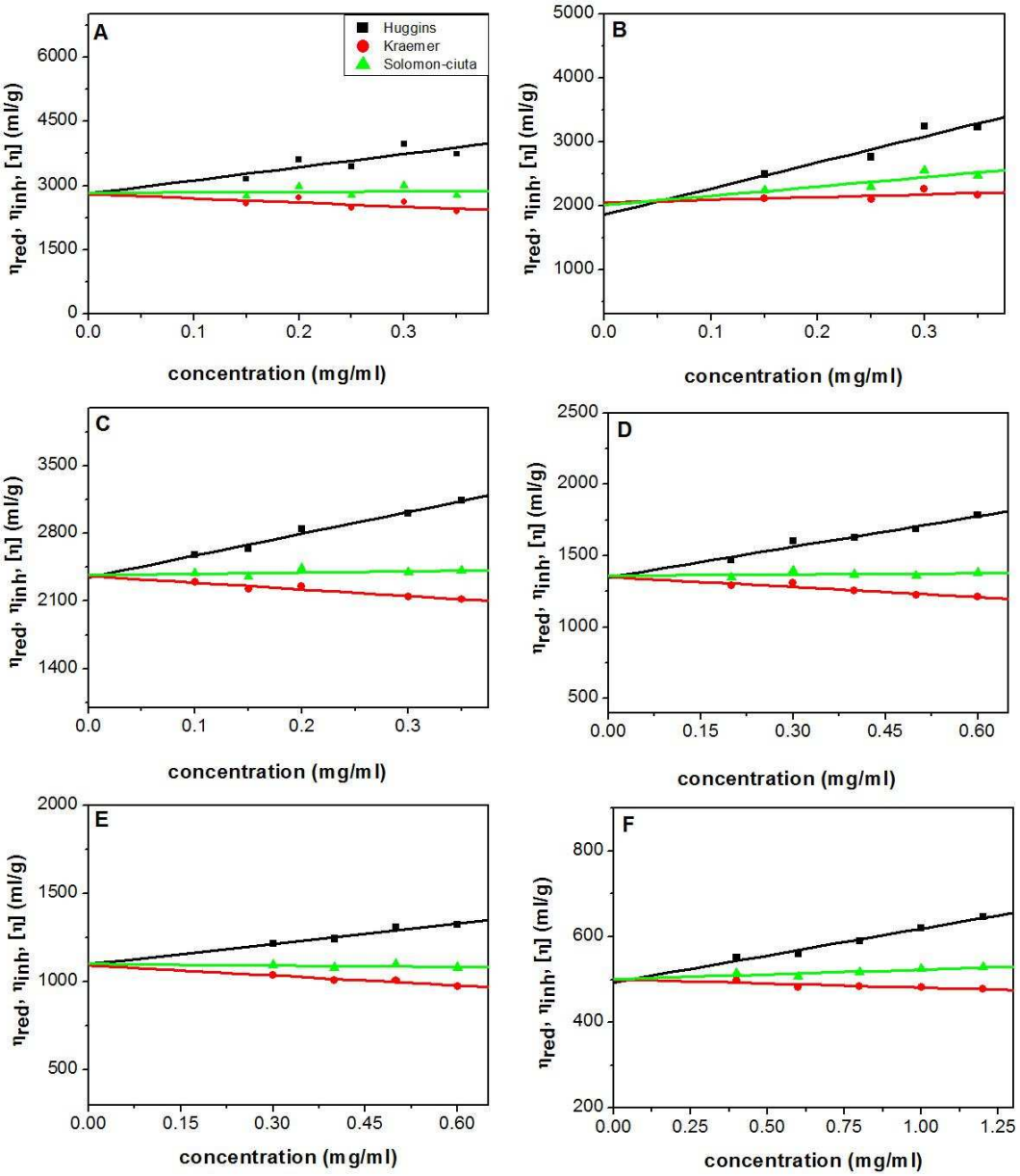


Figure 4.7: The intrinsic viscosity plots from capillary viscometry: Huggins, Kraemer and Solomon-Ciuta extrapolations for gellan samples in 25mM NaI; (A) LAG, (B) LAG1, (C) LAG2, (D) LAG3, (E) LAG4, (F) LAG5.

4.4.5. Conformation Analysis

4.4.5.1. Mark-Houwink-Kuhn-Sakurada Power Law Relationships

The Mark-Houwink-Kuhn-Sakurada (MHKS) or power law relationships is one of the simplest methods to obtain the conformation and flexibility of low acyl gellan in solution using sedimentation coefficient, intrinsic viscosity and molecular weight parameters (Harding et al., 1991c);

$$[\eta] = \kappa_\eta \, M^{\,a} \tag{4.7}$$

$$s^0_{20,w} = \kappa_s \, M^{\,b} \tag{4.8}$$

The MHKS or 'Mark-Houwink' exponents "a" and "b" are obtained from the slopes of double logarithmic plots of intrinsic viscosity, *[η],* and sedimentation coefficient, $s^0_{20,w}$ versus molecular weight M_w, respectively. The values of a and b are then used to determine conformation using 'Haug Triangle', which is a representation of the gross conformation of macromolecules. The three extremes of conformation, compact sphere, random coil and rigid rod, are placed at the corners of triangle (Tombs and Harding, 1997) with the values given at Table 4.4.

Table 4.4. **Mark-Houwink-Kuhn-Sakurada (MHKS) Power Law exponents. Adapted from (Harding, 2005b)**

Conformation	a	b
Sphere	0	0.67
Random coil	0.5-0.8	0.4-0.5
Rod	1.8	0.15

Double logarithmic plot of $s^0_{20,w}$ versus of molecular weight of all gellan samples is presented in Figure 4.8. The overall b parameter which was yielded from slope was found as (0.22 ± 0.04) between the limits of rod (0.15) and coil (0.4-0.5) according to Table 4.4. This b value is similar with chitosan (Fee, 2006, Cölfen et al., 2001).

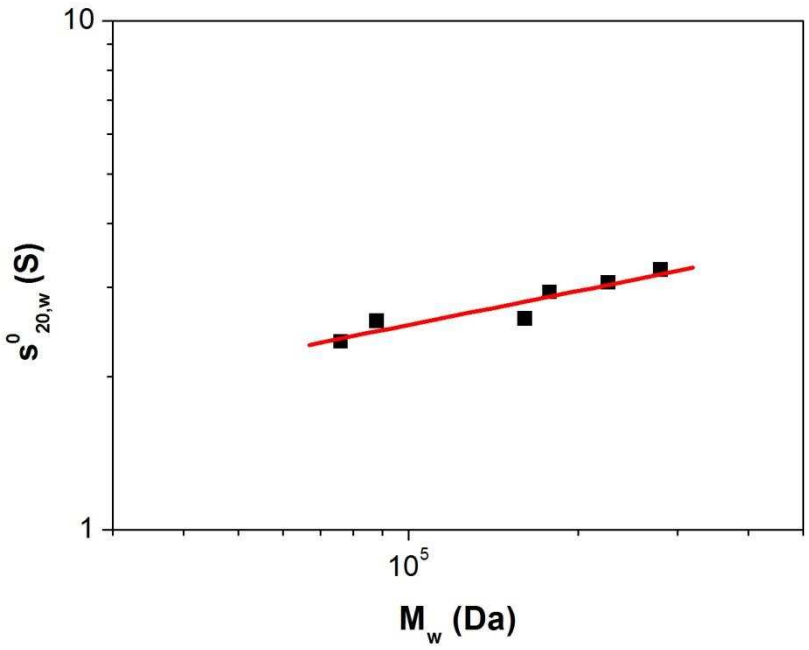


Figure 4.8: Mark–Houwink–Kuhn–Sakurada (MHKS) power law double logarithmic plot of $s^0_{20,w}$ vs M_w for gellan samples.

Figure 4.9 indicates the plot of intrinsic viscosity *[η]* vs. molecular weight, M_w for all gellan samples, where an extrapolation to infinite molecular weight gives a straight line with a slope -the power law exponents a. The obtained overall a values of gellan samples were found as (1.16 ± 0.21) which presents the conformation as a flexible rod and it was consistent with previous study from Takahashi et al. (Takahashi et al., 2004).

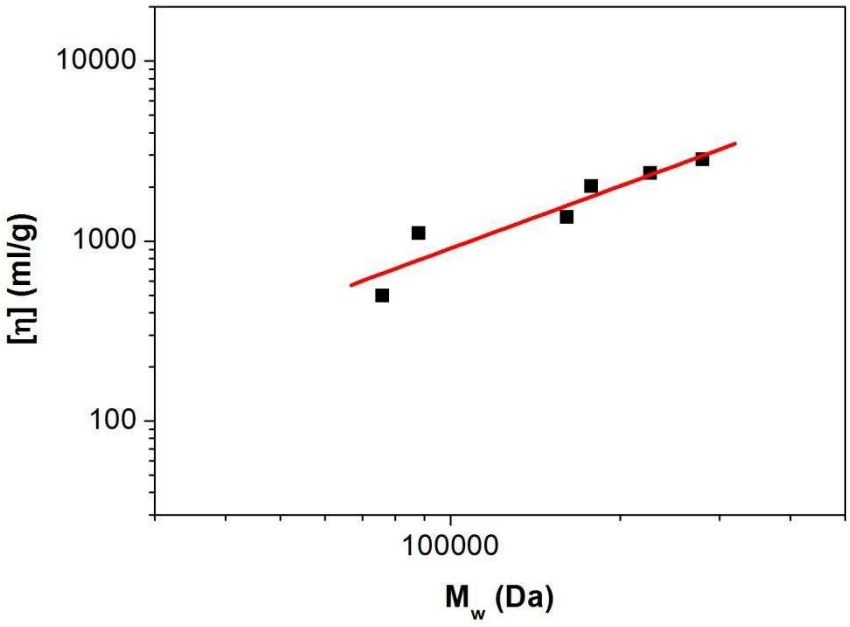


Figure 4.9: Mark–Houwink–Kuhn–Sakurada (MHKS) power law double logarithmic plot for gellan samples.

4.4.5.2. Wales-van Holde Ratio (R)

Wales-van Holde ratio (Wales and Van Holde, 1954) is the simplest guidance/indicator of a molecule conformational flexibility. The limits are ~ 1.6 for a compact sphere or a non-draining random coil (Creeth and Knight, 1965), and <1 for rods (Tombs and Harding, 1998). Wales-van Holde ratio, R is;

$$R = k_s / [\eta] \qquad (4.9)$$

The k_s is concentration dependence coefficient or the Gralen parameter and $[\eta]$ is intrinsic viscosity. The R results of gellan samples were given in Table 4.5 and it appears that all gellan samples are again consistent with rod structures with some flexibility (R ~ 0.5–0.7).

Table 4.5: **Wales-van Holde ration, R, for original low acyl and depolymerised gellan samples.**

Sample	$R= k_s/[\eta]$
LAG	0.53
LAG1	0.52
LAG2	0.58
LAG3	0.46
LAG4	0.53
LAG5	0.66

4.4.5.3. Estimation of the Persistence Length L_p and Mass Per Unit Length M_L

The persistence length L_p and M_L are representations of the bending flexibility of linear polymer chains (worm-like chains) (Harding, 2005a). L_p is defined as the average projection length along the initial direction of the polymer chain and M_L is the mass of the molecule(s) within the polymer divided by its length. Theoretically, $L_p = 0$ is for a random coil whereas $L_p = \infty$ is for the rigid rod (eg. see (Harding, 1997). However in practice limits, for random coil ~1nm (e.g pullulan) and for rigid rod ~200nm (eg. xanthan) are more suitable (Tombs and Harding, 1997). Persistence length can be estimated using different approaches either sedimentation coefficient (Yamakawa and Fujii, 1973, Hearst and Stockmayer, 1962) or intrinsic viscosity (Bohdanecky, 1983, Stockmayer and Fixman, 1963), equations.

4.5.4.3.1. Global analysis method (HYDFIT)

It is clear that using different methods to determine L_p and M_L might lead to some bias and for discrepancies in the results. To prevent this variability, the Multi-HYFIT program was developed by Ortega and Garcia de la Torre (2007) to enable estimates for consensus values of L_p and M_L and chain diameter d. To do this, the program considers two or more data sets of intrinsic viscosity *([η])*, sedimentation coefficient ($s^0_{20,w}$) and where appropriate radius of gyration (R_g) and translational diffusion coefficient (D_t) for varying molecular weights of the same substance. This program carries out minimisation of a target function known as Δ using Bushin-Bohdanecky (Bohdanecky, 1983, Bushin et al., 1981a) and Yamakawa-Fujii (Yamakawa and Fujii, 1973) equations within the several variables. The optimization process can be implemented giving different weightings to each property (Ortega and García de la Torre, 2007). To simplify and accelerate the minimization of the process, the least effective parameter or well defined parameter from known molecular structure (e.g. M_L) can be fixed .The results of simulation analysis showed that L_p is comparatively insensitive to the value chosen d. Then the Multi-HYDFIT program optimizes the parameters in order to obtain the minimisation of the target function, based on the following equations:

$$\Delta^2 = \frac{1}{N_s}\sum_{i=1}^{N_s}\left[(\sum_T W_T)^{-1}\sum_T W_T\left(\frac{a_{T(cal)}-a_{T(exp)}}{a_{T(\exp)}}\right)^2\right] \qquad (4.10)$$

$$\Delta^2 = \frac{1}{N_s}\sum_{i=1}^{N_s}\left[(\sum_I W_I)^{-1}\sum_I W_I\left(\frac{a_{I(cal)}-a_{I(exp)}}{a_{I(\exp)}}\right)^2\right] \qquad (4.11)$$

where N_s is the number of samples, W_T and W_I are the statistical weights for equivalent radii a_T and a_I and the subscripts cal and exp indicates values from

calculated and experimental values, respectively. Therefore, Δ is a dimensionless estimate of the consensus between calculated values for the frictional coefficient, intrinsic viscosity and radius of gyration for a certain persistence length, L_P and the experimentally measured parameters (Ortega et al., 2011, Patel et al., 2008b).

In this study, the chain diameter, d was fixed and L_p and M_L were treated as variables. In this case the best estimates for the persistence lengths and mass per unit lengths of gellan sample was obtained with the minimum value of the target function Δ and shown as contour plots as shown in Figures 4.10. The values of the target (error) function, Δ are represented by the full colour spectrum ranging from blue to red. The x-axis and y-axis represents L_p (nm) and M_L ($g.mol^{-1}.nm^{-1}$), respectively.

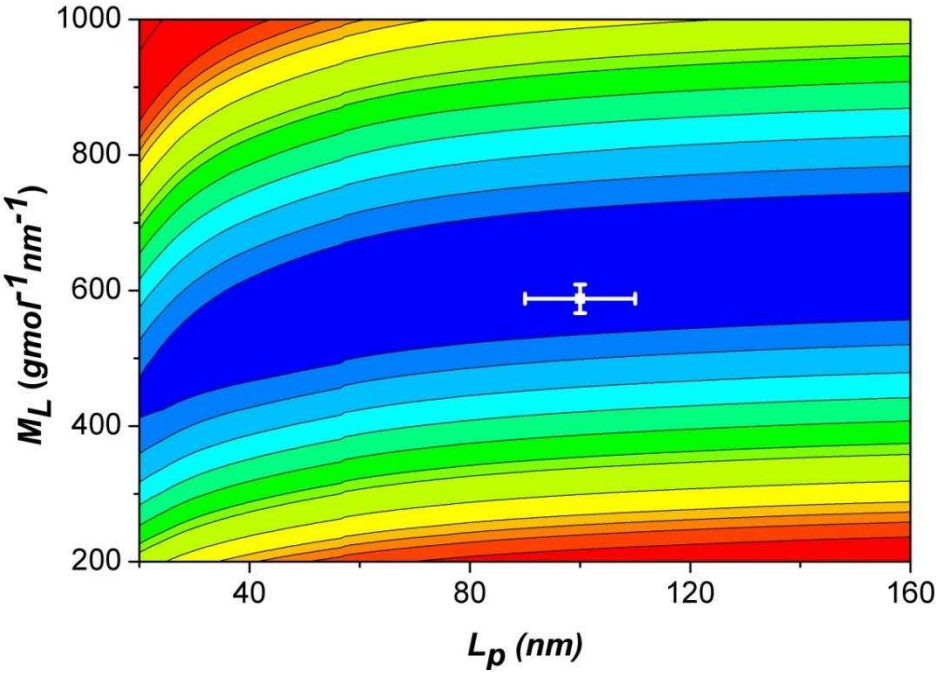


Figure 4.10: Contour plots for gellan samples. The target function, *Δ* calculated based on variables values of L_p and M_L, and are represented on the full colour spectrum from blue (*Δ* = 0.17) to red (*Δ*≥0.95).

The overall L_p and M_L were found as (100 ± 10) nm and (588 ± 21) ($g.mol^{-1}.nm^{-1}$), respectively. These values indicate the rod structure and this range of persistence length is consistent with the result from Okamoto et al. (Okamoto et al., 1993) and Takahashi et al. (Takahashi et al., 2004).

4.4.5.4. Molecular Conformation Zoning

The sedimentation conformation zoning plot provide the estimation of 'overall' solution conformation of a macromolecule ranging from Zone A (extra-rigid rod) to Zone E (globular or branched) by plotting of $k_s M_L$ versus [s]/M_L. (Pavlov et al., 1997, Pavlov, 2013) Thus, it represents the conformation of the polymer in solution based on mass per unit length, M_L and persistent length, L_p parameters. Also, the important parameter is sedimentation coefficient, which can be estimated from the sedimentation coefficient and [s] is evaluated from this equation:

$$[s] = \frac{s^0_{20,w}\eta_{20,w}}{\left(1-\bar{\upsilon}\rho_{20,w}\right)} \tag{4.12}$$

M_L is the mass of the molecule(s) within the polymer divided by its length. In this study, M_L was taken as the estimated values obtained from Multi- HYDFIT analysis as 588 $g.mol^{-1}.nm^{-1}$ and [s] was calculated from sedimentation coefficient data.

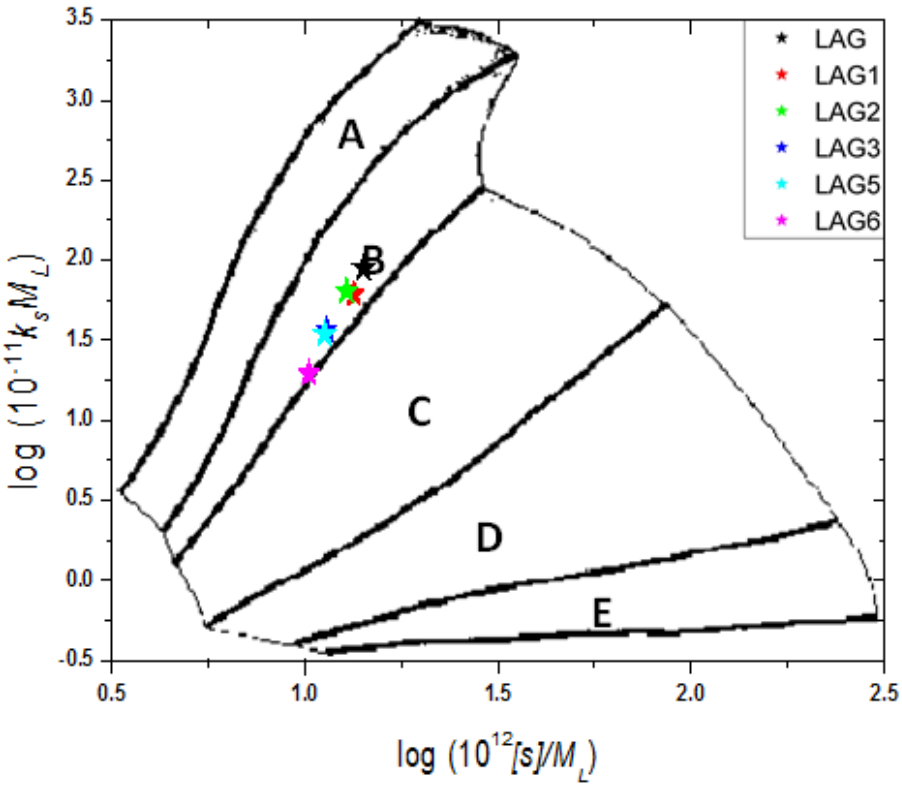


Figure 4.11: The conformation zoning plot for gellan samples which are adapted rigid rod structures (Zone B).

Figure 4.11 demonstrates that the gellan samples have rigid rod conformation with some flexibility in Zone B. This method also shows an excellent agreement with results from the MHKS relationship and Wales van Holde ratio.

4.5. DISCUSSION

The hydrodynamic properties of gellan gum in solution have been investigated using three different approaches based on sedimentation coefficient, $s^0_{20,w}$, molecular weight, M_w and intrinsic viscosity, $[\eta]$. To determine the conformation and the flexibility, the sample was depolymerised by the microwave bomb method which was successfully applied by Kok et al. (2009) and Almutairi (2015). Owing to this

method, gellan samples with different molecular weights were obtained by degradation of the sample. Heat treatment using microwaves in a high-pressure vessel in a short time did not degrade the gellan solution as it was observed in Kok et al. (Kök et al., 2009). Therefore, longer times and higher temperatures were applied and this prompted the degradation of polymer in solution.

According to sedimentation velocity results using in the analytical ultracentrifuge, the samples showed a bimodal sedimentation coefficient distribution; this indicates the heterogeneity of samples. The apparent weight average sedimentation coefficient values increased with decrease in concentration for all gellan samples, which show no evidence of reversible associative behaviour. Although the ranges of the concentrations for the experiment were low, considerable concentration dependence was observed, which shows the effects of non-ideality. Additionally, after heat treatment, both sedimentation coefficients and the concentration dependence parameter k_s, decreased with increasing the heating time.

Since weight average molecular weight is an important parameter for the hydrodynamic characterisation and conformation for gellan samples, they were estimated by the sedimentation equilibrium method in AUC. The molecular weight of gellan has been estimated previously using osmometry (Ogawa et al., 2002), static (Dentini et al., 1988, Okamoto et al., 1993) and dynamic light scattering (Takahashi et al., 1999) but this method was applied for the first time for gellan samples. Working with a series of concentrations and extrapolation to zero concentration helped to eliminate the solution non-ideality effect. The reciprocal plot of $M_{w,app}$ versus concentration gave a linear extrapolation for LAG, LAG1, LAG2 and LAG3. At the same time a second order polynomial fit was applied to the reciprocal plot of $M_{w,app}$ versus concentration for LAG4 and LAG5 because of high non-ideality.

The conformation of gellan in 25mM NaI solution was determined using MHKS (a and b parameter) and Wales van Holde ratio and both results indicated that gellan adopts rod type conformation with some flexibility. These results were also reinforced by sedimentation conformation zoning approach, which also proved that depolymerisation process by microwave bomb technique didn't affect the conformation of gellan. In terms of flexibility, the persistence length, L_p and mass per unit length, M_L were estimated by Multi-HYDFIT method and found as (100 ± 10) nm and (588 ± 21) ($g.mol^{-1}.nm^{-1}$), respectively. These values are similar with earlier studies by Takahashi et al. who suggested L_p as 98nm and M_L as 650 ($g.mol^{-1}.nm^{-1}$) in 25 mM NaCl at 25°C based on $[\eta]$ and M_w data. (Takahashi et al., 2004). Dentini et al. has also found similar L_p value (102 nm) for gellan in tetramethylammonium (TMA) solution but a higher M_L value of 710 ($g.mol^{-1}.nm^{-1}$) (Dentini et al., 1988).

4.6. CONCLUSION

In this study, the untreated low acyl gellan and heat treated-gellan samples were characterised in terms of viscosity, heterogeneity, molecular weight and conformational properties in 25mM NaI solution. Due to electrostatic charge and gel formation in high salt content, SEC-MALL could not be carried out for this sample. However, sedimentation velocity and sedimentation equilibrium in the analytical ultracentrifuge, viscometry and Multi-HYDFIT have successfully been applied to samples. The results from these techniques proved that 25mM NaI is sufficient to supress the electrostatic effects of gellan, which is particularly important for AUC and viscometry experiments. Results from AUC experiments also allowed estimating the conformation and molecular weight of gellan samples. Meanwhile, the

conformation results showed consistency with the previous results, and the rod conformation with some flexibility, which was proved by the MHKS relationship, Wales-van Holde ratio and molecular conformation zoning. This study also shows that since gellan is found as solution form with no aggregates at 25mM NaI and not requiring any further purification to maintain this solution form, the hydrogel formation of gellan with other cationic polymers can be studied for the therapeutic applications, especially for the drug delivery, the mixture of gellan and chitosan as an encapsulating agent may be useful.

CHAPTER 5

MOLECULAR WEIGHT AND CONFORMATION STUDY OF SODIUM HYALURONATE IN AQUEOUS SOLUTION

5.1. INTRODUCTION

Hyaluronic acid or hyaluronan (HA) is a linear, negatively charged and unbranched polysaccharide. It is chemically classified as a glycosaminoglycan and consists of a repeating disaccharide unit of β-(1→4) N-acetyl-D-glucosamine and β-(1→3) linked D-glucuronic acid (Figure 5.1) (Hokputsa, 2003).

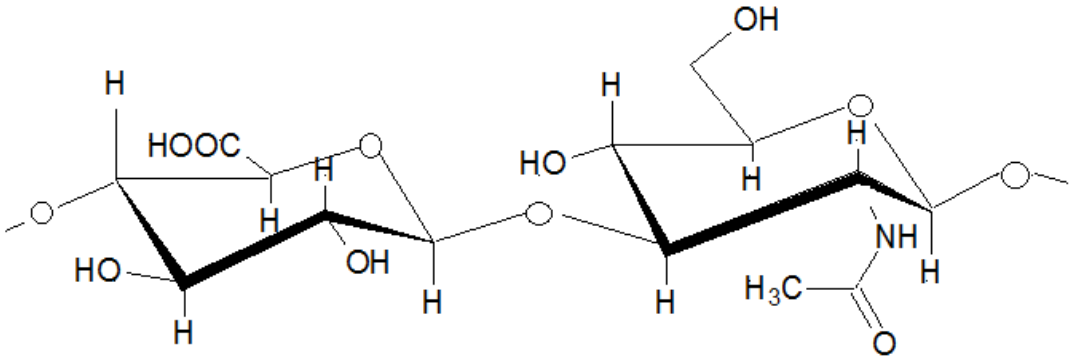


Figure 5.1: Chemical structure of repeating disaccharide unit of hyaluronic acid. Figure reproduced from (Hokputsa, 2003).

HA is found in umbilical cord and the vitreous body of the eye, mammalian synovial fluid, and connective tissues such as rooster comb. (Kogan et al., 2007, Hokputsa et al., 2003a). Additionally, it is also found in the capsules of Streptoccocus species e.g. Streptococcus zooepidemicus and Streptococcus equi (Marcellin et al., 2009). It has been successfully produced via microbial fermentation with less environmental pollution and low production cost compared to rooster comb and other eukaryotic sources. Also, the HA polysaccharide from these microorganisms is obtained at a larger scale, better yield and purity for industrial applications (Haxaire et al., 2000, Milas and Rinaudo, 2004, Liu et al., 2011b).

Due to the distinctive physico-chemical properties of HA, which play an important role in many biological processes, it has been used in several clinical treatments including ophthalmology, orthopaedics, wound healing (Gandolfi et al., 1992, Durrani et al., 1995, Miyazaki et al., 1996, Tascıoglu and Öner, 2003), drug delivery (Luo et al., 2000, Jacobetz et al., 2013) and cosmetic applications. Thus, determination of the molecular properties such as molecular weight (molar mass in $g.mol^{-1}$) and conformation for hyaluronic acid in solution is essential to give a full understanding of its properties and functions for medical and pharmaceutical applications. For example, HA with high molecular weight is used for tissue repair, ophthalmic drug delivery, enhancing nasal adhesion (Saettone et al., 1991, Morimoto et al., 1991, Duranti et al., 1998, Lapčík et al., 1998) whereas HA with low molecular weight has been suggested for the inhibition of tumour growth, initiating the expression of inflammatory moderators and promotion of angiogenesis (West et al., 1985, Zeng et al., 1998, Liu et al., 2011b). The molecular weight estimation for numerous hyaluronic acid samples was extensively studied by different techniques such as gel permeation chromatography, light scattering, osmometry and

sedimentation equilibrium methods (Hokputsa et al., 2003a, Rinaudo, 2008, Preston and Wik, 1992, Choi et al., 2010).

Conformation is also an important property for hyaluronic acid, which is important for an understanding of its interaction with other macromolecules. The conformation of linear HA has been claimed to be a flexible random coil in aqueous solution by (Bothner et al., 1988, Hayashi et al., 1996, Milas and Rinaudo, 2004, Caspersen et al., 2014). Hokputsa and co-workers showed that HA adopts a random coil conformation when $M_w > 10^6$, whereas the stiffness increases with $M_w < 10^6$ as shown by the Mark-Houwink-Kuhn-Sakurada (MHKS) or power-law relationships (Hokputsa et al., 2003b). Another conformation parameter, the persistence length (L_p) -which is indicative of the flexibility of linear polymer chains of HA- was found to have a wide range of values of 4-20 nm from application of the methods including the Yamakawa-Fujii-Yoshizaki and Bushin Bohdanecky approaches and also the application of electric birefringence decay by various researchers - see e.g. (Trimm and Jennings, 1983, Cleland, 1984, Hayashi et al., 1996, Buhler and Boué, 2004).

In this chapter, the properties of different samples of sodium hyaluronate were studied in solution to evaluate structural unity in terms of sedimentation coefficient, molecular weight, intrinsic viscosity, conformation and overall conformational flexibility by taking advantage of the recent advances in hydrodynamic analysis. A new approach was applied using sedimentation equilibrium ("SEDFIT-MSTAR") together with size exclusion chromatography coupled to multi angle light scattering (SEC-MALS) to determine heterogeneity and molecular weight distributions. The flexibility of samples in terms of the persistence length (L_p) and mass per unit length (M_L) values were also estimated using a more recent approach, the global conformational analysis method an algorithm known as Multi-HYDFIT in order to

address some discrepancies in L_p in the literature. (Ortega and García de la Torre, 2007). The Multi-HYDFIT method employs a combination of molecular weight, intrinsic viscosity and sedimentation coefficient data for all sodium hyaluronate samples.

5.2. MATERIALS

The six bacterial sodium hyaluronate samples HAV1, HAV2, HAV3, HAV4, HAV5 and HAV6 were kindly supplied in highly purified form by Vitrolife Ltd. (Sweden). Samples were used as supplied without any further purification. A stock solution of each sodium hyaluronate was prepared by dissolving a known amount in distilled deionised water, at room temperature with gentle stirring for two hours followed by dialysis for a further 18 hours against buffer phosphate-chloride buffer supplemented with NaCl according to Green (1933) at pH 7.0 and an ionic strength (I) of 0.1M. The concentrations, c (g/ml) of the stock sample solutions were measured after - dialysis using an Atago (Japan) DD-7 refractometer calibrated with glucose standards and a refractive increment, dn/dc, of 0.167ml/g (Hokputsa et al., 2003b). The solutions of native HAV1 and HAV2 were microwaved with a microwave synthesiser (Anton Paar Ltd, UK) at 90°C for 45s to produce lower molar mass samples that were named as MHAV1 and MHAV2.

5.3. METHODS

5.3.1. Sedimentation Velocity (SV)

An Optima XL-I (Beckman Instruments, Palo Alto, USA) equipped with Rayleigh interference optics was used to determine the sedimentation behaviour and molecular

homogeneity of hyaluronate samples. Solution concentrations ranging between 0.1 – 3.0 mg/ml for each hyaluronate were studied at a temperature of (20.0 ± 0.1) °C. 400µl of solution and an equal volume of the pH 7.0, I=0.1M reference buffer/solvent (400µl) were injected into the solution and solvent channels, respectively of 12 mm optical path length double sector cells. The Rayleigh interference optical system was used to record changes in the concentration versus radial displacement profiles with time. Scans were taken at 2 min intervals for a run time of approximately 18 hours at 35000 rpm for HAV1, HAV2, HAV3, MHAV1 and MHAV2, and at 45000 rpm for HAV4, HAV5 and HAV6. A partial specific volume, $\bar{\upsilon}$ of -0.6ml/g - was used for all samples (Hokputsa et al., 2003b). For comparison purposes, sedimentation coefficients were normalised to standard solvent conditions, namely the density and viscosity of water at 20.0° C see e.g. (Abdelhameed, 2010, Laue and Stafford III, 1999):

$$s_{20,w} = \{(1-\bar{\upsilon}\rho_{20,w}) / (1-\bar{\upsilon}\rho_0)\} \,.\, \{\eta_0 / \eta_{20,w}\} s_{T,b} \qquad (5.1)$$

where ρ_0 and η_0 are respectively the density and viscosity of the solvent or buffer, b, at temperature T and $\rho_{20,w}$ and $\eta_{20,w}$ the corresponding values of water at 20.0 °C. The data was analysed using the "least squares ls-g(s) model" SEDFIT program of Schuck and colleagues (Dam and Schuck, 2004) in terms of distributions of sedimentation coefficient distribution . The ls-g(s) vs. s profiles were used to provide an assessment of sample polydispersity. The s and $s_{20,w}$ values are 'apparent' values because of non-ideality. To remove this effect, $s_{20,w}$ is extrapolated to zero concentration and $s^0_{20,w}$ is obtained from reciprocal plot of $s_{20,w}$ $(1/s_{20,w})$ vs. concentration (see for example, (Harding, 2005c):

$$1/s_{20,w} = (1/ s°_{20,w}).(1+k_s c) \qquad (5.2)$$

where $s^0_{20,w}$ is sedimentation coefficient at zero concentration and standard condition, k_s is the Gralen parameter (Gralen, 1944); see also (Harding, 2005b).

5.3.2. Sedimentation Equilibrium (SE)

Sedimentation equilibrium experiments were also performed using the Beckman (Palo Alto, California, U.S.A.) Optima XL-I analytical ultracentrifuge and employing Rayleigh interference optics and an automatic on-line data capture system. 12 mm optical path length double-sector titanium cells with sapphire windows were loaded with (~80µl) of dialysed sample as a concentration series (ranging from 0.2-2.0mg/ml) and a matching amount of reference buffer dialysate in appropriate channels. The balanced cells were then loaded into an analytical 8-hole titanium rotor An50-Ti and placed in the AUC. After time was allowed for vacuum formation (≤ 50 microns) and for temperature equilibration (20.0 °C), the rotor was then accelerated to 5000 rpm for HAV1, HAV2, HAV3, MHAV1 and MHAV2, 13000 rpm for HAV4, 16000 rpm for HAV5 and 23000 rpm for HAV6. Using the Rayleigh interference optical system, scans were taken every one hour and equilibrium was reached after approximately 48 hours to 120 hours. Records of the relative concentration distribution of the solute at equilibrium were analysed to give the weight average apparent molecular weight $M_{w,app}$ using the SEDFIT-MSTAR program implemented by Schuck et al. (Schuck et al., 2014) based on the algorithm of Cölfen and Harding (Cölfen and Harding, 1997) and the M* function of Creeth and Harding (Creeth and Harding, 1982).

5.3.3. Size Exclusion Chromatography Coupled to Multi Angle Light Scattering (SEC-MALS)

Molecular weights (weight averages) of the sodium hyaluronate samples were also estimated by using the independent technique of SEC–MALS. This technique has been successfully applied to polysaccharide characterisation since 1991 by applying firstly alginate samples (Horton 1991). The system consisted of a series of size-exclusion chromatography (SEC) columns, namely TSK G5000PW and TSK G6000PW, protected by a similarly packed guard column (Tosoh Bioscience, Tokyo, Japan) coupled on-line to "Helios" multi-angle light scattering (MALS) and refractive index (OptilabrEX) detectors (Wyatt Technology, Santa Barbara, USA). Solutions for injection were prepared for HAV1, HAV2, and HAV3 as 0.5mg/ml, for MHAV1, MHAV2 as 1.0mg/ml, and for HAV4, HAV5, and HAV6 as 5.0 mg/ml. Then, they were filtered through a 0.2 μm syringe filter (Minisart, Surrey, UK) to remove any insoluble material or dust prior to being injected into the columns. The buffer was pumped at a steady, pulse-free flow rate of 0.8 ml/min through the column system. ASTRA (Version 6.1) software (Wyatt Technology, Santa Barbara, USA) was used to analyse the data. A second polynomial fit (for high molecular weight samples) and linear fit (for low molecular weight samples) to the "Debye" plot of Kc/R_θ vs $\sin^2(\theta/2)$, where the terms have their meaning (Wyatt, 2013b) was used for calculating the apparent weight average molecular weight ($M_{w,app}$). The refractive index increment (dn/dc) was taken as 0.167 ml/g which has previously been determined by Hokputsa and co-workers (Hokputsa et al., 2003a).

5.3.4. Capillary and Differential Pressure Viscometry

The flow times of sodium hyaluronate solutions ranging in concentration from 0.1 mg/ml to 5mg/ml and the reference solvent were measured using a 2ml Schott-Geräte Ostwald viscometer system. The temperature was kept constant at 20.0 (± 0.01) °C by suspending the capillary in water bath combined with a cooling sytem. The relative viscosity, (η_{rel} = (t/t_o), was obtained from the ratio of the flow time of the solution t (sec) to the flow time of solvent that was recorded accurately using photosensors. Because of the low concentrations a density correction was deemed unnecessary (Harding, 1997). The reduced viscosity, η_{red}=(η_{rel}-1)/c, and the inherent viscosity, η_{inh} = ($ln\eta_{rel}$)/c were extrapolated to zero concentration to eliminate non-ideality effects with the common intercept at c=0 yielding the intrinsic viscosity *[η]* using the Huggins and Kraemer equations:

$$\eta_{red} = [\eta]\ (1 + K_H.[\eta].c) \tag{5.3}$$

and

$$(ln\eta_{rel})/c = [\eta]\ (1 - K_K.[\eta].c) \tag{5.4}$$

where K_H and K_K are respectively the Huggins (1942) and Kraemer (1938) constants. As an additional check, a combined relation due to Solomon & Ciuta (1962) was also used:

$$[\eta] \sim (1/c).\ [2\ (\eta_{sp} - ln\ (\eta_{rel}\ ))]^{1/2} \tag{5.5}$$

The assumption has been made that there was no shear dependence of *[η]* under creeping flow conditions in the capillary viscometer.

Intrinsic viscosities of samples were also measured by Viscostar (Wyatt Technology) differential pressure viscometer on-line to the SEC-MALS system. Due to the sensitivity of the sensors and high dilution in the column, the concentration is low and because of this, the Solomon-Ciuta equation (5.5) can be applied without any extrapolation (Harding, 1997).

5.4. RESULTS

5.4.1. Sedimentation Velocity (SV)

The sedimentation coefficient, s was obtained for each concentration of each sample using the least square ls-g*(s) distribution method. The sedimentation coefficient distribution profiles in Figure 5.2 shows the high purity and unimodiality with one major peak at each concentration of all sodium hyaluronate samples. The peaks also show an evidence of significant hyper sharpening with increasing the concentration especially for HAV1, HAV2, HAV3 and microwave heated samples MHAV1 and MHAV2. The apparent sedimentation coefficient $s_{20,w}$ increased with reducing concentration which indicates a considerable concentration dependency especially for these same samples. The sedimentation coefficients were found between 1.1S to 6.8S as shown in Table 5.1. The reciprocal plots of sedimentation coefficient versus concentration extrapolated to infinite dilution were shown in Figure 5.3 for all sodium hyaluronate samples. The concentration dependence of sedimentation, k_s was also determined from this extrapolation using Equation 5.2 for each sample and presented in Table 5.1.

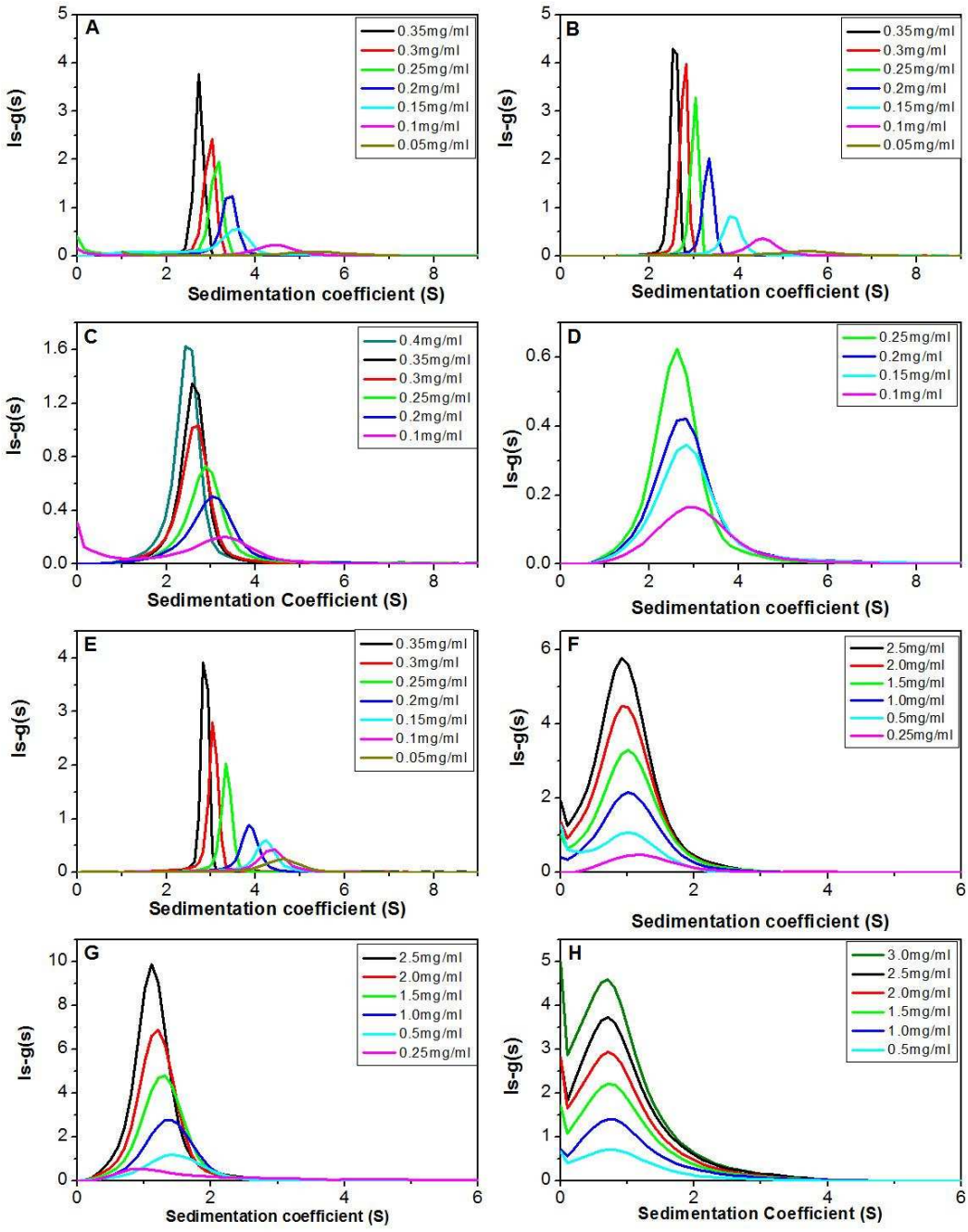


Figure 5.2: Sedimentation coefficient distribution profiles using the least squares g*(s) method of SEDFIT obtained from sedimentation velocity experiment for sodium hyaluronate samples (A) HAV1, (B) HAV2, (C) MHAV1, (D) MHAV2, (E) HAV3, (F) HAV4, (G) HAV5, (H) HAV6.

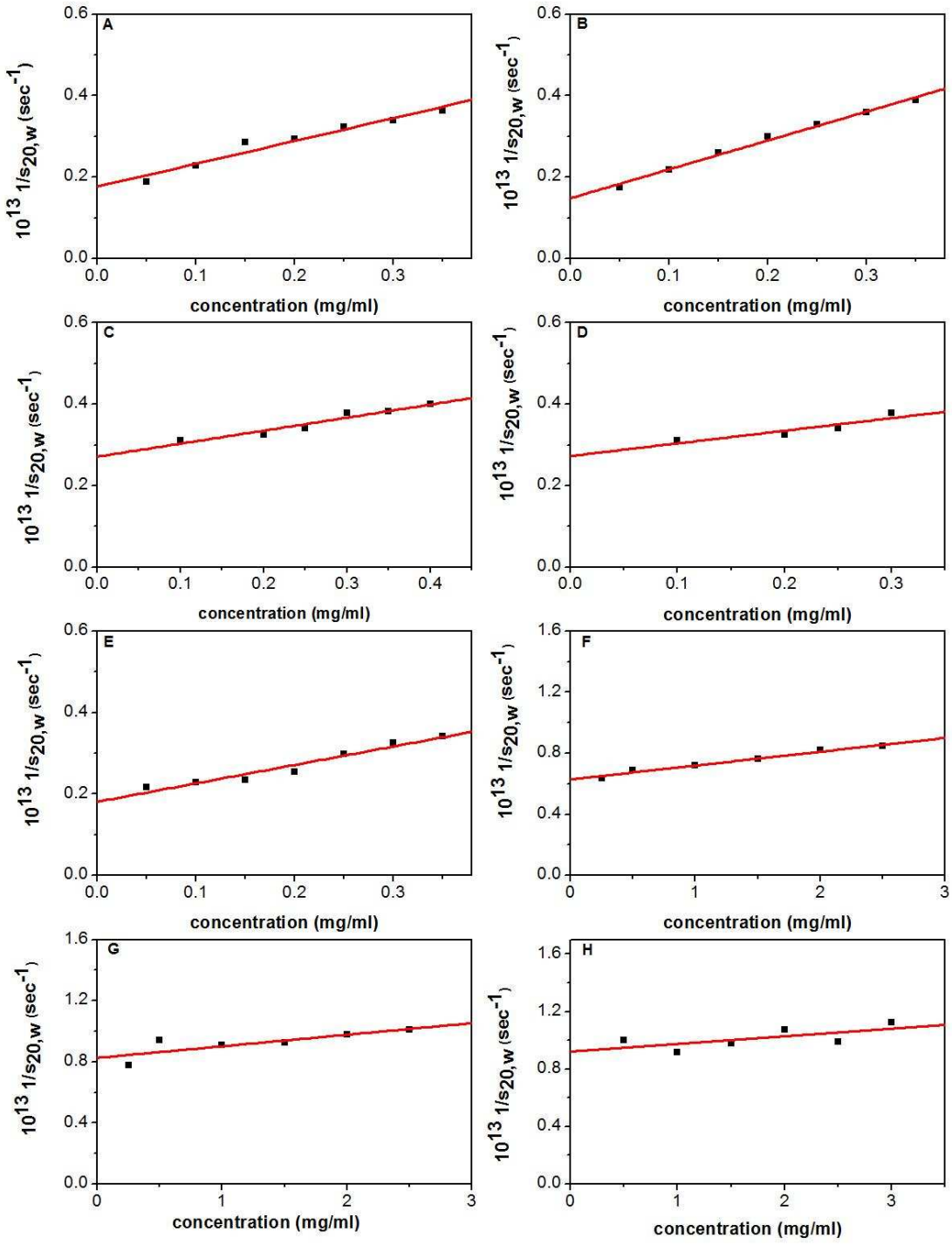


Figure 5.3: Concentration dependence (reciprocal) of the sedimentation coefficient plot (after correction to standard solvent conditions) for sodium hyaluronate samples in 0.1M PBS (A) HAV1, (B) HAV2, (C) MHAV1, (D) MHAV2, (E) HAV3, (F) HAV4, (G) HAV5, (H)HAV6.

Table 5.1: Summary of $s^0_{20,w}$ and k_s for sodium hyaluronate samples.

Sample	$s^\circ_{20,w}$ (S)	k_s (ml/g)
HAV1	5.7 ± 0.40	3180 ± 390
HAV2	6.8 ± 0.30	4800 ± 280
HAV3	5.5 ± 0.30	2500 ± 300
HAV4	1.6 ± 0.02	144 ± 10
HAV5	1.3 ± 0.04	130 ± 20
HAV6	1.1 ± 0.10	60 ± 30
MHAV1	3.7 ± 0.17	1180 ± 170
MHAV2	3.6 ± 0.20	1270 ± 330

5.4.2. Estimation of Molecular Weight

The weight average molecular weight of sodium hyaluronate samples were estimated using both sedimentation equilibrium in the analytical ultracentrifuge and SECMALS. The weight average molecular weight was firstly determined by sedimentation equilibrium. However, for this experiment, the effect of thermodynamic non-ideality in solution needs to be considered. Because of charge effects and excluded volume effects, the solution non-ideality appears and the sodium hyaluronate solutions display strong solvent-polymer interactions that ascend with increase in concentration. To minimise this non-ideality effect, the samples were run at a series of measurements at different loading concentration and extrapolated to infinite concentration. Nevertheless, for HAV1 and HAV2, measurements over a range of concentrations and extrapolating to zero concentration was not successful to eliminate this non-ideality effect even though using long

optical path length cells (20.0 mm) that allows to work at relatively low concentration (0.2 mg /ml).

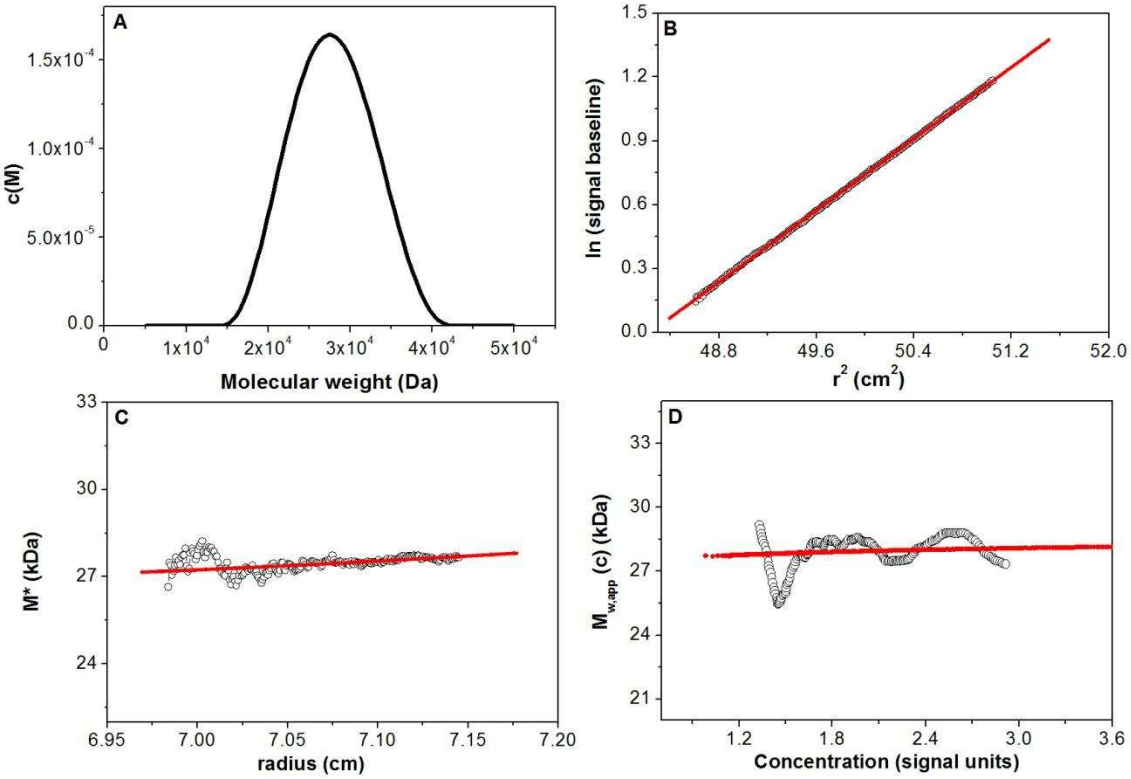


Figure 5.4: SEDFIT-MSTAR analysis of HAV4 in 0.1 M PBS at a loading concentration of 1.0 mg/ml (A) molecular weight distribution, c(M) vs. M plot; (B) log concentration ln c(r) vs. r^2 plot, where r is the radial distance from the centre of rotation; (C) M* vs. r plot: the value of M* extrapolated to the cell base = $M_{w,app}$ the apparent weight average molecular weight for the whole distribution. (D) Point or local apparent weight average molecular weight at radial position r (open circle) plotted against the local concentration c(r).

On the other hand, MHAV1, MHAV2, HAV3, HAV4, HAV5 and HAV6 were run at different concentration ranges from (0.2-2.5mg/ml) and weight average molecular weights were determined by SEDFIT-MSTAR. Figure 5.4 shows an example of this analysis for HAV4 at 1.0mg/ml. The reciprocal plot of $M_{w,app}$ versus concentration

gave a linear extrapolation for samples HAV4, HAV5 and HAV6. At the same time a simple second order polynomial fit was applied to the conventional plot of $M_{w,app}$ versus concentration for HAV3 and reciprocal plot of $M_{w,app}$ versus concentration for MHAV1 and MHAV2 (Figure 5.5). This fit was also applied for kappa-carrageenan and hyaluronic acid at high molecular weight because of high non-ideality by Harding et al. (Harding et al., 1997) and Hokputsa et al. (Hokputsa et al., 2003a). The molecular weight values obtained from these extrapolations are reported in Table 5.2.

Table 5.2: Summary of weight average molecular weights (M_w) results for sodium hyaluronate samples from sedimentation equilibrium and SEC-MALS.

Sample	**10^5 x M_w (Da)[a]**	**10^5 x M_w (Da)[b]**
HAV1	ND	22.7 ± 1.1
HAV2	ND	20.0 ± 3.6
HAV3	25.0 ± 2.0	18.9 ± 3.0
HAV4	0.46 ± 0.11	0.43 ± 0.08
HAV5	0.24 ± 0.04	0.14 ± 0.02
HAV6	0.07 ± 0.01	0.06 ± 0.01
MHAV1	7.35 ± 0.2	5.10 ± 0.10
MHAV2	4.76 ± 1.7	3.90 ± 0.04

a : obtained from sedimentation equilibrium

b : obtained from SEC-MALS

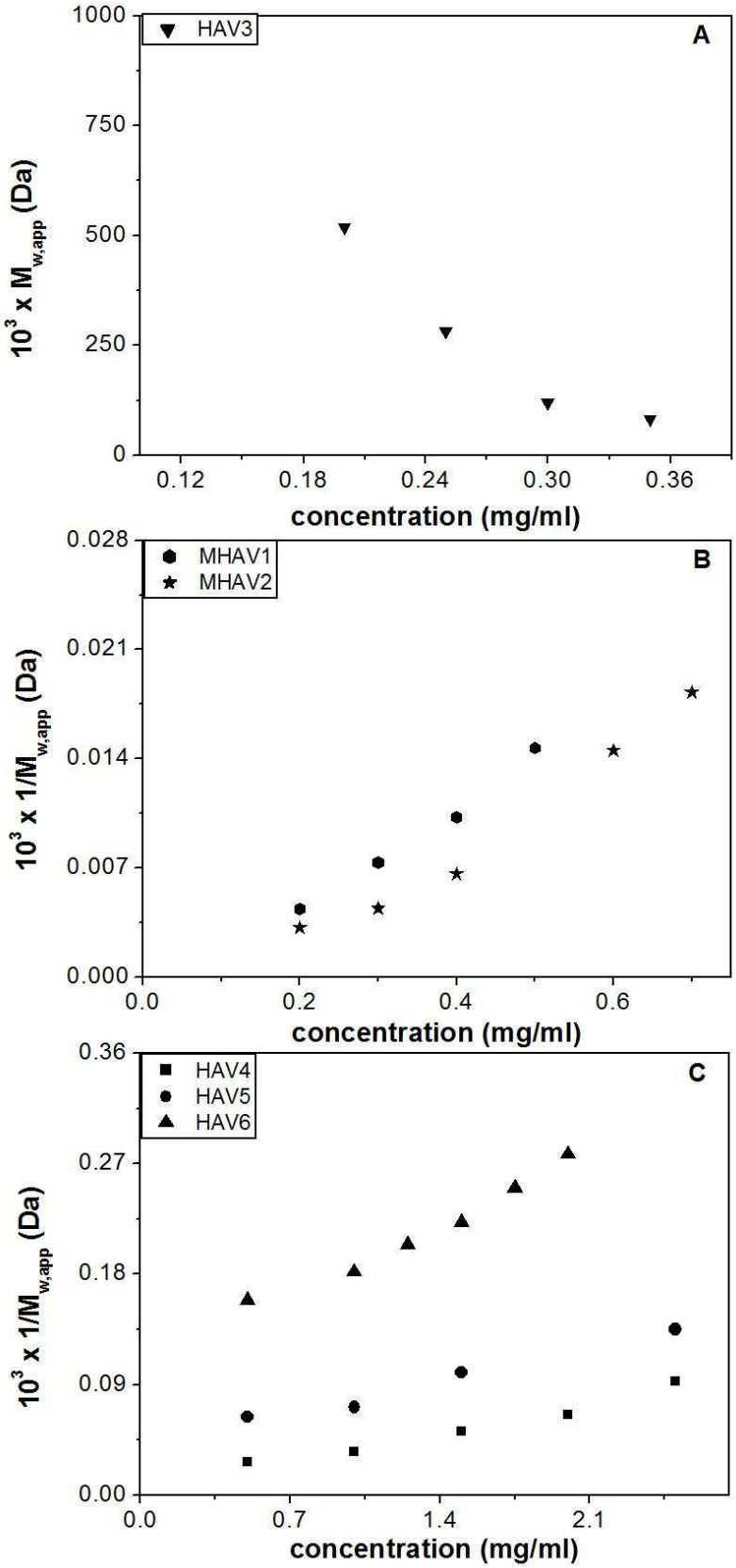


Figure 5.5: Plots of $M_{w,app}$ against concentration for (A) conventional plot of HAV3 (B) reciprocal plot of MHAV1 and MHAV2 (C) reciprocal plot of HAV4, HAV5 and HAV6.

The weight average molecular weight of sodium hyaluronate samples were also determined by SEC-MALS and the values are also presented in Table 5.2. Due to the sample dilution in SEC columns, the non-ideality effect was reduced, which allowed us to obtain the weight average molecular weight of HAV1 and HAV2 directly. The elution volume profiles of samples are given in Figure 5.6 (a and b) and from this figure approximately unimodal profiles are seen for MHAV1, MHAV2, HAV4, HAV5 and HAV6, with some lower molecular weight peaks seen in HAV1, HAV2 and HAV3. The weight average molecular weight results obtained for each sample from SEC-MALS were relatively consistent with those found by sedimentation equilibrium (Table 5.2).

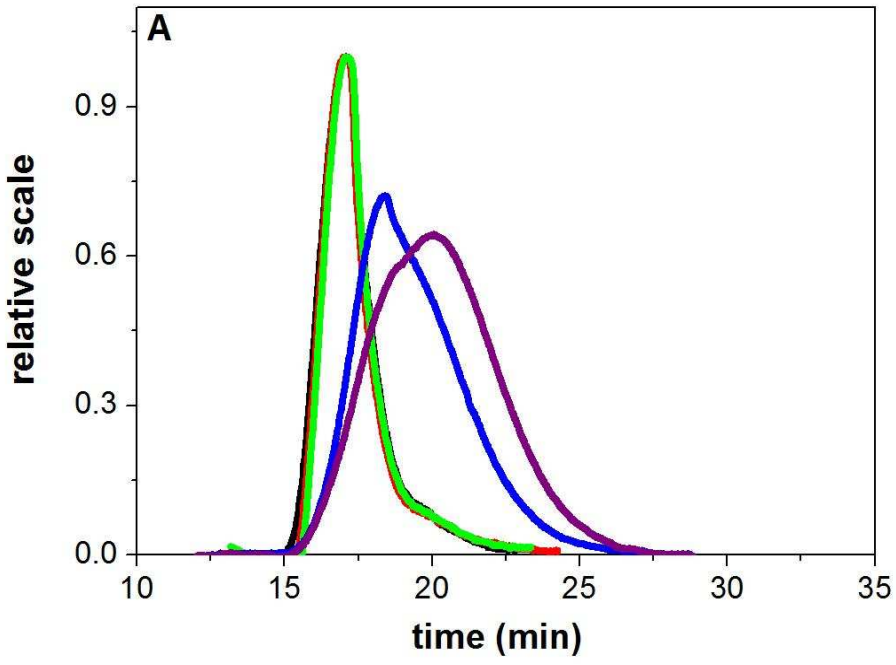


Figure 5.6a: Elution profiles of the sodium hyaluronate samples from dRI detector: HAV1 (black line), HAV2 (red line), HAV3 (green line) at concentration 0.5 mg/ml, MHAV1 (blue line) and MHAV2 (purple line) at concentration 1.0mg/ml examined by SEC-MALS.

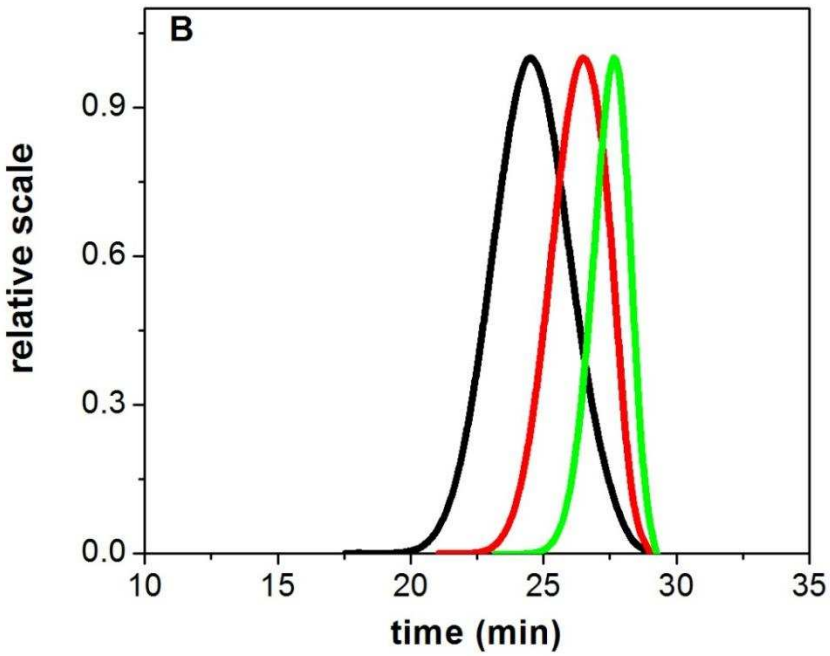


Figure 5.6b: Elution profiles of the sodium hyaluronate samples from dRI detector: HAV4 (black line), HAV5 (red line), HAV6 (green line) at concentration 5.0 mg/ml examined by SEC-MALS.

5.4.3. Intrinsic viscosity

The intrinsic viscosities of samples were measured using both a capillary viscometer and the Viscostar (Wyatt Technology) differential pressure viscometer for each sodium hyaluronate sample. The value of $[\eta]$ were obtained using Huggins, Kraemer and Solomon-Ciuta extrapolations for the capillary viscometer and a good linear extrapolation can be seen from Figure 5.7 for all samples.

The results are presented on Table 5.3 and this table proves that intrinsic viscosity greatly depends on molecular weight and there is a general decrease in intrinsic viscosity with decreasing molecular weight. The intrinsic viscosity result of HAV2 is

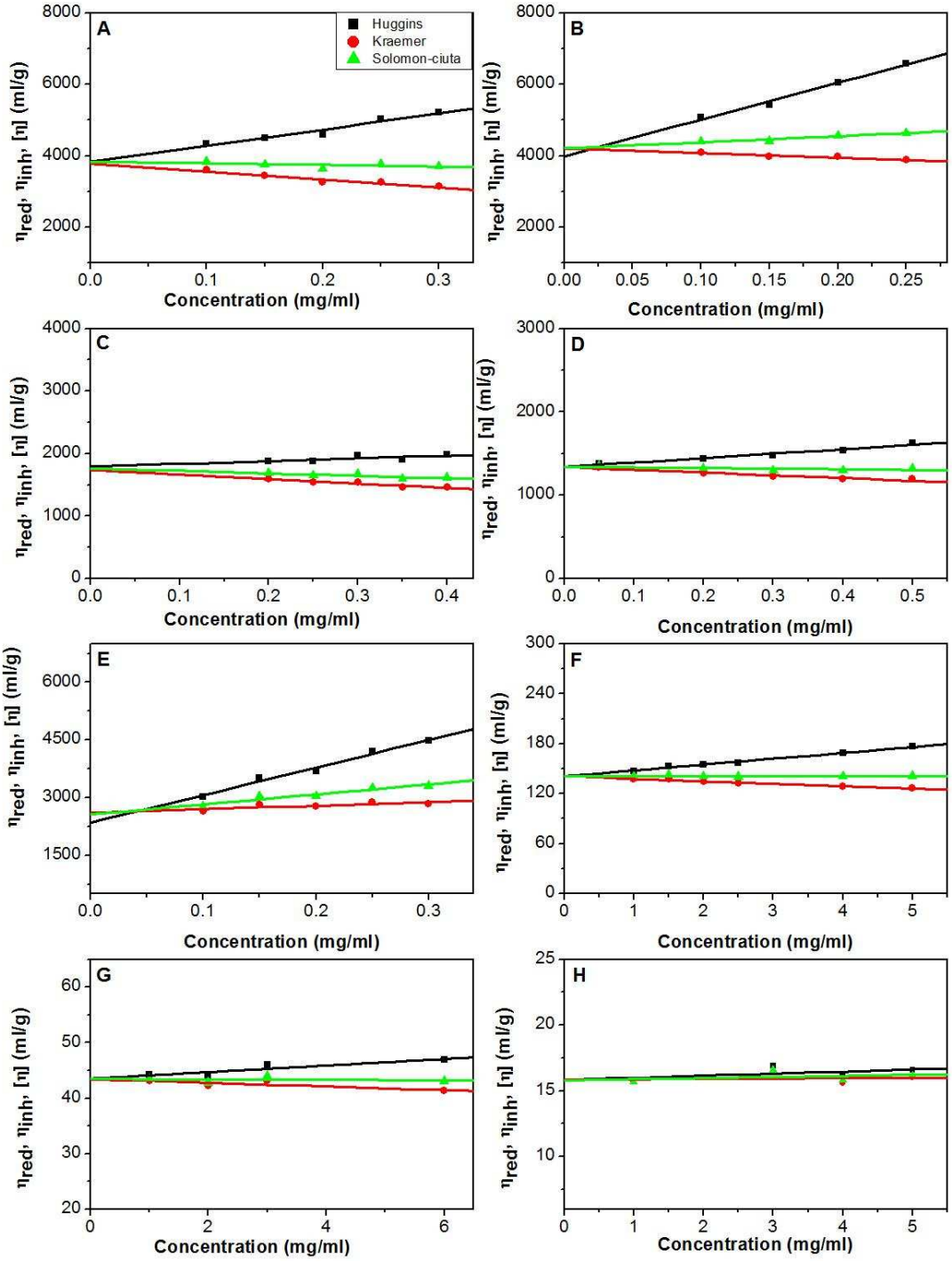


Figure 5.7: The intrinsic viscosity plots from capillary viscometry: Huggins, Kraemer and Solomon-Ciuta extrapolations for sodium hyaluronate samples; (A) HAV1, (B) HAV2, (C) MHAV1, (D) MHAV2, (E) HAV3, (F) HAV4, (G) HAV5, (H) HAV6.

higher than that of the HAV1 though the molecular weight is less. This could be related to the different stiffness of samples and HAV2 could be much stiffer. Table 5.3 also demonstrates the intrinsic viscosity for sodium hyaluronate samples from ViscoStar on-line with SEC-MALS, and the data is consistent with those yielded from capillary viscometer except HAV2 and HAV3. The results of intrinsic viscosity are also within the range previously determined.

Table 5.3: Summary of Intrinsic viscosity values of sodium hyaluronate samples obtained from capillary viscometry and differential pressure viscometry.

Sample	Intrinsic viscosity *[η]* (mL/g)			
	Capillary viscometry			Online viscostar™
	Huggins	Kraemer	Solomon-Ciuta	
HAV1	3840 ± 90	3830 ± 140	3800 ± 80	4320 ± 730
HAV2	3990 ± 130	4210 ± 60	4210 ± 70	4820 ± 40
HAV3	2340 ± 110	2610 ± 80	2560 ± 90	4740 ± 10
HAV4	141 ± 1.0	141 ± 0.8	142 ± 1	144 ± 0.2
HAV5	44 ± 0.6	44 ± 0.6	44 ± 1	44 ± 0.1
HAV6	16 ± 0.6	16 ± 0.6	16 ± 1	16.6 ± 0.1
MHAV1	1840 ± 50	1790 ± 70	1740 ± 45	1640 ± 3.1
MHAV2	1340 ± 20	1340 ± 20	1350 ± 17	1210 ± 3.6

5.4.4. Conformation Analysis

5.4.4.1. Mark-Houwink-Kuhn-Sakurada Power Law Relationships

The Mark-Houwink-Kuhn-Sakurada (MHKS) or power law relationships is one of the simplest methods to obtain for conformation and flexibility of sodium hyaluronate in solution using sedimentation coefficient, intrinsic viscosity and molecular weight parameters (Harding et al., 1991c);

$$[\eta] = \kappa_\eta \, M^{\,a} \tag{5.6}$$

$$s^0_{20,w} = \kappa_s \, M^{\,b} \tag{5.7}$$

The MHKS or 'Mark-Houwink' exponents "a" and "b" are obtained from the slopes of double logarithmic plots of intrinsic viscosity, *[η],* and sedimentation coefficient, $s^0_{20,w}$ versus molecular weight M_w, respectively. The values of a and b are then used to determine conformation using 'Haug Triangle' which is a representation of the gross conformation of macromolecules. The three extremes of conformation, compact sphere, random coil and rigid rod, are placed at the corners of triangle (Tombs and Harding, 1997) with the values given at Table 4.4.

Double logarithmic plot of $s^0_{20,w}$ versus of molecular weight of all sodium hyaluronate samples were presented in Figure 5.8. The overall b parameter which was yielded from slope was found as (0.31 ± 0.02) between the limits of rod (0.15) and coil (0.4-0.5) according to Table 4.4. Within the error estimate the value agrees with that obtained previously by (Hokputsa, 2003).

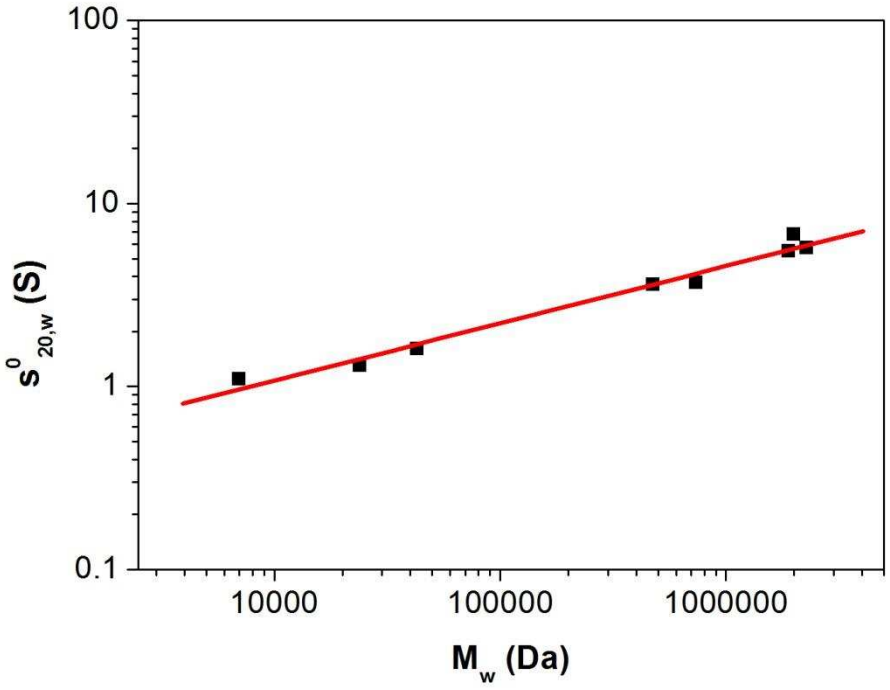


Figure 5.8: Mark–Houwink–Kuhn–Sakurada (MHKS) power law double logarithmic plot of $s^0_{20,w}$ vs M_w for all sodium hyaluronate samples.

Figure 5.9 presents the plot of intrinsic viscosity $[\eta]$ vs. molecular weight M_w for each sodium hyaluronate sample. The obtained a values from these slopes were presented in Table 5.4. As it can be seen from Table 5.4, the a values of sodium hyaluronate samples were found between 0.2 to 0.75 which indicates the conformation as a semi flexible coil and the finding is consistent with previous studies (Bothner et al., 1988, Gura et al., 1998, Bezáková et al., 2008, Caspersen et al., 2014).

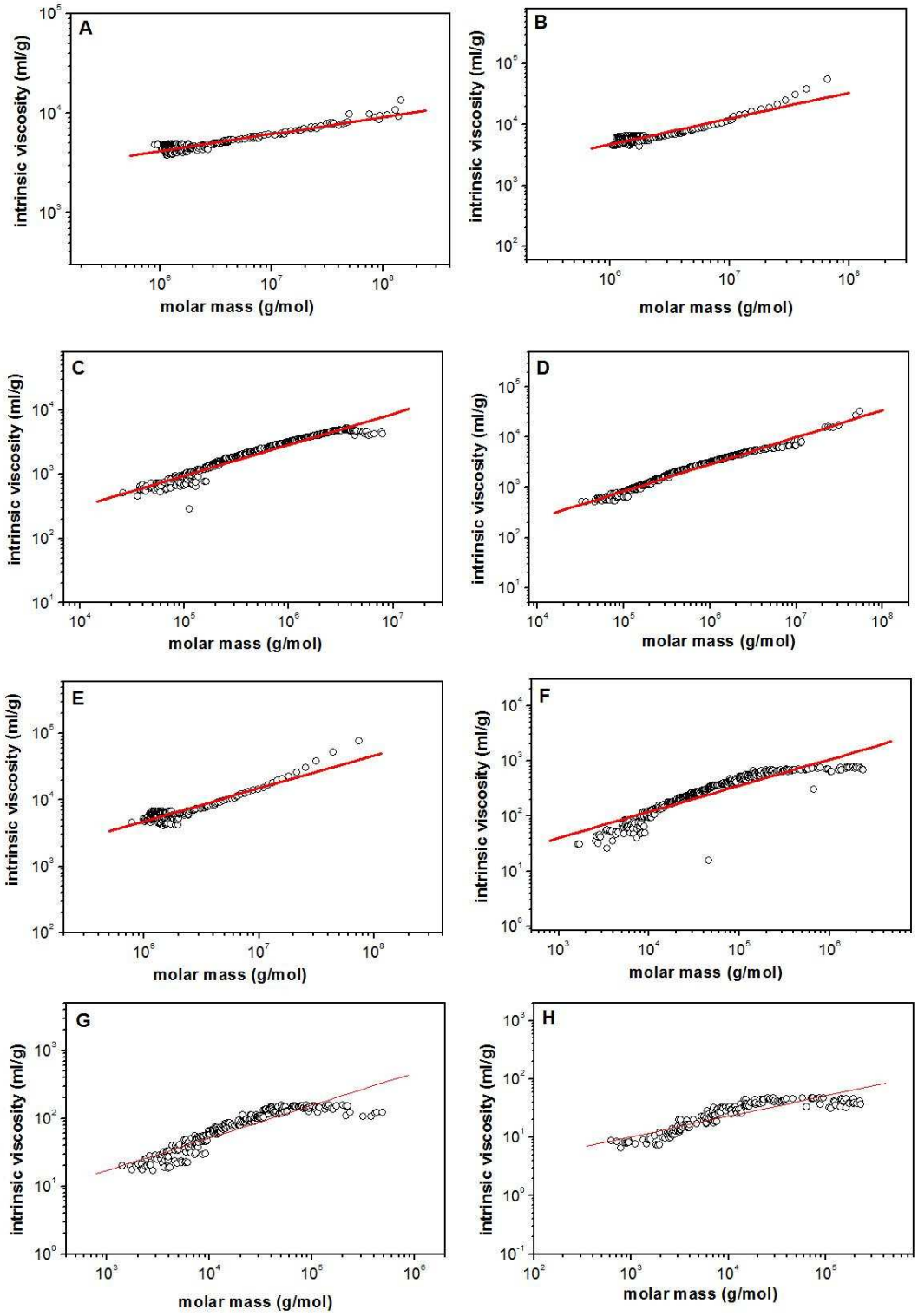


Figure 5.9: Mark–Houwink–Kuhn–Sakurada (MHKS) power law double logarithmic plot from on-line differential pressure viscometry coupled to SEC-MALS for sodium hyaluronate samples; (A) HAV1, (B) HAV2, (C) MHAV1, (D) MHAV2, (E) HAV3, (F) HAV4, (G) HAV5, (H) HAV6.

Table 5.4: Mark-Houwink-Kuhn-Sakurada (MHKS) power law exponent a, from SEC-MALS and Wales-van Holde ratio, R, for sodium hyaluronate samples.

Sample	MHKS a	R= $k_s[\eta]$
HAV1	0.20 ± 0.01	0.8
HAV2	0.43 ± 0.01	1.1
HAV3	0.50 ± 0.01	0.6
HAV4	0.66 ± 0.01	1
HAV5	0.69 ± 0.01	ND
HAV6	0.54 ± 0.01	ND
MHAV1	0.65 ± 0.01	0.7
MHAV2	0.75 ± 0.01	0.7

5.4.4.2. Wales-van Holde Ratio (R)

The Wales-van Holde ratio (Wales and Van Holde, 1954) is the simplest guidance/indicator of a molecule conformational flexibility. The limits are ~ 1.6 for a compact sphere or a non-draining random coil (Creeth and Knight, 1965), and <1 for rods (Tombs and Harding, 1998). Wales-van Holde ratio, R, is;

$$R = k_s / [\eta] \quad (5.8)$$

The k_s is concentration dependence coefficient or the Gralen parameter and $[\eta]$ is intrinsic viscosity. The R results of sodium hyaluronate samples are given in Table 5.4 and it appears that all sodium hyaluronate samples are again consistent with semi-flexible structures (R ~ 0.6–1.0). We also note that our results appear similar to those found previously by Kok et al., Hokputsa et al. and Almutairi et al. (Kök et al., 2009, Hokputsa et al., 2003b, Almutairi et al., 2013).

5.4.4.3. Estimation of the Persistence Length (L_p) and Mass Per Unit Length (M_L)

The persistence length L_p and M_L are representations of the bending flexibility of linear polymer chains (worm-like chains)(Harding, 2005a). L_p is defined as the average projection length along the initial direction of the polymer chain and M_L is the mass of the molecule(s) within the polymer divided by its length. Theoretically, $L_p = 0$ is for a random coil whereas $L_p = \infty$ is for the rigid rod (e.g. see (Harding, 1997). However the practical limits, -for a random coil are ~1nm (e.g pullulan) and for a rigid rod ~200nm (e.g. xanthan) are more suitable (Tombs and Harding, 1997). The persistence length can be estimated using different approaches, either using the sedimentation coefficient (Yamakawa and Fujii, 1973, Hearst and Stockmayer, 1962) or using the intrinsic viscosity (Bohdanecky, 1983, Stockmayer and Fixman, 1963) equations.

5.4.4.3.1. Bushin-Bohdanecky Method

This method is a popular method for estimating chain persistence lengths (L_p) especially for semi-flexible polymers, and has been applied to a range of polysaccharides such as xyloglucan (Patel et al., 2008b), methylcellulose (Morris et al., 2009b) and konjac glucomannan (Kök et al., 2009). The persistence length is estimated using viscosity and molecular weight data from the equation below (Bushin et al., 1981a, Bohdanecky, 1983):

$$\left(\frac{M_W^2}{[\eta]}\right)^{1/3} = A_0 M_L \Phi^{-1/3} + B_0 \Phi^{-1/3} \left(\frac{2L_P}{M_L}\right)^{-1/2} M_w^{1/2} \qquad (5.9)$$

where Φ is the Flory-Fox constant (2.86 x 10^{23} mol^{-1}), A_0 and B_0 are constants and were taken as ~1.32 and ~1.10, respectively (Bushin et al., 1981b). The value of mass per unit length (M_L) of sodium hyaluronate was taken as (~410 $g.mol^{-1}.nm^{-1}$), that was obtained from (Tsutsumi and Norisuye, 1998).

The plot of $(M_w^2/[\eta])^{1/3}$ vs. $M_w^{1/2}$ for all sodium hyaluronate samples are shown in Figure 5.10. The L_p is calculated from slope using the Equation 5.9 and the constants, A_0 and B_0, as given previously. From the slope the L_p was obtained as (9.4 ± 0.03) nm, which is an excellent agreement with (Gamini et al., 1992) and (Hayashi et al., 1996) using the same method.

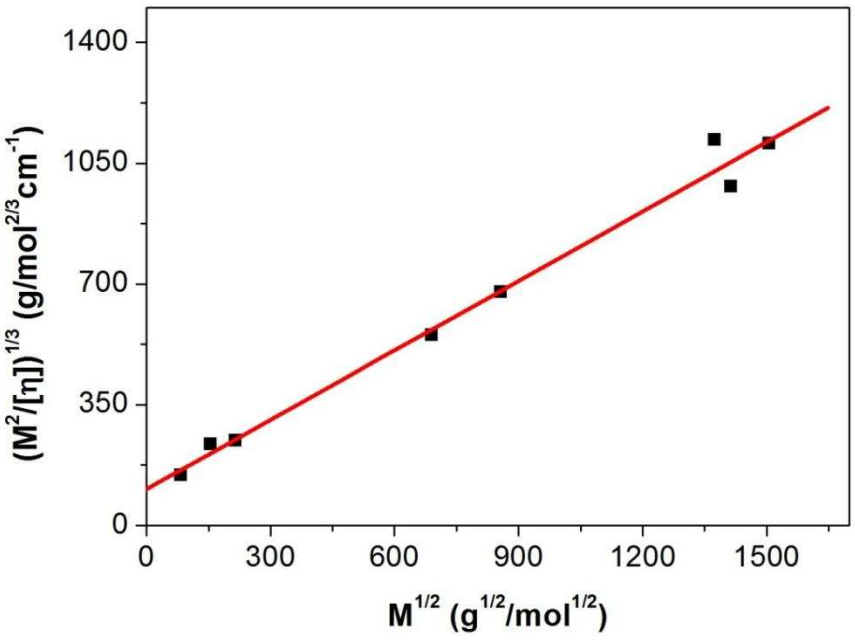


Figure 5.10: Bushin-Bohdanecky plot for sodium hyaluronate samples, where L_p = (9.4 ± 0.03) nm from the slope.

5.4.4.3.2. Global analysis method (HYDFIT)

It is clear that using different methods to determine L_p and M_L might lead to some bias and discrepancies on results. To prevent this variability, the Multi-HYFIT program was developed by Ortega and Garcia de la Torre (2007) to enable estimates for consensus values of L_p and M_L and chain diameter d, by considering two or more data sets of intrinsic viscosity *([η]),* sedimentation coefficient ($s^0_{20,w}$) and where appropriate radius of gyration (R_g) and translational diffusion coefficient (D_t) for varying molecular weights of the same substance. This program carries out minimisation of a target function known as Δ using Bushin-Bohdanecky (Bohdanecky, 1983, Bushin et al., 1981a) and Yamakawa-Fujii (Yamakawa and Fujii, 1973) equations within the several variables. The optimization process can be implemented giving different weightings to each property (Ortega and García de la Torre, 2007). To simplify and accelerate the minimization of the process, the least effective parameter or well defined parameter from known molecular structure (eg. M_L) can be fixed .The results of simulation analysis showed that L_p is comparatively insensitive to the value chosen d. Then the Multi-HYDFIT program optimizes the parameters in order to obtain the minimisation of the target function, based on the following equations:

$$\Delta^2 = \frac{1}{N_s}\sum_{i=1}^{N_s}\left[(\sum_T W_T)^{-1}\sum_T W_T\left(\frac{a_{T(cal)}-a_{T(exp)}}{a_{T(\exp)}}\right)^2\right] \qquad (5.10)$$

$$\Delta^2 = \frac{1}{N_s}\sum_{i=1}^{N_s}\left[(\sum_I W_I)^{-1}\sum_I W_I\left(\frac{a_{I(cal)}-a_{I(exp)}}{a_{I(\exp)}}\right)^2\right] \qquad (5.11)$$

where N_s is the number of samples, W_T and W_I are the statistical weights for equivalent radii a_T and a_I and the subscripts cal and exp indicates values from

calculated and experimental values, respectively. Therefore, Δ is a dimensionless estimate of the consensus between calculated values for the frictional coefficient, intrinsic viscosity and radius of gyration for a certain persistence length, L_p and the experimentally measured parameters (Ortega et al., 2011, Patel et al., 2008b).

In this study, the chain diameter, d was fixed and L_p and M_L were treated as variables. In this case the best estimates for the persistence lengths and mass per unit lengths of each sodium hyaluronate sample were obtained with the minimum value of the target function Δ and shown as contour plots as shown in Figures 5.11. The values of the target (error) function, Δ are represented by the full colour spectrum ranging from blue to red. The x-axis and y-axis represents L_p (nm) and M_L ($g.mol^{-1}.nm^{-1}$), respectively.

The overall L_p and M_L were found as (9.0 ± 0.7) nm and (321 ± 33) $g.mol^{-1}.nm^{-1}$, respectively. The values estimated for each sample were found in the range of 5.0-9.0 nm for L_p, whereas 290-395 $g.mol^{-1}.nm^{-1}$ for M_L, and are given in Table 5.5. The small differences for L_p and M_L might be due to different chemical compositions. Furthermore, these values indicate the semi-flexible random coil structure and the range of persistence length we find is consistent with previous studies (Cleland, 1984, Fouissac et al., 1992, Haxaire et al., 2000, Buhler and Boué, 2004) and with other semi- flexible coil type polysaccharides such as citrus pectin (Morris et al., 2008).

Table 5.5: Summary of the persistence length, L_p and the mass per unit length, M_L values for sodium hyaluronate samples.

Sample	L_p (nm)	M_L (g mol^{-1} nm^{-1})
HAV1	5.5 ± 0.6	385 ± 30
HAV2	9.0 ± 1.5	385 ± 50
HAV3	7.3 ± 0.1	290 ± 30
HAV4	5.0 ± 0.1	300 ± 10
HAV5	5.0 ± 0.1	395 ± 10
HAV6	5.0 ± 0.1	300 ± 10
MHAV1	5.9 ± 0.6	325 ± 20
MHAV2	7.0 ± 0.2	370 ± 10

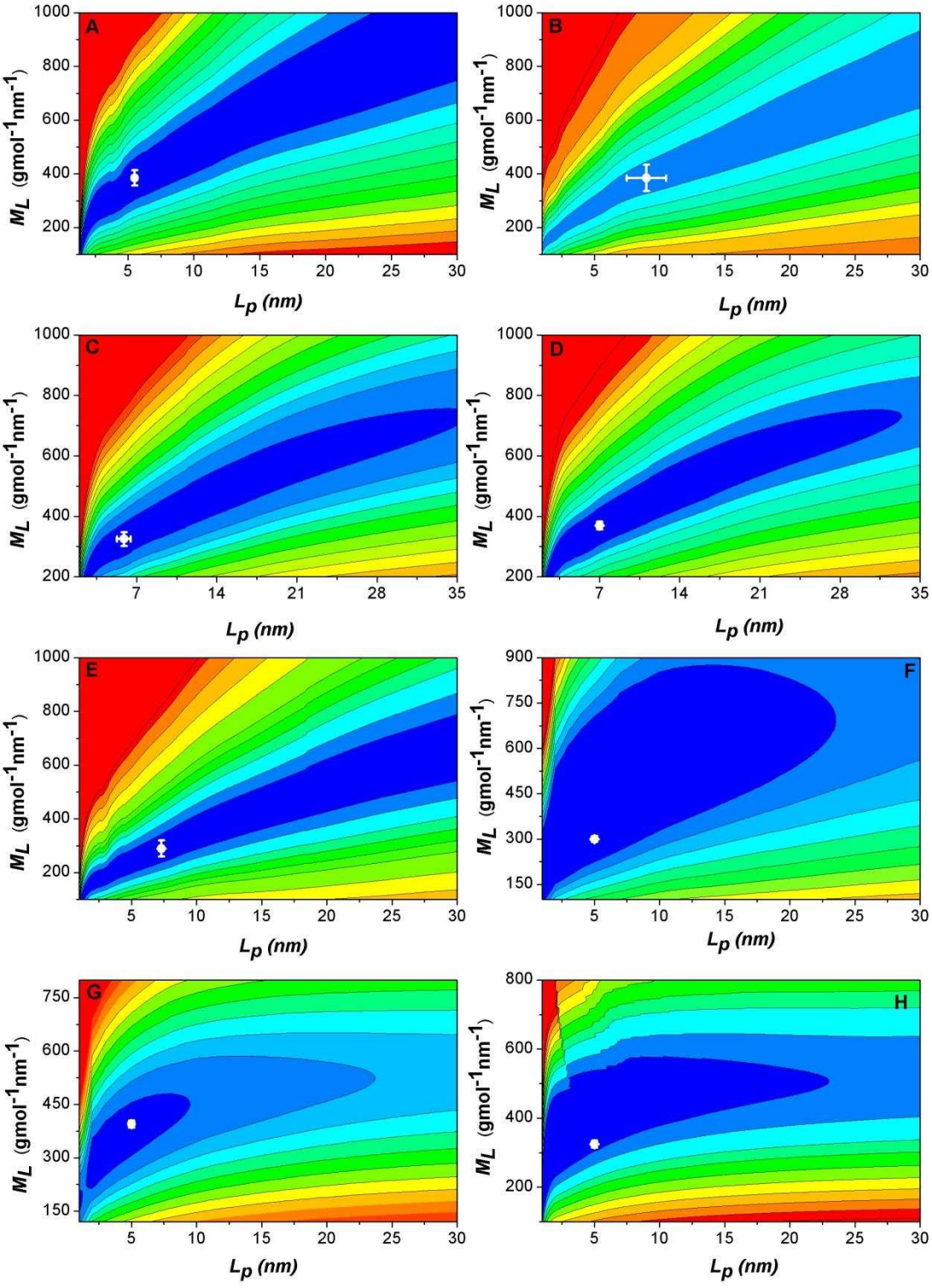


Figure 5.11: Contour plots for sodium hyaluronate samples; (A) HAV1, (B) HAV2, (C) MHAV1, (D) MHAV2, (E) HAV3, (F) HAV4, (G) HAV5, (H) HAV6. The target function, Δ calculated based on variables values of L_p and M_L, and are represented on the full colour spectrum from blue (Δ = 0) to red ($\Delta \geq 0.95$).

5.4.4.4. Molecular Conformation Zoning

The sedimentation conformation zoning plot provide the estimation of 'overall' solution conformation of a macromolecule ranging from Zone A (extra-rigid rod) to Zone E (globular or branched) by plotting of $k_s M_L$ versus [s]/M_L. (Pavlov et al., 1997, Pavlov, 2013). [s] is evaluated from this equation:

$$[s] = \frac{s^0_{20,w}\eta_{20,w}}{\left(1-\bar{\upsilon}\rho_{20,w}\right)} \tag{5.12}$$

M_L is the mass of the molecule(s) within the polymer divided by its length. In this study, M_L was taken as the estimated values obtained from Multi- HYDFIT analysis as 321 $g.mol^{-1}.nm^{-1}$ and [s] was calculated from sedimentation coefficient data.

Figure 5.12 demonstrates that the sodium hyaluronate samples have semi-flexible conformation in Zone C. This method also shows an excellent agreement with results from MHKS and Wales van Holde ratio.

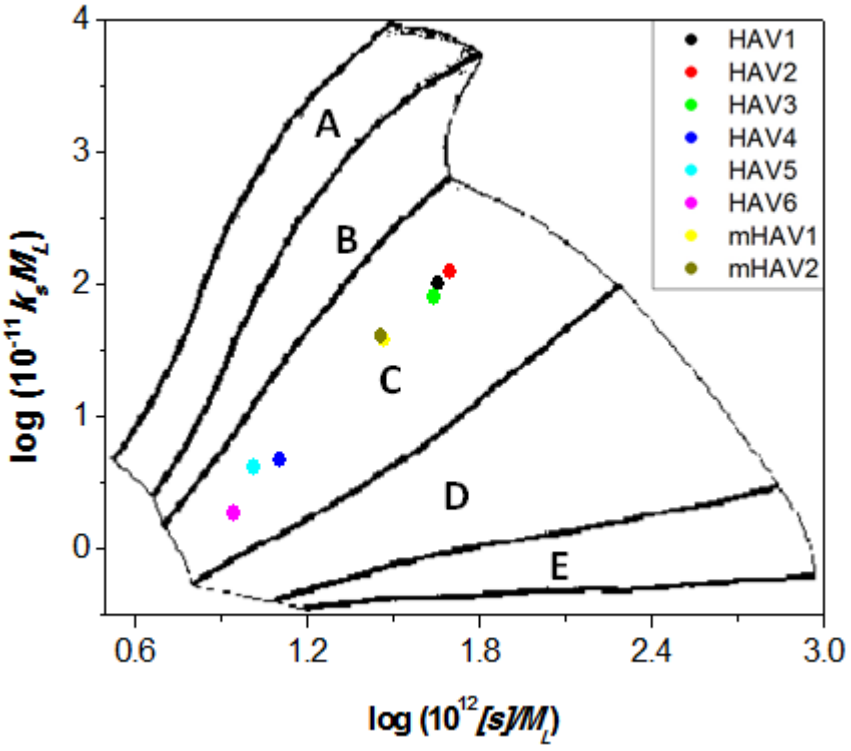


Figure 5.12: The conformation zoning plot for sodium hyaluronate samples. All samples fall in the zone for semi-flexible coil structures (Zone C).

5.5. DISCUSSION

Throughout this study on sodium hyaluronate samples, the samples that have different molecular weight were examined in terms of their hydrodynamic properties (e.g. molecular weight and viscosity) for comparative purposes and the conformational characteristics. According to the plots of g(s) vs s (Svedberg), the purity and homogeneity of samples were represented. As the sedimentation coefficient particularly depends on size (and conformation), the low sedimentation coefficient might be an indicator of low molecular weight samples since Hokputsa and co-workers indicated this result (Hokputsa, 2003). The concentration dependence of sedimentation or Gralén coefficient (k_s) for each sample was obtained

from the reciprocal plots of sedimentation coefficient ($1/s^0_{20,w}$) vs. concentration and it was also used with the intrinsic viscosity results to calculate Wales-van Holde ratios, which provided a simple guidance for the semi-flexible conformation adopted by these polysaccharides.

Molecular weight which is described as 'weight average molecular weight' is an important parameter for the hydrodynamic characterisation of sodium hyaluronate and was measured using two different experimental approaches. Firstly, sedimentation equilibrium in the AUC was used to determine the weight average molecular weight for the whole distribution. Since determination of the molecular mass of sodium hyaluronate by this method relates with eliminating the effects of solution non-ideality, running the samples over a range of concentrations and extrapolating to zero concentration was used to accomplish this effect. For the low molecular mass samples, an extrapolation of $1/M_{w,app}$ versus concentration was sufficient whereas it was not efficient for the two high molecular weight samples HAV1 and HAV2. In this case, SEC-MALS technique has been successfully applied to sodium hyaluronate samples with higher molecular weight since the dilution of the sample into the column was low enough to eliminate non-ideality effect. This state was also observed by Hokputsa et al., (2003) with the high molecular weight samples and the molar mass was achieved by taking advantage of using SEC-MALS. Results of the weight average molecular weight were confirmed by using both sedimentation equilibrium in AUC and SEC-MALS methods, which were consistent with those obtained previously Hokputsa et al. (Hokputsa et al., 2003b), Takahashi et al. (Takahashi et al., 1999) and Caspersen et al. (Caspersen et al., 2014).

SEC-MALS also provided the advantage of coupling online molecular weight and intrinsic viscosity measurements for the samples, which enabled determination of the

conformation by Mark-Houwink-Kuhn-Sakurada (MHKS) and flexibility by Multi-HYDFIT methods. The MHKS results indicated that the all samples adopted a semi-flexible random coil type conformation confirmed by the Wales-van Holde ratio and conformation zoning. In terms of persistence length, two different methods, Bushin-Bohdanecky and Multi-HYDFIT, have been applied to estimate the conformational flexibility of the samples. Both methods confirmed the previous results as a flexible coil conformation. The L_p values varies between 5.0-9.0 nm in agreement with Fouissac et al. (Fouissac et al., 1992) and Buhler and Boue (Buhler and Boué, 2004) who found the L_p of 4.5-8 nm using Odijk's model and Yamakawa-Fujii-Yoshizaki viscosity theory, and L_p of 9 nm from combined light and small-angle neutron scattering data. On the other hand, Hayashi and co-workers determined the L_p as 4 and 10.5nm using Yamakawa-Fujii-Yoshizaki theory combining with Yamakawa-Stockmayer-Shimada theory and by Bushin-Bohdanecky plot (Hayashi et al., 1996). Considering the L_p data from these three techniques above indicates that L_p not only relies on the chain conformation, solubility, side chain aggregation and excluded volume effects but also the method and the parameters that are used.

5.6. CONCLUSION

In this chapter, the characterisation of hyaluronic acid in its sodium salt form has been successfully achieved using the complementary hydrodynamic techniques of AUC (sedimentation velocity and equilibrium), SEC-MALS and viscometry providing knowledge on concerning heterogeneity and conformation of this important substance. The conformation of samples was also revisited by Multi-HYDFIT and molecular conformation zoning. Meanwhile the results from Multi-HYFIT have perfect agreement with the previous results, and the flexible coil

conformation was proved by this technique and the other complementary conformation methods Mark-Houwink-Kuhn-Sakurada (MHKS), Wales van Holde Ratio and molecular conformation zoning.

CHAPTER 6

A STUDY ON SOLUTION PROPERTIES AND MOLECULAR CONFORMATION OF SCHIZOPHYLLAN

6.1. INTRODUCTION

Schizophyllan is a non-ionic, water-soluble microbial homopolysaccharide that is produced by fermentation from the filamentous fungi Schizophyllum commune. It consists of a linear chain of β-D -(1-3)-glucopyranosyl groups, to which β-D-(1-6)-glucopyranosyl groups are attached (e.g. Figure 6.1) (Kumari et al., 2008, Bot et al., 2001). Through the advantage of these glucosyl side-chains being on the outside of a triple helical structure, it is readily dissolved in water (Bot et al., 2001). Owing to its high capacity for immobilising water (in cosmetics-skin and hair products), high heat stability (petroleum recovery) and bioactivity characteristics (antitumor, anti-inflammatory, antibacterial activities), it has been considered for many industrial, medical and pharmaceutical applications (Leathers et al., 2006, Tombs and Harding, 1997).

The solution properties of schizophyllan have previously been studied in different solvents and temperature conditions, e.g. (Norisuye et al., 1980, Sato et al., 1983,

Sato et al., 1984, Yanaki et al., 1980, Kashiwagi et al., 1981, Stokke et al., 1993, Tako, 1996). Early studies had suggested that the conformation of schizophyllan is a

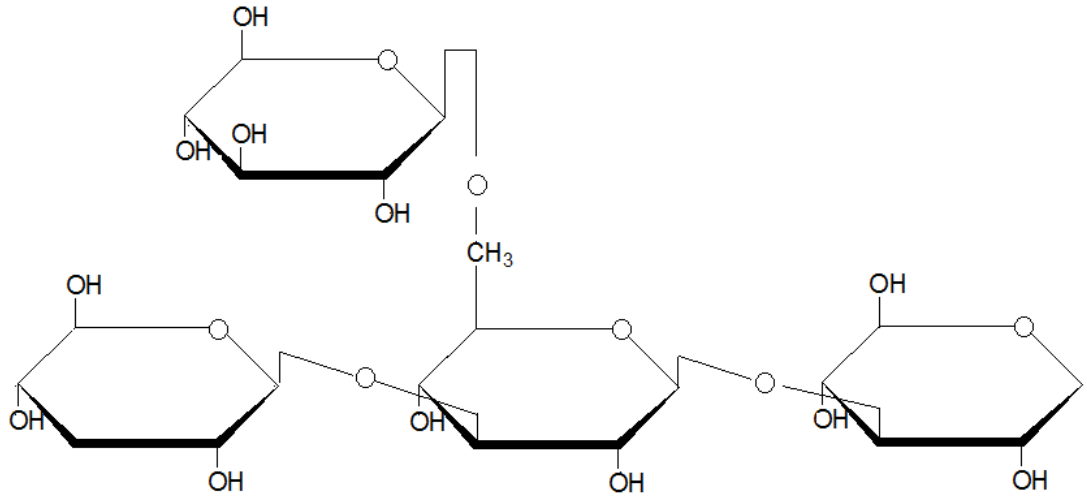


Figure 6.1: Chemical structure of repeating unit of schizophyllan (reproduced from (Takedatsu et al., 2012)

rod-like trimer in water and a single random coil in DMSO or NaOH by using sedimentation equilibrium and light scattering methods. (Norisuye et al., 1980, Yanaki et al., 1980, Kashiwagi et al., 1981, Sato et al., 1983). Light scattering and viscosity results have shown that schizophyllan completely dissolves in 0.01M NaOH and the trimer structure is also maintained (Kashiwagi et al., 1981, Yanaki et al., 1980). The conformational transition from trimers to single chains (thermo-irreversible) can also be generated by heating schizophyllan aqueous solutions above 135 °C (Yanaki et al., 1985, Zentz et al., 1992, Tako, 1996).

Data sets of intrinsic viscosity vs. molecular weight, sedimentation coefficient vs. molecular weight, radius of gyration vs. molecular weight plots have also been used to estimate not only conformation from Mark-Houwink-Kuhn-Sakurada power law relations but also have been used to estimate the persistence length (L_p) (flexibility of

linear polymer chains) and mass per unit length (M_L) (molar mass of the polymer divided by its length: see for example (Laue and Rhodes, 1990). Norisuye et al. (1980), Yanaki et al. (1980) and Kashiwagi et al. (1981) who have estimated (L_p and M_L using the so-called Yamakawa-Fujii relation (Yamakawa and Fujii, 1973) as shown in Table 6.1. Bohdanecky (Bohdanecky, 1983) employed the intrinsic viscosity and molecular weight data from Yanaki and co-workers (Yanaki et al., 1980) to estimate L_p and M_L and - the chain diameter (d)- and the persistence length was found higher (296 nm). Stokke et al. have observed (L_p) and (M_L) in the range of ~104-161 nm and ~2070-2013 $g.mol^{-1}.nm^{-1}$ for three ultrasonicated schizophyllan samples using electron microscopy (Stokke et al., 1993).

Table 6.1. Persistence length L_p and mass per unit length M_L of schizopyhyllan

L_p (nm)	**M_L (g mol^{-1} nm^{-1})**	**Reference**
100-200	-	Norisuye et al. (1980)
200 ± 30	2150 ± 150	Yanaki et al. (1980)
180 ± 30	2170 ± 50	Kashiwagi et al. (1981)
104 - 161	2080 - 2130	Stokke et al. (1993)
274 - 296	1900 - 2050	Bohdanecky (1983)

In a more recent approach, an algorithm known as Multi-HYDFIT (Ortega and García de la Torre, 2007) was applied to previous literature data (s vs. M_w , R_g vs. M_w, $[\eta]$ vs. M_w), by Ortega et al. (Ortega et al., 2011). These researchers obtained values of (150 ± 20) nm for L_p and (2050 ± 90) nm for M_L. However, those

researchers used a very different partial specific volume (0.555 ml/g) instead of Yanaki's - 0.619 ml/g.

In order to address these discrepancies and by taking advantage of the recent advances in hydrodynamic analysis, two different schizophyllan samples with different molecular weight were depolymerised to estimate their hydrodynamic parameters in aqueous solution. Newly published approaches for sedimentation velocity in analytical ultracentrifugation (AUC) (the Extended Fujita approach) and sedimentation equilibrium ("SEDFIT-MSTAR") together with size exclusion chromatography coupled to multi angle light scattering (SEC-MALS) were used to characterise heterogeneity and molecular weight distributions. The flexibility parameters, L_p and M_L values, and the conformation were re-assessed using Multi-HYDFIT and other methods, namely the Wales-van Holde and Conformation Zoning approaches.

6.2. MATERIALS

Two schizophyllan samples GM1 and INV1 were kindly provided by Glycomix Ltd. (Reading, United Kingdom) and Invivogen Ltd (San Diego, USA), respectively. Both samples were used as supplied without any further purification and assumed to be of similar composition. A stock solution for both GM and INV was prepared by dissolving a known amount of schizophyllan in distilled deionised water at room temperature with gentle stirring overnight followed by dialysis for a further 18 hours against phosphate-chloride buffer supplemented with NaCl according to Green (1933) at pH 7.0 and an ionic strength (I) of 0.1M. The concentrations, c (g/ml) of the stock schizophyllan solutions were measured after dialysis using an Atago

(Japan) DD-7 refractometer calibrated with glucose standards, and a refractive increment dn/dc of 0.145ml/g (Norisuye et al., 1980). The solution of native schizophyllan INV was sonicated with a VWR Ultrasonicater Bath-USC 1700 THD series (VWR International, UK) at 480W and 45 kHz for 38 hours to produce different molar mass of sample, INV2. The stock solution of another native schizophyllan GM1 was then also exposed to microwave heating by a microwave synthesiser (Anton Paar Ltd, UK) at 500W and 110°C for 45 seconds to produce GM2. It was observed that heating for a longer period (more than 45 seconds) resulted in discoloration of the sample.

6.3. METHODS

6.3.1. Partial Specific Volume

Density measurements of schizophyllan solutions (ranging from 0.25 to 1.25mg/ml) were performed using a DMA 5000M density meter (Anton Paar, UK) so as to determine the partial specific volume using the mechanical oscillator technique according to the procedure of Kratky et al. (Kratky et al., 1973). The partial specific volume was calculated using the equation below;

$$\bar{\upsilon} = \frac{1 - d\rho/dc}{\rho_0} \tag{6.1}$$

where $\bar{\upsilon}$ is the partial specific volume (ml/g), ρ_0 is the density of the solvent (g/ml), $d\rho/dc$ is the density increment which can be obtained from the limiting slope of the plot of solution density versus concentration.

6.3.2. Sedimentation Velocity (SV)

An Optima XL-I (Beckman Instruments, Palo Alto, USA) equipped with Rayleigh interference optics was used to determine the sedimentation behaviour and molecular homogeneity of schizophyllan samples. Solution concentrations ranging between 0.2 – 1.5 mg/ml for each schizophyllan were studied at a temperature of (20.0 ± 0.1) °C. 400µl of solution and an equal volume of the pH 7.0, I=0.1M reference buffer/solvent (400µl) were injected into the solution and solvent channels respectively of 12 mm optical path length double sector cells. The Rayleigh interference optical system was used to record changes in the concentration versus radial displacement profiles with time. Scans were taken at 2 min intervals for a run time of approximately 18 hours at 40000 rpm. A partial specific volume, $\bar{\upsilon}$ of -0.592 ml/g- was used for the schizophyllan according to the density meter measurements. For comparison purposes, sedimentation coefficients were normalised to standard solvent conditions, namely the density and viscosity of water at 20.0°C -see e.g. (Abdelhameed, 2010, Laue and Stafford III, 1999):

$$s_{20,w} = \{(1-\bar{\upsilon}\rho_{20,w})/(1-\bar{\upsilon}\rho_0)\} \cdot \{\eta_0 / \eta_{20,w}\} s_{T,b} \qquad (6.2)$$

where ρ_0 and η_0 are respectively the density and viscosity of the solvent or buffer, b, at temperature T and $\rho_{20,w}$ and $\eta_{20,w}$ the corresponding values of water at 20.0 °C. The data was analysed using the "least squares ls-g(s) model" SEDFIT program of Schuck and colleagues (Dam and Schuck, 2004) in terms of distributions of sedimentation coefficient distribution . The ls-g(s) vs. s profiles were used to provide an assessment of sample polydispersity. The s and $s_{20,w}$ values are 'apparent' values because of non-ideality. To remove this effect, $s_{20,w}$ is extrapolated to zero

concentration and $s^0_{20,w}$ is obtained from reciprocal plot of $s_{20,w}$ ($1/s_{20,w}$) vs. concentration (see for example, (Harding, 2005c)):

$$1/s_{20,w} = (1/ s°_{20,w}).(1+k_sc) \quad (6.3)$$

where $s^0_{20,w}$ is sedimentation coefficient at zero concentration and standard condition, k_s is the Gralen parameter (Gralen, 1944); see also (Harding, 2005a)

6.3.3. Sedimentation Equilibrium (SE)

Sedimentation equilibrium experiments were also carried out using the Beckman (Palo Alto, California, U.S.A.) Optima XL-I analytical ultracentrifuge and employing Rayleigh interference optics and an automatic on-line data capture system. 12 mm optical path length double-sector titanium cells with sapphire windows were loaded with (~70µl) of dialysed sample as a concentration series (that is ranging from 0.4-1.5mg/ml) and a matching amount of reference buffer dialysate in appropriate channels. The balanced cells were then loaded into an analytical 8-hole titanium rotor An50-Ti and placed in the AUC. After time was allowed for vacuum formation and for temperature equilibration (20.0 °C), the rotor was then accelerated to 3000rpm for GM1 and GM2, and 7000 rpm for INV1 and INV2. Using the Rayleigh interference optical system, scans were taken every one hour and equilibrium was reached after approximately 48 hours for INV1 and INV2, and 96 hours for GM1 and GM2. Record of the relative concentration distribution of the solute at equilibrium was analysed to give the weight average apparent molecular weight $M_{w,app}$ using the SEDFIT-MSTAR program implemented by Schuck et al. (Schuck et al., 2014) based on the algorithm of Cölfen and Harding (Cölfen and

Harding, 1997) and the M* function of Creeth and Harding (Creeth and Harding, 1982).

6.3.4. Size Exclusion Chromatography Coupled to Multi Angle Light Scattering (SEC-MALS)

Molecular weights (weight averages) and molecular weights distribution of all schizophyllan samples were determined using SEC–MALS. The system consisted of a series of size-exclusion chromatography (SEC) columns, namely TSK G5000PW and TSK G6000PW, protected by a similarly packed guard column (Tosoh Bioscience, Tokyo, Japan) coupled on-line to "Helios" multi-angle light scattering (MALS) and refractive index (OptilabrEX) detectors (Wyatt Technology, Santa Barbara, USA). Solutions for injection were prepared as 0.5mg/ml for all samples and were then filtered through a 0.2 μm syringe filter (Minisart, Surrey, UK)—to remove any insoluble material or dust prior to being injected into the columns. The buffer was pumped at a steady, pulse-free flow rate of 0.8 ml/min through the column system. Data was analysed by ASTRA (Version 6.1) software (Wyatt Technology, Santa Barbara, USA). A linear fit to the "Debye" plot of Kc/R_θ vs $\sin^2(\theta/2)$, where the terms have their meaning was used for calculating the absolute weight average molecular weight (M_w) (Wyatt, 2013b). The refractive index increment (dn/dc) value used for data analysis for the schizophyllan was 0.145ml/g (Norisuye et al., 1980).

6.3.5. Capillary and Differential Pressure Viscometry

Schizophyllan solutions ranging from 0.2 mg/ml to 1.2 mg/ml were analysed using a Schott-Geräte Ostwald viscometer system at a temperature of (20.0 ± 0.01) °C. The

relative viscosity, η_{rel}, was obtained from the ratio of the flow time of the solution t (sec) to the flow time of solvent ($\eta_{rel} = (t/t_o)$), where the flow time was recorded accurately using photosensors. Because of the low concentrations, a density correction was deemed unnecessary (Harding, 1997). The reduced viscosity ($\eta_{red} = (\eta_{rel}-1)/c$) and the inherent viscosity ($\eta_{inh} = (ln\eta_{rel})/c$) were extrapolated to zero concentration to eliminate non-ideality effects with the common intercept at c=0 yielding the intrinsic viscosity $[\eta]$ from Huggins and Kraemer equations:

$$\eta_{red} = [\eta] (1 + K_H.[\eta].c) \quad (6.4)$$

and

$$(ln\eta_{rel})/c = [\eta] (1 - K_K.[\eta].c) \quad (6.5)$$

where K_H and K_K are the Huggins (1942) and Kraemer (1938) constants, respectively. As an additional check, a combined Solomon & Ciuta (1962) relation was also used:

$$[\eta] \sim (1/c). [2 (\eta_{sp} - ln (\eta_{rel}))]^{1/2} \quad (6.6)$$

The assumption has been made that there was no shear dependence of $[\eta]$ under creeping flow conditions in the capillary viscometer.

Intrinsic viscosities of samples were also measured by Viscostar (Wyatt Technology) differential pressure viscometer on-line to the SEC-MALS system. Due to sensitivity of the sensors and high dilution in the column, the concentration is low and because of this, Solomon-Ciuta equation (6.6) can be applied without any extrapolation (Harding, 1997).

6.4. RESULTS

6.4.1. Partial Specific Volume

To measure the sedimentation coefficient and weight average molecular weight from sedimentation equilibrium experiment, partial specific volume, $\bar{\upsilon}$ of schizophyllan was required in 0.1M PBS. Thus, the partial specific volume was determined from density measurements and $\bar{\upsilon}$ of (0.59 ± 0.05) ml/g was calculated from the slope of the solution density versus concentration (Figure 6.2). This value is similar to the values for xanthan (Dhami, 1996) and citrus pectin (Harding et al., 1991a).

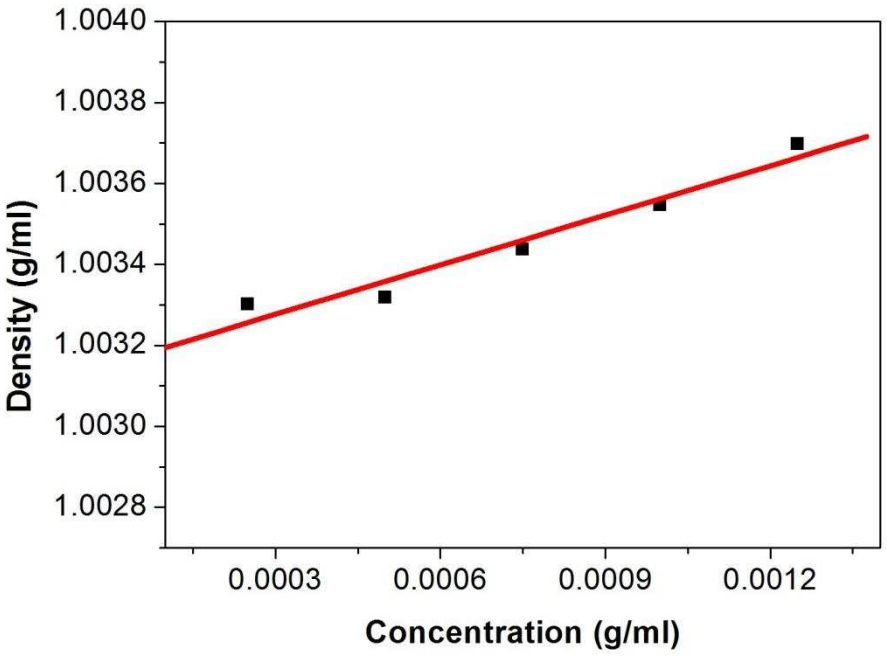


Figure 6.2. Determination of partial specific volume of schizophyllan using density measurement in 0.1M PBS at 20^{o}C.

6.4.2. Sedimentation Velocity (SV)

The sedimentation coefficient (s) of each schizophyllan sample was measured at various concentrations by the least square ls-g*(s) method. The sedimentation coefficient distribution plots (Figure 6.3) indicates that the apparent sedimentation coefficient distributions for all samples appear to be bimodal and showed that the samples are heterogeneous.

Table 6.2: Summary of $s^0_{20,w}$ and k_s for schizophyllan samples.

Sample	$s^0_{20,w}$ (S)	k_s (mL/g)
GM1	10.40 ± 0.2	168 ± 21
GM2	9.53 ± 0.3	186 ± 30
INV1	9.00 ± 0.36	141 ± 44
INV2	8.07 ± 0.13	236 ± 18

According to the distribution plots in Figure 6.3, two peaks were identified for each concentration studied and for all four schizophyllan samples. Peak 1 (the minor peak) is around ~2S which shows the small molecular weight component and peak 2 (the main component) is around ~8S - 9S that indicates higher molecular weight component in the sample.

To eliminate the effect of non-ideality $s_{20,w}$ was extrapolated to zero concentration to obtain $s^0_{20,w}$. The Figure 6.4 shows the reciprocal plots of apparent sedimentation coefficient versus concentration (for the main component). The slope of these plots gives the concentration dependence parameter k_s (Gralén coefficient) for each sample and presented on Table 6.2.

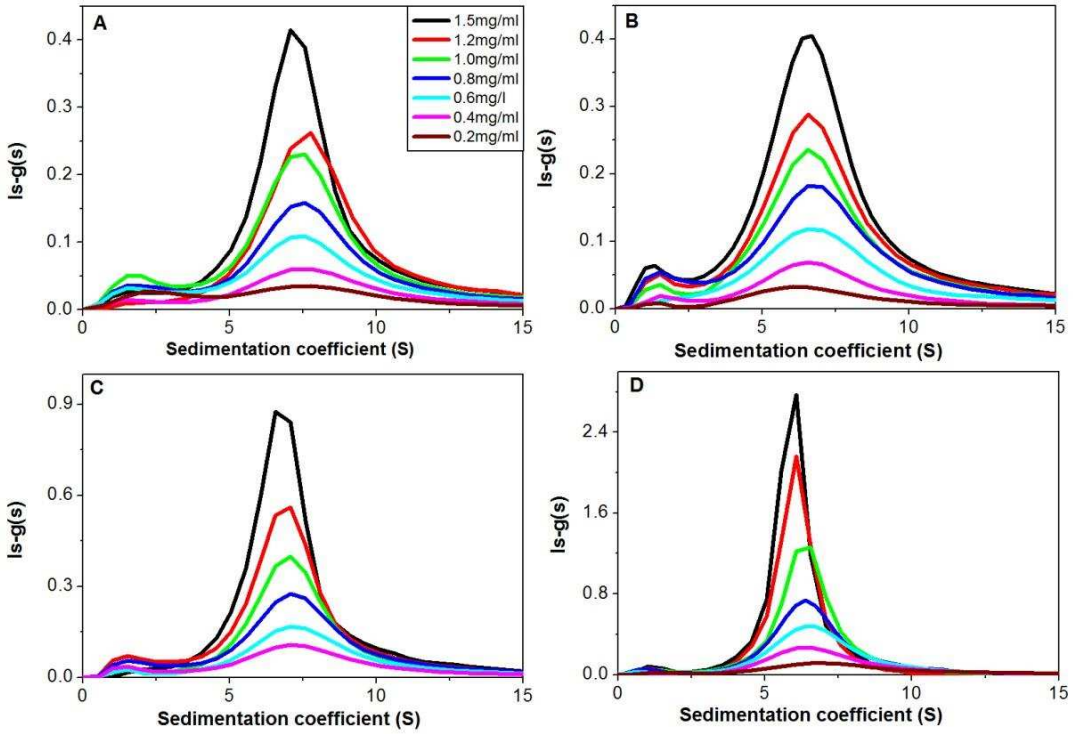


Figure 6.3: Sedimentation coefficient distribution profiles using least squares g*(s) method of SEDFIT obtained from sedimentation velocity experiment for schizophyllan samples (A) GM1, (B) INV1, (C) GM2, (D) INV2.

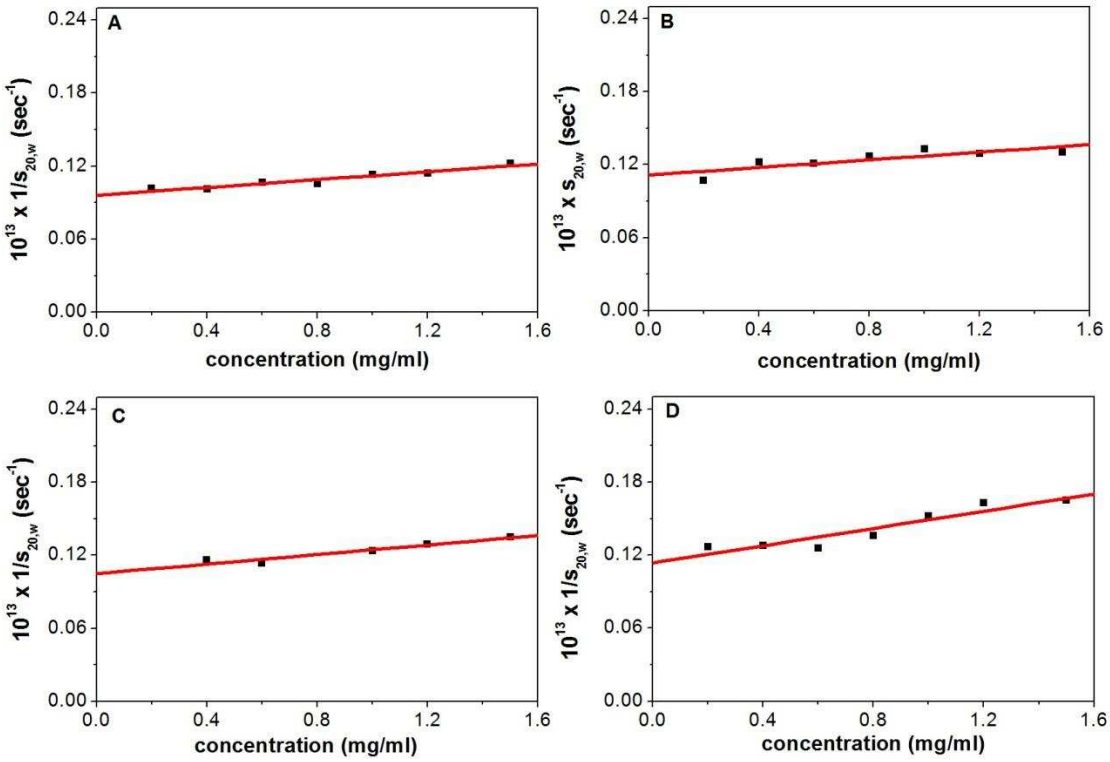


Figure 6.4: Concentration dependence (reciprocal) of the sedimentation coefficient plot (after correction to standard solvent conditions) for schizophyllan samples (main component) in 0.1M PBS at pH 7.0 (A) GM1, (B) INV1, (C) GM2, (D) INV2.

6.4.3 Estimation of Molecular Weight

The weight average molecular weight of schizophyllan samples was determined by the sedimentation equilibrium method in the analytical ultracentrifuge and SECMALS. The values were initially determined from the sedimentation equilibrium method. To eliminate the non-ideality effect in solution from excluded volume and charge effects, the samples were run at different loading concentrations in the range 0.4-1.6mg/ml. The data then was analysed using the SEDFIT-MSTAR program to obtain apparent weight average molecular weight

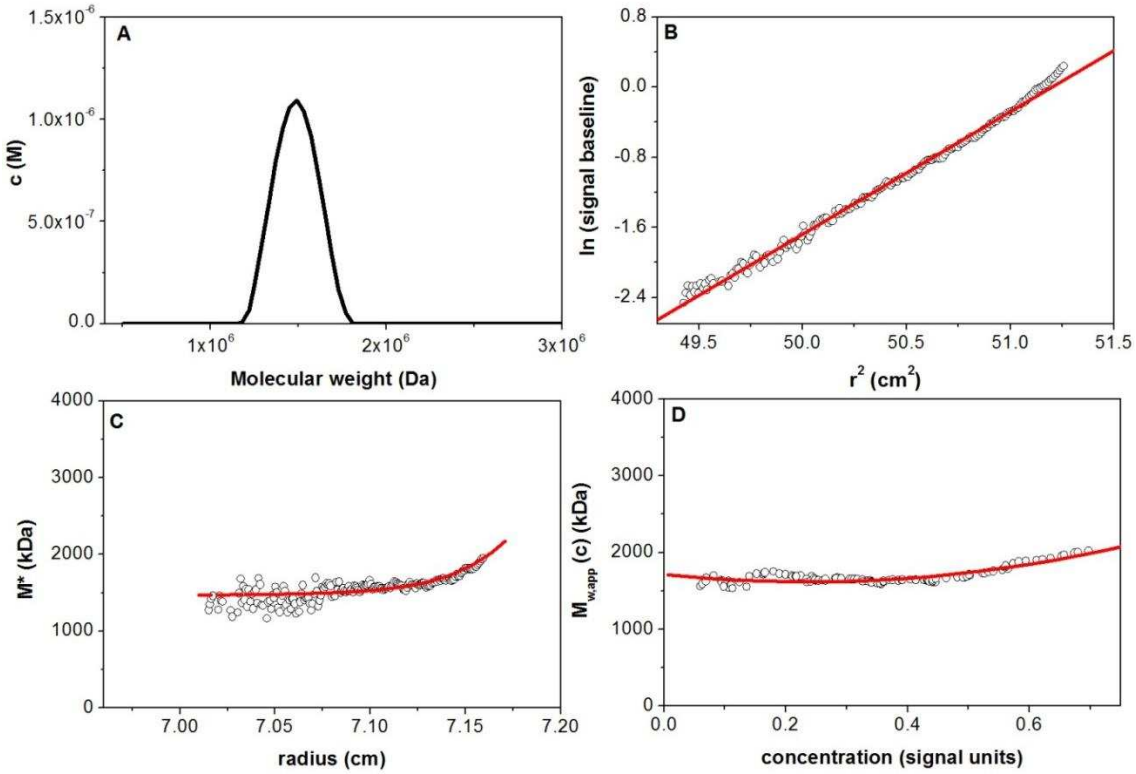


Figure 6.5: As (Figure 5.4) but the analysis of GM1 at a loading concentration of (0.6 mg/ml). $M_{w,app}$ from extrapolation of M* to cell base = 2043 kDa, and the meaning of the fitted lines in "c" and "d" are explained in the legend Figure 6.4.

Table 6.3: Summary of weight average molecular weights (M_w) results for schizophyllan samples from sedimentation velocity, equilibrium and SEC-MALS.

Sample	10^6 x M_w (Da)[a]	10^6 x M_w (Da)[b]	10^6 x M_w (Da)[c]
GM1	2.59 ± 0.6	2.14 ± 0.36	2.82 ± 0.16
GM2	1.94 ± 0.1	1.76 ± 0.19	2.12 ± 0.18
INV1	1.9 ± 0.8	1.93 ± 0.23	1.90 ± 0.33
INV2	1.15 ± 0.1	1.44 ± 0.17	1.50 ± 0.04

a : obtained from sedimentation equilibrium.
b : obtained from SEC-MALS.
c : obtained from molecular weight obtained from sedimentation velocity and the Extended Fujita method.

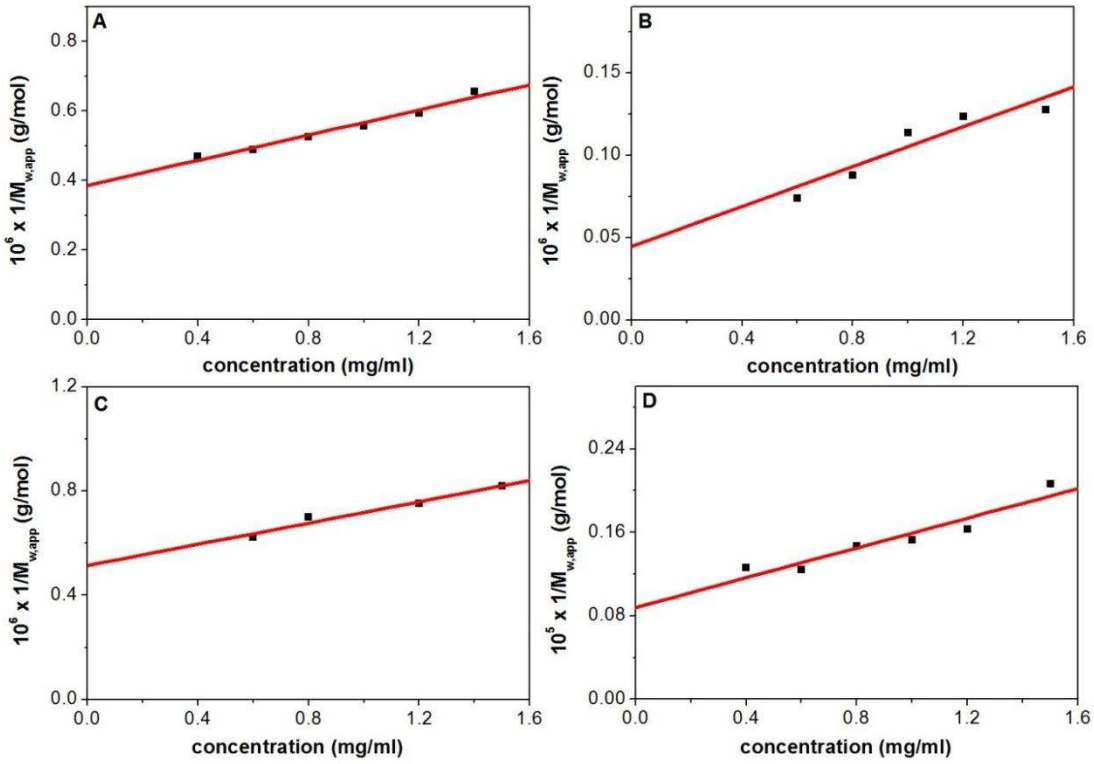


Figure 6.6: The reciprocal plots of the apparent weight average molecular weight ($M_{w,app}$) against concentration c (g/ml) for schizophyllan samples (A) GM1, (B) INV1, (C) GM2, (D) INV2.

(see, for example Figure 6.5). The reciprocal plot of $M_{w,app}$ versus concentration gave linear extrapolations for all samples as shown in Figure 6.6. The weight average molecular weight values were then yielded from the intercept of these extrapolations and presented in Table 6.3.

However, through the ability of studying at low concentrations (by dilution of the solution in the columns) in the light scattering detector of the SEC-MALS system, the non-ideality effects are usually small. Thus, the weight average molecular weight of each schizophyllan sample and its distribution were also obtained by SEC-MALS system and are reported in (Table 6.3). Within the error estimate the weight average

molecular weight results obtained for each sample from SEC-MALS are consistent with those found by sedimentation equilibrium.

The molecular weight distribution of schizophyllan samples was then obtained by transforming a distribution of sedimentation coefficient g(s) vs s into a distribution of molecular weight, f(M) vs M using the Extended Fujita method (Harding et al., 2011).

The transformation from g(s) versus s is as below:

$$f(M) = g(s).\ (ds/dM) \qquad (6.7)$$

with

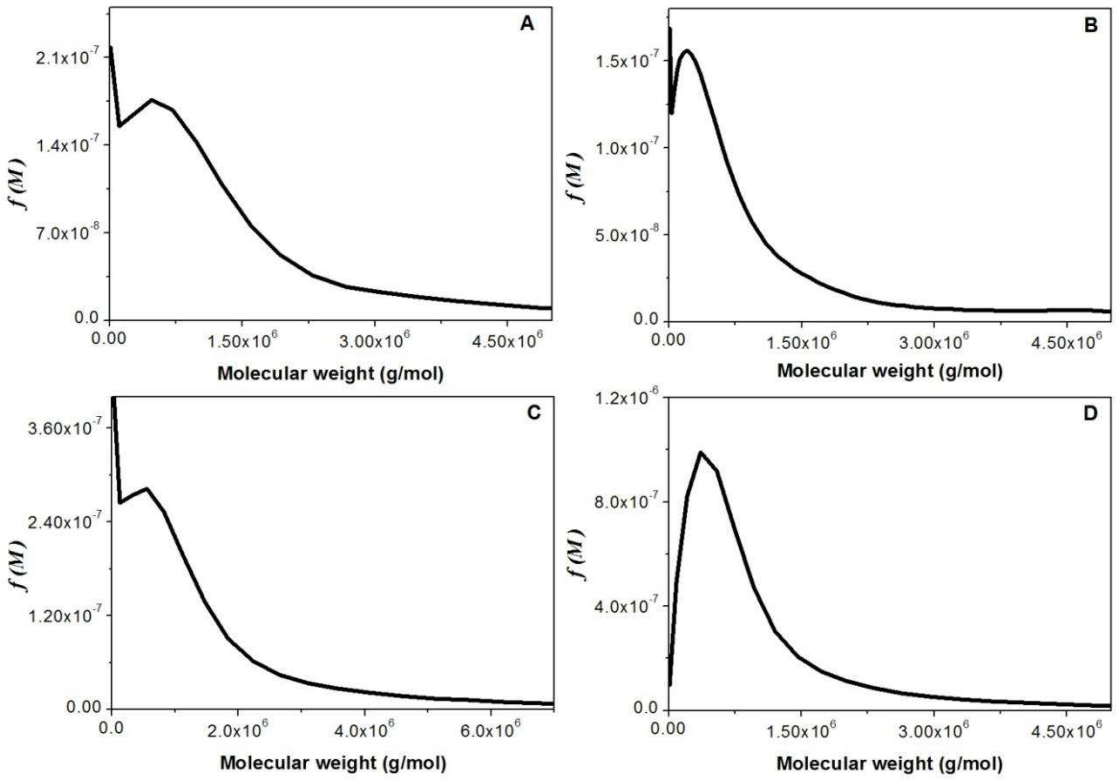


Figure 6.7: Molecular weight distribution for all schizophyllan samples in 0.1 M PBS buffer obtained from transformation of the g(s) versus s distribution using the Extended Fujita method of Harding et al., (2011) (A) GM1 at c=0.2mg/ml, (B) INV1, (C) GM2, (D) INV2 at c=0.4mg/ml.

$$s = \kappa_s . M^b \quad (6.8)$$

and

$$ds/dM = b. \kappa_s^{1/b}. s^{(b-1/b)} \quad (6.9)$$

the conformation parameter (MHKS) b and κ_s has been obtained as 0.28 and 0.162, respectively, from the slopes of double logarithmic plots of sedimentation coefficient versus molecular weight. The molecular weight distributions of samples are presented in Figure 6.7 and are consistent with the results obtained from sedimentation equilibrium and SEC-MALS.

6.4.4. Intrinsic Viscosity

The intrinsic viscosities of all schizophyllan samples were measured using both a capillary viscometer and the Viscostar (Wyatt Technology) differential pressure viscometer for each schizophyllan sample. The value of *[η]* were obtained using Huggins, Kraemer and Solomon-Ciuta extrapolations for the capillary viscometer

Table 6.4: Summary of intrinsic viscosity values of schizophyllan samples obtained from capillary viscometry and differential pressure viscometry.

Sample	Intrinsic viscosity [η] (mL/g)			
	Capillary viscometry			Online viscostar™
	Huggins	Kraemer	Solomon-Ciuta	
GM1	470 ± 10	510 ± 20	500 ± 16	730 ± 10
GM2	670 ± 35	700 ± 20	690 ± 20	730 ± 10
INV1	385 ± 20	430 ± 20	420 ± 20	560 ± 16
INV2	740 ± 65	730 ± 35	740 ± 40	765 ± 3

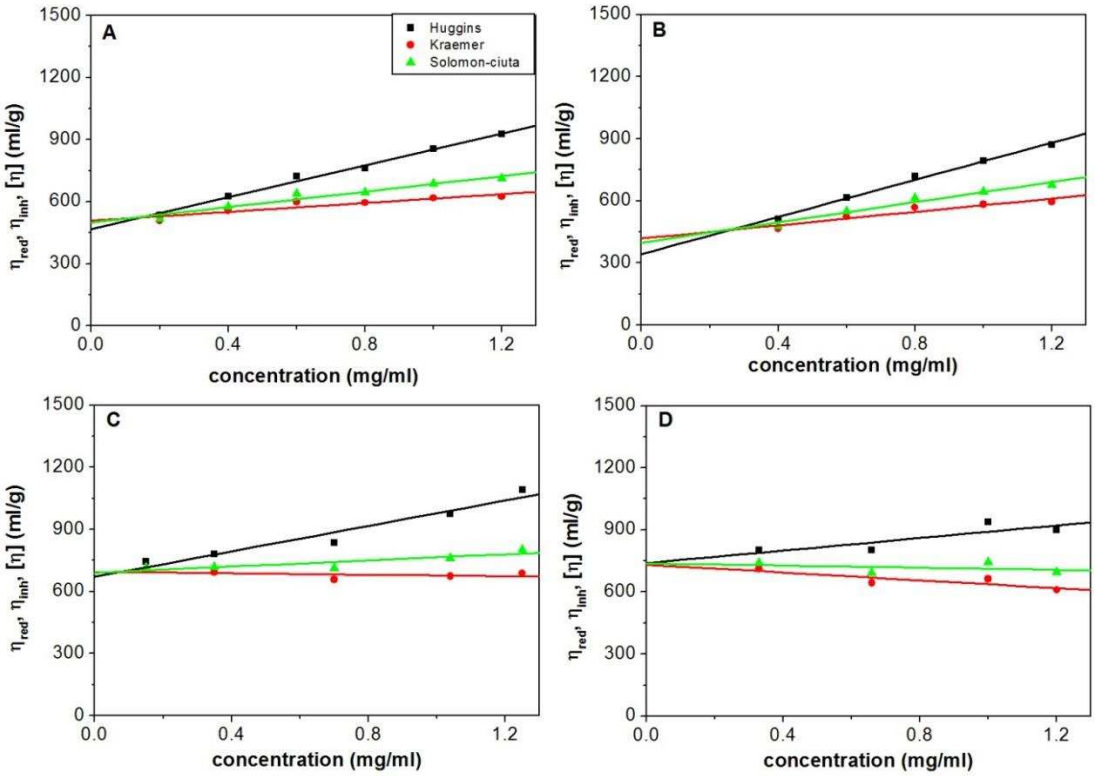


Figure 6.8: Intrinsic viscosity plots from capillary viscometry: Huggins, Kraemer and Solomon-Ciuta extrapolations for schizophyllan samples (A) GM1, (B) INV1, (C) GM2, (D) INV2.

and linear extrapolations can be seen from Figure 6.8 for all samples. The results in Table 6.4 were also in excellent agreement with the previous study by (Norisuye et al., 1980).

6.4.5. Conformation Analysis

6.4.5.1. Mark-Houwink-Kuhn-Sakurada Power Law Relationships

The conformation of schizophyllan samples was assessed based on knowledge of the sedimentation coefficient, $s^0_{20,w}$ and $[\eta]$ with M_w. Initially, the double logarithmic plot of sedimentation coefficient versus molecular weight can give the precise

indication of the gross conformation of the schizophyllan samples in dilute solution from equation 6.8.

The exponent b in equation 6.8 - has values ~0.67 (sphere), ~0.4-0.5 (random coil) and ~0.15-0.2 (rigid rod). As noted above, the overall b parameter for schizophyllan samples was found in this study as (0.28 ± 0.09) from the slope of a double logarithmic plot of $s^0_{20,w}$ versus M_w, which is consistent with a rod like molecule (Figure 6.9). This value agrees with that obtained previously by Yanaki and co-workers (Yanaki et al., 1980).

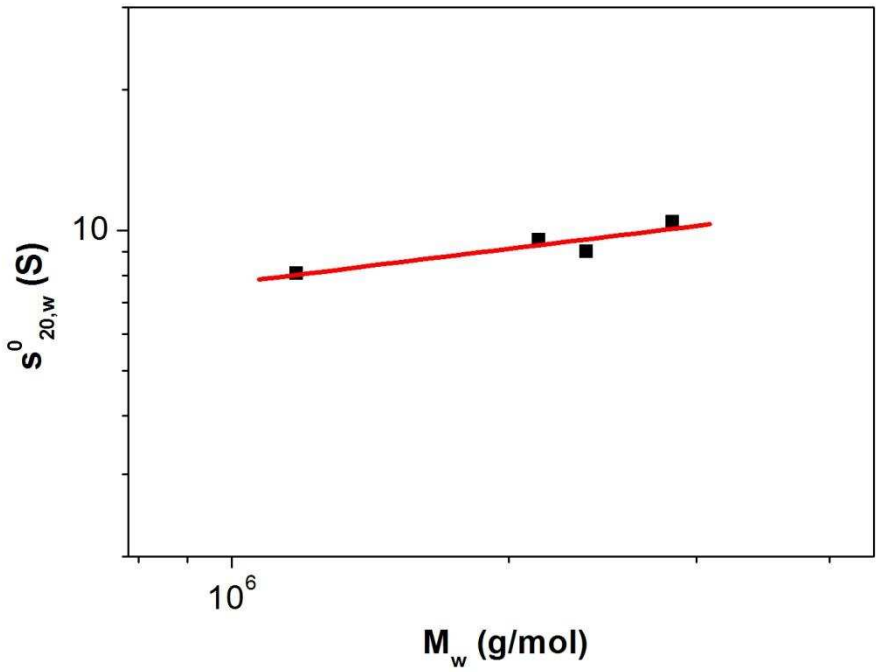


Figure 6.9: Mark–Houwink–Kuhn–Sakurada (MHKS) power law double logarithmic plot of $s^0_{20,w}$ vs M_w for all schizophyllan samples.

A similar MHKS double-logarithmic plot was produced for the intrinsic viscosity, $[\eta]$, data plotted versus molecular weight to obtain the Mark-Houwink exponent a as follows:

$$[\eta] = \kappa_{\eta} .M^{a} \quad (6.10)$$

Owing to the feature of the Viscostar coupled to the on-line fractionation SEC-MALS system, the conformation parameter a was characterised using the (MHKS) power law relation linking $[\eta]$ (from the Viscostar) and M_w (from SEC–MALS). The limiting a values are ~0 for the compact sphere, ~0.5-0-8 for random coil and ~1.8 for a rigid rod. (Harding, 2005b). The exponent of (a) yielded from the slope for all schizophyllan samples are reported in Table 6.5 and the results appeared to suggest the overall conformation as an extended rigid rod structure and similar to that for xanthan (Figure 6.10) (Tombs and Harding, 1997).

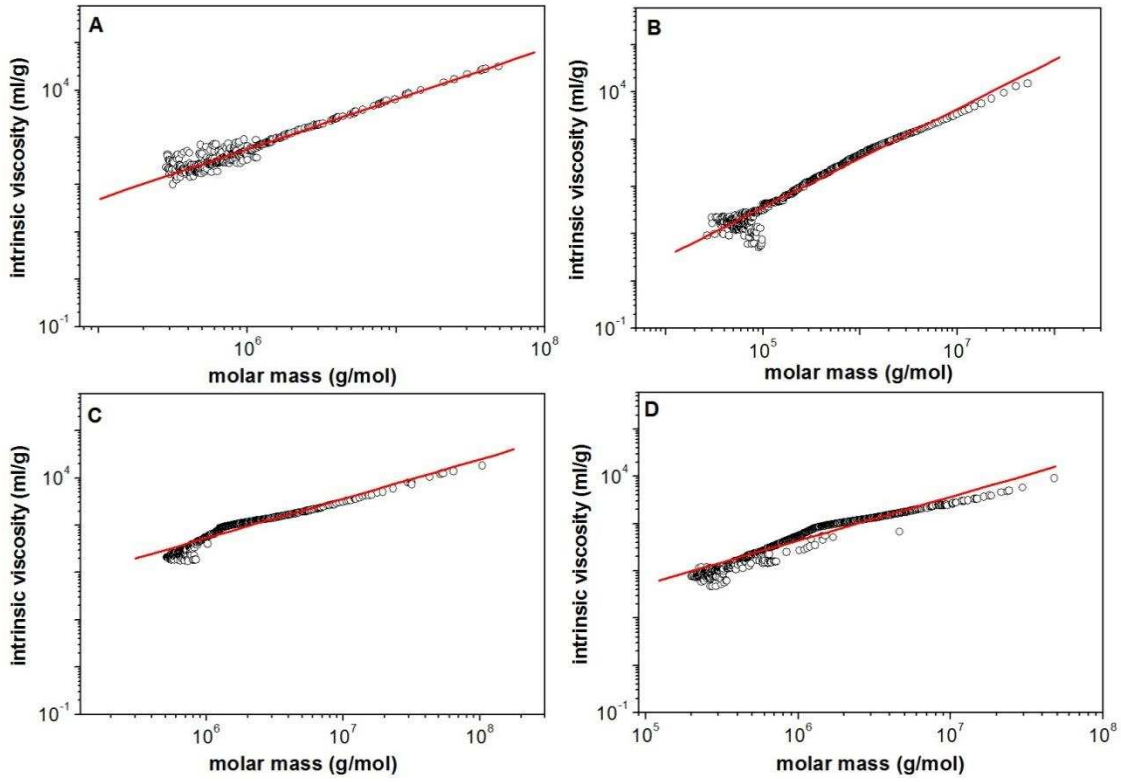


Figure 6.10: Mark–Houwink–Kuhn–Sakurada (MHKS) power law double logarithmic plot from on-line differential pressure viscometry coupled to SEC-MALS for schizophyllan samples (A) GM1, (B) INV1, (C) GM2, (D)INV2.

Table 6.5: Mark-Houwink-Kuhn-Sakurada (MHKS) power law exponent a, from SEC-MALS and Wales-van Holde ration, R, for schizophyllan samples.

Sample	MHKS a	R= $k_s/[\eta]$
GM1	1.06 ± 0.01	0.34
GM2	0.90 ± 0.01	0.27
INV1	1.04 ± 0.01	0.35
INV2	0.92 ± 0.01	0.32

6.4.5.2 Wales-Van Holde Ratio (R)

Another useful indication of the possible conformation for schizophyllan samples in solution can be obtained from the Wales-Van Holde parameter which is the ratio of the sedimentation concentration dependence coefficient, k_s, to the intrinsic viscosity $[\eta]$ (Wales and Van Holde, 1954). The value of this ratio is characteristically ~1.6 for spheres and random coils, and substantially lower, <1 for rods. The R results shown in Table 6.5 indicate an extended rod conformation for these schizophyllan samples

6.4.5.3. Estimation of the Persistence Length L_p and Mass Per Unit Length M_L

The conformational flexibility of linear polymer chains (worm-like chains) were estimated from persistence length L_p and M_L representations (Harding, 2005a). M_L is the mass of the molecule(s) within the polymer divided by its length. L_p is defined as the average projection length along the initial direction of the polymer chain and it can be estimated using different approaches either sedimentation coefficient

(Yamakawa and Fujii, 1973, Hearst and Stockmayer, 1962) or intrinsic viscosity (Bohdanecky, 1983, Stockmayer and Fixman, 1963), equations.

6.4.5.3.1. Yamakawa–Fujii Method

This method provides another way for estimating chain persistence length, L_p using sedimentation coefficient and molecular weight information. The slope of $s^0_{20,w}$ vs $(M_w)^{1/2}$ gives the value of L_p and M_L but it also requires knowledge about one of these parameters (L_p or M_L) (Yamakawa and Fujii, 1973). However, the original equation given by Yamakawa and Fujii (1973) was misprinted. Freire and Garcia de la Torre (Freire and Garcia De La Torre, 1992) provided the corrected relation as follows:

$$s^0 = \frac{M_L(1-\bar{\upsilon}\rho_0)}{3\pi\eta_0 N_A}\, x\, \left[1.843\left(\frac{M_w}{2M_L L_P}\right)^{1/2} + A_2 + A_3\left(\frac{M_w}{2M_L L_P}\right)^{-1/2} + \ldots.\right] \quad (6.11)$$

If the persistence length L_p is much larger than the mean chain diameter, d, Yamakawa and Fujii (Yamakawa and Fujii, 1973) have shown that $A_2 = -\ln(d/2L_p)$ and $A_3 = 0.1382$. Using Yamakawa- Fujii relation from the plot of $s^0_{20,w}$ vs $(M_w)^{1/2}$, the slope was obtained as $(3.74 \pm 0.11) \times 10^6$ (Figure 6.11). By the Equation (6.11) and fixed M_L as 2150 g/mol.nm, the L_p was estimated as (134 ± 4) nm and this value again indicates the extended rod conformation for schizophyllan in solution.

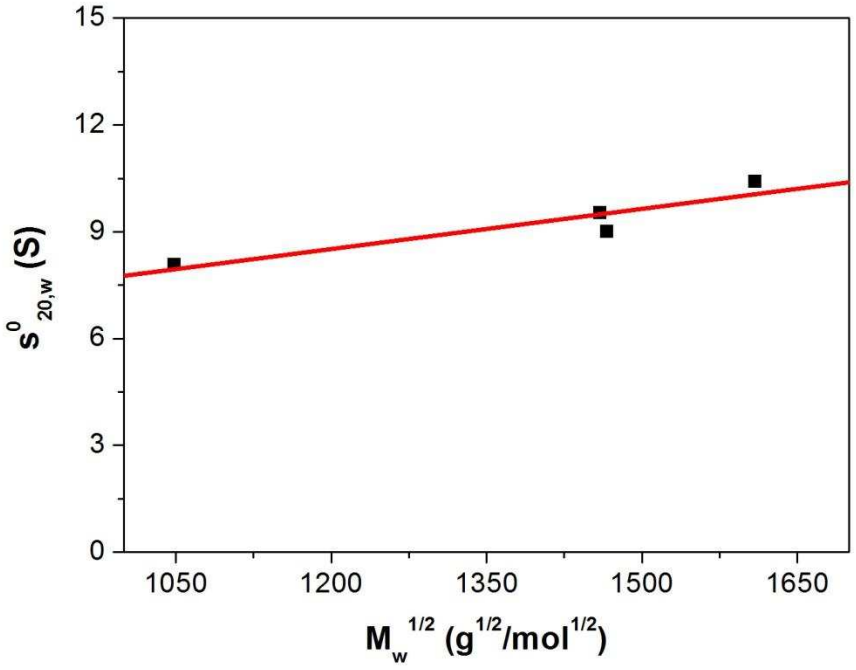


Figure 6.11: Yamakawa-Fujii plot for schizophyllan samples, where L_p = (134 ± 4) nm from the slope and an assumed value for M_L= 2150 $g.mol^{-1}.nm^{-1}$ from (Yanaki et al.).

6.4.5.3.2. Global analysis method (HYDFIT)

The main disadvantage of using the Bushin-Bohdanecky and Yamakawa-Fujii methods separately is requirement of either L_p or M_L to determine the other parameter. Therefore, a new algorithm was developed by Ortega and Garcia de la Torre (Ortega and García de la Torre, 2007), which basically combines both previous methods to estimate L_p and M_L from the two or more data sets of sedimentation coefficient, intrinsic viscosity and molecular weight information of the macromolecule. This programme then optimises the parameters in order to obtain the minimisation of the target function, Δ, based on the equation as above:

$$\Delta^2 = \frac{1}{N_s}\sum_{i=1}^{N_s}\left[(\sum_T W_T)^{-1}\sum_T W_T\left(\frac{a_{T_{(cal)}}-a_{T_{(exp)}}}{a_{T_{(\exp)}}}\right)^2\right] \qquad (6.12)$$

$$\Delta^2 = \frac{1}{N_s}\sum_{i=1}^{N_s}\left[(\sum_I W_I)^{-1}\sum_I W_I\left(\frac{a_{I_{(cal)}}-a_{I_{(exp)}}}{a_{I_{(\exp)}}}\right)^2\right] \qquad (6.13)$$

where N_s is the number of samples, W_T and W_I are the statistical weights for equivalent radii a_T and a_I and the subscripts cal and exp indicate calculated and experimental values, respectively. Therefore, Δ is a dimensionless estimate of the consensus between calculated values for the frictional coefficient, intrinsic viscosity and radius of gyration for a certain persistence length, L_P and the experimentally measured parameters (Ortega et al., 2011, Patel et al., 2008b).

The reported L_p and M_L values in Table 6.6 were obtained by fixing the chain diameter d and with the minimum value of the target function, Δ. Although the theoretical limits are $L_p = 0$ for random coil and $L_p = \infty$ for extra-rigid, practically the range is ~ 1 nm for random coils (e.g. pullulan) and ~ 200 nm for an extra-rigid rod (e.g. xanthan). In this study, the L_p values of schizophyllan were determined to be ~130nm and ~120nm for depolymerised samples and native samples, respectively. These values appear to suggest the conformation has a rigid rod structure. The M_L values were estimated as ~2300 g.mol^{-1}.nm^{-1} and ~2200 g.mol^{-1}.nm^{-1} for GM samples and INV samples, respectively and the M_L values did not appear to change with depolymerisation. These L_p and M_L values are consistent with previous studies (Stokke et al., 1993, Ortega et al., 2011, Norisuye et al., 1980). The contour plots were presented in Figure 6.12 and the target function Δ were represented by the full colour spectrum ranging from blue to red.

Table 6.6: Summary of the persistence length, L_p and the mass per unit length, M_L values for schizophyllan samples.

Sample	L_p (nm)	M_L (Da/nm)
GM1	120 ± 10	2300 ± 10
GM2	130 ± 10	2300 ± 10
INV1	120 ± 15	2200 ± 10
INV2	130 ± 10	2200 ± 10

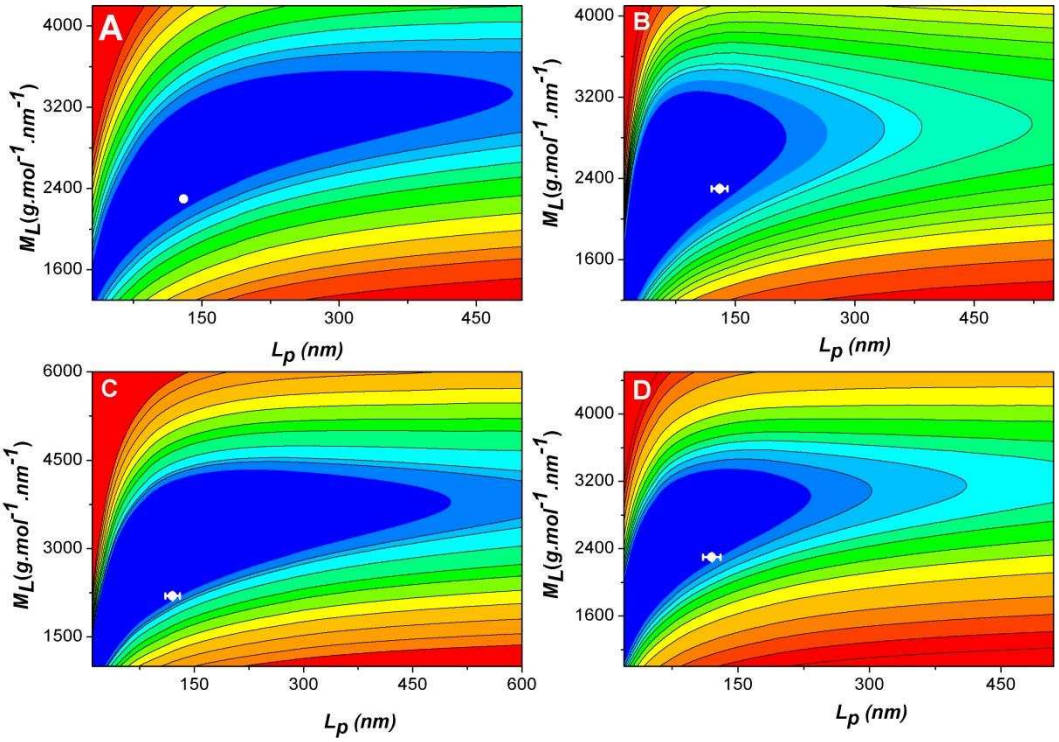


Figure 6.12: Contour plots of schizophyllan samples; (A) GM1, (B) INV1, (C) GM2, (D) INV2. The target function, Δ is calculated based on variables values of L_p and M_L, and are represented on the full colour spectrum from blue (Δ = 0) to red ($\Delta \geq 0.95$).

6.4.5.4. Molecular Conformation Zoning

The sedimentation conformation zoning plot provide the estimation of 'overall' solution conformation of a macromolecule ranging from Zone A (extra-rigid rod) to Zone E (globular or branched) by plotting of $k_s M_L$ versus [s]/M_L. Thus, the molecular conformation type can be estimated using sedimentation coefficient parameter and M_L from the equations as follows:

$$[s] = \frac{s^0_{20,w}\eta_{20,w}}{(1-\bar{\upsilon}\rho_{20,w})} \quad (6.14)$$

and M_L is the mass of the molecule(s) within the polymer divided by its length. In this study, M_L was taken by estimation value from Multi-HYDFIT as 2200 $g.mol^{-1}.nm^{-1}$ and 2300 $g.mol^{-1}.nm^{-1}$ for GM samples and INV samples, respectively. The [s] values were obtained from the sedimentation coefficient data using equation 6.14.

From Figure 6.13, it appears that schizophyllan samples clearly belong to Conformation Zone B rigid rods. These findings are consistent with those yielded from the MHKS and Wales-van Holde approaches, and reinforce those previously found by Yanaki et al. (Yanaki et al., 1980).

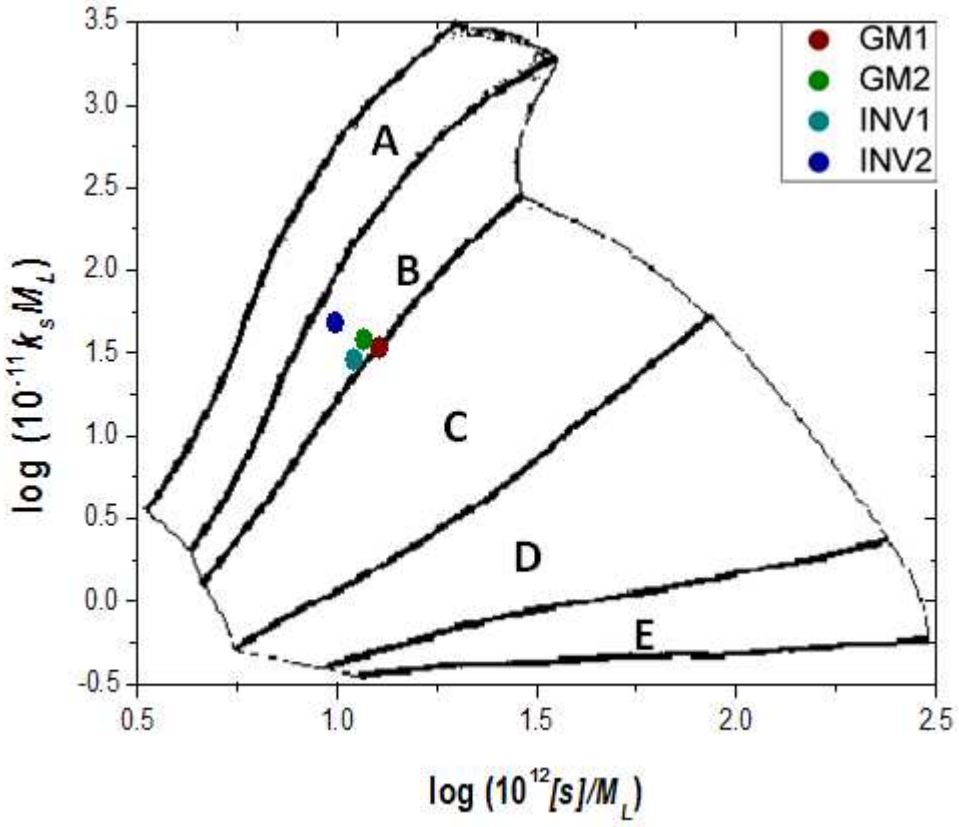


Figure 6.13: The conformation zoning plot for schizophyllan samples which are adapted rigid rod structures (Zone B).

6.5. DISCUSSION

In this study, the hydrodynamic properties of four schizophyllan samples have been characterised with regard to their weight-average molecular weight (M_w), sedimentation coefficient ($s^0_{20,w}$) distribution, and intrinsic viscosities ($[\eta]$). Bimodal distributions were seen from sedimentation coefficient distributions. The weight average molecular weight was firstly determined by sedimentation equilibrium. However, for this experiment, the effect of thermodynamic non-ideality in solution needs to be considered. Because of charge effects and excluded volume effects, the solution non-ideality appears and the schizophyllan solution displays strong solvent-

polymer interactions that ascend with increase in concentration. To minimise this non-ideality effect, the samples were run at a series of measurements at different loading concentration and extrapolated to infinite concentration. As a result, the sedimentation equilibrium method has successfully been applied to schizophyllan samples and the values of molecular weights were obtained for all samples in the range of ~ (1.2-2.6) x 10^6 (Da). Results were confirmed with those obtained from SEC-MALS and the previous studies (Norisuye et al., 1980, Yanaki et al., 1980, Kashiwagi et al., 1981). A third approach was used as a complementary method to determine molecular weight distributions based on sedimentation coefficient – Extended Fujita results were again consistent with those obtained from sedimentation equilibrium and SEC-MALS.

In terms of conformation, SEC-MALS also provided the advantage of coupling online molecular weight and intrinsic viscosity measurements for the samples, which allowed estimating conformation by Mark-Houwink-Kuhn-Sakurada (MHKS) and flexibility by Multi-HYDFIT methods. The MHKS results indicated that the all samples adopted rigid rod type conformation proving by Wales-van Holde ratio and conformation zoning and gaining some flexibility at higher molecular weight (Yanaki et al., 1980).

The flexibility of schizophyllan samples in terms of L_p and M_L, were revisited using the accomplish technique-Multi-HYDFIT and sedimentation conformation zoning. Meanwhile the L_p results from Multi-HYFIT have a perfect agreement with the previous results from Norusiye et al., and Stokke et al. (Stokke et al., 1993), who found L_p of ~100-200nm using the so-called Yamakawa-Fujii relation and ~104-161nm using electron microscopy, respectively. On the other hand, Bohdanecky (Bohdanecky, 1983) employed the intrinsic viscosity and molecular weight data

from Yanaki et al. (Yanaki et al., 1980) to get L_p and M_L and - the chain diameter (d), and the persistence length was found higher (296 nm). The obtained L_p and M_L values also consistent with the result from Ortega et al (2011) who applied the Multi-HYDFIT program to the previous literature data from Yanaki et al. (1980) and found the values of (150 ± 20) nm for L_p and (2050 ± 90) nm for M_L. Consequently, the results also showed that using only single approach to estimate persistence length and mass per unit length can lead to a bias in the results. This emphasizes the need to use more than one independent method, and if possible using complementary hydrodynamic techniques.

6.6. CONCLUSION

The hydrodynamic properties of schizophyllan were determined by the complementary hydrodynamic techniques including AUC (sedimentation velocity and equilibrium), SEC-MALS and viscometry, which provide an important knowledge on the heterogeneity and conformation. The conformation of samples was also revisited by accomplish technique-Multi-HYDFIT and molecular conformation zoning in addition to previous conformation methods. Meantime, the results from Multi-HYFIT have a perfect agreement with the previous results, and the rod type conformation was proved by this technique and the other complementary conformation methods such as Mark-Houwink-Kuhn-Sakurada (MHKS), Wales van Holde Ratio and molecular conformation zoning.

CHAPTER 7

HYDRODYNAMIC CHARACTERISATION OF CHITOSAN AND ITS INTERACTION WITH TWO POLYANIONS: DNA AND XANTHAN

In Chapter 3, we considered in detail the properties of one of the most important industrial microbial polysaccharides – xanthan. However, only very rarely is it used in products by itself. In this chapter, we consider the behaviour of mixtures of the (polyanionic) xanthan with the polycationic polysaccharide chitosan, which is derived for example from chitin from the shells of crustaceans. We use the analytical ultracentrifuge and the principal of co-sedimentation as a marker for interaction. For comparative purposes, we consider also the interactions of chitosan with another double helical polyanionic molecule with strong carbohydrate content – DNA. We firstly examined the hydrodynamic properties of chitosan with different molecular weight, then studied on the interaction in collaboration with F. Almutairi (Almutairi, 2015)

7.1 INTRODUCTION

Chitosan is a cationic polysaccharide which is derived from chitin extracted from the exoskeletons of crustaceans or the cell walls of Basidiomycete fungi. The basic structure of chitosan is comprised of linear β-(1-4) linked to 2-amino-2-deoxy-d-glucopyranose unit with a high degree of N-acetylation as shown in Figure 7.1 (Tombs and Harding, 1997).

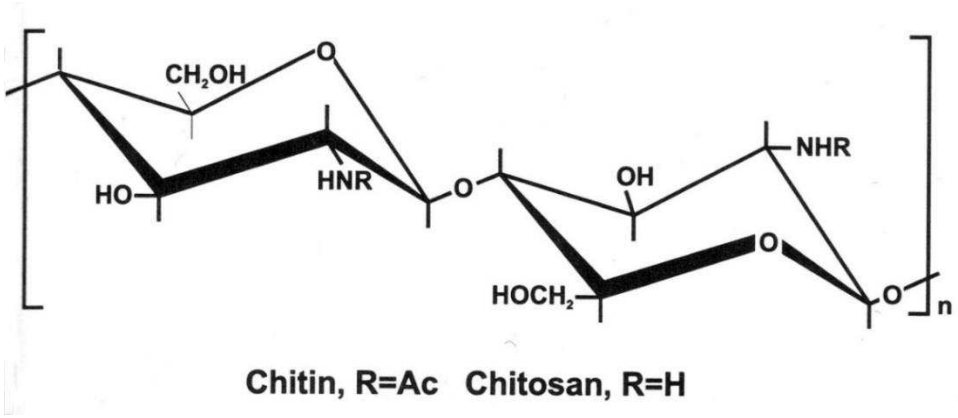


Figure 7.1: Chemical structure of chitosan adapted from Tombs and Harding, (1997). Ac=acetyl

Chitosan is soluble in aqueous acidic solution and due to protonation of amine groups in acidic media, becomes a cationic polyelectrolyte (Fee, 2006). The variation of chitosan in solution derives from differences in the molecular weight, degree of acetylation (DA) and also the distribution of acetyl groups along the chain (Venugopal, 2011).

Owing to the unique properties of chitosan including biocompatibility, biodegradability, hemocompatiblity, antibacterial activity, nontoxic, antitumor,

fungistatic and anticholesteremic (Rinaudo, 2006), it has in itself received attention for use in the food (Argin-Soysal et al., 2009), cosmetics (Dutta et al., 2004), pharmaceutical (Wong, 2009, Bhattarai et al., 2005) and medical applications (Tan et al., 2009, Ma et al., 2003). Chitosan can form polyelectrolyte complex- three-dimensional networks or "hydrogels- with oppositely charged polymers and this complex can be used for controlled drug release by preserving the drug from degradation in the gastrointestinal tract for drug delivery systems. Modifying the chemical structure and solvent conditions of chitosan electrostatic interaction and hydrophobic bonds can be enhanced. Through these interactions, the biomedical applications of chitosan for drug delivery (chitosan–alginate) and gene delivery (chitosan–DNA) (Li et al., 2005, Mansouri et al., 2004) has attracted attention. However, the information of molecular properties of chitosan in solution especially molecular weight and conformation is essential to understand the behaviour of chitosan in the presence of other macromolecules.

Molecular weight (primarily the weight average M_w) or "molar mass" estimations for various chitosan preparations in solution have in the past been investigated using membrane osmometry, multi-angle light scattering (MALS), or light scattering coupled with size exclusion chromatography, or SEC alone (Rinaudo et al., 1993, Kasaai et al., 2000, Berth et al., 1998, Schatz et al., 2003). Due to the possibility of adverse polycationic interactions with column materials, analytical ultracentrifugation (AUC) –another powerful approach which estimates molecular weight is useful in this regard (Fee et al., 2003b) and also as a complementary technique e.g. (Cölfen et al., 2001, Fee, 2006).

By considering the interactions of chitosan with macromolecules, the conformation particularly depends on the source, molecular size range, and degree of acetylation

DA (or degree of de-acetylation). For instance, increasing the deacetylation of the molecule, the conformation is more extended due to the increase in charged amino groups along the chain. In the meantime, increase in ionic strength reduces electrostatic repulsion, which leads to a more compact conformation (Fee, 2006). The conformation of chitosan has been determined ranging from semi-flexible to stiffer conformations (Cölfen et al., 2001, Rinaudo, 2006, Morris et al., 2009b) in which sedimentation and viscometry also plays a key role in these evaluations.

Since chitosan can be applied for nasal and oral drug delivery as an mucadhesive (for example, chitosan–mucin glycoprotein mucoadhesive interactions (Harding, 2003, Harding, 2006), there is an increasing interest in chitosan interactions with oppositely charge polyelectrolytes. Sedimentation velocity was used previously to assay the efficacy of these interactions, where results are reflected in a change in the sedimentation coefficient of the complex with respect to that of the pure component (Fiebrig et al., 1995, Anderson, 1991).

In this study, the hydrodynamic properties of six different chitosan samples in solution were firstly characterised using sedimentation velocity along with sedimentation equilibrium in the AUC, SEC-MALS and viscometry in order to obtain the information of sedimentation coefficient, molecular weight, distribution of molecular weight, intrinsic viscosity and overall conformational flexibility. Then, the possible interaction between chitosan and other oppositely charge polyelectrolytes such as xanthan and for comparison another polyanion, DNA, were investigated. The degree of interaction has been determined by measuring the distribution/weight average of sedimentation coefficient for the complex comparing those of individual polysaccharides.

7.2. MATERIALS

Commercially available chitosans (CHIT1, CHIT2, CHIT3 and CHIT4) were obtained from Sigma Aldrich (USA). A further two chitosans (CHIT5 and CHIT6) referred to as "laboratory chitosans" were prepared at the Teagasc Food Research Centre, Ashtown, Dublin 15, Ireland. Degrees of acetylation (DA) were found to be approximately 25% for CHIT1 to CHIT5 and 15% for CHIT6, as assayed using NMR by suppliers. The samples were used as supplied without any further purification. The chitosan samples were dissolved in I=0.2 M acetate buffer (pH 4.3) with stirring for 24h and used directly for all experiments. For sedimentation equilibrium experiments the samples were dialysed against the buffer solution overnight.

DNA samples were kindly provided by Dr. Alan Mackie, Institute of Food Research (Norwich, UK) in stock solution (5.0 mg/ml) and were diluted in phosphate buffered saline (PBS) at an ionic strength of 0.1M and pH 7.4.

A stock solution of xanthan (supplied by Dupont, Paris), referred to as "xanthan–STD (Standard LMW)" (see chapter 3) was prepared by dissolving a known amount in distilled deionised water, with gentle stirring at 3 h followed by overnight dialysis against phosphate–chloride buffer supplemented with NaCl at pH 7.0 and an ionic strength of 0.1M. The concentrations, c (g/ml) of the stock of chitosans and xanthan solutions were measured using an Atago (Japan) DD-7 refractometer calibrated with glucose standards. The mixtures of DNA–chitosan and xanthan–chitosan were prepared by adding equal volumes and concentration.

7.3. METHODS

7.3.1. Sedimentation Velocity (SV)

An Optima XL-I (Beckman Instruments, Palo Alto, USA) analytical ultracentrifuge equipped with Rayleigh interference optics was used. Sample solution (400 μl) and reference buffer (400 μl) were injected into the respective channels of double sector 12 mm optical path length cells. The Rayleigh interference optical system was used to record changes in the concentration versus radial displacement profiles with time. An initial low rotor speed of 3000 rpm was used to check for the presence of any large sedimenting species and then adjusted to a rotor speed of 40,000 rpm. The standard conditions of density and viscosity of water at 20.0° C were used for adjustment of the sedimentation coefficients s to $s_{20,w}$ values. Scans were taken at 2 min intervals for a run time of ~24 h. The data was analysed using the least squares, ls − g(s) procedure of SEDFIT (Dam and Schuck, 2004), which solves the Lamm equation describing the change of concentration distribution with radial position with time in terms of a distribution of sedimentation coefficients, g(s) vs s, where s is the sedimentation coefficient. The (differential) distribution of sedimentation coefficients g(s) can be defined as population – weight fraction – of species with a sedimentation coefficient between s + ds (Dam and Schuck, 2004, Harding, 2005b). To eliminate the effects of non-ideality (co-exclusion and any residual polyelectrolyte effects) a plot of the reciprocal of the sedimentation coefficient ($1/s_{20,w}$) against concentration, c (g/ml) was made from the intercept at infinite dilution c = 0, the value free of these effects was found: $s^0_{20,w}$ (units seconds, s, or Svedbergs, S, where 1S = 10^{-13}s). The following relation due to (Gralen, 1944) was used for the extrapolations:

$$1/s_{20,w} = (1/s_{20,w}).(1+k_s c) \quad (7.1)$$

where k_s is the "Gralen" coefficient (ml/g).

7.3.2. Sedimentation Equilibrium (SE)

Sedimentation equilibrium experiments were performed also using the Optima XL-I analytical ultracentrifuge. The optical path length (12.0 mm) double-sector cells with sapphire windows were loaded with (~80 μL) of dialysed sample and a matching amount of reference buffer dialysate in appropriate channels. The balanced cells were then loaded into an analytical 8 hole titanium rotor An50–Ti and placed in the AUC. After time was allowed for vacuum formation (≤50 microns) and for temperature equilibration (20.0°C), the rotor was then accelerated to 10000 rpm. Using the Rayleigh interference optical system, scans were taken every 1h and equilibrium was reached after approximately ~72 h. Records of the relative concentration distribution of the solute at equilibrium was analysed to give the weight average apparent weight average molecular weight $M_{w,app}$ using the SEDFIT–MSTAR program implemented by Schuck et al. (Schuck et al., 2014). To account for non-ideality, the conventional/reciprocal of the apparent weight average molecular weight $1/M_{w,app}$ determined over a range of concentrations, c, was extrapolated to zero concentration (Harding, 2005b).

7.3.3. Size Exclusion Chromatography Coupled to Multi Angle Light Scattering (SEC-MALS)

Molecular weights (weight averages) of the chitosan samples were also estimated by using the independent technique of SEC–MALS (Wyatt, 2012), a technique which

has been successfully applied to polysaccharide characterisation since Horton, Harding, and Mitchell (1991). The present set-up comprises a series of size exclusion chromatography (SEC) columns, namely TSK G6000PW and TSK G4000PW, protected by a similarly packed guard column (Tosoh Bioscience, Tokyo, Japan) coupled on-line to "Helios" multi-angle light scattering (MALS) and refractive index (OptilabrEX) detectors (Wyatt Technology, Santa Barbara, USA). Solutions prepared at injected concentrations of 0.5 and 1.0 mg/ml were filtered through a 0.45 μm syringe filter (Whatman, Maidstone, England)—to remove any insoluble material or dust prior to being injected into the columns. The buffer was pumped at a steady, pulse free flow rate of 0.8 ml/min through the column system. ASTRA (Version 5.1.9.1) software (Wyatt Technology, Santa Barbara, USA) was used to analyse the data. A linear fit to the "Debye" plot of Kc/R_θ vs $\sin^2(\theta/2)$, where the terms have their usual meaning (Wyatt, 2013b) was used for calculating the apparent weight average molecular weight ($M_{w,app}$) using a value for the refractive index increment dn/dc = 0.163 ml/g (Rinaudo et al., 1993). Because of the low concentrations after dilution on the columns no correction for non-ideality was assumed necessary, and $M_{w,app} = M_w$, the ideal weight average molecular weight.

7.3.4. Intrinsic viscosity

The relative viscosities (η_{rel}) of chitosan solutions ranging from 0.1 mg/ml to 1.0 mg/ml were measured using a 2ml Schott-Geräte Ostwald viscometer system at a temperature of (20.0 ± 0.01) °C. The reduced ($\eta_{red} = (\eta_{rel}-1)/c$) and the inherent viscosities ($\eta_{inh} = (\ln_{\eta rel})/c$) were extrapolated to zero concentration to eliminate non-ideality effects with the common intercept at c=0 yielding the intrinsic viscosity *[η]*

from Huggins (1942) and Kraemer equations (1938). As an additional check a combined Solomon & Ciuta (1962) relation was also used:

$$[\eta] \sim (1/c).\ [2\ (\eta_{sp} - ln\ (\eta_{rel}))]^{1/2} \quad (7.2)$$

The assumption has been made that there was no shear dependence of $[\eta]$ under creeping flow conditions in the capillary viscometer.

Relative viscosities η_{rel} were also estimated from a Viscostar (WyattTechnology) differential pressure viscometer linked on-line to the SEC–MALS system (Harding, 1997). The differential pressure drop from solution flow versus solvent flow yielded η_{rel} and then the reduced viscosity η_{red} from:

$$\eta_{red}=(\eta_{rel}-1)/c \quad (7.3)$$

Then because of the high dilutions from the column, the assumption that the intrinsic viscosity ~ reduced viscosity can be reasonably made:

$$[\eta] \sim \eta_{red} \quad (7.4)$$

The average $[\eta]$ for the whole undistributed sample can therefore be specified as well as the intrinsic viscosity $[\eta](Ve)$ as a function of elution volume Ve using the Solomun-Ciuta relation (Eq 7.2). Because of the high sensitivity of the sensors and the high dilution from the column, Eq. (7.2) was used to obtain $[\eta]$ (Ve) without a concentration extrapolation.

7.4. RESULTS

7.4.1. Sedimentation Velocity (SV)

Chitosan samples were firstly characterised by sedimentation velocity in an analytical ultracentrifuge to examine their molecular integrity using the least squares ls-g(s) method of Dam & Schuck (2004). The sedimentation coefficient distribution profiles indicated polydisperse distributions in all cases as shown in Figure 7.2. These profiles showed unimodal distributions for all samples and suggested that the samples are homogeneous. Values of the weighted average $s_{20,w}$ increased with decrease in concentration, showing no evidence of associative effects. The sedimentation coefficient, $s^0_{20,w}$ of each sample was obtained ranging from 1.8S to 2.7S as reported in (Table 7.1). These values are consistent with previous studies (Cölfen et al., 2001, Fee, 2006, Morris et al., 2009a).

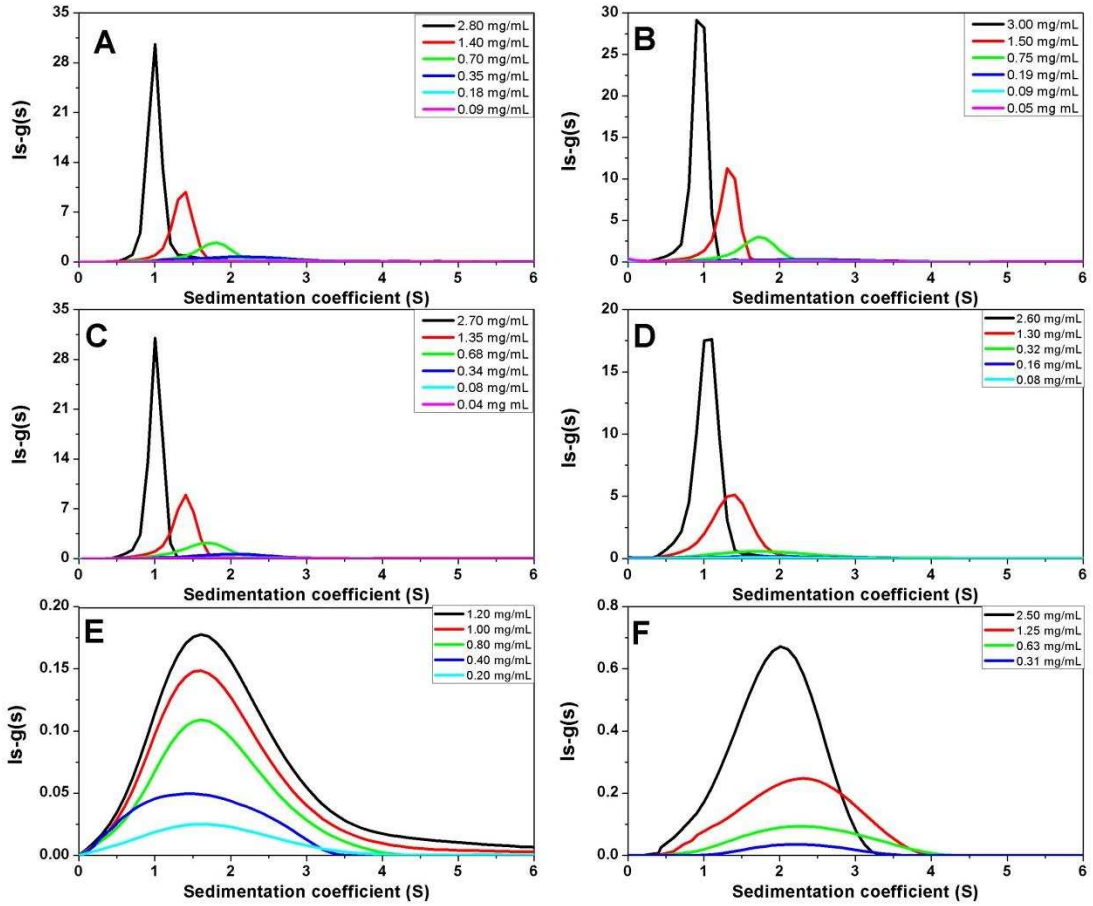


Figure 7.2: Sedimentation coefficient distribution profiles using least squares g*(s) method of SEDFIT obtained from sedimentation velocity experiment for chitosan samples (A) CHIT1, (B) CHIT2, (C) CHIT3, (D) CHIT4, (E) CHIT5, (F) CHIT6.

Additionally, the concentration dependence parameter, k_s (Gralén coefficient) for each sample was yielded from the slope of the reciprocal plots of apparent sedimentation coefficient versus concentrationand this parameter is an indicative of non-ideality (Figure 7.3).

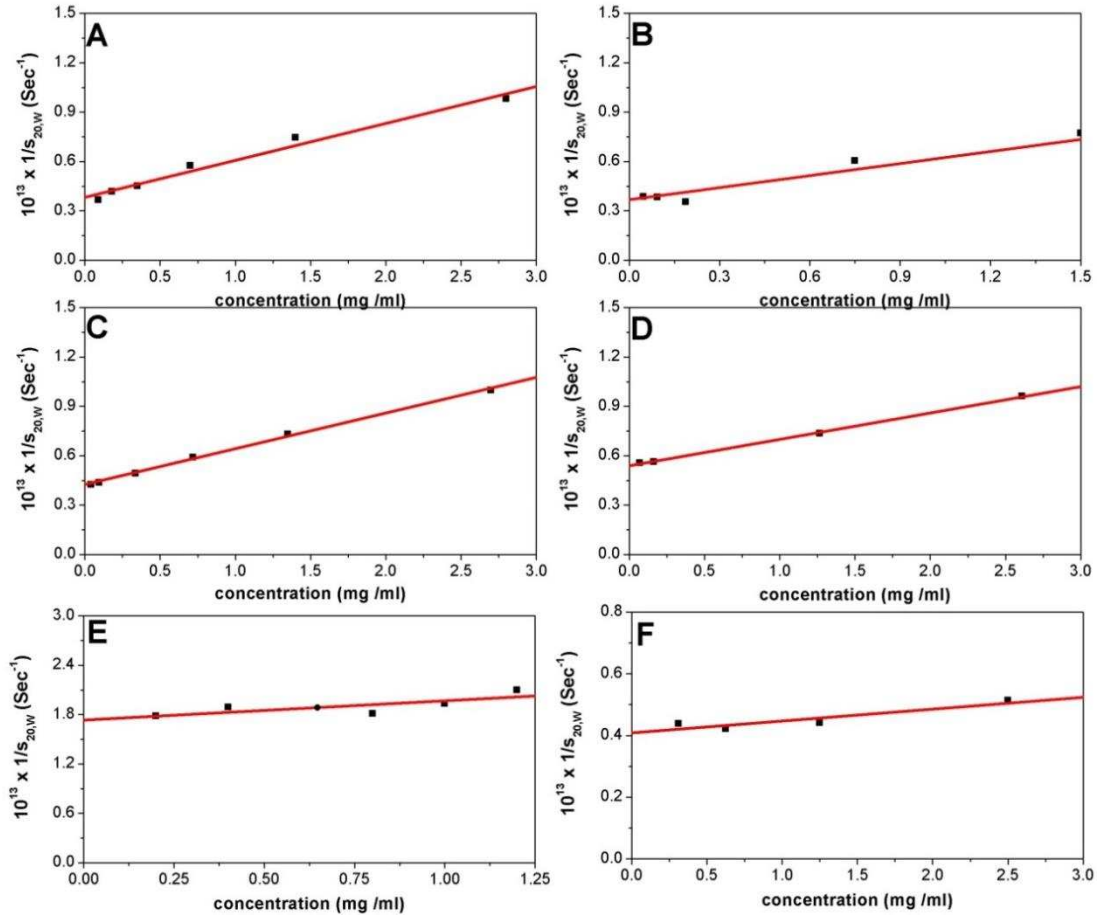


Figure 7.3: Concentration dependence (reciprocal) of the sedimentation coefficient plot for chitosan samples (A) CHIT1 (B) CHIT2 (C) CHIT3 (D) CHIT4 (E) CHIT5 (F) CHIT6.

Table 7.1: Summary of $s^{0}_{20,w}$ and k_s for chitosan samples.

Sample	$s^{\circ}_{20,w}$ (S)	k_s (ml/g)
CHIT1	2.5 ± 0.2	650 ± 50
CHIT2	2.7 ± 0.2	750 ± 70
CHIT3	2.3 ± 0.1	600 ± 30
CHIT4	1.85 ± 0.1	300 ± 10
CHIT5	1.8 ± 0.1	100 ± 30
CHIT6	2.4 ± 0.1	120 ± 30

7.4.2. Estimation of Molecular Weight

The weight average molecular weights of chitosan samples were determined by sedimentation equilibrium method in analytical ultracentrifuge and SEC-MALS. The values at first of all were determined by the sedimentation equilibrium method. The chitosan samples were run at different loading concentration ranges 0.5-2.0mg/ml to eliminate the non-ideality effect in solution from excluded volume and charge effects. Apparent weight average molecular weights ($M_{w,app}$) were then obtained using SEDFIT–MSTAR (see, for example Fig. 7.4).

Plots of $M_{w,app}$ versus concentration for commercial samples (CHIT1 to CHIT4) gave a non-linear extrapolation, showing a significant concentration dependence consistent with non-ideal behaviour and consistent with the sedimentation velocity results (Fig. 7.5a) (Harding, 2005b, Schuck et al., 2014). Meanwhile, a second order polynomial fit was used to obtain the molecular weight values which are presented in (Table 7.2). Similar behaviour has also been observed for hyaluronic acid at high molecular weight (see Chapter 5). The reciprocal plot of $1/M_{w,app}$ versus concentration was then applied for the laboratory-prepared samples (CHIT5 and CHIT6) (Fig. 7.5b), and M_w values obtained from the linear extrapolation (Table 7.2).

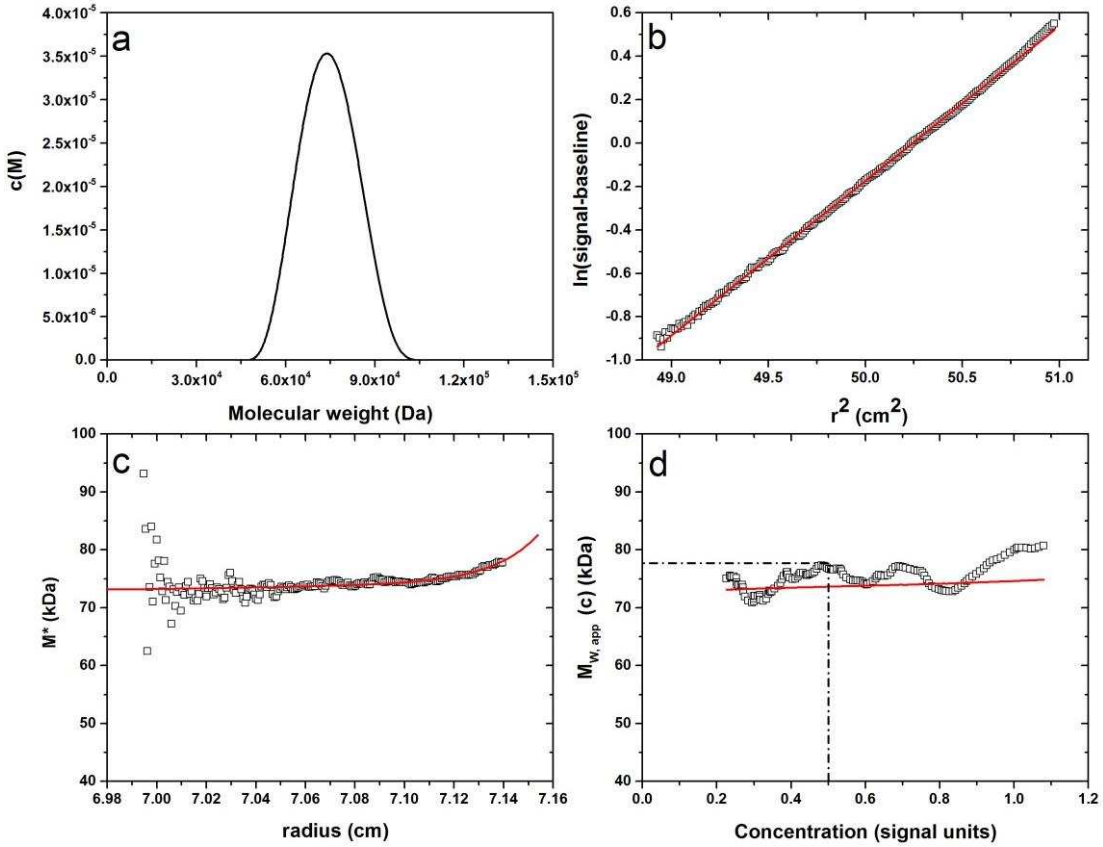


Figure 7.4: SEDFIT–MSTAR output for analysis of CHIT4 at a loading concentration of 0.5 mg/ml sedimentation equilibrium experiment (a) molecular weight distribution, c(M) vs M plot; (b) log concentration ln c(r) vs r^2 plot, where r is the radial distance from the centre of rotation; (c) M* vs r plot (open circle) and fit based on the M* transformations of the c(M) fit of the raw data (red line): the value of M* extrapolated to the cell base = $M_{w,app}$ the apparent weight average molecular weight for the whole distribution. (d)Point or local apparent weight average molecular weight at radial position r (open circle) plotted against the local concentration c(r) for different radial positions: red line is the fit based on the equivalent transformations of the c(M) fit of the raw data.

The weight average molecular weight of chitosan samples were also determined by SEC-MALS systems and the values were presented in Table 7.2. Due to the sample dilution in SEC columns, the non-ideality effect was reduced. The elution volume

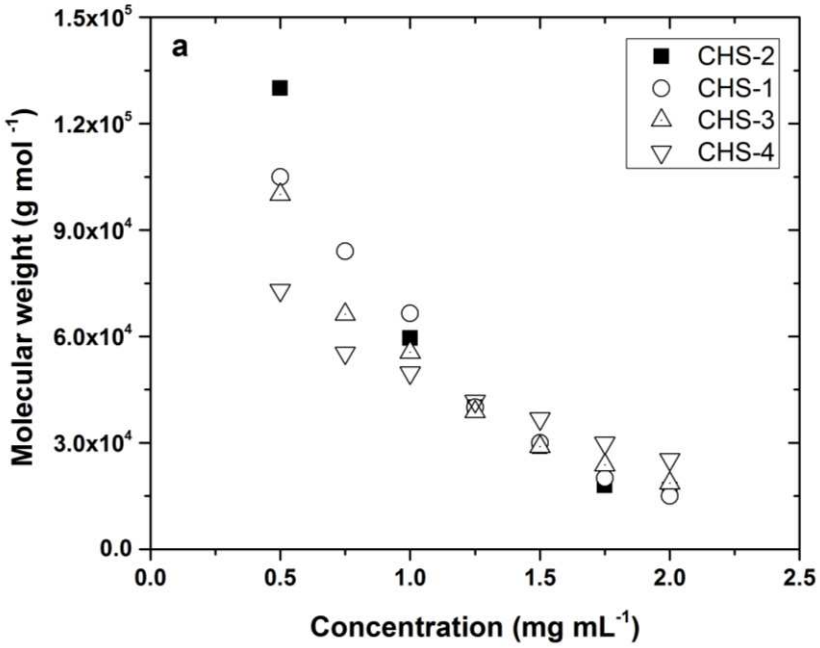


Figure 7.5a: The conventional plot of the apparent weight average molecular weight ($M_{w,app}$) against concentration c (g/ml) ($M_{w,app}$ vs c).

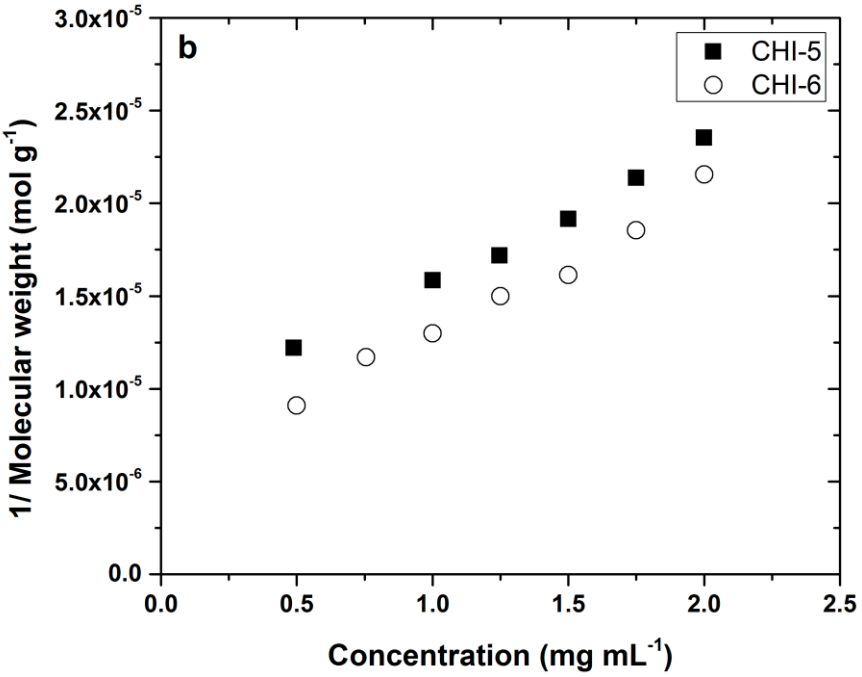


Figure 7.5b: The reciprocal plot of the apparent weight average molecular weight ($M_{w,app}$) against concentration c (g/ml) ($M_{w,app}$ vs c).

profiles of samples were given in Figure 7.6. Results were consistent with estimates from sedimentation equilibrium (Figure 7.6, Table 7.2) and values are similar to those found previously (Errington et al., 1993, Fee et al., 2003b). The elution volume profiles of samples for chitosan samples indicated earlier elution times for commercial samples (CHIT1 to CHIT4), in contrast to laboratory-prepared samples (CHIT5 and CHIT6) although similar molecular weights were observed (Figure 7.6).

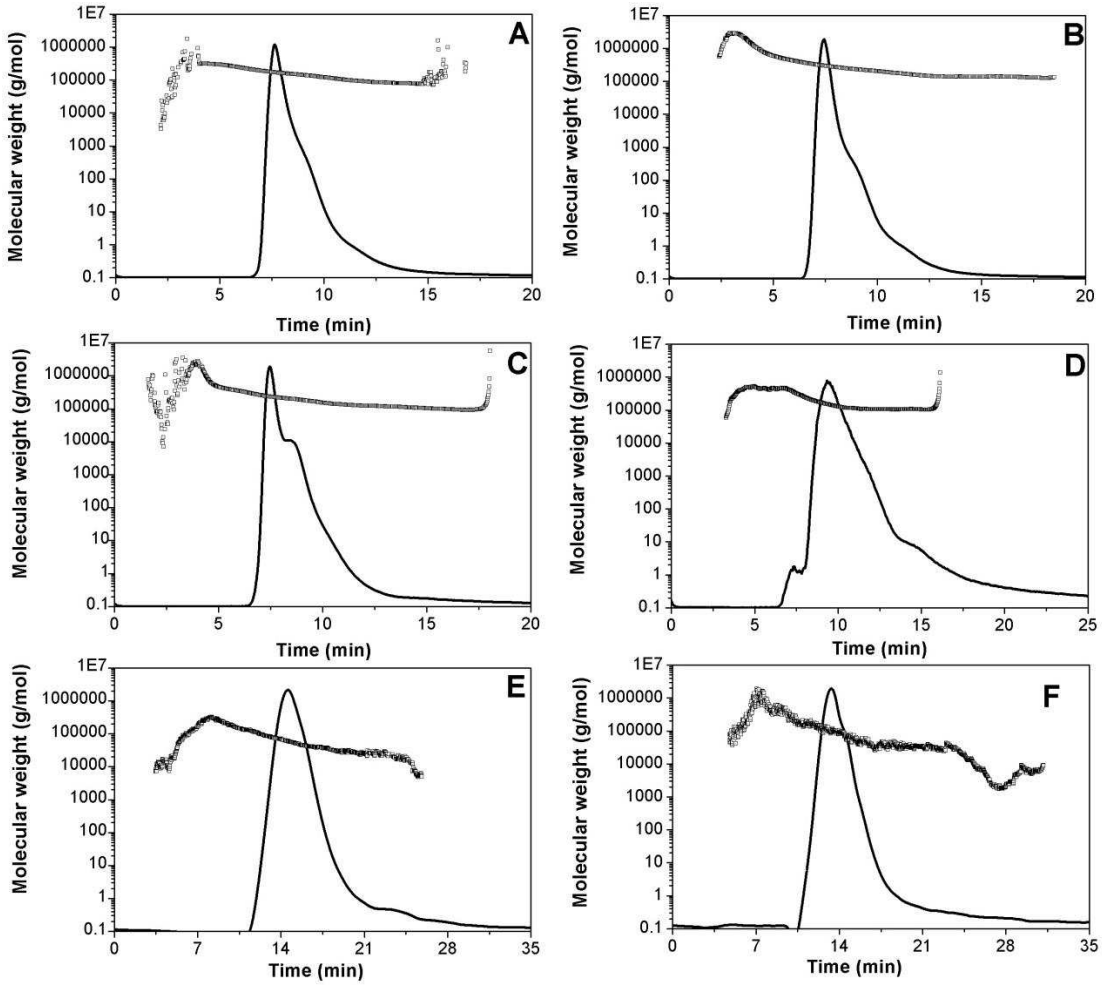


Figure 7.6: Elution profile of commercial and laboratory-prepared chitosan samples from dRI detector in 0.2 M, pH 4.3, acetate buffer, (A) CHIT1 (B) CHIT2 (C) CHIT3 (D) CHIT4 (E) CHIT5 (F) CHIT6 (black line) examined by SEC-MALS at concentration 0.5 mg/ml. The open squares correspond to molecular weights calculated from SEC-MALS.

Table 7.2: Summary of weight average molecular weights (M_w) results for chitosan samples from sedimentation velocity, equilibrium and SEC-MALS.

Sample	10^3 x M_w (Da)[a]	10^3 x M_w (Da)[b]	10^3 x M_w (Da)[c]
CHIT1	170 ± 10	170 ± 5.0	160 ± 10
CHIT2	230 ± 10	260 ± 10	220 ± 10
CHIT3	130 ± 10	140 ± 5.0	120 ± 20
CHIT4	85 ± 5.0	110 ± 20	90 ± 10
CHIT5	95 ± 10	85 ± 5.0	95 ± 10
CHIT6	170 ± 30	170 ± 10	140 ± 30

a : obtained from sedimentation equilibrium.
b : obtained from SEC-MALS.
c :obtained from molecular weight obtained from sedimentation velocity and the Extended Fujita method

Additionally, the third method to estimate the molecular weight of chitosan samples is transforming a distribution of sedimentation coefficient g(s) vs s into a distribution of molecular weight, f(M) vs M using the Extended Fujita method (Harding et al., 2011).

The transformation from g(s) versus s is as below:

$$f(M) = g(s).\ (ds/dM) \quad (7.5)$$

with

$$s = \kappa_s . M^b \quad (7.6)$$

and

$$ds/dM = b.\ \kappa_s^{1/b} . s^{(b-1/b)} \quad (7.7)$$

the conformation parameter (MHKS) b has already been determined by Fee et al. (Fee, 2006) and κ_s can be yielded form equation (7.6) with at least one value of M_w (e.g. M_w from sedimentation equilibrium) and the corresponding of s (e.g. the weight average s value). The molecular weight distributions of samples were presented in Figure 7.7 and agreed with the results obtained from sedimentation equilibrium and SEC-MALS (Table 7.2).

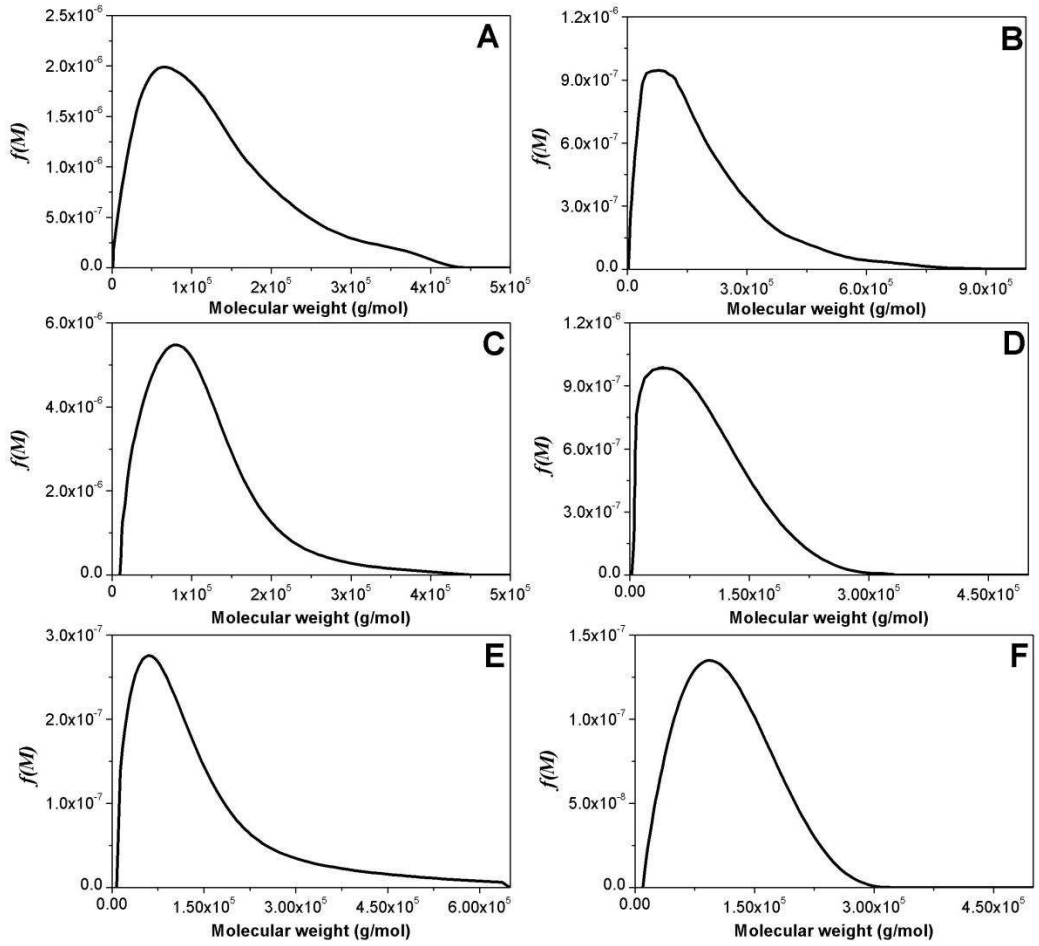


Figure 7.7: Molecular weight distribution for all chitosan samples in 0.2 M, pH 4.3, acetate buffer obtained from transformation of the g(s) versus s distribution at concentration (0.2 mg/ml), using the Extended Fujita method of Harding et al., (2011) (A) CHIT1 (B) CHIT2 (C) CHIT3 (D) CHIT4 (E) CHIT5 (F) CHIT6.

7.4.3. Intrinsic Viscosity

The intrinsic viscosities of chitosan samples were measured using both, a capillary viscometer and the Viscostar (Wyatt Technology) differential pressure viscometer for each chitosan sample. The value of $[\eta]$ were obtained using Huggins, Kraemer and Solomon-Ciuta extrapolations from the capillary viscometer and these extrapolations are indicated in Figure 7.8 for all samples. The obtained intrinsic viscosity values were presented in Table 7.3. The differences between these values can be seen and they indicate the effect of different preparations and source of the samples on viscosity.

Table 7.3: Intrinsic viscosity values of (Commercial) and (Laboratory-prepared) chitosan samples obtained from capillary viscometry and differential pressure viscometry.

Sample	Intrinsic viscosity $[\eta]$ (ml/g)			
	Capillary viscometry			Online viscostar™
	Huggins	Kraemer	Solomon-ciuta	
CHIT1	830 ± 20	815 ± 15	825 ± 15	885 ± 20
CHIT2	775 ± 50	805 ± 20	810 ± 25	820 ± 5
CHIT3	730 ±10	740 ± 5	740 ± 5	730 ± 5
CHIT4	440 ± 5	430 ± 5	435 ± 5	500 ± 10
CHIT5	130 ± 10	130 ± 5	130 ± 5	230 ± 20
CHIT6	295 ± 10	295 ± 5	295 ± 5	300 ± 20

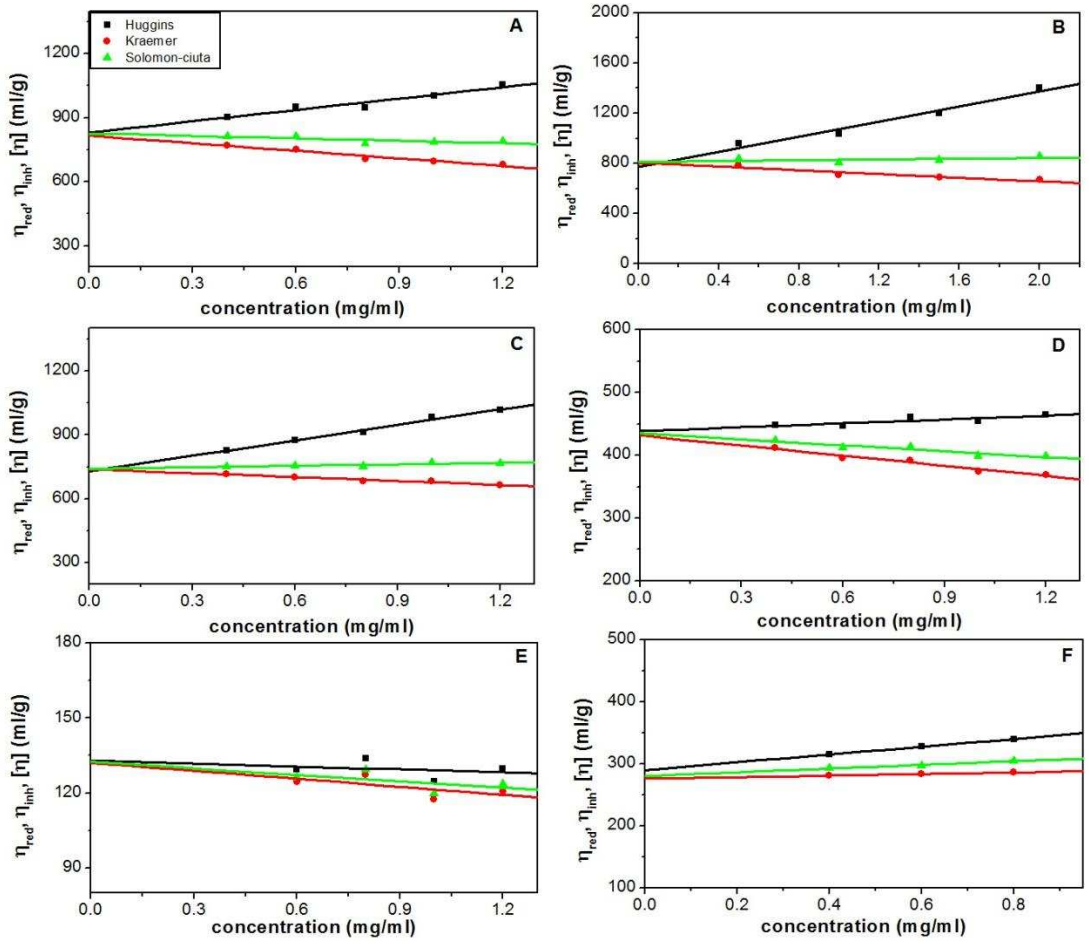


Figure 7.8: The intrinsic viscosity plots from capillary viscometry: Huggins, Kraemer and Solomon-Ciuta extrapolations for chitosan samples (a) CHIT1 (b) CHIT2 (c) CHIT3 (d) CHIT4 (e) CHIT5 (f) CHIT6.

7.4.4. Conformational Analysis

7.4.4.1. Mark-Houwink-Kuhn-Sakurada Power Law Relationship

The Mark-Houwink-Kuhn-Sakurada (MHKS) relation is one of the simplest methods to provide conformation and flexibility information of polysaccharides. According to equation (7.6) and the slope of the double logarithmic plot of $s^0_{20,w}$ versus M_w (Figure 7.9), the exponent b was found as (0.35 ± 0.06). This value suggests the conformation of chitosan samples are between the limits of rod (0.15) and coil (0.4-0.5). Within the error estimate the value is similar to those obtained previously by Cölfen et al., and Fee et al., (Cölfen et al., 2001, Fee, 2006).

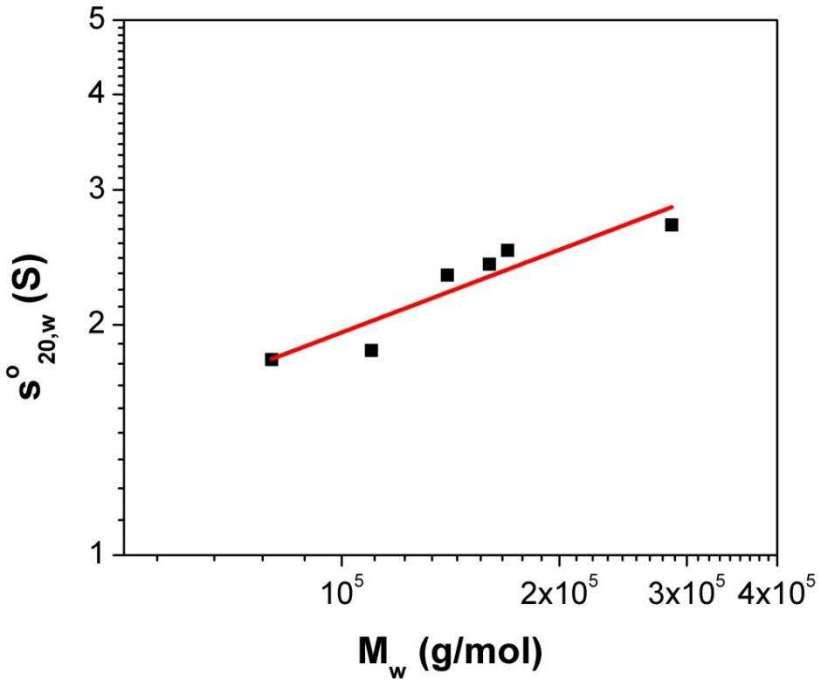


Figure 7.9: Mark–Houwink–Kuhn–Sakurada (MHKS) power law double logarithmic plot of $s^0_{20,w}$ vs M_w for all chitosan samples.

Taking advantage of the feature of viscostar coupled on-line to SEC–MALS system, the most common used MHKS equation relates the intrinsic viscosity [η] to molecular weight:

$$[\eta] = \kappa_{\eta} . M^{a} \quad (7.8)$$

Figure 7.10 shows the double logarithmic plots of intrinsic viscosity *[η] versus* M_w for all chitosan samples and the a exponent yielded from the slope of this plot was presented in Table 7.4. The values of a for the chitosans are all consistent with semi-flexible type molecules (the limits are 0.5-0.8 for a flexible coil, 0 for a compact sphere and 1.8 for a rigid rod), and again consistent with previous studies (Brugnerotto et al., 2001, Wan et al., 2003, Morris et al., 2009b).

Table 7.4: Mark-Houwink-Kuhn-Sakurada (MHKS) power law exponent a, from SEC-MALS and Wales-van Holde ration, R for chitosan samples.

Sample	MHKS a	R= $k_s/[\eta]$
CHIT1	0.98 ± 0.01	0.75
CHIT2	0.92 ± 0.01	0.90
CHIT3	0.98 ± 0.01	0.83
CHIT4	0.90 ± 0.01	0.60
CHIT5	0.70 ± 0.01	0.45
CHIT6	0.85 ± 0.01	0.40

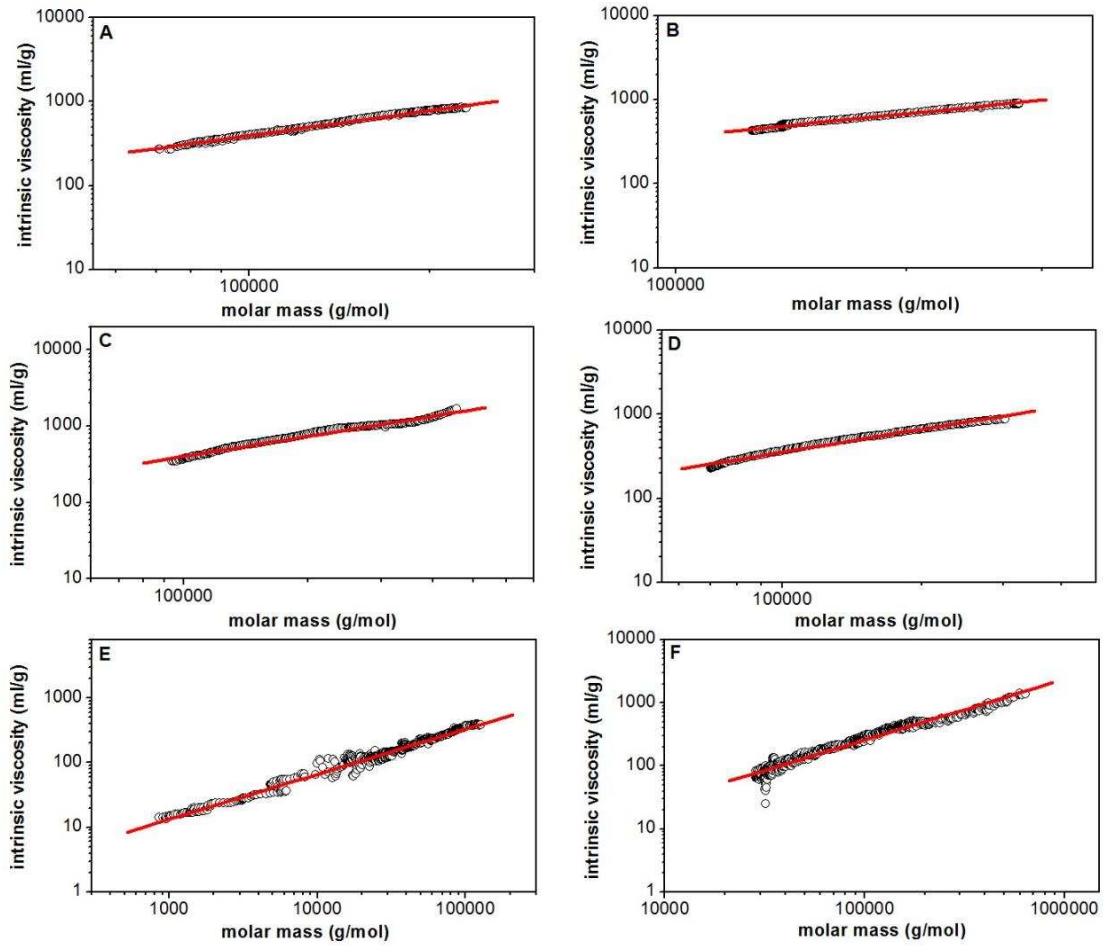


Figure 7.10: Mark–Houwink–Kuhn–Sakurada (MHKS) power law double logarithmic plot for chitosan samples (A) CHIT1 (B) CHIT2 (C) CHIT3 (D) CHIT4 (E) CHIT5 (F) CHIT6.

7.4.4.2. Wales-van Holde Ratio

The conformation of chitosan samples in solution was also obtained using the Wales-Van Holde parameter. The ratio of the sedimentation concentration dependence coefficient, k_s, to the intrinsic viscosity $[\eta]$ was used to measure the parameter and the value for ~1.6 for spheres and random coils, and substantially lower, <1 for rods. The R results in Table 7.4 appear that all chitosan samples adopted semi-flexible structures with the values between (R ~ 0.4–0.9). These results again agree with the previous work from Cölfen et al. (Cölfen et al., 2001).

7.4.4.3. Estimation of the Persistence Length L_p and Mass Per Unit Length M_L

The flexibility of linear polymer chains (worm-like chains) were estimated by determining the persistence length L_p and M_L representations (Harding, 2005a). L_p is defined as the average projection length along the initial direction of the polymer chain while M_L is the mass of the molecule(s) within the polymer divided by its length. These both parameters can be estimated using different approaches either viscosity (Stockmayer and Fixman, 1963, Bohdanecky, 1983) or sedimentation coefficient (Hearst and Stockmayer, 1962, Yamakawa and Fujii, 1973).

7.4.4.3.1. Bushin-Bohdanecky Method

Referring with section (6.4.4.3.1), this method was applied to estimate the chain persistence length (L_p) using the equation below:

$$\left(\frac{M_w^2}{[\eta]}\right)^{1/3} = A_0 M_L \Phi^{-1/3} + B_0 \Phi^{-1/3} \left(\frac{2L_P}{M_L}\right)^{-1/2} M_w^{1/2} \qquad (7.9)$$

where Φ is the Flory-Fox constant (2.86 x 10^{23} mol^{-1}), B_0 taken as ~ 1.10 (Bohdanecky, 1983) and M_L ~ 450 ($g.mol^{-1}.nm^{-1}$) obtained from (Morris et al., 2009b). Figure 7.11 showed the plot of $(M_w^2/[\eta])^{1/3}$ vs. $M_w^{1/2}$ for all chitosan samples. The L_p was obtained from the slope of this plot as (10 ± 1) nm.

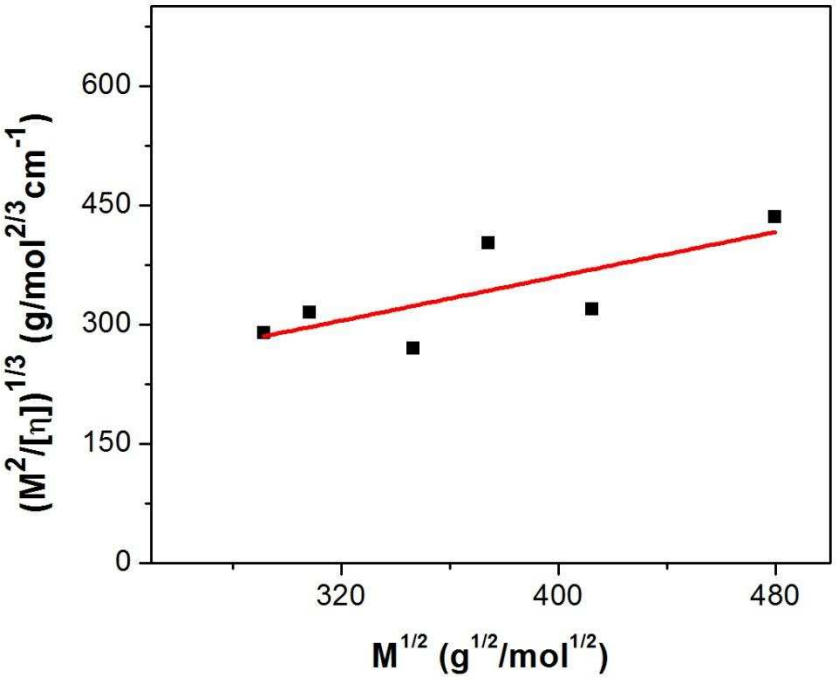


Figure 7.11: Bushin-Bohdanecky plot for commercial (CHIT1 to CHIT4) and laboratory-prepared (CHIT5 and CHIT6) chitosan samples, where L_p = (10 ± 1) nm from the slope.

7.4.4.3.2. Yamakawa–Fujii Method

Another approach to estimate chain persistence length, L_p is Yamakawa Fujii method by using sedimentation coefficient and molecular weight information (Please refer to section 6.4.5.3.1) (Yamakawa and Fujii, 1973). The slope of $s^0_{20,w}$ vs $(M_w)^{1/2}$ plot gives the value of L_p and M_L by using the following equation, which Freire and Garcia de la Torre were provided the corrected version (Freire and Garcia De La Torre, 1992):

$$s^0 = \frac{M_L(1-\bar{\upsilon}\rho_0)}{3\pi\eta_0 N_A}\, x\, \left[1.843\left(\frac{M_w}{2M_L L_P}\right)^{1/2} + A_2 + A_3\left(\frac{M_w}{2M_L L_P}\right)^{-1/2} + \ldots.\right] \quad (7.10)$$

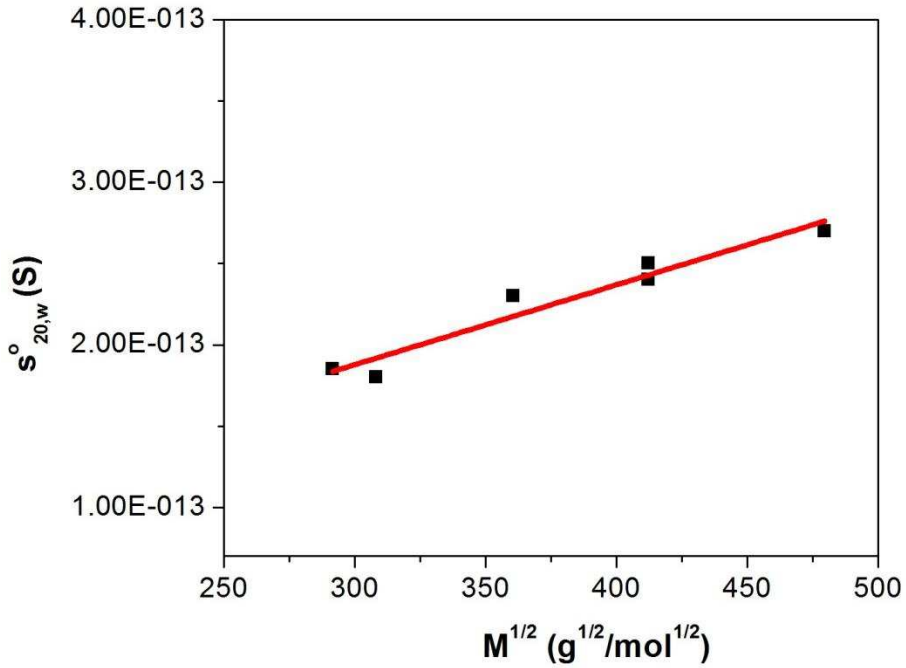


Figure 7.12: Yamakawa-Fujii plot for commercial and laboratory-prepared chitosan samples, where L_p = (18 ± 1) nm from the slope.

Using the equation above and from the slope of $s^0_{20,w}$ vs $(M_w)^{1/2}$ (Figure 7.12) the L_p was yielded as (18 ± 1) nm by fixing M_L as 450 ($g.mol^{-1}.nm^{-1}$).

7.4.4.3.3. Global analysis method (HYDFIT)

Clearly using one method can bias the result of L_p and M_L and additionally it requires either L_p or M_L to determine the other parameter. Therefore, a new algorithm was developed by Ortega and Garcia de la Torre which basically combines both previous methods to estimate L_p and M_L from the two or more data sets of sedimentation coefficient, intrinsic viscosity and molecular weight information of the

macromolecule. This programme then optimises the parameters in order to obtain the minimisation of the target function, Δ.

In this study, the L_p and M_L were estimated by fixing the chain diameter d and with the minimum value of the target function, Δ. The L_p and M_L values estimated using this procedure reported in in Table 7.5 The contour plot for each chitosan sample was presented in Figure 7.13.

Although the theoretical limits are $L_p = 0$ for random coil and $L_p = \infty$ for extra-rigid, practically the range is ~ 1 nm for the random coils (e.g. pullulan) and ~ 200 nm for an extra-rigid (e.g. xanthan). In this study, the L_p values of chitosan were determined in the range 7-16 nm for L_p, whereas 390-560 ($g.mol^{-1}.nm^{-1}$) as they were shown in Table 7.5. The differences between chitosan samples in persistence length and mass per unit length may result from slight differences in the intrinsic viscosity and the sedimentation coefficient. These values agree with a semi-flexible rod structure and also from previous studies (Berth et al., 1998, Brugnerotto et al., 2001, Cölfen et al., 2001, Morris et al., 2009b).

Table 7.5: Summary of the persistence length L_p and the mass per unit length M_L values for chitosan samples obtained from global HYDFIT analyses.

Sample	L_p (nm)	M_L (nm)
CHIT1	16 ± 0.2	500 ± 30
CHIT2	14 ± 0.2	560 ± 40
CHIT3	10 ± 1.0	400 ± 30
CHIT4	7 ± 0.4	400 ± 20
CHIT5	7 ± 0.1	390 ± 40
CHIT6	16 ± 1.0	550 ± 20

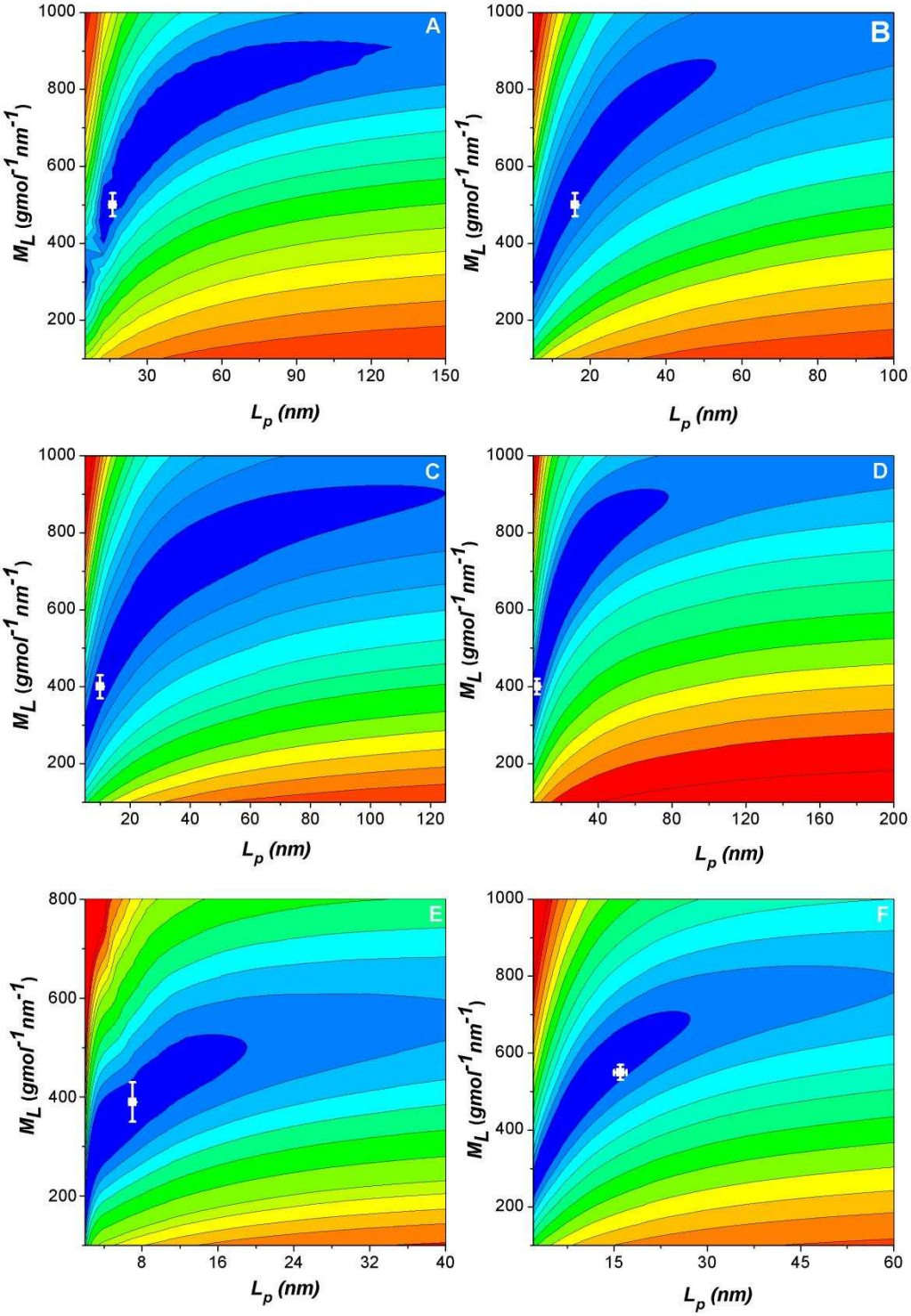


Figure 7.13: Contour plots of chitosan samples (A) CHIT1, (B) CHIT2, (C) CHIT3, (D) CHIT4, (E) CHIT5 and (F) CHIT6. The target function, Δ calculated based on variables values of L_p and M_L, and are represented on the full colour spectrum from blue (Δ = 0) to red (Δ≥0.95).

7.4.4.4. Molecular Conformation Zoning

The overall solution conformation can be determined using a sedimentation conformation zoning plot by plotting of $k_s M_L$ versus [s]/M_L (Pavlov et al., 1997) (see section 5.4.4.4). Figure 7.14 indicates that commercial chitosan samples (CHIT1 to CHIT4) adapted a rigid rod structure in zone (B) while laboratory-prepared (CHIT5 and CHIT6) adapted the semi-flexible structure in zone (C). These results are also consistent with those obtained from the MHKS and Wales-van Holde approaches.

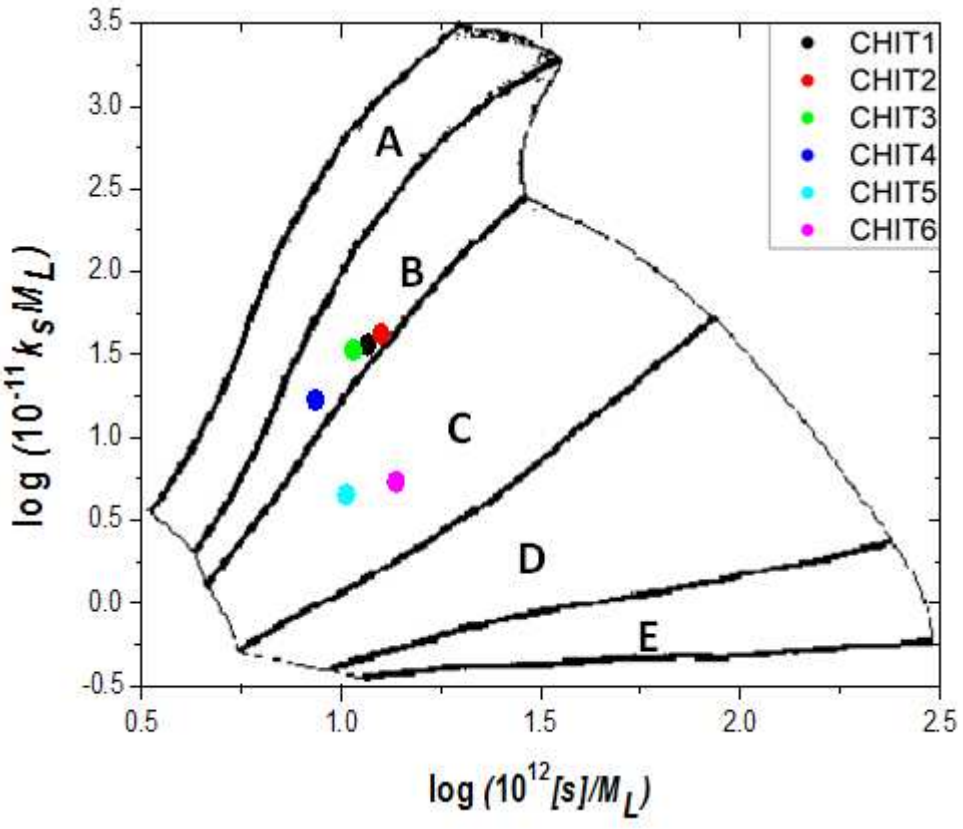


Figure 7.14: The conformation zoning plot for chitosan samples, commercial (CHIT1 to CHIT4) which have rigid rod structures, and laboratory-prepared (CHIT5 and CHIT6) which have semi-flexible coil structures.

7.4.5. Interaction with Two Polyanions: DNA and Xanthan

7.4.5.1. Chitosan-DNA Interaction

The principle of co-sedimentation in the analytical ultracentrifuge - previously successfully employed to study chitosan–mucin interactions (Harding, 2003, Harding, 2006)- is used to explore this situation further. Solutions of the two laboratory-prepared chitosan samples CHIT5 and CHIT6 with different molecular weights and degrees of acetylation were studied in mixtures with the DNA of M_w, estimated from the Extended Fujita method (Harding et al., 2011) as approximately 300 kDa. First, CHIT5, CHIT6 and DNA were characterised separately at a concentration of 1.0 mg/ml and a temperature of 20.0°C, using analytical ultracentrifugation based on sedimentation velocity. Unimodal distributions were seen in all cases, and the apparent weight average sedimentation coefficient $s_{20,w}$ obtained for CHIT5, CHIT6 were 1.9S and 2.3S, respectively, and 6.8S for DNA as reported in Table 7.6. Each chitosan preparation was then mixed in a 1:1 w/w ratio with the DNA to a total concentration of 1.0 mg/ml. A clear shift to a high s value is observed in both cases, with nothing sedimenting at the rate of uncomplexed chitosan suggesting that the interaction had gone to completion. From the shoulder of the complex in Figure 7.15, some unreacted DNA was seen remaining.

The effect of degree of acetylation has been examined by providing a greater $s_{20,w}$ distribution at low acetylation ratio (CHIT6) compared to that of a higher acetylation ratio (CHIT5).

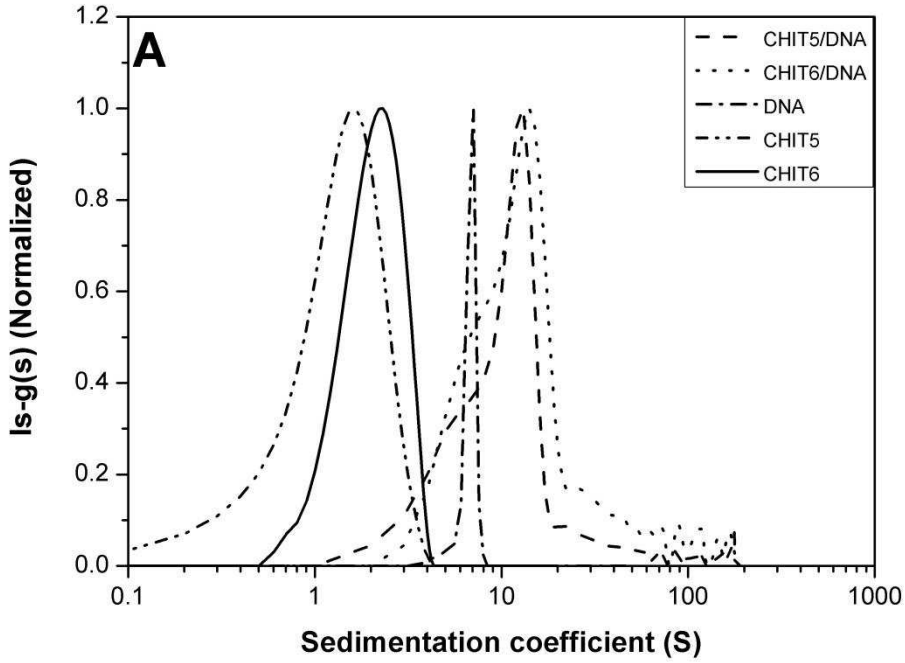


Figure 7.15: Normalized sedimentation coefficient distribution profiles obtained from sedimentation velocity experiment for unmixed controls and mixture for chitosan samples (CHIT5 and CHIT6) with DNA.

Table 7.6: Sedimentation coefficients at $s_{20,w}$ at a total concentration of 1.0 mg/ml, for chitosan, DNA, xanthan and chitosan-DNA and chitosan-xanthan complexes.

Sample	$s_{20,w}$ (S)	% unreacted chitosan	% unreacted DNA	% unreacted xanthan
CHIT5	1.9			
CHIT6	2.3			
DNA	6.8			
xanthan	4.8			
CHIT5-DNA	17	0	28	
CHIT6-DNA	20	0	17	
CHIT5-xanthan	10	0		0
CHIT6-xanthan	10	0		0

7.4.5.2. Chitosan-Xanthan Interaction

Xanthan is a double helical highly polyanionic polymer and can generate hydrogel with other polysaccharides. The characteristics of chitosan and xanthan mixtures as hydrogels have been extensively studied for over two decades (Chu et al., 1995, Magnin et al., 2003, Popa et al., 2010, Draganescu et al., 2013). The chitosan and xanthan mixture was examined with a co-sedimentation method in this study. The molecular weight of the standard pyruvated xanthan (LMW-STD) was found previously to be $\sim 3.2 \times 10^3$ kDa using sedimentation equilibrium in the analytical ultracentrifuge (see Chapter 3).

As with the DNA study, the sedimentation coefficient profile of xanthan was firstly characterised at 1.0 mg/ml yielding a unimodal g(s) vs s plot with a weighted-average $s^0_{20,w}$ of 4.8S. Then the 1:1 by weight mixtures with CHIT5 and CHIT6 at a total concentration of 1.0 mg/ml, were studied and the results shown in Figure 7.16 and Table 7.6. Unlike chitosan–DNA, all the chitosan was complexed, and no residual chitosan or xanthan were left behind for both CHIT5 and CHIT6 complexes. Weighted average $s_{20,w}$ for the complexes of 10.3S and 10.1S for CHIT5-xanthan and CHIT6-xanthan, respectively were obtained.

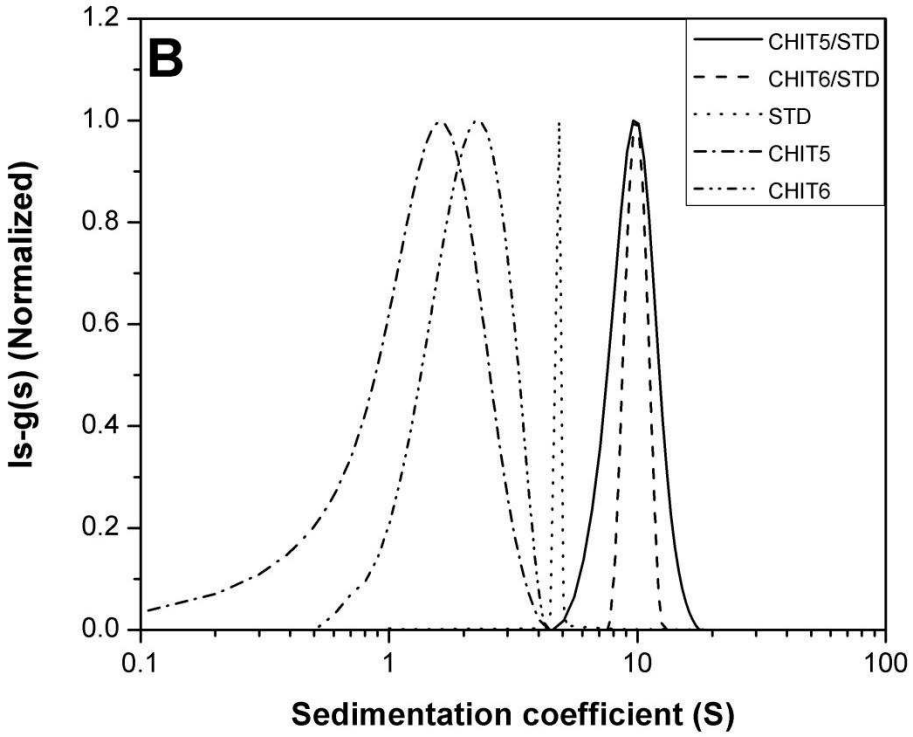


Figure 7.16: Normalized sedimentation coefficient distribution profiles obtained from sedimentation velocity experiment for unmixed controls and mixture for chitosan samples (CHIT5 and CHIT6) with xanthan-STD.

7.5. DISCUSSION

In this chapter, the six chitosan samples-commercial (C) and laboratory (L) prepared samples- with different molecular weights and degrees of acetylation (25% and 15%) have been characterised in terms of hydrodynamic properties to investigate further application for their interaction with polyanionic polymers. The weight-average molecular weight (M_w), sedimentation coefficient ($s^0_{20,w}$) distribution, and intrinsic viscosities *([η]*) of chitosan samples were assessed by hydrodynamic approaches using sedimentation equilibrium, sedimentation velocity and SEC–MALS. The

unimodal distributions were obtained from sedimentation coefficient distributions for all chitosan samples. The higher values of concentration dependence (k_s) have been yielded for commercial samples (CHIT1 to CHIT4) whereas not for the laboratory-prepared samples (CHIT5 and CHIT6), which might indicate very high non-ideal behaviour. The methods of sedimentation equilibrium, sedimentation velocity-extended Fujita Method- and SEC–MALS provided the weight average molecular weight values for each sample in the range of ~(85-260) x 10^3 (Da). The values obtained from those were all consistent within the error estimate.

The conformation of chitosan depends on the degree of acetylation of the molecule and the ionic strength of the solvent in which it was studied (Schatz et al., 2003). Therefore, knowledge of the dependence of $[\eta]$ and $s^0_{20,w}$ with corresponding M_w enables the investigation of the conformation of chitosan samples. The results indicated the conformation as semi-flexible rod and sample greater flexibility was observed for CHIT5. These results were confirmed with the Wales-van Holde and sedimentation conformation zoning methods. Different chemical composition, molecular weight and ionic strength may result in the discrepancy in the conformational flexibility of chitosan samples (Varum and Smidsrød, 2004). Therefore, using more than one hydrodynamic method can overcome to this problem while characterising the macromolecules. Regarding the persistence length, three different methods -Bushin-Bohdanecky and Yamakawa-Fujii, Multi HYDFIT- have been used to estimate the flexibility of chitosan structures. The results appear that chitosan samples adopt a semi-flexible rod type conformation, which is consistent with those calculated from MHKS and Wales-van Holde ratio. The results also reinforced the earlier study by Brugneretto et al. (2001) who found the stiffness of the chain was not affected from DA ratio (up to 60%). Examining the physical

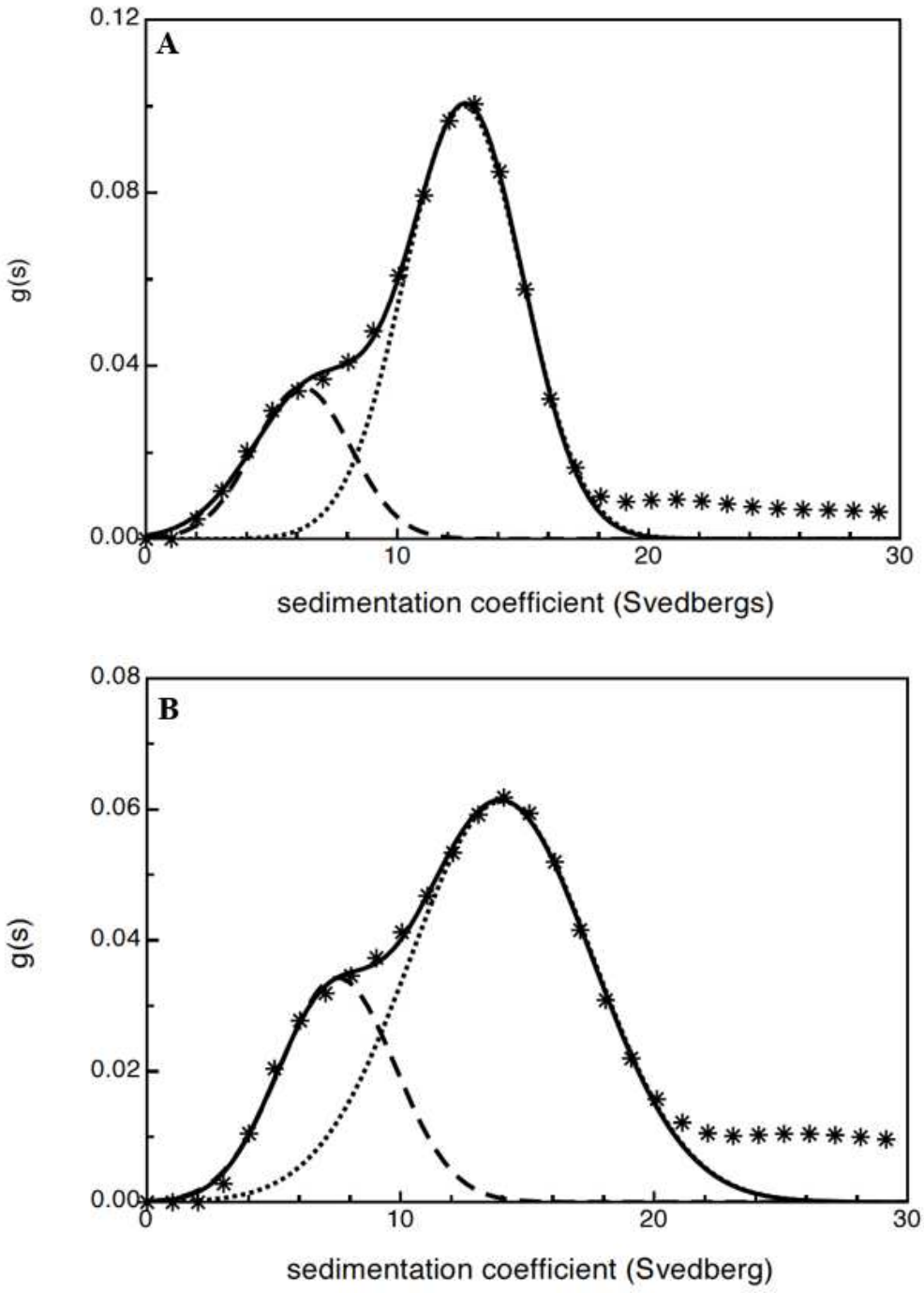


Figure 7.17: Multi-Gaussian fit using MULTIG (locally written software, run under pro Fit™, interactive Preview Window, floating the position (s value), area and standard deviation of each peak Quansoft, Zurich) (A) Multi-Gaussian fit to the CHIT5-DNA mixture and (B) Multi-Gaussian fit to the CHIT6-DNA mixture. With the routine MULTIG fitting was initially performed manually via the interactive Preview Window, floating the position (s value), area and standard deviation of each peak.

properties of chitosans in solution provide information about the biophysical characteristics of molecules and this information enable the study of their behaviour in mixture with the DNA and xanthan. The principle of co-sedimentation successfully applied to examine interactions between the chitosan–DNA and chitosan-xanthan mixtures, where the laboratory prepared chitosan samples (CHIT5 and CHIT6) were used. Interactions were observed by quantified from the changes in the sedimentation coefficient distribution of the mixture compared to unmixed controls using the sedimentation velocity approach. The effect of molecular weight on interaction can be particularly seen from the chitosan-DNA interaction.

In terms of the shoulder of the chitosan-DNA complex, some unreacted DNA was observed (Figure 7.15). Multi-Gaussian analysis of the g(s) vs s distribution for the complex using the routine MULTIG suggests ~ 28% DNA had not interacted for CHIT5 (Figure 7.17A) and ~17% for CHIT6 (Figure 7.17B). The s-distribution of the complex is very broad, even on a logarithmic scale, with material in excess of 100S, with the larger molecular weight chitosan CHIT6 showing the highest degree of complexation. The chitosan-xanthan mixture indicated that all chitosan and xanthan interact so there was no remaining unreacted polymer.

7.7. CONCLUSION

A combined hydrodynamic approach using sedimentation equilibrium, sedimentation velocity and SEC–MALS provides three methods for assessing the molecular weight and molecular weight distribution of chitosans—and all in agreement for the six samples studied. Combination with viscosity has been shown to yield estimates for the conformational flexibility parameter consistent with previous measurements.

This study also demonstrates that the principle of co-sedimentation can be used to study interactions with polyanions such as xanthan and DNA as it has been successfully applied previously to the study of chitosan–mucin glycoprotein interactions. Furthermore, the interaction of chitosan-xanthan is important to evaluate the potential medical and food applications such as drug delivery and flavour encapsulation. The latter interaction between chitosan-xanthan may prove useful for the assay of potential chitosan based materials with especially xanthan for controlled release of entrapped materials such as therapeutic agents, enzymes and bacteria particularly if it used in conjunction with mucoadhesive phenomena (Deacon et al., 2000).

CHAPTER 8

CONCLUDING REMARKS AND SUGGESTIONS FOR FUTURE WORK

The principal aim of this thesis was to provide a comprehensive hydrodynamic characterisation of a selected group of microbial polysaccharides, which are of particular commercial/therapeutic potential use. The solution properties of these polysaccharides -in terms of their molecular integrity, size distribution, conformation and interactions with other biopolymers have been investigated using analytical ultracentrifugation (AUC), size exclusion chromatography coupled with multi angle light scattering (SEC-MALS) and viscometry as our main tools of enquiry. The virtue of combining these methods together has also been demonstrated.

8.1. Characterisation of Xanthans

We considered the solution behaviour of four commercial xanthan samples: two with identical degrees of pyruvalation ("Standard pyruvate" 3.9%), but different molecular weights (high molecular weight HMW and low molecular weight LMW), and two further ones of different degrees of pyruvalation-namely "High" (6.5%) and "Low" (2%) The hydrodynamic parameters such as viscosity, molecular weight were determined using AUC, viscometry and dynamic light scattering (DLS) techniques, but the samples were too large for adequate characterisation by size exclusion

chromatography coupled to multi-angle light scattering (SEC-MALS). Therefore, the SEC-MALS experiment could not be carried out.

Sedimentation velocity revealed unimodal sedimentation coefficient distributions, which confirmed the purity of all the xanthan preparations. The molecular weights were determined using the sedimentation velocity-MHKS power law and sedimentation equilibrium methods. Due to the low value of the "critical overlap concentration" (c*) and large thermodynamic non-ideality of these macromolecules, normal "infinite dilution" extrapolation methods to eliminate non-ideality in sedimentation equilibrium were difficult to apply. However, taking advantage of the earlier study by Dhami et al. (1995) and using the value obtained for the 2nd thermodynamic virial coefficient B, correct apparent weight average molecular weights or thermodynamically ideal weight average molecular weights were obtained. For the conformation, the results revealed a rigid rod conformation, from both the Wales van Holde Ratio and using molecular conformation zoning. In terms of the ionic strength effect, the three xanthan samples- xanthan Standard LMW, High pyruvate and Low pyruvate - showed increasing rigidity with increasing ionic strength.

8.2. Characterisation of Gellan

The hydrodynamic properties of low acyl gellan (LAG) in low ionic strength (25mM) NaI solution were determined in terms of viscosity, heterogeneity, molecular weight and conformational properties. At this ionic strength of NaI buffer, the gellan exists in solution form (gellan - especially of low purity can easily form gels in the presence of higher concentrations of mono-and-divalent cations). The LAG sample was used without any further purification and it was irradiated for

varying times using microwave heating in a high pressure vessel to produce a series of polymers of different degrees of degradation or molecular weight, i.e. a "homologous" series of polymers. Estimating how hydrodynamic parameters varied with molecular weight provided us with a means of estimating conformation. According to sedimentation velocity all samples showed a bimodal sedimentation coefficient distribution. With depolymerisation, a clear reduction in weight-average sedimentation coefficient, molecular weight, concentration dependence parameter k_s, and viscosity was observed with increased heating time in the microwave. The results showed that microwave treated gellan most likely adopted a rod conformation with some flexibility when it dissolves in 25mM NaI. The Wales-Van Holde ratio indicated a rigid rod structure (R = 0.5 – 0.7), which was reinforced by Mark-Houwink-Kuhn-Sakurada (MHKS) and conformation zoning methods. For the quantitative determination of flexibility of gellan, a new software package, HYDFIT (Ortega and García de la Torre, 2007), which considers data sets of both intrinsic viscosities for different molecular weights and sedimentation coefficients for different molecular weights was used: values for the persistence length L_p of (100 ± 10) were again consistent with a rod conformation.

8.3. Characterisation of Microbial Hyaluronic Acid

We also investigated the solution behaviour of six different hyaluronic acid preparations (in their sodium salt form) and two further microwave irradiated samples. The sedimentation coefficient distribution plots, g*(s) vs. s plots again, like xanthan, showed unimodal behaviour. Both sedimentation equilibrium in the analytical ultracentrifuge and SEC-MALS were applied to estimate molecular weights. According to the MHKS method, the conformations of sodium hyaluronate

samples were all estimated as semi-flexible random coil type conformation, a conclusion which was reinforced by the Wales-van Holde ratio and conformation zoning methods. A combination of molecular weight with viscosity data was also used to determine the persistence length of the samples. The Multi-HYDFIT and Bushin Bohdanecky approaches were applied to estimate the quantitative conformational flexibility of the polysaccharides through their persistence lengths (L_p) and mass per unit lengths (M_L). Those determinations indicated semi flexible random coil structures confirming results from other conformation determination methods.

8.4. Characterisation of Schizophyllan

We then considered the solution properties of two samples of schizophyllan (INV1 and GM1) with different molecular weights, which were irradiated using microwave heating (GM1) and ultrasonication (INV1) to provide a homologous polymer series for analysis. Again, according to the sedimentation coefficient distribution profiles, all samples presented bimodal distributions with two peaks, which indicated the high and low molecular weight component in all schizophyllan samples. The molecular weights were estimated using three different approaches- sedimentation equilibrium and sedimentation velocity in the analytical ultracentrifuge and SEC-MALS by SEDFIT-MSTAR, the Extended Fujita, f(M) approach, (Harding et al., 2011) and ASTRA (Version 6.1) analysis methods, respectively. The results showed an agreement on M_w values from these three different approaches for all samples, which proved the importance of comparing different methods for the determination of molecular weight of polysaccharides. SEC-MALS also provided data to estimate the conformation by Mark-Houwink-Kuhn-Sakurada (MHKS) and flexibility by Multi-

HYDFIT methods by the advantage of coupling online molecular weight and intrinsic viscosity measurements for all samples. The conformation results by the MHKS approach demonstrated that all four schizophyllan samples adopted rigid-rod type conformation confirmed by the Wales-van Holde ratio and conformation zoning. The polymers were shown to gain increased flexibility at higher molecular weight (Yanaki et al., 1980). Further conformation analysis for the quantitative determination of flexibility of the schizophyllan samples (The L_p and M_L values) was done using the Multi-HYDFIT and Yamakawa-Fujii approaches. The L_p and M_L values of each sample and the results all pointed to a rigid-rod conformation with L_p values of ~120-130 nm, which were also consistent with previous studies (Norisuye et al., 1980, Stokke et al., 1993).

8.5. Characterisation of chitosan – used as an interactant with xanthan and DNA

Finally, the hydrodynamic properties of commercial (C) and laboratory (L) prepared chitosan samples with different molecular weight and degrees of acetylation were studied in Chapter 7. The hydrodynamic techniques- namely sedimentation equilibrium, sedimentation velocity, SEC-MALS and viscometry were used for characterisation. The molecular integrity of chitosan samples were examined by sedimentation velocity and the g*(s) vs. s (S) plots reflected the homogeneity of samples with unimodal distributions. The weight average molecular weights of chitosan samples were estimated by sedimentation equilibrium, sedimentation velocity method in analytical ultracentrifuge and SEC-MALS, and the values from sedimentation equilibrium method were consistent with those obtained from SEC-MALS and the complementary Extended Fujita method of Harding et al. (Harding et

al., 2011). Knowledge of the intrinsic viscosity $[\eta]$ and $s^0_{20,w}$ with molecular weight (M_w) made it possible to investigate the conformation of chitosan samples by MHKS method and $[\eta]$ values with M_w values were yielded from SEC-MALS for each chitosan sample. Mark–Houwink–Kuhn–Sakurada (MHKS) results suggested a semi-flexible coil conformation for the chitosan samples and this conformation was confirmed with the other approaches such as Wales–van Holde ratio and conformation zoning. The flexibility in terms of the persistence length (L_p) of all chitosan samples were estimated using three different approaches-Bushin-Bohdanecky, Yamakawa-Fujii and Multi-HYDFIT. The results again indicated a semi-flexible coil conformation for all commercial and laboratory-prepared chitosan samples in solution (L_p ~7 to 16 nm).

The principle of co-sedimentation in the analytical ultracentrifuge was applied to study interactions of chitosan with two polyanions - xanthan and DNA, which is important when evaluating these mixtures for the potential medical and food applications such as gene delivery, drug delivery and flavour encapsulation. This may prove useful for the assay of potential chitosan based materials with especially xanthan for controlled release of entrapped materials such as therapeutic agents, enzymes and bacteria (Chellat et al., 2000). If this complex is particularly used along with mucoadhesive phenomena as an imaging probes, it can give better understanding for the drug delivery application in digestive track (Deacon et al., 2000).

8.6. Suggestion for Future Work

It is clear that there are a number of areas which can be covered in future studies:

- ✓ Although the efficacy of hydrodynamic methods – including co-sedimentation – to explore xanthan-chitosan interaction has been clearly presented, the interaction can also be explored with different conditions such as the buffer, pH value, ionic strengths and mixing ratio with this methodology.
- ✓ The interaction between hyaluronic acid and chitosan can be investigated with the co-sedimentation methods with different mixing ratio, buffer and ionic strength
- ✓ Since gellan is solution form in 25mM NaI and not requiring the any further purification to maintain as a solution form, the hydrogel formation of gellan-chitosan can be studied in different pH values and concentrations with rheometer, Differential scanning calorimetry (DSC) and atomic force microscopy (AFM) and dynamic light scattering (DLS) methods as an addition to analytical ultracentrifugation method.
- ✓ These additional methods which were mentioned above (eg. rheometer, DSC, AFM, DLS can also be useful to examine the interaction of xanthan-chitosan and xanthan-hyaluronic acid mixtures, which will provide more information to develop better healthcare therapies and food applications.

REFERENCES

ABDELHAMEED, A. S. 2010. Molecular Conformation and Integrity of Polysaccharide based Meningitis Vaccines. PhD Thesis, University of Nottingham.

ABDELHAMEED, A. S., ANG, S., MORRIS, G. A., SMITH, I., LAWSON, C., GAHLER, R., WOOD, S. & HARDING, S. E. 2010. An analytical ultracentrifuge study on ternary mixtures of konjac glucomannan supplemented with sodium alginate and xanthan gum. Carbohydrate Polymers, 81**,** 145-148.

ALMUTAIRI, F. M. 2015. A Molecular Hydrodynamic Study of Marine Based Non-Digestible Fibre Polysaccharides Considered for Use in Health Products. PhD, University of Nottingham.

ALMUTAIRI, F. M., ADAMS, G. G., KÖK, M. S., LAWSON, C. J., GAHLER, R., WOOD, S., FOSTER, T. J., ROWE, A. J. & HARDING, S. E. 2013. An analytical ultracentrifugation based study on the conformation of lambda carrageenan in aqueous solution. Carbohydrate polymers, 97**,** 203-209.

ALTMAN, R. D. Intra-articular sodium hyaluronate in osteoarthritis of the knee. Seminars in arthritis and rheumatism, 2000. Elsevier, 11-18.

ANDERSON, M. T. 1991. The Interaction of Mucous Glycoproteins with Polymeric Materials. PhD, University of Nottingham.

ARGIN-SOYSAL, S., KOFINAS, P. & LO, Y. M. 2009. Effect of complexation conditions on xanthan–chitosan polyelectrolyte complex gels. Food Hydrocolloids, 23**,** 202-209.

BENNY, I. S., GUNASEKAR, V. & PONNUSAMI, V. 2014. Review on Application of Xanthan Gum in Drug Delivery. International Journal of PharmTech Research, 6.

BERGERET-GALLEY, C., LATOUCHE, X. & ILLOUZ, Y. 2001. The value of a new filler material in corrective and cosmetic surgery: DermaLive and DermaDeep. Aesthetic plastic surgery, 25**,** 249-255.

BERTH, G., DAUTZENBERG, H., CHRISTENSEN, B. E., HARDING, S. E., ROTHER, G. & SMIDSRØD, O. 1996. Static light scattering studies on xanthan in aqueous solutions. Macromolecules, 29**,** 3491-3498.

BERTH, G., DAUTZENBERG, H. & PETER, M. G. 1998. Physico-chemical characterization of chitosans varying in degree of acetylation. Carbohydrate Polymers, 36**,** 205-216.

BEZÁKOVÁ, Z., HERMANNOVÁ, M., DŘÍMALOVÁ, E., MALOVÍKOVÁ, A., EBRINGEROVÁ, A. & VELEBNÝ, V. 2008. Effect of microwave irradiation on the molecular and structural properties of hyaluronan. Carbohydrate polymers, 73**,** 640-646.

BHATTARAI, N., RAMAY, H. R., GUNN, J., MATSEN, F. A. & ZHANG, M. 2005. PEG-grafted chitosan as an injectable thermosensitive hydrogel for sustained protein release. Journal of Controlled Release, 103**,** 609-624.

BINDAL, A., NARSIMHAN, G., HEM, S. L. & KULSHRESHTHA, A. 2007. Structural Changes in Xanthan Gum Solutions During Steam Sterilization for Sterile Preparations. Pharmaceutical Development and Technology, 12**,** 159-167.

BOHDANECKY, M. 1983. New method for estimating the parameters of the wormlike chain model from the intrinsic viscosity of stiff-chain polymers. Macromolecules, 16**,** 1483-1492.

BOHN, J. A. & BEMILLER, J. N. 1995. (1→ 3)-β-D-Glucans as biological response modifiers: a review of structure-functional activity relationships. Carbohydrate polymers, 28**,** 3-14.

BOT, A., SMORENBURG, H. E., VREEKER, R., PÂQUES, M. & CLARK, A. H. 2001. Melting behaviour of schizophyllan extracellular polysaccharide gels in the temperature range between 5 and 20 C. Carbohydrate polymers, 45**,** 363-372.

BOTHNER, H., WAALER, T. & WIK, O. 1988. Limiting viscosity number and weight average molecular weight of hyaluronate samples produced by heat degradation. International Journal of Biological Macromolecules, 10**,** 287-291.

BRADSHAW, I., NISBET, B., KERR, M. & SUTHERLAND, I. 1983. Modified xanthan—its preparation and viscosity. Carbohydrate Polymers, 3**,** 23-38.

BROWN, M. & JONES, S. A. 2005. Hyaluronic acid: a unique topical vehicle for the localized delivery of drugs to the skin. Journal of the European Academy of Dermatology and Venereology, 19**,** 308-318.

BRUGNEROTTO, J., DESBRIÈRES, J., ROBERTS, G. & RINAUDO, M. 2001. Characterization of chitosan by steric exclusion chromatography. Polymer, 42**,** 09921-09927.

BUHLER, E. & BOUÉ, F. 2004. Chain Persistence Length and Structure in Hyaluronan Solutions: Ionic Strength Dependence for a Model Semirigid Polyelectrolyte. Macromolecules, 37**,** 1600-1610.

BUSHIN, S., TSVETKOV, V., LYSENKO, Y. B. & YEMELYANOV, V. 1981a. Conformational properties and rigidity of molecules of ladder polyphenylsiloxane in solutions according the data of sedimentation-diffusion analysis and viscometry. Vysokomolekulyarnye Soedineniyaseriyaa, 23**,** 2494-2503.

BUSHIN, S., TSVETKOV, V., LYSENKO, Y. B. & YEMELYANOV, V. 1981b. Conformational properties and rigidity of molecules of ladder polyphenylsiloxane in solutions according the data of sedimentation-diffusion analysis and viscometry. VYSOKOMOLEKULYARNYE SOEDINENIYA SERIYA A, 23**,** 2494-2503.

CAGGIONI, M., SPICER, P., BLAIR, D., LINDBERG, S. & WEITZ, D. 2007. Rheology and microrheology of a microstructured fluid: The gellan gum case. Journal of Rheology (1978-present), 51**,** 851-865.

CALLET, F., MILAS, M. & RINAUDO, M. 1987. Influence of acetyl and pyruvate contents on rheological properties of xanthan in dilute solution. International Journal of Biological Macromolecules, 9**,** 291-293.

CASAS, J. & GARCÍA-OCHOA, F. 1999. Viscosity of solutions of xanthan/locust bean gum mixtures. Journal of the Science of Food and Agriculture, 79**,** 25-31.

CASPERSEN, M. B., ROUBROEKS, J. P., QUN, L., SHAN, H., FOGH, J., RUIDONG, Z. & TØMMERAAS, K. 2014. Thermal degradation and stability of sodium hyaluronate in solid state. Carbohydrate polymers, 107**,** 25-30.

CHAZEAU, L., MILAS, M. & RINAUDO, M. 1995. Conformations of xanthan in solution: analysis by steric exclusion chromatography. International Journal of Polymer Analysis and Characterization, 2**,** 21-29.

CHEETHAM, N. W. H. & NIK NORMA, N. M. 1989. The effect of pyruvate on viscosity properties of xanthan. Carbohydrate Polymers, 10**,** 55-60.

CHELLAT, F., TABRIZIAN, M., DUMITRIU, S., CHORNET, E., RIVARD, C.-H. & YAHIA, L. 2000. Study of biodegradation behavior of chitosan-xanthan microspheres in simulated physiological media. Journal of biomedical materials research, 53**,** 592-599.

CHOI, H. M. & YOO, B. 2009. Steady and dynamic shear rheology of sweet potato starch–xanthan gum mixtures. Food Chemistry, 116**,** 638-643.

CHOI, J.-I., KIM, J.-K., KIM, J.-H., KWEON, D.-K. & LEE, J.-W. 2010. Degradation of hyaluronic acid powder by electron beam irradiation, gamma ray irradiation, microwave irradiation and thermal treatment: A comparative study. Carbohydrate Polymers, 79**,** 1080-1085.

CHONG, B. F., BLANK, L. M., MCLAUGHLIN, R. & NIELSEN, L. K. 2005. Microbial hyaluronic acid production. Applied Microbiology and Biotechnology, 66**,** 341-351.

CHU, C.-H., SAKIYAMA, T. & YANO, T. 1995. pH-sensitive swelling of a polyelectrolyte complex gel prepared from xanthan and chitosan. Bioscience, biotechnology, and biochemistry, 59**,** 717-719.

CLAES, P., DUNFORD, M., KENNEY, A. & VARDY, P. 1992. An On-Line Dynamic Light Scattering Instrument for Macromolecular Characterisation. In: HARDING, S. E., SATTELLE, D. B. & BLOOMFIELD, V. A. (eds.) Laser Light Scattering in Biochemistry. Cambridge, UK: The Royal Society of Chemistry.

CLELAND, R. L. 1984. Viscometry and sedimentation equilibrium of partially hydrolyzed hyaluronate: Comparison with theoretical models of wormlike chains. Biopolymers, 23**,** 647-666.

COLE, J. L., LARY, J. W., P. MOODY, T. & LAUE, T. M. 2008. Analytical Ultracentrifugation: Sedimentation Velocity and Sedimentation Equilibrium. In: DR. JOHN, J. C. & DR. H. WILLIAM DETRICH, III (eds.) Methods in Cell Biology. Academic Press.

CÖLFEN, H., BERTH, G. & DAUTZENBERG, H. 2001. Hydrodynamic studies on chitosans in aqueous solution. Carbohydrate Polymers, 45**,** 373-383.

CÖLFEN, H. & HARDING, S. E. 1997. MSTARA and MSTARI: interactive PC algorithms for simple, model independent evaluation of sedimentation equilibrium data. European Biophysics Journal, 25**,** 333-346.

CREETH, J. & KNIGHT, C. 1965. On the estimation of the shape of macromolecules from sedimentation and viscosity measurements. Biochimica et Biophysica Acta (BBA)-Biophysics including Photosynthesis, 102**,** 549-558.

CREETH, J. M. & HARDING, S. H. 1982. Some observations on a new type of point average molecular weight. Journal of biochemical and biophysical methods, 7**,** 25-34.

CUVELIER, G. & LAUNAY, B. 1986. Concentration regimes in xanthan gum solutions deduced from flow and viscoelastic properties. Carbohydrate Polymers, 6**,** 321-333.

DAM, J. & SCHUCK, P. 2004. Calculating sedimentation coefficient distributions by direct modeling of sedimentation velocity concentration profiles. Methods in enzymology, 384**,** 185-212.

DEACON, M., MCGURK, S., ROBERTS, C., WILLIAMS, P., TENDLER, S., DAVIES, M., DAVIS, S. & HARDING, S. 2000. Atomic force microscopy of gastric mucin and chitosan mucoadhesive systems. Biochem. J, 348**,** 557-563.

DENTINI, M., COVIELLO, T., BURCHARD, W. & CRESCENZI, V. 1988. Solution properties of exocellular microbial polysaccharides. 3. Light scattering from gellan and from the exocellular polysaccharide of Rhizobium trifolii (strain TA-1) in the ordered state. Macromolecules, 21**,** 3312-3320.

DHAMI, R. 1996. Hydrodynamic Studies of Xanthan and Xylan Systems. PhD Thesis, University of Nottingham.

DHAMI, R., HARDING, S. E., JONES, T., HUGHES, T., MITCHELL, J. R. & TO, K. 1995. Physico-chemical studies on a commercial food-grade xanthan—I. Characterisation by sedimentation velocity, sedimentation equilibrium and viscometry. Carbohydrate polymers, 27**,** 93-99.

DRAGANESCU, D., SILION, M., IGNAT, I., SARGHIE, C. & POPA, M. I. 2013. Entrapment Of Flaxseed Extract Into Xanthan-Chitosan Complex. Cellulose Chemistry and Technology, 47**,** 231-238.

DURANTI, F., SALTI, G., BOVANI, B., CALANDRA, M. & ROSATI, M. L. 1998. Injectable hyaluronic acid gel for soft tissue augmentation. Dermatologic surgery, 24**,** 1317-1325.

DURRANI, A., FARR, S. & KELLAWAY, I. 1995. Influence of molecular weight and formulation pH on the precorneal clearance rate of hyaluronic acid in the rabbit eye. International journal of pharmaceutics, 118**,** 243-250.

DUTTA, P. K., DUTTA, J. & TRIPATHI, V. 2004. Chitin and chitosan: Chemistry, properties and applications. Journal of Scientific and Industrial Research, 63**,** 20-31.

ERRINGTON, N., HARDING, S., VÅRUM, K. & ILLUM, L. 1993. Hydrodynamic characterization of chitosans varying in degree of acetylation. International journal of biological macromolecules, 15**,** 113-117.

FEE, M. 2006. Evaluation of Chitosan Stability in Aqueous Systems. PhD, University of Nottingham.

FEE, M., ERRINGTON, N., JUMEL, K., ILLUM, L., SMITH, A. & HARDING, S. E. 2003a. Correlation of SEC/MALLS with ultracentrifuge and viscometric data for chitosans. Eur Biophys J, 32**,** 457-464.

FEE, M., ERRINGTON, N., JUMEL, K., ILLUM, L., SMITH, A. & HARDING, S. E. 2003b. Correlation of SEC/MALLS with ultracentrifuge and viscometric data for chitosans. European Biophysics Journal, 32**,** 457-464.

FIEBRIG, I., HARDING, S. E., ROWE, A. J., HYMAN, S. C. & DAVIS, S. S. 1995. Transmission electron microscopy studies on pig gastric mucin and its interactions with chitosan. Carbohydrate polymers, 28**,** 239-244.

FOUISSAC, E., MILAS, M., RINAUDO, M. & BORSALI, R. 1992. Influence of the ionic strength on the dimensions of sodium hyaluronate. Macromolecules, 25**,** 5613-5617.

FREIRE, J. & GARCIA DE LA TORRE, J. 1992. Sedimentation coefficients of flexible chain polymers. In: HARDING, S. E., ROWE, A. J. & HORTON, J. C. (eds.) Analytical ultracentrifugation in biochemistry and polymer science. Cambridge, UK: The Royal Society of Chemistry.

GAMINI, A., PAOLETTI, S. & ZANETTI, F. 1992. Chain Rigidity of Polyuronides: Static Light Scattering of Aqueous Solutions of Hyaluronate and Alginate. In: HARDING, S. E., SATTELLE, D. B. & BLOOMFIELD, V. A. (eds.) Laser Light Scattering in Biochemistry. Cambridge,UK: The Royal Society of Chemistry.

GANDOLFI, S. A., MASSARI, A. & ORSONI, J. G. 1992. Low-molecular-weight sodium hyaluronate in the treatment of bacterial corneal ulcers. Graefe's archive for clinical and experimental ophthalmology, 230**,** 20-23.

GARCÍA-OCHOA, F., SANTOS, V., CASAS, J. & GÓMEZ, E. 2000. Xanthan gum: production, recovery, and properties. Biotechnology advances, 18**,** 549-579.

GIAVASIS, I. 2013. Production of microbial polysaccharides for use in food. In: MCNEIL, B., ARCHER, D., GIAVASIS, I. & HARVEY, L. (eds.) Microbial Production of Food Ingredients, Enzymes and Nutraceuticals. Cambridge, UK: Woodhead Publishing.

GIAVASIS, I. 2014. Bioactive fungal polysaccharides as potential functional ingredients in food and nutraceuticals. Current opinion in biotechnology, 26**,** 162-173.

GIAVASIS, I. & BILIADERIS, C. 2007a. Microbial polysaccharides. CRC Press, Boca Raton, FL, USA.

GIAVASIS, I. & BILIADERIS, C. 2007b. Microbial polysaccharides. In: BILIADERIS, C. G. & IZYDORCZYK, M. S. (eds.) Functional Food Carbohydrates. Boca Raton, FL, USA: CRC Press, Taylor and Francis.

GRALEN, N. 1944. Sedimentation and Diffusion Measurements on Cellulose and Cellulose Derivatives. PhD thesis, University of Uppsala.

GREEN, A. A. 1933. The preparation of acetate and phosphate buffer solutions of known pH and ionic strength. Journal of the American Chemical Society, 55**,** 2331-2336.

GUNNING, A., KIRBY, A., RIDOUT, M., BROWNSEY, G. & MORRIS, V. 1996. Investigation of gellan networks and gels by atomic force microscopy. Macromolecules, 29**,** 6791-6796.

GURA, E., HÜCKEL, M. & MÜLLER, P.-J. 1998. Specific degradation of hyaluronic acid and its rheological properties. Polymer degradation and stability, 59**,** 297-302.

GURNY, R., IBRAHIM, H., AEBI, A., BURI, P., WILSON, C., WASHINGTON, N., EDMAN, P. & CAMBER, O. 1987. Design and evaluation of controlled release systems for the eye. Journal of Controlled Release, 6**,** 367-373.

HARDING, S. 2003. Mucoadhesive interactions. Biochemical Society Transactions, 31**,** 1036-1041.

HARDING, S. 2012. Viscometry, analytical ultracentrifugation and light scattering probes for carbohydrate stability. In: HARDING, S. E. (ed.) Stability of complex carbohydrate structures: Biofuels, foods, vaccines and shipwrecks. Croydon, UK: RSC Publishing.

HARDING, S., ALMUTAIRI, F., ADAMS, G. G., MORRIS, G., LAWSON, C. J., WOOD, S. & GAHLER, R. J. 2012. Dilute Solution Viscometry Studies on a Therapeutic Mixture of Non-digestible Carbohydrates. International Journal of Biotechnology for Wellness Industries, 1**,** 107-114.

HARDING, S. E. 1992. Sedimentation Analysis of Polysaccharides. In: HARDING, S. E., ROWE, A. J. & HORTON, J. C. (eds.) Analytical Ultracentrifugation in Biochemistry and Polymer Science. Royal Soc. Chem.

HARDING, S. E. 1997. The intrinsic viscosity of biological macromolecules. Progress in measurement, interpretation and application to structure in dilute solution. Progress in biophysics and molecular biology, 68**,** 207-262.

HARDING, S. E. 1999. Diffusion. In: CREIGHTON, T. E. (ed.) Encyctopedoia of Molecular Biology. John Wiley & Sons, Inc.

HARDING, S. E. 2005a. Analysis of Polysaccharides by Ultracentrifugation. Size, Conformation and Interactions in Solution. In: HEINZE, T. (ed.) Polysaccharides I. Springer Berlin Heidelberg.

HARDING, S. E. 2005b. Analysis of polysaccharides size, shape and interactions. Analytical ultracentrifugation techniques and methods**,** 231-252.

HARDING, S. E. 2005c. Challenges for the modern analytical ultracentrifuge analysis of polysaccharides. Carbohydrate Research, 340**,** 811-826.

HARDING, S. E. 2006. Trends in muco-adhesive analysis. Trends in food science & technology, 17**,** 255-262.

HARDING, S. E., BERTH, G., BALL, A., MITCHELL, J. R. & DE LA TORRE, J. G. 1991a. The molecular weight distribution and conformation of citrus pectins in solution studied by hydrodynamics. Carbohydrate Polymers, 16**,** 1-15.

HARDING, S. E., DAY, K., DHAMI, R. & LOWE, P. M. 1997. Further observations on the size, shape and hydration of kappa-carrageenan in dilute solution. Carbohydrate Polymers, 32**,** 81-87.

HARDING, S. E. & JOHNSON, P. 1985a. The concentration-dependence of macromolecular parameters. Biochem. J, 231**,** 543-547.

HARDING, S. E. & JOHNSON, P. 1985b. Physicochemical studies on turnip-yellow-mosaic virus. Homogeneity, relative molecular masses, hydrodynamic radii and concentration-dependence of parameters in non-dissociating solvents. Biochem. J, 231**,** 549-555.

HARDING, S. E., ROWE, A. J. & HORTON, J. C. (eds.) 1992. Analytical Ultracentrifugation in Biochemistry and Polymer Science, Cambridge, UK: Royal Society of Chemistry.

HARDING, S. E., SATTELLE, D. B. & BLOOMFIELD, V. A. 1990. Laser Light Scattering in Biochemistry, Cambridge, UK, Royal Scoiety of Chemsitry.

HARDING, S. E., SCHUCK, P., ABDELHAMEED, A. S., ADAMS, G., KÖK, M. S. & MORRIS, G. A. 2011. Extended Fujita approach to the molecular weight distribution of polysaccharides and other polymeric systems. Methods, 54**,** 136-144.

HARDING, S. E., VÅRUM, K., STOKKE, B. R. T. & SMIDSRØD, O. 1991b. Molecular weight determination of polysaccharides. Advances in carbohydrate analysis, 1.

HARDING, S. E., VARUM, K. M., STOKKE, B. T. & SMIDSROD, O. 1991c. Molecular Weight Determination of Polysaccharides Advances in Carbohydrate Analysis., 1**,** 63-144.

HAXAIRE, K., BRACCINI, I., MILAS, M., RINAUDO, M. & PÉREZ, S. 2000. Conformational behavior of hyaluronan in relation to its physical properties as probed by molecular modeling. Glycobiology, 10**,** 587-594.

HAYASHI, K., TSUTSUMI, K., NORISUYE, T. & TERAMOTO, A. 1996. Electrostatic contributions to chain stiffness and excluded-volume effects in sodium hyaluronate solutions. Polymer journal, 28**,** 922-928.

HEARST, J. E. & STOCKMAYER, W. H. 1962. Sedimentation constants of broken chains and wormlike coils. The Journal of Chemical Physics, 37**,** 1425-1433.

HOCHBERG, M. C. Role of intra-articular hyaluronic acid preparations in medical management of osteoarthritis of the knee. Seminars in arthritis and rheumatism, 2000. Elsevier, 2-10.

HOKPUTSA, S. 2003. Chemical and Hydrodynamic Investigations of Polysaccharides with Pharmaceutical Importance. PhD, University of Nottingham

HOKPUTSA, S., JUMEL, K., ALEXANDER, C. & HARDING, S. E. 2002. Hydrodynamic characterisation of chemically degraded hyaluronic acid. Carbohydrate Polymers, 52**,** 111-117.

HOKPUTSA, S., JUMEL, K., ALEXANDER, C. & HARDING, S. E. 2003a. A comparison of molecular mass determination of hyaluronic acid using SEC/MALLS and sedimentation equilibrium. European Biophysics Journal, 32**,** 450-456.

HOKPUTSA, S., JUMEL, K., ALEXANDER, C. & HARDING, S. E. 2003b. Hydrodynamic characterisation of chemically degraded hyaluronic acid. Carbohydrate polymers, 52**,** 111-117.

HOTTA, H., HAGIWARA, K., TABATA, K., ITO, W. & HOMMA, M. 1993. Augmentation of protective immune responses against Sendai virus infection by fungal polysaccharide schizophyllan. International journal of immunopharmacology, 15**,** 55-60.

HUBER, K. C., MCDONALD, A. & BEMILLER, J. N. 2005. Carbohydrate Chemistry. In: HUI, Y. H. (ed.) Handbook of Food Science, Technology, and Engineering. Boca Raton, Florida, USA: Taylor and Francis.

IZYDORCZYK, M. 2005. Understanding the chemistry of food carbohydrates. In: CUI, S. W. (ed.) Food Carbohydrates: Chemistry, Physical Properties, and Applications. CRC Press, Boca Raton, FL, USA.

JACOBETZ, M. A., CHAN, D. S., NEESSE, A., BAPIRO, T. E., COOK, N., FRESE, K. K., FEIG, C., NAKAGAWA, T., CALDWELL, M. E. & ZECCHINI, H. I. 2013. Hyaluronan impairs vascular function and drug delivery in a mouse model of pancreatic cancer. Gut, 62**,** 112-120.

JANIN, M. 2015. Functionality of new xanthan gums. PhD, University of Nottingham.

JIN, Y.-J., UBONVAN, T. & KIM, D.-D. 2010. Hyaluronic acid in drug delivery systems. J Pharm Invest, 40**,** 33-43.

JUMEL, K., HO, M. M. & BOLGIANO, B. 2002. Evaluation of meningococcal C oligosaccharide conjugate vaccines by size-exclusion chromatography/multi-angle laser light scattering. Biotechnol. Appl. Biochem., 36**,** 219-226.

KACINIK, V., LYON, M., PURNAMA, M., REIMER, R., GAHLER, R., GREEN, T. & WOOD, S. 2011. Effect of PGX, a novel functional fibre supplement,

on subjective ratings of appetite in overweight and obese women consuming a 3-day structured, low-calorie diet. Nutrition & diabetes, 1**,** e22.

KAKUMU, S., ISHIKAWA, T., WAKITA, T., YOSHIOKA, K., ITO, Y. & SHINAGAWA, T. 1991. Effect of sizofiran, a polysaccharide, on interferon gamma, antibody production and lymphocyte proliferation specific for hepatitis B virus antigen in patients with chronic hepatitis B. International journal of immunopharmacology, 13**,** 969-975.

KANI, K., HORINAKA, J.-I. & MAEDA, S. 2005. Effects of monovalent cation and anion species on the conformation of gellan chains in aqueous systems. Carbohydrate Polymers, 61**,** 168-173.

KASAAI, M. R., ARUL, J. & CHARLET, G. 2000. Intrinsic viscosity–molecular weight relationship for chitosan. Journal of Polymer Science Part B: Polymer Physics, 38**,** 2591-2598.

KASHIWAGI, Y., NORISUYE, T. & FUJITA, H. 1981. Triple helix of Schizophyllum commune polysaccharide in dilute solution. 4. Light scattering and viscosity in dilute aqueous sodium hydroxide. Macromolecules, 14**,** 1220-1225.

KAWAHARA, K., OHTA, K., MIYAMOTO, H. & NAKAMURA, S. 1984. Preparation and solution properties of pullulan fractions as standard samples for water-soluble polymers. Carbohydrate polymers, 4**,** 335-356.

KAWAKAMI, K. & NORISUYE, T. 1991. Second virial coefficient for charged rods: sodium xanthan in aqueous sodium chloride. Macromolecules, 24**,** 4898-4903.

KHOURYIEH, H., HERALD, T., ARAMOUNI, F. & ALAVI, S. 2007. Intrinsic viscosity and viscoelastic properties of xanthan/guar mixtures in dilute solutions: Effect of salt concentration on the polymer interactions. Food research international, 40**,** 883-893.

KHOURYIEH, H. A. M. 2006. Rheological Characterization Of Xanthan-Guar Mixtures In Dilute Solutions. PhD Thesis, Kansas State University.

KIMURA, Y., TOJIMA, H., FUKASE, S. & TAKEDA, K. 1994. Clinical evaluation of sizofilan as assistant immunotherapy in treatment of head and neck cancer. Acta Oto-laryngologica, 114**,** 192-195.

KOGAN, G., ŠOLTÉS, L., STERN, R. & GEMEINER, P. 2007. Hyaluronic acid: a natural biopolymer with a broad range of biomedical and industrial applications. Biotechnology letters, 29**,** 17-25.

KOJIMA, T., TABATA, K., ITOH, W. & YANAKI, T. 1986. Molecular weight dependence of the antitumor activity of schizophyllan. Agricultural and biological chemistry, 50**,** 231-232.

KÖK, M. S., ABDELHAMEED, A. S., ANG, S., MORRIS, G. A. & HARDING, S. E. 2009. A novel global hydrodynamic analysis of the molecular flexibility of the dietary fibre polysaccharide konjac glucomannan. Food Hydrocolloids, 23**,** 1910-1917.

KOOL, M. M., GRUPPEN, H., SWORN, G. & SCHOLS, H. A. 2014. The influence of the six constituent xanthan repeating units on the order–disorder transition of xanthan. Carbohydrate Polymers, 104**,** 94-100.

KRATKY, O., LEOPOLD, H. & STABINGER, H. 1973. The determination of the partial specific volume of proteins by the mechanical oscillator technique. Methods in enzymology, 27**,** 98.

KUMAR, A. S. & MODY, K. 2009. Microbial exopolysaccharides: variety and potential applications. In: REHM, B. H. A. (ed.) Microbial production of biopolymers and polymer precursors. Applications and Perspectives. Norfolk, UK: Caister Academic Press

KUMARI, M., SURVASE, S. A. & SINGHAL, R. S. 2008. Production of schizophyllan using Schizophyllum commune NRCM. Bioresource Technology, 99**,** 1036-1043.

LAPČÍK, L., LAPCIK, L., DE SMEDT, S., DEMEESTER, J. & CHABRECEK, P. 1998. Hyaluronan: preparation, structure, properties, and applications. Chemical reviews, 98**,** 2663-2684.

LAUE, T. & STAFFORD III, W. 1999. Modern applications of analytical ultracentrifugation. Annual review of biophysics and biomolecular structure, 28**,** 75-100.

LAUE, T. M. & RHODES, D. G. 1990. Determination of size, molecular weight, and presence of subunits. Methods in enzymology, 182**,** 566-587.

LEATHERS, T., NUNNALLY, M. & PRICE, N. 2006. Co-production of Schizophyllan and Arabinoxylan from Corn Fiber. Biotechnology Letters, 28**,** 623-626.

LI, J., KAMATH, K. & DWIVEDI, C. 2001. Gellan film as an implant for insulin delivery. Journal of biomaterials applications, 15**,** 321-343.

LI, Z., RAMAY, H. R., HAUCH, K. D., XIAO, D. & ZHANG, M. 2005. Chitosan–alginate hybrid scaffolds for bone tissue engineering. Biomaterials, 26**,** 3919-3928.

LIAO, Y.-H., JONES, S. A., FORBES, B., MARTIN, G. P. & BROWN, M. B. 2005. Hyaluronan: pharmaceutical characterization and drug delivery. Drug delivery, 12**,** 327-342.

LIU, H., NAKAGAWA, K., KATO, D.-I., CHAUDHARY, D. & TADÉ, M. O. 2011a. Enzyme encapsulation in freeze-dried bionanocomposites prepared from chitosan and xanthan gum blend. Materials Chemistry and Physics, 129**,** 488-494.

LIU, L., LIU, Y., LI, J., DU, G. & CHEN, J. 2011b. Microbial production of hyaluronic acid: current state, challenges, and perspectives. Microb Cell Fact, 10**,** 1-9.

LOKESHWAR, V. B., ÖBEK, C., PHAM, H. T., WEI, D., YOUNG, M. J., DUNCAN, R. C., SOLOWAY, M. S. & BLOCK, N. L. 2000. Urinary hyaluronic acid and hyaluronidase: markers for bladder cancer detection and evaluation of grade. The Journal of urology, 163**,** 348-356.

LUO, Y., KIRKER, K. R. & PRESTWICH, G. D. 2000. Cross-linked hyaluronic acid hydrogel films: new biomaterials for drug delivery. Journal of Controlled Release, 69**,** 169-184.

LUPPI, B., BIGUCCI, F., MERCOLINI, L., MUSENGA, A., SORRENTI, M., CATENACCI, L. & ZECCHI, V. 2009. Novel mucoadhesive nasal inserts based on chitosan/hyaluronate polyelectrolyte complexes for peptide and protein delivery. Journal of Pharmacy and Pharmacology, 61**,** 151-157.

MA, L., GAO, C., MAO, Z., ZHOU, J., SHEN, J., HU, X. & HAN, C. 2003. Collagen/chitosan porous scaffolds with improved biostability for skin tissue engineering. Biomaterials, 24**,** 4833-4841.

MÄCHTLE, W. & BÖRGER, L. 2006. Analytical ultracentrifugation of polymers and nanoparticles, Springer Science & Business Media.

MAGNIN, D., DUMITRIU, S. & CHORNET, E. 2003. Immobilization of enzymes into a polyionic hydrogel: ChitoXan. Journal of Bioactive and Compatible Polymers, 18**,** 355-373.

MANSOURI, S., LAVIGNE, P., CORSI, K., BENDERDOUR, M., BEAUMONT, E. & FERNANDES, J. C. 2004. Chitosan-DNA nanoparticles as non-viral vectors in gene therapy: strategies to improve transfection efficacy. European Journal of Pharmaceutics and Biopharmaceutics, 57**,** 1-8.

MARCELLIN, E., CHEN, W. & NIELSEN, L. K. 2009. Microbial Hyaluronic Acid Biosynthesis. In: REHM, B. H. A. (ed.) Microbial Production of Biopolymers and Polymer Precursors. Norwich, UK: Caister Academic Press.

MILAS, M. & RINAUDO, M. 1996. The gellan sol-gel transition. Carbohydrate Polymers, 30**,** 177-184.

MILAS, M. & RINAUDO, M. 2004. Characterisation and properties of hyaluronic acid. In: DUMITRIU, S. (ed.) Polysaccharides: structural diversity and functional versatility. New York, USA: CRC press.

MILAS, M., SHI, X. & RINAUDO, M. 1990. On the physicochemical properties of gellan gum. Biopolymers, 30**,** 451-464.

MIYAZAKI, T., MIYAUCHI, S., NAKAMURA, T., TAKESHITA, S. & HORIE, K. 1996. The effect of sodium hyaluronate on the growth of rabbit corneal epithelial cells in vitro. Journal of ocular pharmacology and therapeutics, 12**,** 409-415.

MIYOSHI, E., TAKAYA, T. & NISHINARI, K. 1994. Gel-sol transition in gellan gum solutions. I. Rheological studies on the effects of salts. Food Hydrocolloids, 8**,** 505-527.

MIYOSHI, E., TAKAYA, T., WILLIAMS, P. A. & NISHINARI, K. 1996. Effects of sodium chloride and calcium chloride on the interaction between gellan gum and konjac glucomannan. Journal of Agricultural and Food Chemistry, 44**,** 2486-2495.

MORIMOTO, K., YAMAGUCHI, H., IWAKURA, Y., MORISAKA, K., OHASHI, Y. & NAKAI, Y. 1991. Effects of viscous hyaluronate–sodium solutions on the nasal absorption of vasopressin and an analogue. Pharmaceutical research, 8**,** 471-474.

MORRIS, E. R., NISHINARI, K. & RINAUDO, M. 2012. Gelation of gellan–a review. Food Hydrocolloids, 28**,** 373-411.

MORRIS, G. & HARDING, S. 2013. Hydrodynamic Modeling of Carbohydrate Polymers. In: ROBERTS, G. K. (ed.) Encyclopedia of Biophysics. Springer Berlin Heidelberg.

MORRIS, G., LI, P., PUAUD, M., LIU, Z., MITCHELL, J. & HARDING, S. 2001. Hydrodynamic characterisation of the exopolysaccharide from the halophilic cyanobacterium< i> Aphanothece halophytica</i> GR02: a comparison with xanthan. Carbohydrate polymers, 44**,** 261-268.

MORRIS, G. A. 2001. Hydrodynamic Investigation of Polysaccharides and Their Interactions With Casein. PhD Thesis, University of Nottingham.

MORRIS, G. A., CASTILE, J., SMITH, A., ADAMS, G. G. & HARDING, S. E. 2009a. The kinetics of chitosan depolymerisation at different temperatures. Polymer Degradation and Stability, 94**,** 1344-1348.

MORRIS, G. A., CASTILE, J., SMITH, A., ADAMS, G. G. & HARDING, S. E. 2009b. Macromolecular conformation of chitosan in dilute solution: A new global hydrodynamic approach. Carbohydrate Polymers, 76**,** 616-621.

MORRIS, G. A., FOSTER, T. J. & HARDING, S. E. 2002. A hydrodynamic study of the depolymerisation of a high methoxy pectin at elevated temperatures. Carbohydrate Polymers, 48**,** 361-367.

MORRIS, G. A., PATEL, T. R., PICOUT, D. R., ROSS-MURPHY, S. B., ORTEGA, A., GARCIA DE LA TORRE, J. & HARDING, S. E. 2008. Global hydrodynamic analysis of the molecular flexibility of galactomannans. Carbohydrate Polymers, 72**,** 356-360.

MORRIS, V. J. 2006. Bacterial Polysaccharides. In: STEPHEN, A. M., PHILLIPS, G. O. & WILLIAMS, P. A. (eds.) Food Polysaccharides and Their Applications. Boca Raton, FL, USA: CRC Press.

MORRISON, N., CLARK, R., CHEN, Y., TALASHEK, T. & SWORN, G. 1999. Gelatin alternatives for the food industry. Physical chemistry and industrial application of gellan gum. Springer.

NARINS, R. S., BRANDT, F., LEYDEN, J., LORENC, Z. P., RUBIN, M. & SMITH, S. 2003. A randomized, double-blind, multicenter comparison of the efficacy and tolerability of Restylane versus Zyplast for the correction of nasolabial folds. Dermatologic surgery, 29**,** 588-595.

NITTA, Y., KIM, B. S., NISHINARI, K., SHIRAKAWA, M., YAMATOYA, K., OOMOTO, T. & ASAI, I. 2003. Synergistic gel formation of

xyloglucan/gellan mixtures as studied by rheology, DSC, and circular dichroism. Biomacromolecules, 4**,** 1654-1660.

NORISUYE, T., YANAKI, T. & FUJITA, H. 1980. Triple helix of a Schizophyllum commune polysaccharide in aqueous solution. Journal of Polymer Science: Polymer Physics Edition, 18**,** 547-558.

NORTON, A. B., COX, P. W. & SPYROPOULOS, F. 2011. Acid gelation of low acyl gellan gum relevant to self-structuring in the human stomach. Food Hydrocolloids, 25**,** 1105-1111.

OGAWA, E. 1999. Temperature dependence of the conformational properties of sodium-type gellan gum in aqueous solutions. Physical Chemistry and Industrial Application of Gellan Gum. Springer.

OGAWA, E., MATSUZAWA, H. & IWAHASHI, M. 2002. Conformational transition of gellan gum of sodium, lithium, and potassium types in aqueous solutions. Food Hydrocolloids, 16**,** 1-9.

OKAMOTO, T., KUBOTA, K. & KUWAHARA, N. 1993. Light scattering study of gellan gum. Food Hydrocolloids, 7**,** 363-371.

ORTEGA, A., AMOROS, D. & GARCÍA DE LA TORRE, J. 2011. Global fit and structure optimization of flexible and rigid macromolecules and nanoparticles from analytical ultracentrifugation and other dilute solution properties. Methods, 54**,** 115-123.

ORTEGA, A. & GARCÍA DE LA TORRE, J. 2007. Equivalent radii and ratios of radii from solution properties as indicators of macromolecular conformation, shape, and flexibility. Biomacromolecules, 8**,** 2464-2475.

OSMAŁEK, T., FROELICH, A. & TASAREK, S. 2014. Application of gellan gum in pharmacy and medicine. International journal of pharmaceutics, 466**,** 328-340.

PALANIRAJ, A. & JAYARAMAN, V. 2011. Production, recovery and applications of xanthan gum by Xanthomonas campestris. Journal of Food Engineering, 106**,** 1-12.

PATEL, T. 2007. Solution Structure and Interactions of Therapeutic Polysaccharides. PhD, University of Nottingham.

PATEL, T. R., MORRIS, G. A., DE LA TORRE, J. G., ORTEGA, A., MISCHNICK, P. & HARDING, S. E. 2008a. Molecular flexibility of methylcelluloses of differing degree of substitution by combined

sedimentation and viscosity analysis. Macromolecular bioscience, 8**,** 1108-1115.

PATEL, T. R., MORRIS, G. A., EBRINGEROVÁ, A., VODENIČAROVÁ, M., VELEBNÝ, V., ORTEGA, A., GARCIA DE LA TORRE, J. & HARDING, S. E. 2008b. Global conformation analysis of irradiated xyloglucans. Carbohydrate polymers, 74**,** 845-851.

PAVLOV, G. M. 2013. Hydrodynamics of Macromolecules: Conformation Zoning for General Macromolecules. Encyclopedia of Biophysics. Springer.

PAVLOV, G. M., ROWE, A. J. & HARDING, S. E. 1997. Conformation zoning of large molecules using the analytical ultracentrifuge. TrAC Trends in Analytical Chemistry, 16**,** 401-405.

PELLETIER, E., VIEBKE, C., MEADOWS, J. & WILLIAMS, P. 2001. A rheological study of the order-disorder conformational transition of xanthan gum. Biopolymers, 59**,** 339-346.

PERSIN, Z., STANA-KLEINSCHEK, K., FOSTER, T. J., VAN DAM, J. E., BOERIU, C. G. & NAVARD, P. 2011. Challenges and opportunities in polysaccharides research and technology: The EPNOE views for the next decade in the areas of materials, food and health care. Carbohydrate Polymers, 84**,** 22-32.

PHAECHAMUD, T. & RITTHIDEJ, G. C. 2008. Formulation variables influencing drug release from layered matrix system comprising chitosan and xanthan gum. Aaps PharmSciTech, 9**,** 870-877.

PHILO, J. & ARAKAWA, T. 2000. Alliance protein laboratories: Laser light scattering http://www.ap-lab.com/light_scattering.htm [Online].

PICONE, C. S. F. & CUNHA, R. L. 2013. Chitosan–gellan electrostatic complexes: Influence of preparation conditions and surfactant presence. Carbohydrate polymers, 94**,** 695-703.

PICOUT, D. R., ROSS-MURPHY, S. B., JUMEL, K. & HARDING, S. E. 2002. Pressure cell assisted solution characterization of polysaccharides. 2. Locust bean gum and tara gum. Biomacromolecules, 3**,** 761-767.

PINTO, E. P., FURLAN, L. & VENDRUSCOLO, C. T. 2011. Chemical Deacetylation Natural Xanthan (Jungbunzlauer□). Polímeros, 21**,** 47-52.

POPA, N., NOVAC, O., PROFIRE, L., LUPUSORU, C. E. & POPA, M. I. 2010. Hydrogels based on chitosan–xanthan for controlled release of theophylline. Journal of Materials Science: Materials in Medicine, 21**,** 1241-1248.

PRAJAPATI, V. D., JANI, G. K., ZALA, B. S. & KHUTLIWALA, T. A. 2013. An insight into the emerging exopolysaccharide gellan gum as a novel polymer. Carbohydrate polymers, 93**,** 670-678.

PRESTON, B. N. & WIK, K. O. 1992. Non-ideality of hyaluronan as determined by sedimentation equilibrium studies. In: HARDING, S. E., ROWE, A. J. & HORTON, J. C. (eds.) Analytical Ultracentrifugation in Biotechnology and Polymer Science. Cambridge,UK: Royal Society of Chemistry.

RALSTON, G. B. 1993. Introduction to analytical ultracentrifugation, Beckman Instruments.

RENIER, D., BELLATO, P., BELLINI, D., PAVESIO, A., PRESSATO, D. & BORRIONE, A. 2005. Pharmacokinetic behaviour of ACP gel, an autocrosslinked hyaluronan derivative, after intraperitoneal administration. Biomaterials, 26**,** 5368-5374.

RINAUDO, M. 2006. Chitin and chitosan: Properties and applications. Progress in Polymer Science, 31**,** 603-632.

RINAUDO, M. 2008. Main properties and current applications of some polysaccharides as biomaterials. Polymer International, 57**,** 397-430.

RINAUDO, M., MILAS, M., BRESOLIN, T. & GANTER, J. Physical properties of xanthan, galactomannan and their mixtures in aqueous solutions. Macromolecular Symposia, 1999. Wiley Online Library, 115-124.

RINAUDO, M., MILAS, M. & LE DUNG, P. 1993. Characterization of chitosan. Influence of ionic strength and degree of acetylation on chain expansion. International Journal of Biological Macromolecules, 15**,** 281-285.

RODD, A., DUNSTAN, D. & BOGER, D. 2000. Characterisation of xanthan gum solutions using dynamic light scattering and rheology. Carbohydrate Polymers, 42**,** 159-174.

RODRíGUEZ-HERNÁNDEZ, A. I. & TECANTE, A. 1999. Dynamic viscoelastic behavior of gellan-ι-carrageenan and gellan-xanthan gels. Food Hydrocolloids, 13**,** 59-64.

ROSALAM, S. & ENGLAND, R. 2006. Review of xanthan gum production from unmodified starches by Xanthomonas comprestris sp. Enzyme and Microbial Technology, 39**,** 197-207.

SAETTONE, M., GIANNACCINI, B., CHETONI, P., TORRACCA, M. & MONTI, D. 1991. Evaluation of high-and low-molecular-weight fractions of sodium hyaluronate and an ionic complex as adjuvants for topical ophthalmic vehicles containing pilocarpine. International journal of pharmaceutics, 72**,** 131-139.

SANDFORD, P. A., PITTSLEY, J. E., KNUTSON, C. A., R., W. P., CADMUS, M. C. & JEANES, A. 1977. Variation in Xanthomonas campestris NRRL B-1459: Characterization of Xanthan Products of Differing Pyruvic Acid Content. In: SANDFORD, P. A. & LASKIN, A. (eds.) Extracellular Microbial Polysaccharides. American Chemical Society.

SATO, T., NORISUYE, T. & FUJITA, H. 1983. Triple helix of Schizophyllum commune polysaccharide in dilute solution. 5. Light scattering and refractometry in mixtures of water and dimethyl sulfoxide. Macromolecules, 16**,** 185-189.

SATO, T., NORISUYE, T. & FUJITA, H. 1984. Double-stranded helix of xanthan in dilute solution: Evidence from light scattering. Polymer journal, 16**,** 341-350.

SATTLER, R., KITYK, A. & WAGNER, C. 2007. Molecular configurations in the droplet detachment process of a complex liquid. Physical Review E, 75**,** 051805.

SCHATZ, C., VITON, C., DELAIR, T., PICHOT, C. & DOMARD, A. 2003. Typical physicochemical behaviors of chitosan in aqueous solution. Biomacromolecules, 4**,** 641-648.

SCHUCK, P. 1998. Sedimentation analysis of noninteracting and self-associating solutes using numerical solutions to the Lamm equation. Biophysical Journal, 75**,** 1503-1512.

SCHUCK, P., GILLIS, R. B., BESONG, T. M., ALMUTAIRI, F., ADAMS, G. G., ROWE, A. J. & HARDING, S. E. 2014. SEDFIT–MSTAR: molecular weight and molecular weight distribution analysis of polymers by sedimentation equilibrium in the ultracentrifuge. Analyst, 139**,** 79-92.

SCHUCK, P., PERUGINI, M. A., GONZALES, N. R., HOWLETT, G. J. & SCHUBERT, D. 2002. Size-distribution analysis of proteins by analytical ultracentrifugation: strategies and application to model systems. Biophysical Journal, 82**,** 1096-1111.

SCOTT, D. J., HARDING, S. E. & ROWE, A. J. (eds.) 2005. Analytical Ultracentrifugation Techniques and Methods, Cambridge, UK: Royal Society of Chemistry.

SCOTT, D. J. & SCHUCK, P. 2005. A brief introduction to the analytical ultracentrifugation of proteins for beginners. In: SCOTT, D. J., HARDING, S. E. & ROWE, A. J. (eds.) Modern Analytical Ultracentrifugation: Techniques and Methods. Cambridge: The Royal Society of Chemistry.

SECOUARD, S., GRISEL, M. & MALHIAC, C. 2007. Flavour release study as a way to explain xanthan–galactomannan interactions. Food Hydrocolloids, 21**,** 1237-1244.

SHATWELL, K. P., SUTHERLAND, I. W. & ROSS-MURPHY, S. B. 1990. Influence of acetyl and pyruvate substituents on the solution properties of xanthan polysaccharide. International Journal of Biological Macromolecules, 12**,** 71-78.

SMITH, I., SYMES, K., LAWSON, C. & MORRIS, E. 1981. Influence of the pyruvate content of xanthan on macromolecular association in solution. International Journal of Biological Macromolecules, 3**,** 129-134.

SOUTHWICK, J., MCDONNELL, M., JAMIESON, A. & BLACKWELL, J. 1979. Solution studies of xanthan gum employing quasielastic light scattering. Macromolecules, 12**,** 305-311.

SOUTHWICK, J. G., LEE, H., JAMIESON, A. M. & BLACKWELL, J. 1980. Self-association of xanthan in aqueous solvent-systems. Carbohydrate Research, 84**,** 287-295.

STOCKMAYER, W. & FIXMAN, M. On the estimation of unperturbed dimensions from intrinsic viscositiesxcin. Journal of Polymer Science Part C: Polymer Symposia, 1963. Wiley Online Library, 137-141.

STOKKE, B. T., ELGSAETER, A., HARA, C., KITAMURA, S. & TAKEO, K. 1993. Physicochemical properties of (1→ 6)-branched (1→ 3)-β-D-glucans. 1. Physical dimensions estimated from hydrodynamic and electron microscopic data. Biopolymers, 33**,** 561-573.

SUTHERLAND, I. W. 1998. Novel and established applications of microbial polysaccharides. Trends in biotechnology, 16**,** 41-46.

SUTHERLAND, I. W. 2006. Biotechnology of Microbial Polysaccharides in Food. In: SHETTY, K., PALIYATH, G., POMETTO, A. & LEVIN, R. E. (eds.) Food Biotechnology. Second ed. Boca Raton, FL, USA: CRC Press, Taylor and Francis.

SWORN, G. 2009. Xanthan gum. In: WILLIAMS, G. O. P. A. P. A. (ed.) Handbook of hydrocolloids. Second ed. Cambridge , UK: Woodhead Publishing Limited.

TAKADA, Y., SATO, T. & TERAMOTO, A. 1991. Dynamics of stiff-chain polymers in isotropic solution. 2. Viscosity of aqueous solutions of xanthan, a rigid double-helical polysaccharide. Macromolecules, 24**,** 6215-6219.

TAKAHASHI, R., KUBOTA, K., KAWADA, M. & OKAMOTO, A. 1999. Effect of molecular weight distribution on the solution properties of sodium hyaluronate in 0. 2 M NaCl solution. Biopolymers, 50**,** 87-98.

TAKAHASHI, R., TOKUNOU, H., KUBOTA, K., OGAWA, E., OIDA, T., KAWASE, T. & NISHINARI, K. 2004. Solution properties of gellan gum: Change in chain stiffness between single-and double-stranded chains. Biomacromolecules, 5**,** 516-523.

TAKEDATSU, H., MITSUYAMA, K., MOCHIZUKI, S., KOBAYASHI, T., SAKURAI, K., TAKEDA, H., FUJIYAMA, Y., KOYAMA, Y., NISHIHIRA, J. & SATA, M. 2012. A new therapeutic approach using a schizophyllan-based drug delivery system for inflammatory bowel disease. Molecular Therapy, 20**,** 1234-1241.

TAKO, M. 1996. Molecular origin for the thermal stability of schizophyllan. Polymer Gels and Networks, 4**,** 303-313.

TAKO, M. & NAKAMURA, S. 1984. Rheological properties of deacetylated xanthan in aqueous media. Agricultural and Biological Chemistry, 48**,** 2987-2993.

TAN, H., CHU, C. R., PAYNE, K. A. & MARRA, K. G. 2009. Injectable in situ forming biodegradable chitosan–hyaluronic acid based hydrogels for cartilage tissue engineering. Biomaterials, 30**,** 2499-2506.

TANFORD, C. 1961. Physical chemistry of macromolecules, Wiley.

TASCIOGLU, F. & ÖNER, C. 2003. Efficacy of intra-articular sodium hyaluronate in the treatment of knee osteoarthritis. Clinical rheumatology, 22**,** 112-117.

THIESEN, A., JOHANN, C., DEACON, M. P. & HARDING, S. E. 2000. Refractive increment data book, Nottingham, United Kingdom.

TOMBS, M. P. & HARDING, S. E. 1997. An Introduction to Polysaccharide Biotechnology London, UK, Taylor & Francis Ltd.

TRIMM, H. H. & JENNINGS, B. R. 1983. Study of hyaluronic acid flexibility by electric birefringence. Biochem. J, 213**,** 671-677.

TSUTSUMI, K. & NORISUYE, T. 1998. Excluded-volume effects in sodium hyaluronate solutions revisited. Polymer journal, 30**,** 345-349.

TSVETKOV, V. N., ESKIN, V. E. & FRENKEL, S. I. 1971. Structure of macromolecules in solution, National Lending Library for Science and Technology.

TUINIER, R., ZOON, P., OLIEMAN, C., COHEN STUART, M. A., FLEER, G. J. AND DE KRUIF, C. G. 1998. Isolation and physical characterization of an exocellular polysaccharide. biopolymers, 49**,** 1-9.

VALLI, R. C. & MISKIEL, F. J. 2001. Gellan Gum. In: CHO, S. S. & DREHER, M. L. (eds.) Handbook of dietary fiber. New York, USA: Marcel Dekker.

VAN HOLDE, K. 1985. Physical Biochemistry, New Jersey, USA, Prentice-Hall Inc.

VAN HOLDE, K., JOHNSON, W. C. & HO, P. S. 2006a. Principles of Physical Biochemistry, New Jersey, Pearson Prentice Hall.

VAN HOLDE, K. E., JOHNSON, W. C. & HO, P. S. 2006b. Principles of Physical Biochemistry, USA, Pearson Education ,Inc.

VENUGOPAL, V. 2011. Marine polysaccharides: Food applications, CRC Press.

VIEBKE, C. 2005. Order–Disorder Conformational Transition of Xanthan Gum. In: DUMITRIU, S. (ed.) Polysaccharides, Structural Diversity and Functional Versatility. 2 ed. New York, USA: Marcel Dekker.

VILELA, J. A. P., DE ASSIS PERRECHIL, F., PICONE, C. S. F., SATO, A. C. K. & DA CUNHA, R. L. 2015. Preparation, characterization and in vitro digestibility of gellan and chitosan–gellan microgels. Carbohydrate polymers, 117**,** 54-62.

WALES, M. & VAN HOLDE, K. 1954. The concentration dependence of the sedimentation constants of flexible macromolecules. Journal of Polymer Science, 14**,** 81-86.

WAN, Y., CREBER, K. A., PEPPLEY, B. & BUI, V. T. 2003. Ionic conductivity of chitosan membranes. Polymer, 44**,** 1057-1065.

WANG, Q. & CUI, S. W. 2005. Understanding the physical properties of food polysaccharides. Food Carbohydrates: Chemistry, Physical Properties, and Applications**,** 161.

WATERS, J. & LEISKE, D. 2005. Characterization of hyaluronic acid with on-line differential viscometry, multiangle light scattering, and differential refractometry. LC GC Magazine-North America-Solutions for Separation Scientists, 23**,** 302-311.

WEST, D. C., HAMPSON, I. N., ARNOLD, F. & KUMAR, S. 1985. Angiogenesis induced by degradation products of hyaluronic acid. Science, 228**,** 1324-1326.

WONG, T. W. 2009. Chitosan and its use in design of insulin delivery system. Recent patents on drug delivery & formulation, 3**,** 8-25.

WYATT, P. J. 1993. Light scattering and the absolute characterization of macromolecules. Analytica chimica acta, 272**,** 1-40.

WYATT, P. J. 2013a. Multiangle Light Scattering from Separated Samples (MALS with SEC or FFF). In: ROBERTS, G. (ed.) ln Encyclopedia of Biophysics, . Berlin: Springer Verlag.

WYATT, P. J. 2013b. Multiangle light scattering from separated samples (MALs with SEC or FFF). Encyclopedia of Biophysics. Springer.

XU, X., LI, B., KENNEDY, J., XIE, B. & HUANG, M. 2007. Characterization of konjac glucomannan–gellan gum blend films and their suitability for release of nisin incorporated therein. Carbohydrate Polymers, 70**,** 192-197.

YAMAKAWA, H. & FUJII, M. 1973. Translational friction coefficient of wormlike chains. Macromolecules, 6**,** 407-415.

YANAKI, T., NORISUYE, T. & FUJITA, H. 1980. Triple helix of Schizophyllum commune polysaccharide in dilute solution. 3. Hydrodynamic properties in water. Macromolecules, 13**,** 1462-1466.

YANAKI, T., TABATA, K. & KOJIMA, T. 1985. Melting behaviour of a triple helical polysaccharide schizophyllan in aqueous solution. Carbohydrate Polymers, 5**,** 275-283.

YANG, J. T. 1962. The viscosity of macromolecules in relation to molecular conformation. Advances in protein chemistry, 16**,** 323-400.

ZENG, C., TOOLE, B. P., KINNEY, S. D., KUO, J. W. & STAMENKOVIC, I. 1998. Inhibition of tumor growth in vivo by hyaluronan oligomers. International journal of cancer, 77**,** 396-401.

ZENTZ, F., VERCHÈRE, J.-F. & MULLER, G. 1992. Thermal denaturation and degradation of schizophyllan. Carbohydrate polymers, 17**,** 289-297.

ZHANG, Y., KONG, H., FANG, Y., NISHINARI, K. & PHILLIPS, G. O. 2013. Schizophyllan: A review on its structure, properties, bioactivities and recent developments. Bioactive Carbohydrates and Dietary Fibre, 1**,** 53-71.

APPENDIX

Publications:

1. ERTEN, T., ADAMS, G., FOSTER, T.J. and HARDING, S.E., 2014. Comparative heterogeneity, molecular weights and viscosities of xanthans of different pyruvate and acetate content, Food Hydrocolloids, 42, 335-341.
2. ALMUTAIRI, F.M., ERTEN, T., ADAMS, G.G., HAYES, M., MCLOUGHLIN, P., KOK, M.S., MACKIE, A.R., ROWE, A.J. and HARDING, S.E., 2015. Hydrodynamic characterisation of chitosan and its interaction with two polyanions: DNA and xanthan, Carbohydrate Polymers, 122, 359-366.
3. HARDING SE, GILLIS RB, ALMUTAIRI F, ERTEN T, KÖK MŞ and ADAMS GG, 2015. Recent advances in the analysis of macromolecular interactions using the matrix-free method of sedimentation in the analytical ultracentrifuge. Biology. 4(1), 237-50.
4. HARDING, S. E., G. G. ADAMS, F. ALMUTAIRI, Q. ALZAHRANI, T. ERTEN, M. S. KÖK AND R. B. GILLIS (2015). "Chapter Eighteen-Ultracentrifuge Methods for the Analysis of Polysaccharides, Glycoconjugates, and Lignins." Methods in Enzymology, 562: 391-439.

Posters:

1. Erten T., Foster T., Adams G., Harding S. 2013. Hydrodynamic characterisation of commercial xanthan samples. Nice, France, 3rd EPNOE International Polysaccharide Conference, 21-24 October 2013.
2. Erten T., Kok M.S., Foster T., Adams G., Harding S. 2015. Hydrodynamic Characterisation of Soluble Dietary Fibre: Gellan. Paris, France, 6th International Dietary Fibre Conference DF15, 1-3 June 2015.

Biology **2015**, 4, 237-250; doi:10.3390/biology4010237

OPEN ACCESS

biology

ISSN 2079-7737

www.mdpi.com/journal/biology

Review

Recent Advances in the Analysis of Macromolecular Interactions Using the Matrix-Free Method of Sedimentation in the Analytical Ultracentrifuge

Stephen E. Harding [1,*], Richard B. Gillis [1], Fahad Almutairi [1], Tayyibe Erten [1], M. Şamil Kök [2] and Gary G. Adams [1,3]

[1] National Centre for Macromolecular Hydrodynamics, University of Nottingham, Sutton Bonington LE12 5RD, UK; E-Mails: stxrbg@nottingham.ac.uk (R.B.G.); stxfa7@nottingham.ac.uk (F.A.); stxte@nottingham.ac.uk (T.E.); gary.adams@nottingham.ac.uk (G.G.A.)

[2] Department of Food Engineering, Abant Izzet Baysal University, Bolu 14280, Turkey; E-Mail: kok_s@ibu.edu.tr

[3] Faculty of Medicine and Health Sciences, University of Nottingham, Clifton Boulevard, Nottingham NG7 2RD, UK

***** Author to whom correspondence should be addressed; E-Mail: steve.harding@nottingham.ac.uk; Tel.: +44-115-951-6148; Fax: +44-115-951-6142.

Academic Editor: Thorsten Berg

Received: 1 December 2014 / Accepted: 16 February 2015 / Published: 6 March 2015

Abstract: Sedimentation in the analytical ultracentrifuge is a matrix free solution technique with no immobilisation, columns, or membranes required and can be used to study self-association and complex or "hetero"-interactions, stoichiometry, reversibility and interaction strength of a wide variety of macromolecular types and across a very large dynamic range (dissociation constants from 10^{-12} M to 10^{-1} M). We extend an earlier review specifically highlighting advances in sedimentation velocity and sedimentation equilibrium in the analytical ultracentrifuge applied to protein interactions and mucoadhesion and to review recent applications in protein self-association (tetanus toxoid, agrin), protein-like carbohydrate association (aminocelluloses), carbohydrate-protein interactions (polysaccharide-gliadin), nucleic-acid protein (G-duplexes), nucleic acid-carbohydrate (DNA-chitosan) and finally carbohydrate-carbohydrate (xanthan-chitosan and a ternary polysaccharide complex) interactions.

Keywords: protein; carbohydrate; nucleic acid; interaction; hydrodynamics

1. Introduction

We recently [1] gave a detailed consideration of how the Analytical Ultracentrifuge—a matrix-free separation technique for the analysis of the concentration distributions of a protein solute in solution at high centrifugal field—can be used to investigate either how this concentration distribution changes with time (known as sedimentation velocity), or (at relatively lower centrifugal fields using the same instrumentation) the final steady state concentration distribution after sedimentation and diffusive forces have come to equilibrium (sedimentation equilibrium), can be applied to the study of protein interactions. The choice of the appropriate optical system was shown to be important, with sometimes combined optics (refractometic and UV absorption) proving useful via the process of co-sedimentation, especially when used to study mucoadhesive interactions for drug delivery applications [2,3], and protein-cofactor binding [1].

Since that time there have been some important developments in terms of analysis, particularly for the sedimentation velocity and equilibrium analysis of heterogeneous materials. We will briefly review those developments and then consider very recent applications to protein self-association (tetanus toxoid, the yeast exoribonuclease co-factor Rrp47 and mini-agrin), protein-like carbohydrate self-association (aminocelluloses), carbohydrate-protein interactions (polysaccharide-gliadin), nucleic acid-carbohydrate (DNA-chitosan), carbohydrate-carbohydrate (xanthan-chitosan and PGX® complex) interactions and nucleic acid-protein interactions (G-quadruplex—RNA helicase).

2. Analytical Ultracentrifugation

The analytical ultracentrifuge is a high speed (to 60,000 rpm) ultracentrifuge with one or more optical systems to allow the analysis of the redistribution of macromolecular solute under the influence of a centrifugal field [4,5]. This can be either a sedimentation velocity experiment where the change in concentration distribution with time is followed, or a sedimentation equilibrium experiment—performed at lower speeds—where the steady state distribution of the macromolecular solute is recorded following equilibration of centrifugal and diffusive forces. The following are common types of optical systems used to register concentration distributions: (i) UV/visible—useful for proteins and nucleic acids which generally absorb in the UV, and coloured macromolecules like the cytochromes which absorb in the visible; (ii) refractometric or interferometric optics, which can be used for any macromolecular system. Two other types of optical system are used; (iii) fluorescence optics, permitting detection at very low concentration; and (iv) refractive index gradient or “Schlieren” optics, available on some older equipment.

3. Sedimentation Velocity

In sedimentation velocity we measure the sedimentation coefficient distribution g(s) vs. s—a measure of the purity/heterogeneity of the sample. The s value of individual components present can be related to the molecular weight and (from the frictional properties) shape. The greater the molecular

weight or more compact the macromolecule is, the larger its s value. It is often converted to standard conditions (the density and viscosity of water at 20.0 °C)—to give $s_{20,w}$. Modern software, such as the highly popular SEDFIT suite of algorithms of Schuck and colleagues [6,7] provides also:

(i) A correction to the sedimentation coefficient distribution for diffusion broadening (this assumes all particles in the distribution have the same frictional ratio f/f_o (ratio of the friction coefficient of a macromolecule to the friction coefficient of a sphere of the same mass and anhydrous volume)—the resulting corrected distribution is known as a c(s) vs. s distribution.

(ii) Conversion of g(s) vs. s or c(s) vs. s for a discrete distribution (i.e., of a small number of resolvable components) to a molecular weight distribution (again, assuming particles of the same shape/frictional ratio), known as g(M) vs. M or c(M) vs. M.

(iii) For continuous distributions, a recently published algorithm known as the Extended Fujita algorithm [8] was incorporated into SEDFIT.

The transformation in the Extended Fujita algorithm is as follows:

$$f(M) = (ds/dM).\ g(s) \quad (1)$$

with

$$M = (s/\kappa_s)^{1/b} \quad (2)$$

and

$$ds/dM = b.\kappa_s^{\ 1/b}.s^{(b-1)/b} \quad (3)$$

b is a conformation parameter (~2/3 for globular macromolecules, decreasing for more asymmetric structures down to ~0.15 for rigid rods). κ_s can be found from Equation (2) provided that at least one value of M (e.g., M_w from sedimentation equilibrium) is known for one value of s (e.g., the weight average s value). This method for determination of molecular weight distribution is useful for large glycoconjugates [9] and associative complexes of very large molecular weight which are out of reach of other methods of analysis.

Interactions can manifest themselves in the appearance of material of a higher sedimentation coefficient, and if the reaction is reversible (or partially reversible) an increase in the slope of a plot of sedimentation coefficient $s_{20,w}$ vs. concentration, c (the normal trend—due to non-ideality effects—is a decrease). The proportion of higher molecular weight component(s) should increase as the concentration increases and vice versa.

4. Sedimentation Equilibrium

In sedimentation equilibrium we analyse the steady state distribution of solute concentration c(r) as a function of radial displacement r from the centre of rotation to obtain an estimate for the molecular weight. For an interacting system it can in principle tell us the stoichiometry of the system, the average molecular weight of all the components in the solution being analysed (principally the weight average M_w but also z-average M_z and number average information M_n) and also how the local or "point" average values $M_w(r)$ (and also $M_z(r)$ and $M_n(r)$) vary with r and c(r). From this, and the help of various diagnostic plots it is possible also to ascertain association/interaction K_a or dissociation K_d constants (often expressed in μM^{-1} or μM respectively) from the way the molecular weight changes

with concentration. A popular algorithm in the past has been MSTAR based on the M* function of Creeth and Harding [10] and this has very recently been incorporated into SEDFIT as the very easy to use SEDFIT-MSTAR algorithm [11] which provides an estimate for M_w, $M_w(r)$ vs. r or c(r) and through a smart-smooth procedure an estimate for the molecular weight distribution c(M) vs. M. Except at very small concentrations (<1 mg/mL for proteins, <0.3 mg/mL for large glycoconjugates) thermodynamic non-ideality (co-exclusion and polyelectrolyte effects) can be significant—estimates will then be of the apparent molecular weight (e.g., $M_{w,app}$).

An associated algorithm MULTISIG [12] provides accurate estimates of $M_n(r)$ vs. c(r), $M_z(r)$ vs. c(r) as well as $M_w(r)$ vs. c(r) and is proving very useful in the diagnosis of reversibility in interaction processes [13,14].

For non-interacting systems the conventional way of correcting for non-ideality is to measure $M_{w,app}$ at a series of concentrations and extrapolate back to zero concentration. Unfortunately if reversible concentration dependent interactive effects are being studied, this procedure is inappropriate. However the extent of non-ideality (as manifested by the 2nd thermodynamic virial coefficient B) can be predicted if the molecular weight and shape of the interacting species are known using the excluded volume theory of Rallison and Harding [15] and incorporated into the COVOL algorithm [16]: examples were demonstrated in the Harding and Rowe [1] review.

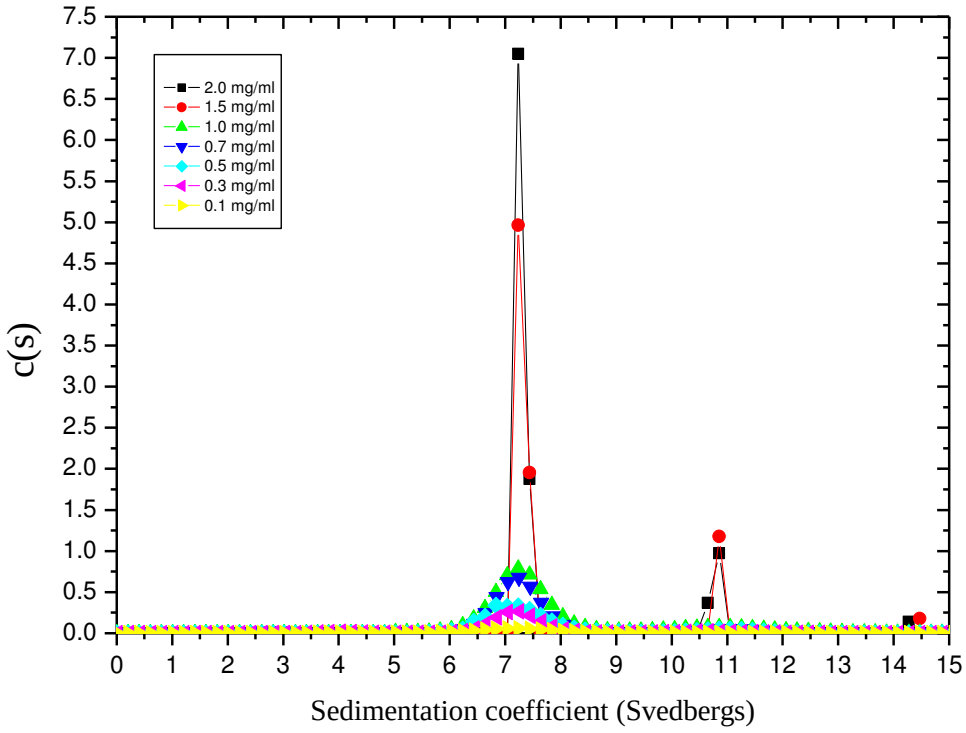
5. Protein Self-Association

Recent examples include the application of AUC to the analysis of the self-association of the tetanus toxoid protein and agrin.

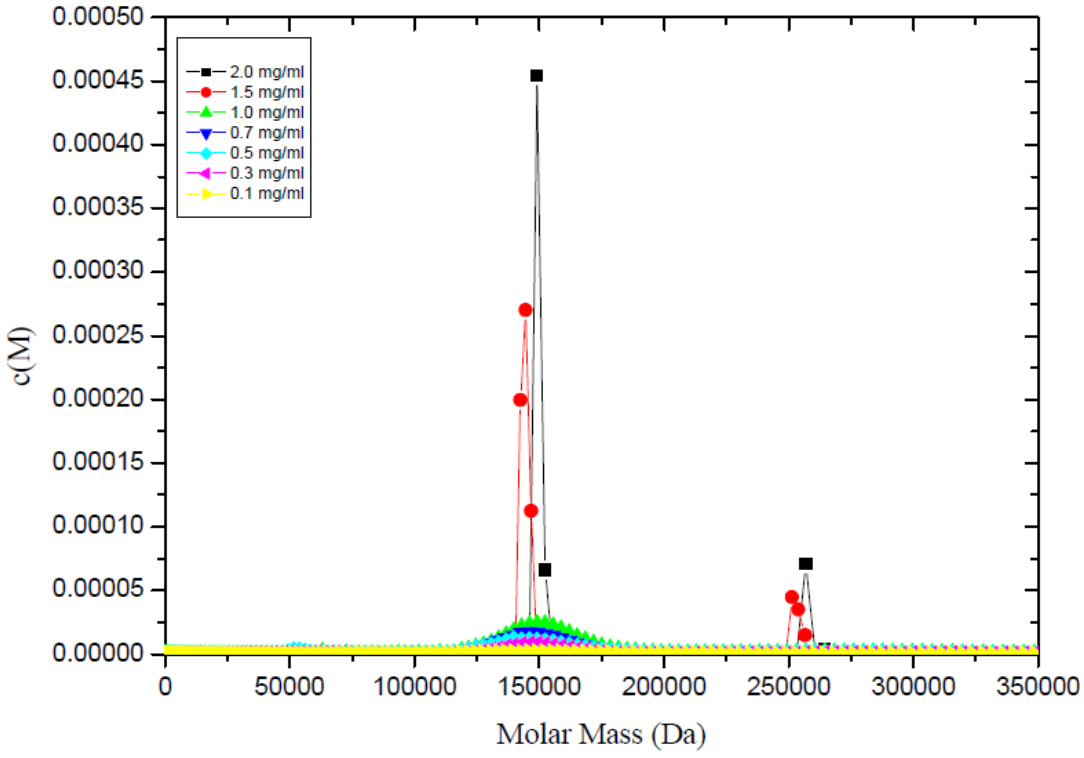
5.1. Tetanus Toxoid Protein

The tetanus toxoid (TT) protein is a chemically detoxified form of the tetanus toxin produced from Clostridium tetani. The tetanus neurotoxin is a 1292 amino acid protein consisting of two chains (N-terminal light chain of 52 kDa and C-terminal heavy chain of 98 kDa) linked by a single disulfide bridge. In addition to being a potent antigen, tetanus toxoid has been frequently used as the carrier protein in conjugate vaccines (see for example [17]), adding much greater efficacy to carbohydrate vaccines (see, e.g., [18]). Sedimentation coefficient c(s) vs. s profiles (Figure 1a) revealed the presence of two clear components with approximately 86% monomer sedimenting at ~7S and a 2nd component at ~11S (expected for the dimer, if $s \sim M^{2/3}$). The proportions of each do not seem to alter significantly with increasing total loading concentration (Figure 1a): this implies that these two components are not in reversible equilibrium. Extrapolation of $s_{20,w}$ values of both components to c = 0 yielded $s°_{20,w}$ values of (7.6 ± 0.1)S and (11.6 ± 0.2)S for the two components. The corresponding c(M) vs. M plots (Figure 1b) yielded molecular weight values of ~(150,000 ± 5000) g/mol for the main peak and (270,000 ± 15,000) g/mol for the minor peak, consistent (within experimental error) with a monomer-dimer system, results which were consistent with sedimentation equilibrium and SEC-MALS (size exclusion chromatography coupled with multi-angle light scattering). Furthermore, from the sedimentation coefficient for the monomer combined with the intrinsic viscosity, it was possible, after allowing for a range of plausible hydration values [18], to estimate the overall shape of the TT protein in terms of a prolate ellipsoid, and the measurements are consistent with an asymmetric protein of aspect ratio

~(3 ± 1):1 (Figure 1c), coincidentally similar to the cartoon representation of it presented some years earlier by Astronomo and Burton [17]. Such a structure presents a greater surface area for conjugation with polysaccharide than a more globular structure, underpinning its popular choice as a conjugation protein for glycoconjugate vaccines.

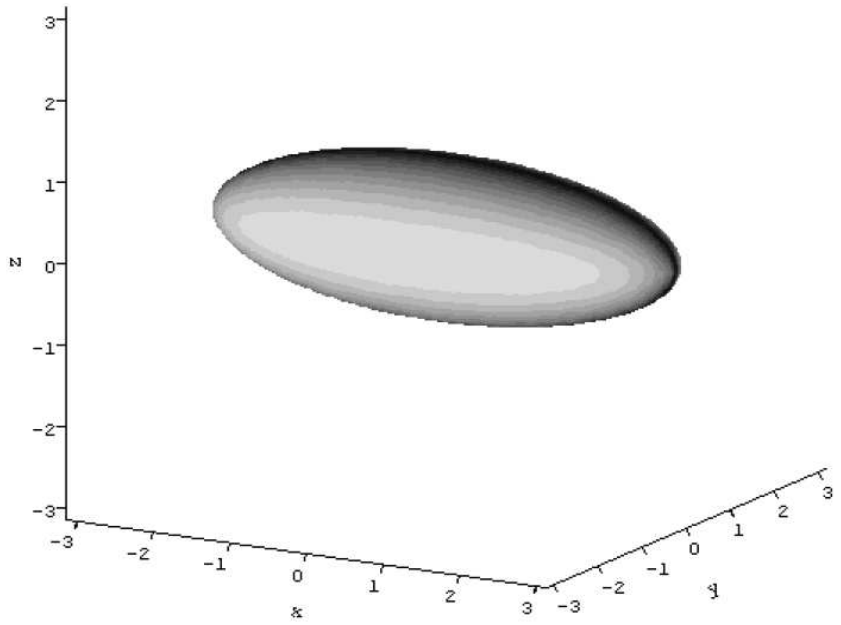


(**a**)



(**b**)

Figure 1. Cont.



(**c**)

Figure 1. (**a**) Sedimentation coefficient distribution profiles, c(s) vs. s, for tetanus toxoid protein at different concentrations, showing mostly monomer with a smaller proportion of dimer not in reversible equilibrium; (**b**) Corresponding molecular weight distribution plots c(M) vs. M; (**c**) Low resolution structure of tetanus toxoid protein using the simple ellipsoid modelling routine ELLIPS1 showing clearly its extended form of axial ratio ~3:1. Reproduced from reference 18 with permission from Elsevier.

5.2. Yeast Exoribonuclease Rrp6 Associated Cofactor Rrp47

In contrast to the TT-protein, recent measurements [19] using both sedimentation velocity and sedimentation equilibrium have established that the protein Rrp47, which plays an important part in RNA processing and degradation events, is a pure dimer at least under the conditions analysed, with an s value of (2.7 ± 0.1)S and M ~ 54,000 g/mol, but like TT-protein it has large frictional ratio (~1.6) corresponding to an axial ratio of ~6:1 [19].

5.3. Mini-Agrin

Mini-agrin [20] is a miniaturized form of agrin—an extracellular matrix proteoglycan that induces acetylcholine receptor aggregation at the neuromuscular junction, miniaturized so that it just contains 4-domains, the N-terminal domain and 3 globular C-terminal domains, considered to be potentially important in the treatment of congenital muscular dystrophy. Unlike the tetanus toxoid system sedimentation velocity in the analytical ultracentrifuge showed no direct evidence of associative behaviour from the c(s) vs. s plots but the weight average $s°_{20,w}$ value (4.7 ± 0.2)S combined with an estimate from dynamic light scattering for the translational diffusion coefficient $D°_{20,w}$ ~ (3.3 ± 0.2) × 10^{-7} cm^2/s yielded an estimate of the M of (127,000 ± 12,000) g/mol using the Svedberg equation, well in excess of the sequence monomer molecular weight of 106,650 g/mol suggestive of associative behaviour. This was confirmed

by SEC-MALS which revealed a value for the 2nd virial coefficient B of -6.5×10^{-4} mL·mol·g^{-2}. On the grounds that return of a negative value for B signifies that thermodynamic non-ideality in the classical sense (exclusion volume and polyelectrolyte effects) is +ve and we observe –ve values confirms that self-association is significant. Re-analysis of the sedimentation equilibrium data using a routine which specifically considers the evaluation of the association/dissociation constants yielded and estimate of 0.24 L/g for the association constant—corresponds to a molar dimerization constant $K_d \sim (4.2 \pm 0.4)$ μM.

The low value for the sedimentation coefficient for such a large ~100 kDa protein suggests the agrin monomer is asymmetric with an axial ratio ~3.8, coincidentally similar to the tetanus toxoid protein. Further experiments using small angle x-ray scattering and modelling the angular distributions of scattered x-rays reinforced this view and indicates dimerization via an end-to-end rather than a side-by-side process [20].

6. Carbohydrate Self-Association

Certain classes of carbohydrate polymer are known to form double or triple helices (for example xanthan and schizophyllan respectively) but these tend to be non-reversible equilibria, i.e., by "reversible" we mean by changing the concentration one can reversibly change the relative amount of oligomerization. Two systems have been shown to give reversible behaviour—one a very weak dimerization (xyloglucan) the other a stronger oligomerisation (aminocelluloses).

6.1. Xyloglucans

A very weak reversible dimerization was observed for xyloglucans—these are β(1–4) linked xylose polymers with arabinose (sometimes esterified with phenolic acids) side chains [21]. Evidence for dimerization comes not from the appearance of an extra component in the sedimentation coefficient distribution plots but from the concentration dependence of the sedimentation coefficient after allowing for non-ideality. For example one xyloglucan (PO2) gave a dissociation constant value $K_d \sim (340 \pm 50)$ μM at 20 °C. Intriguingly decreasing the temperature to 5 °C greatly suppressed the interaction($K_d > 3000$ μM) whereas raising the temperature to 30 °C increased the dimerization strength ($K_d \sim 140$ μM): this decrease in K_d (increase in dimerization) with increase in temperature is systematic of a reversible hydrophobic interaction [21].

6.2. Aminocelluloses

Even more unusual protein-like association has been observed in solutions of the water soluble carbohydrates known as the 6-deoxy-6-(ω-aminoalkyl) aminocelluloses which had previously been reported to produce controllable self-assembling films for enzyme immobilisation and other applications [22]. c(s) vs. s distributions show multiple components (up to pentamers) all related according to $s \sim M^{2/3}$ (Figure 2). Not only had such oligomerisation—of the sort seen for example in antibody aggregation processes—never been seen in polysaccharides, the power law coefficient of 2/3 is more appropriate for globular proteins rather than carbohydrates [13]. The oligomerisation was at least partially reversible (the proportion of the lower molecular weight components decreasing as the total concentration is increased). One particular aminocellulose exhibited a completely reversible tetramerisation behaviour [14] as deduced on the basis of (i) point average molecular weights, $M_n(r)$,

$M_w(r)$ and $M_z(r)$ all converging to the same (monomer value) M_1 = 3250 at zero concentration (and converging to the tetramer value at higher concentration) in plots of these point averages vs. c(r) using the MULTISIG routine and (ii) overlap of plots of $M_z(r)$ vs. c(r) for different loading concentrations. This completely reversible tetramerisation (and subsequent assembly into larger structures) resembled more like the behaviour of sickle cell deoxyhemoglobin than any carbohydrate, possibly revising traditional views of what is "protein-like" and what is "carbohydrate-like" behaviour (see [14] and references therein).

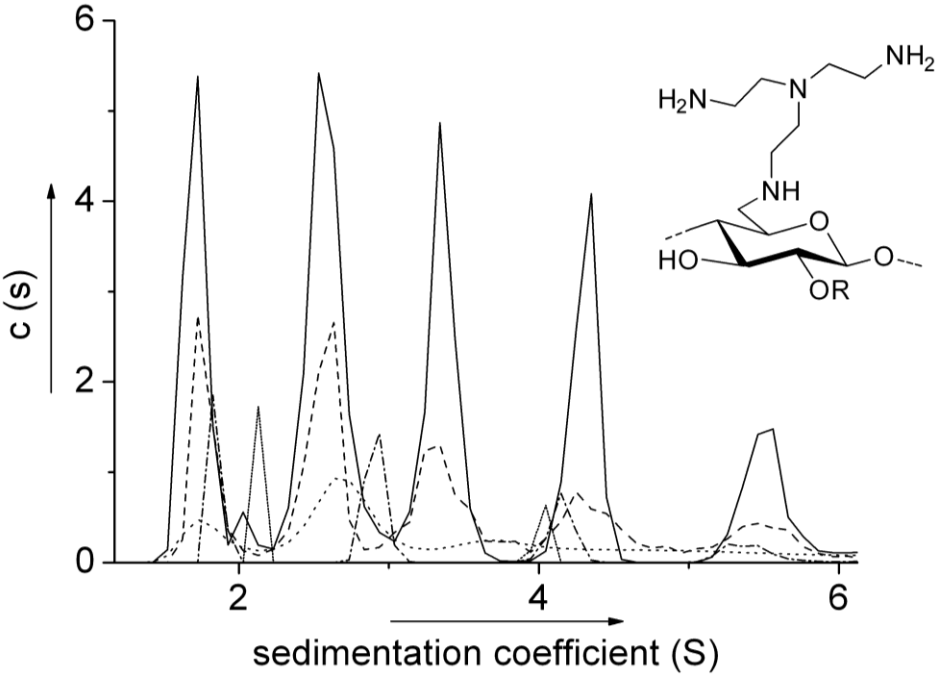


Figure 2. Sedimentation coefficient distributions of a 6-deoxy-6-amino cellulose (BAEA cellulose) at various concentrations: solid (——) 2.0 mg/mL; dash (– –) 1.0 mg/mL; dot (·····) 0.5 mg/mL; dash dot (– · – ·) 0.25 mg/mL; short dot (·····) 0.125 mg/mL. Reproduced from [13] with permission from Wiley.

7. Carbohydrate-Protein Interactions

Recent work on carbohydrate-protein interactions has been focusing on the possible use of fibre polysaccharides as a macromolecular block trying to stop gliadins reaching the mucosal epithelia and causing an immune response in people with gluten intolerance or coeliac disease. The work is currently on going, but an assay procedure based on sedimentation velocity in the analytical ultracentrifuge monitoring for co-sedimentation has been developed. The assay procedure takes advantage of the fact that gliadins absorb ultraviolet light at a wavelength ~280 nm whereas polysaccharides do not. For example iota-carrageenan [23]. Figure 3 shows sedimentation concentration distribution plots for a co-sedimentation experiment involving a mixture of gliadin and iota-carrageenan, showing a significant amount of what appears to be complexed material picked up by the UV absorption system at 280 nm and sedimenting at ~4.5S, well in excess of unbound gliadin. A comprehensive survey of fibre polysaccharides as potential macromolecular barriers to gliadin will be published in the near future (see also ref. [24]).

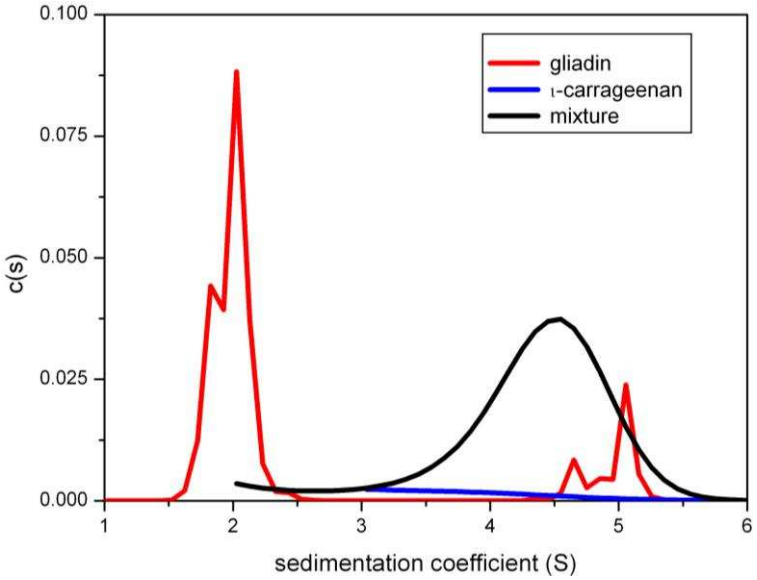


Figure 3. Sedimentation coefficient distribution diagrams for gliadins and iota carrageenan in aqueous phosphate-chloride buffer. c(s) = the population of species with a sedimentation coefficient between s and ds. UV-absorption optics at 280 nm were used showing only the gliadins—and whatever they may have interacted with. Red line: gliadin only control at 5.0 mg/mL loading concentration showing material sedimenting at 2S and a small amount of aggregated material at ~5S. Blue line: iota- carrageenan control at 1.0 mg/mL. The sedimenting material is almost transparent at 280 nm. Black line (same concentrations): mixture showing a substantial amount of material sedimenting at ~4.5S: this may indicate an interaction with gliadin. Reproduced with permission from [23].

8. Nucleic Acid-Carbohydrate Interactions

There is increasing interest in the use of polycationic polysaccharides as histone analogues for condensing nucleic acids in DNA/RNA therapies against disease. Chitosans have been the focus of particular attention: these are soluble derivatives of chitin (poly N-acetyl glucosamine). Reducing the degree of acetylation (DA) yields the soluble polycationic form of chitin known as chitosan. In a recent study [25] (Almutairi et al., 2014), the principle of co-sedimentation was used to explore the effectiveness of chitosans for binding to DNA, in a similar way to earlier studies applied to the study of chitosan "mucoadhesive" types of interaction with mucins [1–3]. In the Almutairi et al. study, solutions of two chitosans samples of different degrees of acetylation, known as "CHIT5" (DA = 25%) and "CHIT6" (15%) and different weight average molecular weights M_w (95,000 g/mol and 170,000 g/mol respectively) from sedimentation equilibrium were characterised and then studied in mixtures with the DNA of M_w, estimated from the Extended Fujita method of Harding et al. [8] to be approximately 300,000 g/mol.

Sedimentation velocity of 1.0 mg/mL solutions of the chitosans CHIT5 or CHIT6 with DNA at a temperature of 20.0 °C all gave unimodal distributions with respective weight average sedimentation coefficients $s_{20,w}$ 1.9S, 2.3S and 6.8S respectively. Each chitosan preparation was then mixed in a 1:1 w/w ratio with the DNA to a total concentration of 1.0 mg/mL. A clear shift to a high s value is observed in both cases, with nothing sedimenting at the rate of uncomplexed chitosan suggesting that the interaction had gone to completion. From the shoulder of the complex, some unreacted DNA appears remaining (Figure 4a). Multi-Gaussian analysis of the g(s) vs. s distribution for the complex

(Figure 4c) using the routine MULTIG suggests ~72% DNA had interacted with CHIT5 and ~83% for CHIT6. The s-distribution of the complex is very broad, even on a logarithmic scale, with material in excess of 100S, with the larger molecular weight and highest positively charged chitosan CHIT6 showing the greatest degree of complexation [4]. For a more detailed quantification of the nature of the interaction, other factors such as the differences in partial specific volume between DNA and carbohydrate would need to be taken into consideration.

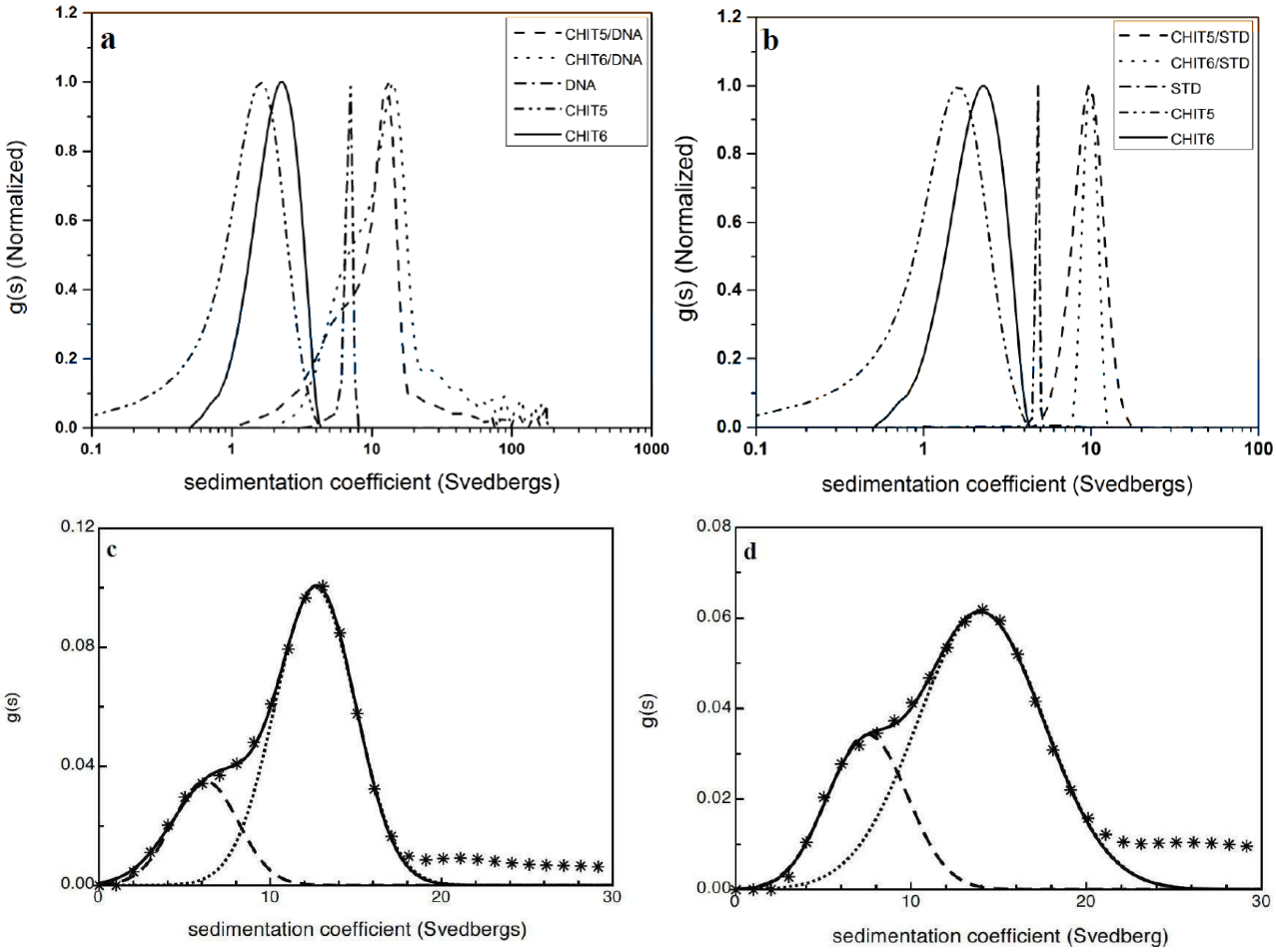


Figure 4. Normalized sedimentation coefficient distribution profiles obtained from sedimentation velocity experiments for unmixed controls and mixtures (**a**) chitosan with DNA; (**b**) chitosan with xanthan-STD; (**c**) multi-Gaussian fit to the CHIT5-DNA mixture; (**d**) multi-Gaussian fit to the CHIT6-DNA mixture. Reproduced from [25] with permission from Elsevier.

9. Carbohydrate-Carbohydrate Interactions

9.1. Chitosan-Xanthan Interactions

The advantageous properties of mixtures of chitosan and xanthan as hydrogels have been considered for some while [26–28] but only very recently has the biophysical basis behind this interaction been studied by analytical ultracentrifugation, again using co-sedimentation [25]. Xanthan, like DNA is a double helical highly polyanionic polymer obtained from the microorganism Xanthomonas campestris, and is widely used in the Food Industry as a thickener. The molecular weight of the particular xanthan

used in the study of Almutairi et al. [25]—known as "xanthan-STD"—had been found previously to be ~3.2×10^3 kDa using sedimentation equilibrium in the analytical ultracentrifuge [29].

As with the chitosan-DNA study, the sedimentation velocity profile of xanthan was first characterised at 1.0 mg/mL yielding a unimodal g(s) vs. s plot with weighted-average $s_{20,w}$ of 4.8S. Then the 1:1 by weight mixtures with CHIT5 and CHIT6 at a total concentration of 1.0 mg/mL, were studied and the results shown in Figure 4b,d. As with chitosan-DNA, all the chitosan was complexed, but unlike chitosan-DNA, for xanthan-DNA there was no residual xanthan were left behind for both CHIT5 and CHIT6 complexes. Weighted average $s_{20,w}$ for the complexes of 10.3S and 10.1S for CHIT5-xanthan and CHIT6-xanthan, respectively were obtained.

9.2. PGX®

Sedimentation coefficient distribution profiling has also been used to good effect for detecting interactions in mixed polysaccharide systems used for health applications. An example is the proprietary commercial product PGX® (PolyGlycopleX®) which is manufactured from konjac glucomannan, xanthan and sodium alginate using a proprietary manufacturing process (EnviroSimplex®, Inovobiologic inc. Burnaby, Canada). This product has been successfully used as a dietary/satiety product for help towards obesity control. Detailed analysis by co-sedimentation [30,31] showed clear evidence for a ternary interaction between the components at low ionic strength reinforcing experiments on the rheological properties of this system [32]. Interactions were shown to be clearly ionic strength dependent, clearly illustrating the importance of the solvent environment in the behaviour of polyelectrolyte polymers in solution.

10. Concluding Remarks

In our earlier review [1], we showed how powerful the analytical ultracentrifuge—with its intrinsic separation and analysis ability without the need for a separation matrix—was for characterising the strength, stoichiometry and reversibility for interacting protein (or glycoprotein) systems, and how potentially complicating issues such as thermodynamic non-ideality could be adequately dealt with.

In the present study, we have shown the considerable diversity of systems that the two main AUC techniques of sedimentation velocity and sedimentation equilibrium can be applied to with examples from very recently published studies, particularly using the principle of co-sedimentation. Particularly exciting is the application of the method for scrutinising the stability and behaviour of antibody based therapies—where the method is already considered as a gold standard—and also glyco-vaccine and DNA based therapy systems and the design of macromolecular based therapies against allergies and obesity. Other exciting developments include the improvement of ways of using and applying the analytical ultracentrifuge to high concentration systems, as is important for example in the development of monoclonal antibody formulations. This can provide a highly crowded macromolecular environment with a concomittant situation of high nonideality, well beyond the dilute solution situations considered in refs [15] and [16]. The use of tracer preparative (as opposed to analytical) ultracentrifugation in this regard, as pioneered by Minton, Rivas and others [33] has now been extended to centrifugal separation followed by subsequent analysis by solid state NMR ([34,35] and references therein).

For details of some of the latest developments and publications in the application of the analytical ultracentrifuge to the study of macromolecular interaction phenomena the interested

reader is advised to refer to the web pages (and links given therein) of the National Centre for Macromolecular Hydrodynamics (www.nottingham.ac.uk/ncmh) and that of the SEDFIT user group: www.analyticalultracentrifugation.com/.

Acknowledgements

Richard B. Gillis is grateful for a BBSRC (UK) Studentship, Fahad Almutairi is grateful to the support of the University of Tabuk, Saudi Arabia for a studentship and Tayyibe Erten is grateful to the Turkish Ministry of National Education for a studentship.

Conflicts of Interest

The authors declare no conflict of interest.

References

1. Harding, S.E.; Rowe, A.J. Insight into protein-protein interactions from analytical ultracentrifugation. Biochem. Soc. Trans. **2010**, 38, 901–907.
2. Harding, S.E. Mucoadhesive interactions. Biochem. Soc. Trans. **2003**, 31, 1036–1041.
3. Harding, S.E. Trends in mucoadhesive analysis. Trends Food Sci. Tech. **2006**, 17, 255–262.
4. Harding, S.E.; Rowe, A.J.; Horton, J.C. Analytical Ultracentrifugation in Biochemistry and Polymer Science; Royal Society of Chemistry: Cambridge, UK, 1992.
5. Scott, D.J.; Harding, S.E.; Rowe, A.J. Analytical Ultracentrifugation. Techniques and Methods; Royal Society of Chemistry: Cambridge, UK, 2005.
6. Schuck, P. Size-distribution analysis of macromolecules by sedimentation velocity ultracentrifugation and Lamm equation modeling. Biophys. J. **2000**, 78, 1606–1619.
7. Dam, J.; Schuck, P. Calculating sedimentation coefficient distributions by direct modeling of sedimentation velocity concentration profiles. Meth. Enzymol. **2004**, 384, 185–212.
8. Harding, S.E.; Schuck, P.; Abdelhammed, A.S.; Adams, G.; Kök, M.S.; Morris, G.A. Extended Fujita approach to the molecular weight distribution of polysaccharides and other polymer systems. Methods **2011**, 54, 136–144.
9. Gillis, R.B.; Adams, G.G.; Wolf, B.; Berry, M.; Besong, T.M.D.; Corfield, A.; Kök, S.M.; Sidebottom, R.; Lafond, D.; Rowe, A.J.; et al. Molecular weight distribution analysis by ultracentrifugation: Adaptation of a new approach for mucins. Carbohyd. Polym. **2003**, 93, 178–183.
10. Creeth, J.M.; Harding, S.E. Some observations on a new type of point average molecular weight. J. Biochem. Biophys. Methods **1982**, 7, 25–34.
11. Schuck, P.J.; Gillis, R.B.; Besong, D.; Almutairi, F.; Adams, G.G.; Rowe, A.J.; Harding, S.E. SEDFIT-MSTAR: Molecular weight and molecular weight distribution analysis of polymers by sedimentation equilibrium in the ultracentrifuge. Analyst **2014**, 139, 79–92.
12. Gillis, R.B.; Adams, G.G.; Heinze, T.; Nikolajski, M.; Harding, S.E.; Rowe, A.J. MultiSig: A new high-precision approach to the analysis of complex biomolecular systems. Europ. Biophys. J. **2013**, 42, 777–786.

13. Heinze, T.; Nikolajski, M.; Daus, S.; Besong, T.M.D.; Michaelis, N.; Berlin, P.; Morris, G.A.; Rowe, A.J.; Harding, S.E. Protein-like oligomerisation of carbohydrates. Ang. Chem. Int. Ed. **2011**, 50, 8602–8604.
14. Nikolajski, M.; Adams, G.G.; Gillis, R.B.; Besong, D.T.; Rowe, A.J.; Heinze, T.; Harding, S.E. Protein-like fully reversible tetramerisation and super-association of an aminocellulose. Sci. Rep. **2014**, 4, doi:10.1038/srep03861.
15. Rallison J.M.; Harding, S.E. Excluded volumes for pairs of triaxial ellipsoids at dominant Brownian motion. J. Coll. Int. Sci. **1985**, 103, 284–289.
16. Harding, S.E.; Horton, J.C.; Jones, S.; Thornton, J.M.; Winzor, D.J. COVOL: An interactive program for evaluating second virial coefficients from the triaxial shape or dimensions of rigid macromolecules. Biophys. J. **1999**, 76, 2432–2438.
17. Astronomo, R.D.; Burton, D.R. Carbohydrate vaccines: Developing sweet solutions to sticky situations? Nat. Rev. Drug Discov. **2010**, 9, 308–324.
18. Abdelhameed, A.S.; Morris, G.A.; Adams, G.G.; Rowe, A.J.; Laloux, O.; Cerny, L.; Bonnier, B.; Duvivier, P.; Conrath, K.; Lenfant, C.; et al. An asymmetric and slightly dimerized structure for the tetanus toxoid protein used in glycoconjugate vaccines. Carbohyd. Polym. **2012**, 90, 1831–1835.
19. Feigenbutz, M.; Jones, R.; Besong, T.D.; Harding, S.E.; Mitchell, P. Assembly of the yeast exoribunuclease Rrp6 with its associated cofactor Rrp47 occurs in the nucleus and is critical for the controlled expression of Rrp47. J. Biol. Chem. **2013**, 288, 15959–15970.
20. Patel, T.R.; Besong, T.M.D.; Patel, N.; Meier, M.; Harding, S.E.; Winzor, D.J.; Stetefeld, J. Evidence for self-association of a miniaturized version of agrin from hydrodynamic and small-angle X-ray scattering measurements. J. Phys. Chem. B **2011**, 115, 11286–11293.
21. Patel, T.R.; Harding, S.E.; Ebringerova, A.; Deszczynski, M.; Hromadkova, Z.; Togola, A.; Paulsen, B.S.; Morris, G.A.; Rowe, A.J. Weak self-association in a carbohydrate system. Biophys. J. **2007**, 93, 741–749.
22. Jung, A.; Berlin, P. New water-soluble and film-forming aminocellulose tosylates as enzyme support matrices with Cu2+-chelating properties. Cellulose **2005**, 12, 67–84.
23. Kök, M.S.; Gillis, R.; Ang, S.; Lafond, D.; Tatham, A.S.; Adams, G.; Harding, S.E. Can dietary fibre help provide safer food products for sufferers of gluten intolerance? A well-established biophysical probe may help towards providing an answer. BMC Biophys. **2012**, 5, doi:10.1186/2046-1682-5-10.
24. Gillis, R. Protein Polysaccharide Complexes: Permanent/Nonpermanent Interactions between Polysaccharides and Polypeptides. PhD Thesis, University of Nottingham, Nottingham, UK, 2015.
25. Almutairi, F.M.; Erten, T.; Adams, G.G.; Hayes, M.; McGloughlin, P.; Kök, M.S.; Mackie, A.R.; Rowe, A.J.; Harding, S.E. Hydrodynamic characterisation of chitosan and its interaction with two polyanions: DNA and xanthan. Carbohyd. Polym. **2015**, doi:10.1016/j.carbpol.2014.09.090.
26. Dumitriu, S.; Magny, P.; Montane, D.; Vidal, P.; Chornet, E. Polyionic hydrogels obtained by complexation between xanthan and chitosan: Their properties as supports for enzyme immobilization. J. Bioact. Compat. Polym. **1994**, 9, 184–209.
27. Martínez-Ruvalcaba, A.; Chornet, E.; Rodrigue, D. Viscoelastic properties of dispersed chitosan/xanthan hydrogels. Carbohyd. Polym. **2007**, 67, 586–595.

28. Shchipunov, Y.; Sarin, S.; Kim, I.; Ha, C.-S. Hydrogels formed through regulated self-organization of gradually charging chitosan in solution of xanthan. Green Chem. **2010**, 12, 1187–1195.
29. Erten, T.; Adams, G.G.; Foster, T.J.; Harding, S.E. Comparative heterogeneity, molecular weights and viscosities of xanthans of different pyruvate and acetate content. Food Hydrocoll. **2014**, 42, 335–341.
30. Abdelhameed, A.S.; Ang, S.; Morris, G.A.; Smith, I.; Lawson, C.; Gahler, R.; Wood, S.; Harding, S.E. An analytical ultracentrifuge study on ternary mixtures of konjac glucomannan supplemented with sodium alginate and xanthan gum. Carbohyd. Polym. **2010**, 81, 145–148.
31. Harding, S.E.; Smith, I.H.; Lawson, C.J.; Gahler, R.J.; Wood, S. Studies on macromolecular interactions in ternary mixtures of konjac glucomannan, xanthan gum and sodium alginate Carbohyd. Polym. **2011**, 83, 329–338.
32. Smith, I.H.; Lawson, C.J.; Harding, S.E.; Gahler, R.J.; Lyon, M.R.; Wood, S. Viscosity development during aqueous dispersion and dissolution: A comparison of PGX® with other dietary supplements and individual polysaccharides. Food Hydrocoll. **2014**, 38, 152–162.
33. Rivas, G.; Minton, A. Beyond the second virial coefficient: Sedimentation equilibrium in highly non-ideal solutions. Methods **2011**, 54, 167–174.
34. Bertini, I.; Luchinat, C.; Parigi, G.; Ravera, E.; Reif, B.; Turano, P. Solid-state NMR of proteins sedimented by ultracentrifugation. Proc. Nat. Acad. Sci. USA **2011**, 108, 10396–10399.
35. Bertini, I.; Luchinat, C.; Parigi, G.; Ravera, E. SedNMR: On the edge between solution and solid-state NMR. Acc. Chem. Res. **2013**, 46, 2059–2069.

© 2015 by the authors; licensee MDPI, Basel, Switzerland. This article is an open access article distributed under the terms and conditions of the Creative Commons Attribution license (http://creativecommons.org/licenses/by/4.0/).